(12)

ECAC-HDBK-82-049

DEPARTMENT OF DEFENSE
Electromagnetic Compatibility Analysis Center
Annapolis, Maryland 21402

RADIO WAVE PROPAGATION: A HANDBOOK OF PRACTICAL TECHNIQUES FOR COMPUTING BASIC TRANSMISSION LOSS AND FIELD STRENGTH

SEPTEMBER 1982

HANDBOOK

Prepared by

M. Weissberger, R. Meidenbauer,
H. Riggins, and S. Marcus

IIT Research Institute
Under Contract to
Department of Defense

Approved for public release; distribution unlimited.

ECAC-HDBK-82-049

This report was prepared by the IIT Research Institute as part of AF Project 649E under Contract F-19628-80-C-0042 with the Electronic Systems Division of the Air Force Systems Command in support of the DoD Electromagnetic Compatibility Analysis Center, Annapolis, Maryland.

This report has been reviewed and is approved for publication.

Reviewed by

Mark A. Weissberger

MARK A. WEISSBERGER
Project Manager, IITRI

Kalle R. Kontson

KALLE R. KONTSON
Assistant Director
Contractor Operations

Approved by

Charles L. Flynn

CHARLES L. FLYNN, Col, USAF
Director

A. M. Messer

A. M. MESSER
Chief, Plans & Resources Mgt.

UNCLASSIFIED

SECURITY CLASSIFICATION OF THIS PAGE (When Data Entered)

REPORT DOCUMENTATION PAGE		READ INSTRUCTIONS BEFORE COMPLETING FORM
1. REPORT NUMBER ECAC-HDBK-82-049	2. GOVT ACCESSION NO. AD-A122 090	3. RECIPIENT'S CATALOG NUMBER
4. TITLE (and Subtitle) RADIO WAVE PROPAGATION: A HANDBOOK OF PRACTICAL TECHNIQUES FOR COMPUTING BASIC TRANSMISSION LOSS AND FIELD STRENGTH		5. TYPE OF REPORT & PERIOD COVERED Handbook 6. PERFORMING ORG. REPORT NUMBER ECAC-HDBK-82-049
7. AUTHOR(s) M. Weissberger, R. Meidenbauer, H. Riggins, S. Marcus		8. CONTRACT OR GRANT NUMBER(s) F-19628-80-C-0042 CDRL # 10M
9. PERFORMING ORGANIZATION NAME AND ADDRESS Electromagnetic Compatibility Analysis Center North Severn, Annapolis, MD 21402		10. PROGRAM ELEMENT, PROJECT, TASK AREA & WORK UNIT NUMBERS
11. CONTROLLING OFFICE NAME AND ADDRESS		12. REPORT DATE September 1982 13. NUMBER OF PAGES 366
14. MONITORING AGENCY NAME & ADDRESS(if different from Controlling Office)		15. SECURITY CLASS. (of this report) UNCLASSIFIED 15a. DECLASSIFICATION/DOWNGRADING SCHEDULE

16. DISTRIBUTION STATEMENT (of this Report)

Approved for public release; distribution unlimited.

17. DISTRIBUTION STATEMENT (of the abstract entered in Block 20, if different from Report)

UNLIMITED

18. SUPPLEMENTARY NOTES

19. KEY WORDS (Continue on reverse side if necessary and identify by block number)

RADIO WAVE PROPAGATION
BASIC TRANSMISSION LOSS
FIELD STRENGTH

20. ABSTRACT (Continue on reverse side if necessary and identify by block number)

This Handbook contains a set of validated models for the computation of the basic transmission loss between a transmitter and a remotely sited receiver. Emphasis is on terrestrial, air-ground, air-air, and earth-satellite circuits in the 10 kHz - 30 GHz band. The effects of the imperfectly conducting, irregularly-shaped earth's surface, the troposphere, and the ionosphere are accounted for, as are meteorological variations and ray path obstruction by vegetation and urban structures. Only one model

DD FORM 1 JAN 73 1473 EDITION OF 1 NOV 68 IS OBSOLETE

UNCLASSIFIED

SECURITY CLASSIFICATION OF THIS PAGE (When Data Entered)

20. ABSTRACT (Continued)

is presented for each type of circuit. The rationale for the selection is discussed. In most cases a version of this model is presented in the form of graphs, tables, or formulas that can be evaluated with hand-held calculators.

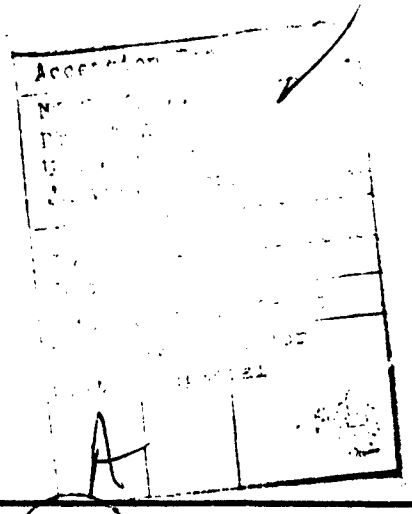

TABLE OF CONTENTS

TABLE OF CONTENTS (Continued)

TABLE OF CONTENTS (Continued)

TABLE OF CONTENTS (Continued)

TABLE OF CONTENTS (Continued)

TABLE OF CONTENTS (Continued)

TABLE OF CONTENTS (Continued)

TABLE OF CONTENTS (Continued)

LIST OF ILLUSTRATIONS

TABLE OF CONTENTS (Continued)

LIST OF ILLUSTRATIONS (Continued)

TABLE OF CONTENTS (Continued)

LIST OF ILLUSTRATIONS (Continued)

TABLE OF CONTENTS (Continued)

Figure — Page

LIST OF ILLUSTRATIONS (Continued)

TABLE OF CONTENTS (Continued)

LIST OF ILLUSTRATIONS (Continued)

TABLE OF CONTENTS (Continued)

Figure — Page

LIST OF ILLUSTRATIONS (Continued)

TABLE OF CONTENTS (Continued)

Figure — Page

LIST OF ILLUSTRATIONS (Continued)

LIST OF TABLES

Table

TABLE OF CONTENTS (Continued)

Table — Page

LIST OF TABLES (Continued)

TABLE OF CONTENTS (Continued)

LIST OF TABLES (Continued)

TABLE OF CONTENTS (Continued)

Appendix Page

LIST OF APPENDIXES

CHAPTER 1

INTRODUCTION

By: M. Weissberger

1.1 BACKGROUND

The Department of Defense Electromagnetic Compatibility Analysis Center (ECAC) has a twenty-plus year tradition of providing state-of-the-art solutions to spectrum-sharing problems. Many of these problems involve the use of radio-wave propagation models to compute the levels of the desired and interfering signals at the input terminals of a receiver, or to compute a field intensity at a location.

1.2 OBJECTIVE

The objective of this document is to provide ECAC project engineers with a set of manual propagation models - graphs, tables, or analytic expressions amenable to evaluation with a hand-held calculator.

1.3 APPROACH

The models were selected for the handbook following a review of recent ECAC model-development studies and documents in the open literature. Accuracy, as demonstrated through comparisons with measured results, was used as the primary criterion for recommending one model from among several that had been developed for solution of a given category of problem. In many instances, the most accurate model for a particular type of problem is a sophisticated computer program. Graphs of typical outputs of most of these programs were prepared and added to this document.

A summary of the validation effort used to select each model has been included for the following reasons:

1. It allows the engineer to account for the magnitude of the uncertainty in the model's predictions when doing an analysis.
2. It reveals the specific subsets of problems for which the model has been shown to be accurate, so that caution may be used when applying it in other parameter regions.
3. It enables the engineer to evaluate the desirability of using models that were not reviewed in this edition of the handbook.
4. It will help guide future model development efforts.
5. It provides a decision-making aid for members of the multi-agency Propagation Standards Coordinating Committee, of which ECAC is a charter member.

For the benefit of analysts at ECAC, information on the availability of computer-automated versions of each model was included.

To assist researchers from other disciplines, a chapter explaining the parameter "basic transmission loss" and its relationship to field strength, power density and received power was provided.

1.4 INDEX OF PROBLEM CATEGORIES

A list of the categories of problems addressed in the Handbook, together with the Chapter that contains the propagation-modeling information, is presented below.

A. Propagation in the 10 - 100 kHz band: Chapter 3

B. Propagation in the 100 kHz - 40 MHz band:
   - o Skywave, 0.5 - 1.6 MHz, Chapter 4
   - o Skywave, 2 - 30 MHz, Chapter 5
   - o Groundwave, 0.1 - 40 MHz, Chapter 6

C. Propagation in the 40 MHz - 30 GHz Band:

- Earth-space propagation, 100 MHz - 30 GHz, Chapter 7
- Air-air and air-ground propagation, 100 MHz - 16 GHz,[a] Chapter 8
- Terrestrial propagation, 40 MHz - 20 GHz:
  - Median loss, Chapter 9
  - Time variability, Chapter 10 (annotated bibliography)
  - Obstructions by vegetation and manmade structures, Chapter 11

D. Propagation at frequencies above 30 GHz:

- 30-300 GHz, Chapter 12 (annotated bibliography)
- IR and optical, Chapter 13 (annotated bibliography)

E. Coupling over an airframe: Chapter 14.

1.5 INDEX OF MODEL NAMES

TABLE 1-1 is an alternate index to this Handbook. It is an alphabetical list of the models that are addressed in the text. The frequency limits given are nominal. The Handbook text and/or source documents should be consulted for the range over which the model has actually been validated.

[a]Air-air and air-ground propagation, 40-100 MHz, is in Chapter 6.

TABLE 1-1

INDEX OF MODEL NAMES

(Page 1 of 3)

Model	Band	Notes	Handbook Section No.
AAPG	≥ 50 MHz	Coupling between antennas on a perfectly conducting airframe.	14.3
ADSEM	1-40 GHz	Line-of-sight propagation. Atmospheric effects.	10
Allsebrook	10-600 MHz	Correction to knife-edge diffraction for buildings.	11.7
AMSAA	50-450 MHz	Terrestrial propagation in Maryland hills. Statistical.	9.2
Artic (Palmer)	150-450 MHz	Terrestrial propagation in Artic areas. Statistical.	9.2, 9.4
ARPROP	--	See Longley-Rice.	
ATADU	--	See IF-77.	
AVPAK	≥ 50 MHz	Coupling between antennas on a perfectly conducting airframe.	14.2,14.3
BARNETT	--	See Vignato.	
Barrick	2-100 MHz	Attenuation due to propagation over a rough sea.	6.2.3, 6.4.1.5
BBC Co-channel	470-960 MHz	Terrestrial propagation over irregular terrain. Point-to-Point.	9.3
Barry (1966)	≥ 10 KHz	Groundwave propagation over a smooth spherical earth.	6.4.1.8
British Aircraft	40-110 MHz	Terrestrial propagation. Statistical and point-to-point versions. Based on measurements in FRG.	9.2-9.4
Bullington Knife-Edge Diffraction	≥ 30 MHz	Nomograph for knife-edge diffraction.	11.3, 11.7, 14.2.4
Bullington Plane Earth	All	Theory of propagation over a plane earth, including surface wave effects.	9.2, A
Cairo Model	0.5-1.6 MHz	Field strength due to skywave propagation.	4.4
CCIR Rec. 435-3	0.15-1.60 MHz	Field strength due to skywave propagation.	4.2, 4.4
CCIR Rep. 236-4	30 MHz-10 GHz	Attenuation due to propagation in a forest environment.	11.2, 11.5
CCIR Rep. 564-1	2-40 GHz	Earth-space propagation model.	7.4.1
CCIR Rep. 569-1	0.5-40 GHz	Calculation of interference fields due to ducting and rain scatter coupling.	10
CCIR Rep. 724	1-40 GHz	Calculation of worst case interference fields due to ducting and rain-scatter coupling.	10
Crane-79 (Global-79)	1-100 GHz+	Attenuation on earth-space links. Rain attenuation on terrestrial links.	7.2.3, 7.4.1
DUCT (ECAC Ducting Model)	65 MHz-3.3 GHz+	Coupling in a ducting environment.	10
EFFSECC	0.1 MHz-20 GHz	Propagation between two antennas over a smooth earth.	6.3
Egli (Fine, FCC 1951)	40-910 MHz	Terrestrial broadcast model. Statistical.	9.2

"+" implies that the limit shown is the highest frequency used by the author of the model in his examples. The model, in theory, is applicable to higher frequencies.

TABLE 1-1

(Page 2 of 3)

Model	Band	Notes	Handbook Section No.
EOSAEL-80	10-350 GHz, 8.3×10^2 cm^{-1} - 4×10^4 cm^{-1}	Effects of atmosphere, smoke and dust on transmittance and scattering.	13.2
EPM-73	1 MHz-10 GHz	Terrestrial propagation model for fairly smooth terrain. Statistical.	9.2, 9.4
Empenschied-Anderson-Bailey	17-60 MHz	Terrestrial propagation. Empirical.	3.4
Exercise Support Program (ESP)	4.4-5.0 GHz	Reliability of terrestrial links. Point-to-point.	10
Exponential Decay (Saxton and Lane)	100 MHz-3.3 GHz	Used in this report to designate a model for the loss due to propagation through a grove of trees.	11.2.3, A
Free Space Loss	All	Attenuation in a vacuum. Inverse-square-law spreading loss.	2.2
FCC MF Groundwave	0.5-1.6 MHz	Field strength due to groundwave propagation.	6.4.1.8
FCC MF Skywave (Clear Channel)	0.5-1.6 MHz	Field strength due to skywave propagation.	4.4, 4.5
FCC TV-FM Model (R-6602, TVFMFS)	50-900 MHz	Terrestrial broadcast model. Statistical.	9.4
GEMCS	10 MHz-40 MHz	Coupling between antennas on an airframe that may be lossy.	14.3
Global-78	1-30 GHz+	Rain attenuation on earth-space and terrestrial links.	7.2.3, 7.4.1
GRWAVE	--	Name of Berry's 1966 program. (see listing in this table). Also name of Rotheram's (Marconi's) program (see Reference 3-18).	
GWAVE	--	See FCC Groundwave.	
Hata	150-2000 MHz	Analytical expressions for Okumura's model. Statistical.	9.2, 11.4
HFMUFES-4	2-30 MHz	Loss between real antennas due to skywave propagation.	5.2, 5.3, Annex to Chapter 2.
HYDRO	1-40 GHz	Non-great circle coupling due to scatter from rain.	9.5.5, 9.5.6
IF-77	100 MHz-16 GHz	Air-ground and air-air propagation.	8
IONCAP	2-30 MHz	Loss between real antennas due to skywave propagation.	5.2, 5.3
IPS	1 MHz-20 GHz	Propagation between two antennas over a smooth earth.	6.3
Jansky and Bailey	25-400 MHz	Empirical loss between two low antennas in a tropical jungle.	11.5
Kinase	3 MHz-1 GHz	Terrestrial broadcast model with factor for urban clutter.	9.2, 11.4
Knife-Edge Diffraction	$\geq$ 20 MHz	Loss along a circuit with an infinitely thin, opaque, planar obstruction.	9.2, 9.3, 9.5 11.3, 11.7
Lateral-Wave	1-200 MHz	Theoretical model for paths including tropical jungle.	11.5.3
Lenkurt	--	See Vigants.	
LFSNR	60-600 kHz	Skywave and groundwave terrestrial propagation.	3.4
Longley-Rice (ARPROP)	20 MHz-20 GHz	Terrestrial propagation model; statistical and point-to-point modes.	9.2, 9.4, 9.5

"+" implies that the limit shown is the highest frequency used by the author of the model in his examples. The model, in theory, is applicable to higher frequencies.

TABLE 1-1

(Page 3 of 3)

Model	Band	Notes	Handbook Section No.
LOWTRAN-5	350-40,000 cm^{-1}	Atmospheric transmittance.	13.2
Malaga	3-450 MHz	Terrestrial propagation between two low antennas in urban and suburban environments. Statistical.	9.2
Millington	All	Coupling between antennas on a smooth earth with inhomogeneous ground constants	3.5, 6.2.2, 6.4.2.1
MINIMUF	2-30 MHz	Computes maximum usable frequency.	5.2.1.2
MIXPATH (ECAC Mixed-Path Model, MPM)	0.1 MHz-20 GHz	Computer implementation of "Millington".	3.5, 6.2.2, 6.4.2.1
MSMPROP	1-300 GHz	Atmospheric effects on line-of-sight links	12.2
Modified Exponential Decay (MED)	200 MHz-95 GHz	Attenuation due to propagation through a grove of trees.	11.1-11.2
Modified Plane Earth		See Bullington plane earth.	
NBS TN 101	40 MHz-10 GHz	Terrestrial propagation model, primarily point-to-point.	9.2, 9.3, 9.5
NLAMBDA	0.1 MHz-20 GHz	Propagation between two antennas over a smooth earth.	6.2-6.4
Ohio University	100-300 MHz+	Line-of-sight air-ground propagation over irregular terrain. Point-to-point.	9.3
Okumura	150-2000 MHz	Terrestrial broadcast model with factor for urban clutter.	9.2, 11.4
POPROP	20 MHz-200 GHz	Terrestrial and air-ground paths over rough terrain. Point-to-point.	9.3
RPP (VPI-79)	1-30 GHz+	Rain attenuation on earth-space links.	7.2.3, 7.4.1
SATPROP	100 MHz-30 GHz+	Earth-space propagation model	7
SCSE	—	Part of IPS.	
SKYWAVE	—	See FCC MF Skywave. Name also used for MFHUFES-4 and IONCAP.	
Smooth-sphere diffraction	All	Two antennas on or above a spherical earth.	3, 6, 8, 11.3
STGM	—	Part of IPS.	
TERRAIN	40 MHz-10 GHz	Line-of-sight propagation over irregular terrain. Point-to-point.	9.3
TIREM	40 MHz-20 GHz	Terrestrial paths over rough terrain. Point-to-point.	9.3-9.7, 11.3
Vigants	2-11 GHz	Bell Labs empirical model for multipath fading on line-of sight links.	10
VLF (ECAC VLF and LF Prop. Model)	10-100 kHz	Terrestrial propagation including effects of groundwave and skywave.	3
VPI-79	--	See RPP.	
WAGNER	< 60 MHz	Terrestrial propagation over irregular terrain with inhomogeneous ground constants. Point-to-point.	6.2.2, 6.4.2, 3.5
Wang	0.5-1.6 MHz	Field strength due to skywave propagation.	4.2-4.4

"+" implies that the limit shown is the highest frequency used by the author of the model in his examples. The model, in theory, is applicable to higher frequencies.

CHAPTER 2

BASIC EQUATIONS, COUPLING IN FREE-SPACE

By: M. Weissberger

2.1 INTRODUCTION

This chapter begins with a presentation of equations to compute the power density and field strength produced by a transmitter in "Free Space", i.e., a region in which there are no substances to reflect, absorb, refract or otherwise affect the radio waves. Then the equation is given for computing the power available at the terminals of a receiving antenna that is illuminated by the transmitting antenna. The parameter "basic free-space transmission loss" (L_{bfs}) is introduced to allow this received power to be computed with a compact formula.

These equations are followed by expressions that can be used when the path between the transmitter and receiver (or observation point) is not free-space. The parameter "basic transmission loss" (L_b) is introduced to allow convenient calculations for these general-environment problems. The remaining chapters of this Handbook present methods for computing L_b.

In order to assist engineers not yet experienced in such matters, straightforward derivations of each equation are presented along with examples of conversions between equations in logarithmic (decibel) units and those in non-logarithmic units.

2.2 FREE-SPACE RELATIONS

2.2.1 Power Density in Free-Space

Assume that p_t(watts) are input to an antenna that is 100% efficient and radiates isotropically. Consider observation points at a distance of r (meters) from the transmitter. The power density at these points is now the power per unit area flowing through a spherical shell of radius r with a

center at the transmitting antenna. At any point on this sphere the power density, p_d, is:

$$p_d = \frac{p_t}{4\pi r^2} \qquad (2\text{-}1)$$

where:

p_d is power density, in W/m^2
p_t is the power delivered to the transmitting antenna, in W.
r is distance, in m.

If the distance r is in statute miles:

$$p_d = \frac{p_t}{r^2(mi)} \times 30.73 \times 10^{-9}, \qquad (2\text{-}1a)$$

since there are 1609 meters in one statute mile.

If the problem input parameters remain as now stated, but the desired output is in dB above 1 mW/m^2 (i.e., dBm/m^2), then:

$$P_D\ (dBm/m^2) = 10 \log \frac{p_d(mW/m^2)}{r^2(m)}$$

$$= 10 \log \left[\frac{p_t(W)}{r^2(mi)} \times 30.73 \times 10^{-9} \times 10^3 \right]$$

$$= 10 \log p_t(W) - 20 \log r(mi) + 10 \log (30.73 \times 10^{-6})$$

$$= 10 \log p_t(W) - 20 \log r(mi) - 45.12 \qquad (2\text{-}1b)$$

If the transmitted power is expressed in dBm, i.e., dB above 1 mW:

$$P_T(dBm) = 10 \log p_t(mW) = 10 \log p_t(W) + 30 \qquad (2\text{-}1c)$$

So that:

$$P_D(dBm/m^2) = P_T(dBm) - 20 \log r(mi) - 75.12 \qquad (2\text{-}1d)$$

A general form of this equation is:

$$P_D(dBm/m^2) = P_T(dBm) - 20 \log r\ (units) - K_1 \qquad (2\text{-}1e)$$

where K_1, shown in TABLE 2-1, depends on the units of r.

TABLE 2-1

CONSTANTS FOR EQUATIONS 2-1e AND 2-6

Units of r	K_1	K_2
Statute miles	75.12	36.58
Nautical miles	76.34	37.80
Kilometers	70.99	32.45
Feet	0.67	-37.87
Meters	10.99	-27.55

2.2.2 Received Power in Free-Space

The effective aperture, A_e', of an antenna is defined by:

$$A_e' = \frac{P_r}{P_d} \qquad (2\text{-}2)$$

where:

P_r = the power delivered to a matched load at the terminals of the receiving antenna, in W

P_d = the power density incident on the antenna, in W/m^2.

This aperture is computed by:[2-1,2-2]

[2-1] Kraus, J. T., Antennas, McGraw Hill, New York, NY, 1950, p. 42 and p. 50.

[2-2] Collin, R. E. and Zucker, F. J., Antenna Theory, McGraw Hill, New York, NY, Part 1, 1969.

$$A_e' = \frac{g\lambda^2}{4\pi} \qquad (2\text{-}2a)$$

where:

g = the power gain of the antenna expressed as a ratio relative to the gain of an isotropic antenna that is 100% efficient

λ = the wavelength of the radiation, in meters.

For an isotropic antenna that is 100% efficient, $g = 1$, and:

$$A_e' = \frac{\lambda^2}{4\pi} \qquad (2\text{-}2b)$$

A formula for the power received by such an antenna in free space can be obtained by entering Equations 2-1 and 2-2b into Equation 2-2. The result is:

$$p_r = p_d A_e' = p_t \left(\frac{\lambda}{4\pi r}\right)^2 \qquad (2\text{-}3)$$

Here, λ and r have the same units, and p_r and p_t have the same non-logarithmic units (e.g., watts, milliwatts, etc.). If the problem is specified in terms of frequency rather than wavelength, then one can substitute:

$$\lambda \text{ (meters)} = \frac{300}{f(\text{MHz})} \qquad (2\text{-}3a)$$

into the preceding equation and obtain:

$$P_r = \frac{569.9\ p_t}{(f(MHz) \times r(meters))^2} \qquad (2\text{-}4)$$

where p_t and p_r are in the same non-logarithmic units.

If the transmitted power and received power are expressed in the same logarithmic units, e.g., dBm or dBW, then the proper equation can be obtained by taking the logarithm (base 10) of each side of this equation and multiplying the results by 10. Thus:

$$P_R = P_T - 20 \log (f(MHz)) - 20 \log (r(meters)) + 27.55 \qquad (2\text{-}4a)$$

This can be adapted to other units; e.g., if r is in statute miles:

$$P_R = P_T - 20 \log f(MHz) - 20 \log (r(miles)) - 36.58 \qquad (2\text{-}4b)$$

Equation 2-4b is frequently written as:

$$P_R = P_T - L_{bfs} \qquad (2\text{-}5)$$

where the basic free-space transmission loss, L_{bfs}, is given by:

$$L_{bfs} = 20 \log (r(units)) + 20 \log (f(MHz)) + K_2, \qquad (2\text{-}6)$$

where values of K_2 appear in TABLE 2-1 for different units of r, the slant range.

The preceding equations for received power are for lossless (i.e., 100% efficient) isotropic antennas at both ends of the link. If the transmitting antenna is not like this, then the power density, p_d, in front of the receiving antenna changes to:

$$p_d = \frac{p_t g_t}{4\pi r^2} \qquad (2\text{-}7)$$

where g_t is the transmitting antenna gain, in the direction of the receiver, relative to a lossless isotropic antenna (dimensionless units.) If the receiving antenna is also not lossless and isotropic, its effective aperture is given by Equation 2-2a, not 2-2b. Inserting Equations 2-7 and 2-2a into 2-2 yields:

$$p_r = p_t g_t g_r \left(\frac{\lambda}{4\pi r}\right)^2 \qquad (2\text{-}8)$$

In logarithmic units (and allowing use of f instead of λ):

$$P_R\ (dBW) = P_T(dBW) + G_T + G_R - 20 \log (r(miles)) - 20 \log (f(MHz)) - 36.58 \qquad (2\text{-}9)$$

where

$G_T\ (dBi) = 10 \log g_t$

$G_R\ (dBi) = 10 \log g_r$

dBi = decibels above the gain of lossless (100% efficient) isotropic antenna.

NOTE: Some manufacturers specify gain relative to a lossless $\frac{1}{2}\lambda$ dipole, rather than relative to an isotropic antenna. In this case, add 2.15 dB to the manufacturers' values before using them in Equation 2-9.

Combining Equations 2-6 and 2-9 yields this equation for the power available at the terminals of the receiving antenna when the transmission medium is free space:

$$P_R = P_T + G_T + G_R - L_{bfs} \qquad (2\text{-}10)$$

The formula is sometimes called, "The Friis Equation."[2-3, 2-4] Reference 2-4 presents an alternate derivation based on intuitive physical principles.

2.3 EQUATIONS WHEN THE ANTENNAS ARE NOT IN FREE-SPACE

2.3.1 A General Equation for Received Power

Equation 2-10 accounts for the $1/(4\pi R^2)$ spreading loss in "free-space," a region free from reflecting, absorbing or refracting materials. The terms G_T and G_R are the transmitter and receiver antenna gains in dBi. These terms also account for losses within the antennas due to lack of 100% radiation efficiency.

[2-3] Friis, H. T., "A Note on a Simple Transmission Loss Formula," BSTJ, 1946.

[2-4] Friis, H.T., "Introduction to Radio and Antennas," IEEE Spectrum, April, 1971.

There may be other losses between the outputs of the transmitter and the transmitting antenna. These can be ohmic losses, for example, in transmission lines, wave guides or antenna couplers; mismatch losses can also occur. Similar losses may exist between the receiving antenna and the input to the receiver. Also, there may be differences in the polarization of transmitting and receiving antennas. To account for these losses when calculating the power at the input terminals of the receiver, P'_R, Equation 2-10 should be modified to read:

$$P'_R = P'_T + G_T + G_R - L_{bfs} - \sum (\text{OTHER LOSSES}) \qquad (2\text{-}11)$$

where P'_T is the power available at the output of the transmitter.

In general, the space between the two antennas will contain the atmosphere and/or the earth. Thus, the basic free-space transmission loss, L_{bfs}, will frequently not be appropriate. Instead, the more general "basic transmission loss", L_b, is needed. The received power equation becomes:

$$P'_R = P'_T + G_T + G_R - L_b - \sum (\text{OTHER LOSSES}) \qquad (2\text{-}12)$$

The remaining sections of this handbook describe procedures that can be used to calculate L_b.

APPENDIX A presents the derivation of two equations for L_b. One allows calculation of the loss due to absorption by atmospheric constituents. The other accounts for the effect of reflection from the earth's surface on the loss between two antennas that are within line-of-sight. These derivations are included in the Handbook so that engineers can gain an intuitive feel for the means of quantifying L_b. They are excluded from the body of the text, since they are only building blocks for the more general models described in the forthcoming chapters.

The antenna gains as used in all preceding equations in this chapter have been defined as power gains relative to a lossless isotropic antenna. Thus, the terms G_T and G_R (and g_t and g_r) differ from the directivities of the transmitter and receiver antennas, D_T and D_R (see, e.g., Reference 2-1), in that the former terms include the effects of the antennas not having 100% efficiency. (An antenna that is 100% efficient will radiate all of the power that is input to it.) The difference between directivity and gain can be very large, especially if the radiation resistance is low relative to the ohmic resistance. This often is the case when the antenna is much smaller than $\frac{1}{4}$ of a wavelength. Measured values of efficiency in the HF band are discussed in References 2-5 and 2-6.

2.3.2 The General Equation for Power Density

An equation for predicting power density in a non-free-space environment can be obtained by entering Equations 2-12 and 2-2a into Equation 2-2 and solving for P_D. The result is:

$$P_D\ (dBm/m^2) = P_T'\ (dBm) + G_T - L_b + 20 \log\ (f(MHz)) \qquad (2\text{-}13)$$

$$- 38.54 - (\text{Losses between the transmitter output and the transmitting antenna}).$$

2-5 Lane, George and Charles Masen, Ground Resistance for MF/HF Design Analysis Of Grounded Antenna Systems, EMEP-76-7, U.S. Army Communications Electronics Engineering Installation Agency, Fort Huachuca, Arizona, April 1976.

2-6 Logan, J. C., AN/PRC-104 Antenna Study, Final Report, Naval Electronics Laboratory Center, NELC/TR 1980, February 1976.

2.4 COMPUTING THE ELECTRIC FIELD STRENGTH

If the engineer/analyst needs to know the electric field strength at a point in space, it may be computed from the power density. In the far field of the transmitting antenna these quantities are related by:

$$p_d \text{ (watts/m}^2\text{, avg)} = \frac{E^2 \text{ (volts/meter, rms)}}{\eta} \qquad (2\text{-}14)$$

where η is the impedance of free-space, = 120$\pi\Omega$, or $\approx$377Ω. (See, for example, Reference 2-7.)

TABLE 2-2, is a set of conversion equations for a variety of units.

2.5 SUPPLEMENTARY DEFINITIONS

In using some references, analysts may come across other terms that are used in the calculation of received power. To aid in correlating with the terms used in this chapter, some of the more common ones are defined below.

Antenna Factor. This is 10 log of the square of the ratio of the electric field intensity (V/m) at an antenna to the terminal voltage (V). Antenna gain can be computed from antenna factor through this equation:

$$G = 20 \log f - A_f - 30 \qquad (2\text{-}15)$$

where G is the gain in dB, and A_f is the antenna factor in dB.

2-7 Hayt, W. H., Engineering Electromagnetics, 3rd Edition, McGraw Hill, New York, NY, 1967.

TABLE 2-2

CONVERSION OF POWER DENSITY TO ELECTRIC FIELD STRENGTH

$E_{RMS} = 19.42\ (p_{avg})^{1/2}$	E_{RMS} in volts/m, p_{avg} in watts/m^2
$E_{RMS} = .61 \times 10^{P_{avg}/20}$	E_{RMS} in volts/m, P_{avg} in dBm/m^2
$E_{RMS} = P_{avg} + 115.8$	E_{RMS} in dBμv/m, P_{avg} in dBm/m^2
$E_{PK} = 1.41\ E_{RMS}$	E_{PK} in volts/m, E_{RMS} in volts/m
$E_{PK} = E_{RMS} + 3.0$	E_{PK} in dBμV/m, E_{RMS} in dBμv/m
$P_{avg} = \frac{(E_{RMS})^2}{376.99}$	p_{avg} in watts/m^2, E_{RMS} in volts/m
$P_{avg} = 20 \log E_{RMS} + 4.24$	P_{avg} in dBm/m^2, E_{RMS} in volts/m
$P_{avg} = E_{RMS} - 115.8$	P_{avg} in dBm/m^2, E_{RMS} in dBμv/m
$P_{PK} = P_{avg} + 3.0$	P_{PK} in dBm/m^2, P_{avg} in dBm/m^2

where:

E_{RMS} = RMS electric field strength,
E_{PK} = peak electric field strength,
P_{avg} = average power density,
P_{PK} = peak power density.

NOTES: 1) The terms peak and average refer to the time frame of one sinusoidal carrier frequency cycle. Transmitter duty cycle effects must be taken into account independently, as must all non-sinusoidal waveforms.

2) All relations apply only in the far field.

Transmission Loss[2-8]. This is 10 log of the ratio of the power input to the transmitting antenna to the power available from the receiving antenna. If it is designated as L, in dB, it can be related to L_b through:

$$L = L_b - G_T - G_R \qquad (2\text{-}16)$$

The reader is cautioned that in some widely used references[2-9], the quantity computed with Equation 2-16 is called "System Loss". These references use the term "Transmission Loss" to mean $L_b - D_T - D_R$.

[2-8] CCIR (International Radio Consultative Committee), Recommendations and Reports of the CCIR, XIVth Plenary Assembly, International Telecommunication Union, Geneva 1978, Report 227-2.

[2-9] Rice, P.L., Longley, A.G., and Norton, K.A., and Barsis, A.P., Transmission Loss Predictions for Tropospheric Communication Circuits, Technical Note 101, National Bureau of Standards, Boulder, CO, Revised January 1967.

CHAPTER 3

PROPAGATION IN THE 10-100 kHz BAND

By: S. Marcus and M. Weissberger

3.1 INTRODUCTION

Modeling for the 10-100 kHz band is discussed in this chapter. Section 3.2 provides a description of the physical phenomena. Graphs of typical field strength-versus-distance behavior are presented. Section 3.3 describes the ECAC VLF/LF computer code. Section 3.4 summarizes the results of comparing the code predictions with measurements. The accuracy of other prediction techniques is described. Section 3.5 contains concluding remarks.

3.2 PROPAGATION PHENOMENA AND CURVES OF TYPICAL RESULTS

Low and very low frequency waves, radiated by a transmitting antenna at or near the earth's surface, propagate within a shell bounded by the earth's surface and the ionosphere. At small circumferential distances ($d < 300$ km) from the transmitter, most of the energy is propagated by the direct and ground-reflected waves (over line-of-sight distances) and by the surface wave. The combination of these three is referred to as the ground wave. As the distance from the transmitter increases, an additional contribution to the radiated field becomes appreciable as a result of reflection of the incident field from the lowest layer of the ionosphere. As the distance from the transmitter increases still further, the contribution of multiply-reflected waves (i.e., waves following an earth-ionosphere-earth-ionosphere-earth path) must be considered as well. The reflected waves are referred to as skywaves. Phase differences between the skywave and groundwave can cause constructive and destructive interference. As a result, the composite field can vary significantly from point to point over the propagation path. These variations are apparent in the sample results illustrated in Figures 3-1 through 3-3. (All curves in this Chapter are for 1 kW radiated.) The representation of the field in terms of the sum of the ground wave and discrete skywaves will be called the ray-theory approach in this report.

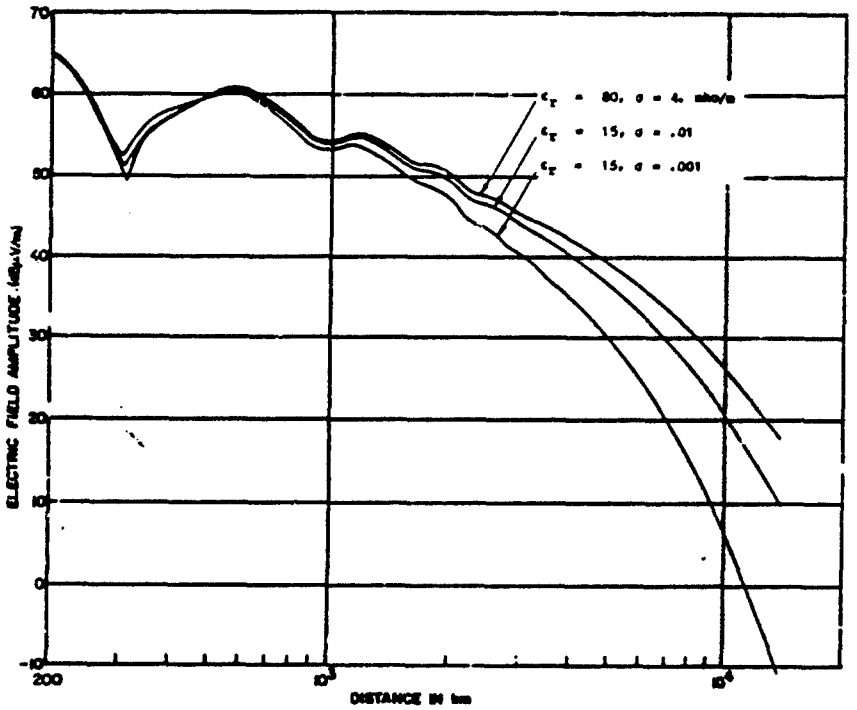

a. Day time.

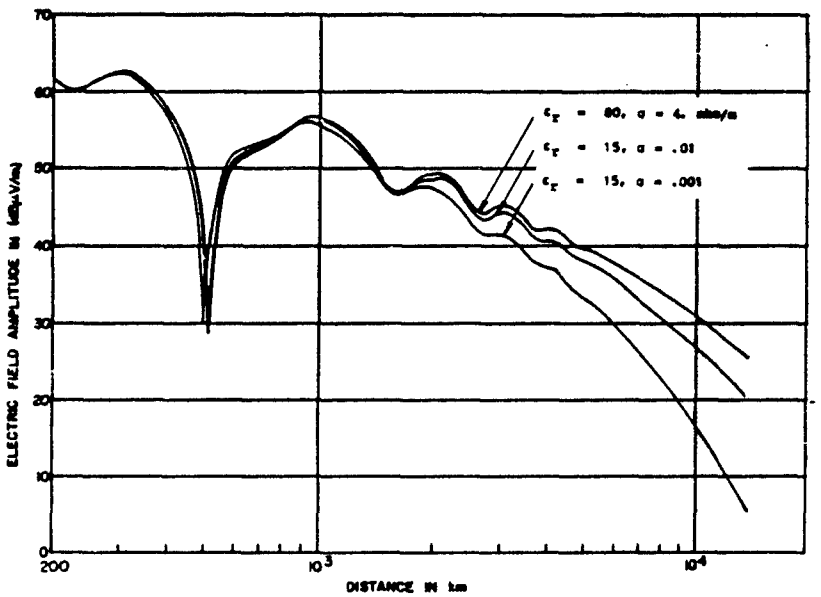

b. Night time.

Figure 3-1. Predicted propagation results for a 10.9 kHz transmission over three types of ground.

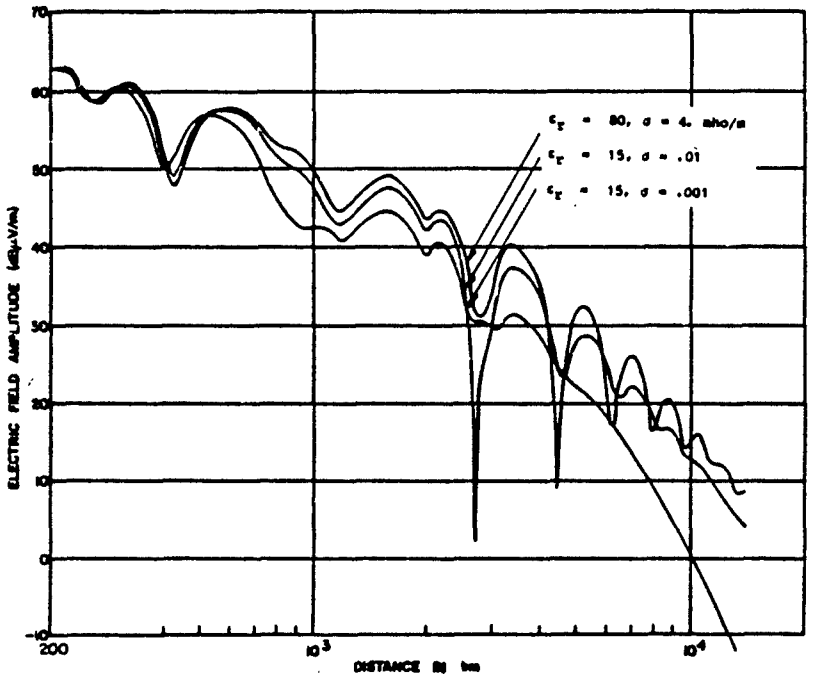

a. Day time.

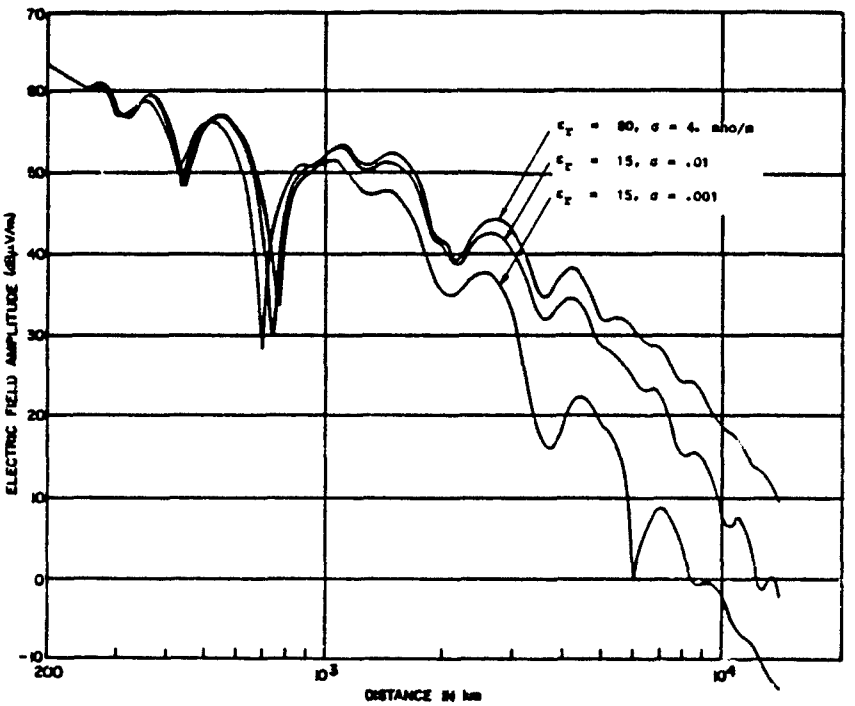

b. Night time.

Figure 3-2. Predicted propagation results for a 28.02 kHz transmission over three types of ground.

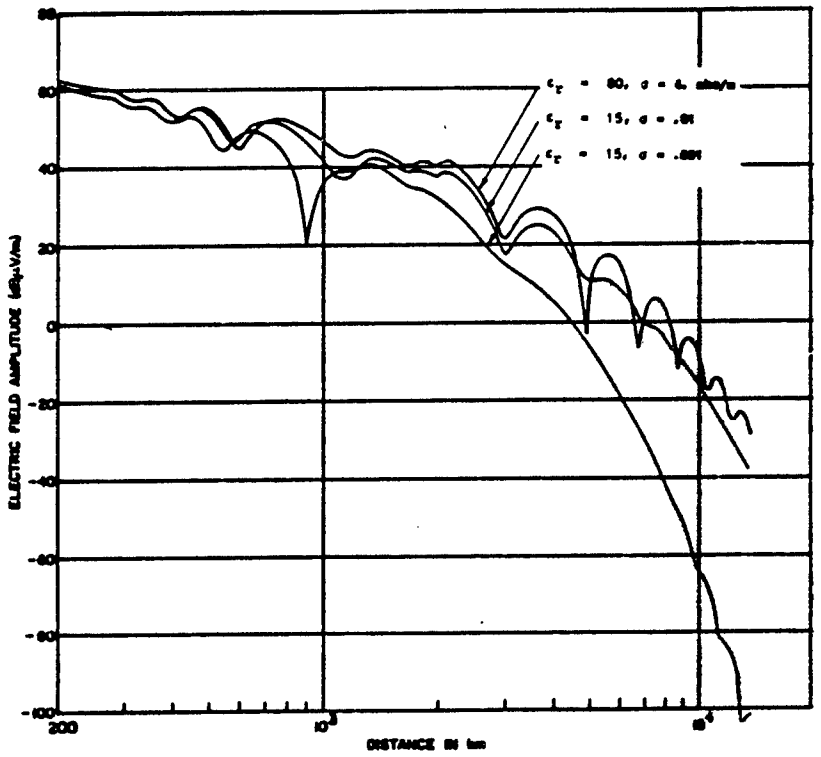

a. Day time.

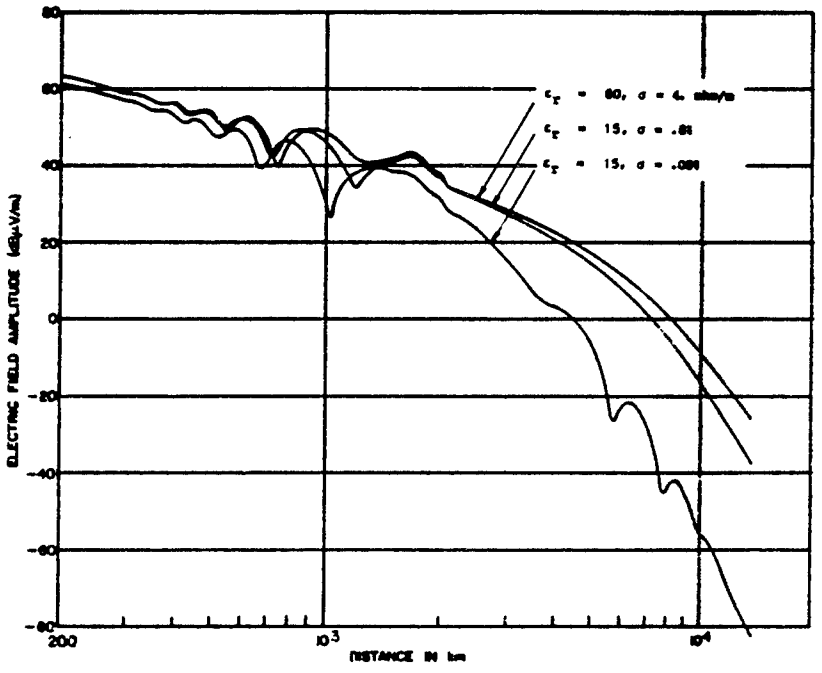

b. Night time.

Figure 3-3. Predicted propagation results for a 56.04 kHz transmission over three types of ground.

The propagation characteristics are dependent on the electrical characteristics of the ground and the ionosphere, as well as on the ionospheric height. The ground conductivity σ and permittivity ε affect the ground-wave behavior as well as the ground-reflection coefficient, which must be taken into account when considering multiply reflected skywaves. Ground conductivity is not constant over long paths. The variation in ground-conductivity values in North America is illustrated in Figure 3-4 (excerpted from Reference 3-1). The reflection coefficient and height of the ionsophere affect the strength and phase of all the sky waves. The latter quantities vary with time of day, season, and location. Typical effective ionosphere heights at VLF/LF are 70 km during daytime and 87 km at night.

As distances from the transmitter are increased, the number of ionospheric reflections, or "sky-hops", becomes large and the mathematical expressions become unwieldly. For these distances, it is convenient to think of the propagation mechanism as one of modes propagating in a wave guide, the walls of which consist of the earth and the ionosphere. Fluctuations in the curves of Figures 3-1 through 3-3 can be interpreted as constructive/destructive interference caused by adding the contributions of two or more wave-guide modes. Of course, the same propagation phenomena exist regardless of whether the ray-theory representation or the wave-guide representation is used to describe them.

3-1 CCIR Report 717, World Atlas of Ground Conductivity, Recommendations and Reports of the CCIR, Volume 5, p. 62, XIVth Plenary Assembly, Kyoto, 1978.

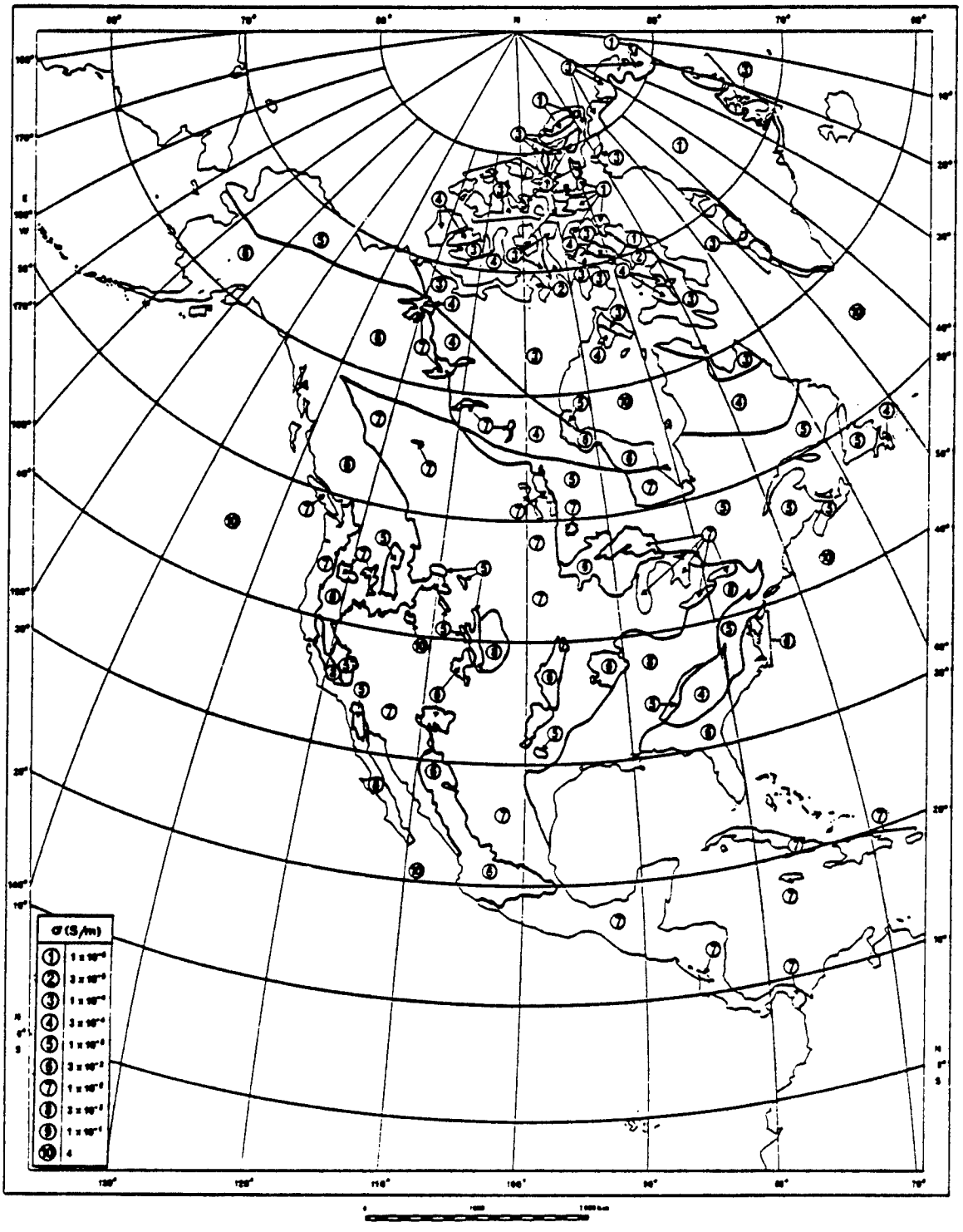

Figure 3-4. Estimated ground conductivity values, 10 - 30 kHz. (Reference 3-1.) (S/m represents Siemens/meter, which are equivalent to mhos/meter).

3.3 COMPUTER MODELING

The ECAC computer code for calculating VLF/LF fields is discussed in detail in Reference 3-2. It is applicable for frequencies between 10 and 100 kHz, and at distances (in km) between $5\lambda_m^{1/3}$ and 15,000, where λ_m is the wavelength in meters. The ray-theory approach, as documented in Sections 3.2 and 3.3 of Reference 3-3, is utilized for $d \leq 2000$ km. For $d > 2000$ km, the wave-guide mode approach, as documented in Reference 3-4, is employed. In this way, solutions usually can be provided by making computations involving no more than five sky-hops or no more than three wave guide modes.

In both the ray-theory and the wave-guide-mode methods of solution, the model assumes the earth's surface and the ionosphere boundary to be perfectly smooth and circumferentially homogeneous, and ignores the effects of the geomagnetic field. The ground is characterized by constant values of σ and ε. Estimates of these values applicable to the 10 - 30 kHz frequency segment are documented in Reference 3-5. (This was the basis of CCIR Report 717 and Figure 3-4.) For the United States, estimates of the parameters for the frequencies around 100 kHz may be obtained from an empirical study done in

---

3-2 Snyder, S. and Kuebler, W., Radio Wave Propagation at VLF and LF, ECAC-TN-74-05, ECAC, Annapolis, MD, July, 1974.

3-3 Watt, A. D., VLF Radio Engineering, Pergamon Press, 1967.

3-4 Wait, J. R. and Spies, K. P., Characteristics of the Earth-Ionosphere Waveguide for VLF Radio Waves, NBS Tech. Note 300, December 30, 1964.

3-5 Morgan, R. R., World-Wide VLF Effective-Conductivity Map, Westinghouse Report 80133F-1, 15 January 1968. AD 675771.

the 160 - 190 kHz band.[3-6] Electric field strength is relatively insensitive to the value of ε.

In the model, the ionosphere is characterized by an exponentially increasing conductivity, given by

$$\sigma(z) = \sigma_o e^{(z-h)/L_1} \qquad (3\text{-}1)$$

where:

$\sigma(z)$ is the conductivity of the ionosphere at height z
σ_o is the conductivity at the reference height, h
z is the height of interest above the earth
L_1 is the conductivity gradient.

As noted above, h and L_1 are dependent on the time of day, season, and path location. Values of L_1 range from 2 to 4 km; values of h are near 70 km during the day and near 90 km at night.[3-7]

Since the present skywave-groundwave-combination computer model assumes horizontal homogeneity, a single "effective" ground conductivity must be employed when considering a propagation path over different ground materials (e.g., land, sea, ice). For the cases investigated, this approach has produced reasonable results. As is noted in the next subsection, rigorous approaches to predicting the combined groundwave-and-skywave field have been devised for the inhomogeneous-ground problem. Subsection 6.2.2 of this Handbook contains a procedure for accounting for inhomogeneity in cases where the path is short enough so that the groundwave is much stronger than the skywave.

[3-6] Lawson, M. R., and Hurst, H. E., Low Frequency Propagation Tests, TR-0177-71.01, Gautney & Jones Communications, Inc., Falls Church, VA, June 1971.

[3-7] Comparison of Predicted VLF/LF Signal Levels with Propagation Data, DCA Report 960-TP-74-5, 21 January 1974.

The predicted effects of varying homogeneous ground characteristics are illustrated in Figures 3-1 through 3-3 for day and night transmissions at three different frequencies.

Perhaps more significant than the requirement that the ground parameters be constant, the homogeneity assumption in the present model requires that single values of L_1 and h be used, with these depending on the time of day. In this regard, it should be noted that signals are generally weaker when sunrise or sunset occurs at midpath than when the path is entirely in day time or entirely in night time.

3.4 VALIDATION AND COMPARISON WITH OTHER MODELS

Computer predictions using the ECAC VLF/LF code have been compared with measured data appearing in Reference 3-7 for frequencies between 10 and 60 kHz, distances between 100 and 5000 km, and magnetic latitudes greater than 20°. The mean (μ), root mean square (RMS), standard deviation (σ) and maximum deviation (D_{MAX}) of these predictions from the measurements are listed in TABLES 3-1 and 3-2. These tables also compare the measurements with predictions using the Espenschied-Anderson-Bailey (EAB) empirical formula:[3-8]

$$E(\mu V/m) = \sqrt{P}\ \frac{298 \times 10^3}{d}\ e^{-0.005d\left(\frac{f}{300}\right)^{1.25}} \qquad (3\text{-}2)$$

where

p = power, in kW
d = the distance in km
f = the frequency in kHz

[3-8] Espenschied, L., Anderson, C. N., and Bailey, A., "Transatlantic Radio Telephone Transmission," Proceedings of the Institute of Radio Engineers, 1926, 14, p. 7.

TABLE 3-1

REGIONAL DEVIATIONS OF PREDICTIONS FROM MEASUREMENTS

	ECAC VLF Code (dB)				EAB Formula (dB)			
Region	μ	RMS	σ	D_{max}	μ	RMS	σ	D_{max}
Pacific	-1.3	4.6	4.5	13.0	-7.1	9.2	5.8	22.0
U.S.	0.7	2.7	2.6	12.0	-0.8	4.1	4.0	17.0
High Latitude	-1.3	3.8	3.6	12.0	-2.9	4.7	3.7	13.0
Overall	-0.9	3.8	3.7	13.0	-4.3	6.9	5.4	22.0

TABLE 3-2

DIURNAL DEVIATIONS OF PREDICTIONS FROM MEASUREMENTS

	ECAC VLF Code (dB)				EAB Formula (dB)			
Time	μ	RMS	σ	D_{max}	μ	RMS	σ	D_{max}
Day	0.2	3.0	3.0	12.0	-3.8	5.8	4.4	17.0
Night	-2.8	5.4	4.6	13.0	-5.2	8.5	6.7	22.0

The predictions using the computer code are superior to those using the EAB formula. It will also be noticed that the day-time prediction results are more accurate than the results for night-time transmissions. (These tables originally appeared in Reference 3-9. Plots of the predictions and measurements for the actual paths also appear in that report.)

3-9 Marcus, S., Evaluation and Validation of the ECAC Computer VLF/LF Propagation Model, ECAC-TN-79-034, Electromagnetic Compatibility Analysis Center, Annapolis, MD.

Figures 3-5 through 3-7 show measurements documented in Reference 3-10 and predictions using the ECAC VLF/LF code, for day-time and night-time transmissions between Hawaii and California at three different frequencies. The predictions agree well with the measurements in five out of the six cases. In Figure 3-7b a substantial discrepancy is seen for path lengths greater than about 1500 km. A study to minimize model prediction errors suggests that choice of a value of L_1 in the 0.8 - 1.4 km range would have led to a smaller error.[3-10]

The Institute of Telecommunication Sciences (ITS) of the Department of Commerce and the Naval Ocean Systems Center (NOSC) also have developed VLF/LF computer codes. The accuracy of these codes has not yet been compared with that of the ECAC VLF/LF model. The features of these models are described below.

ITS - Developed Groundwave Models[3-11]

Program names: IT SNR/WAGNER
Nominal frequency range: 10-2000 kHz
Ground constants can vary along path?: Yes
Terrain profile taken into account?: Yes
Polarizations: Vertical and Horizontal
Maximum antenna height: Varies with path
Includes noise model: Yes/No

3-10 Determination of Effective Ionospheric Electron Density Profiles for VLF/LF Propagation, DCA Report C650-TP-76-4, 1 January 1976.

3-11 Berry, L. A., User's Guide to Low Frequency Radio Coverage Programs, OT Technical Memorandum 78-247, January 1978.

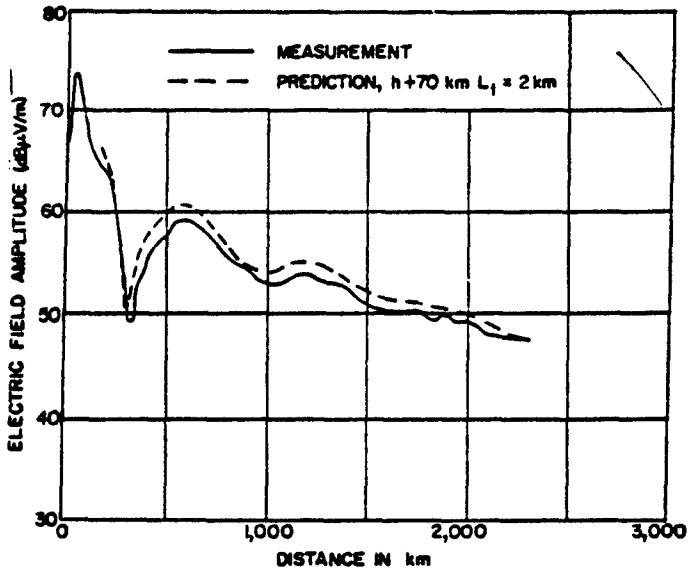

a. Day time.

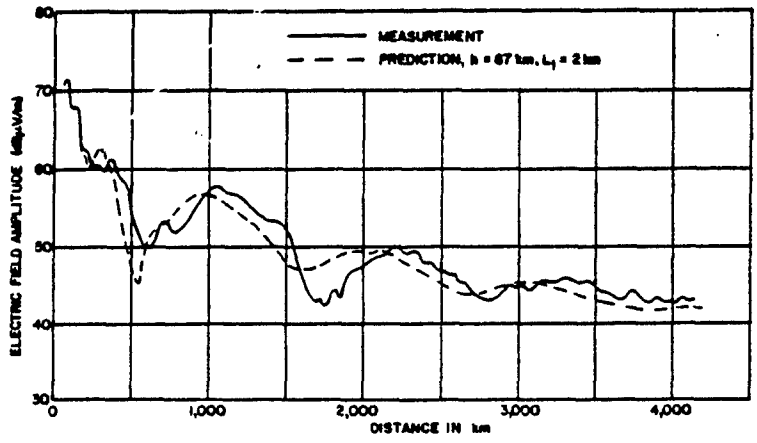

b. Night time.

Figure 3-5. Comparison of measured and predicted results for propagation over the Pacific Ocean (f = 10.9 kHz).

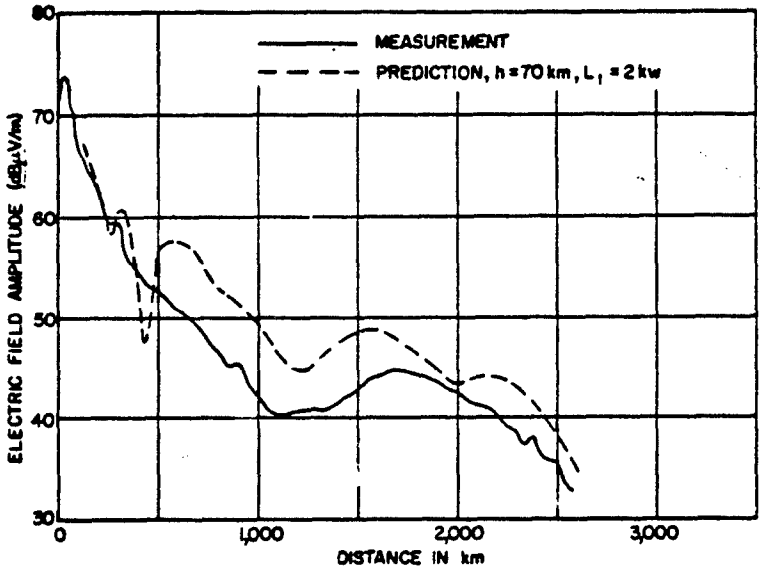

a. Day time.

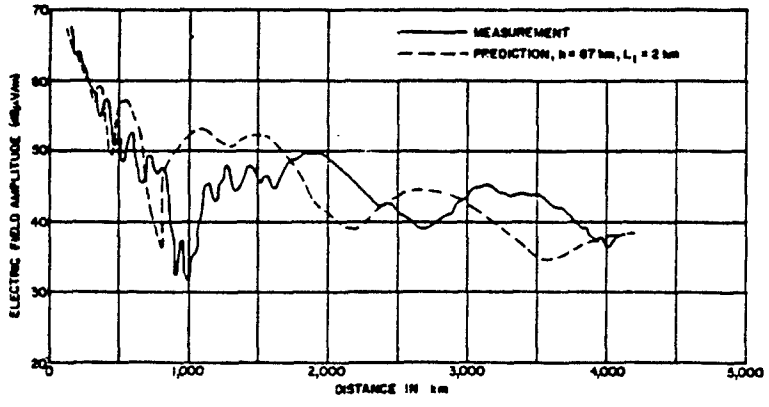

b. Night time.

Figure 3-6. Comparison of measured and predicted results for propagation over the Pacific Ocean (f = 28.02 kHz).

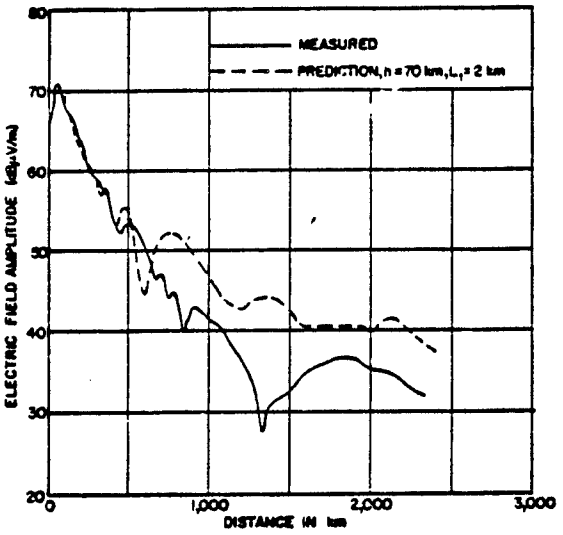

a. Day time.

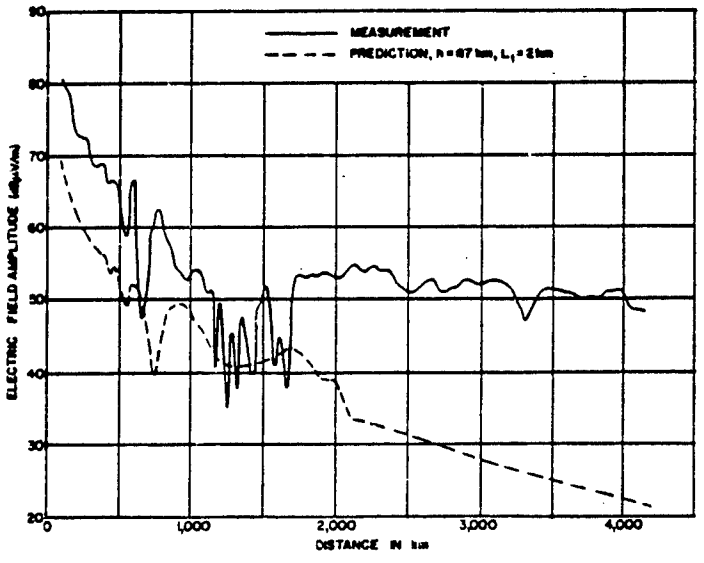

b. Night time.

Figure 3-7. Comparison of measured and predicted results for propagation over the Pacific Ocean (f = 56.04 kHz).

ITS - Developed Skywave-With-Groundwave Models[3-11]

Program names: LF SNR/ANIHOP
Nominal frequency range: 30-650 kHz/60-550 kHz
Anisotropic ionosphere?: No/Yes
Stored model of ionosphere?: Yes/No
Ionosphere can vary along path?: No*
Groundwave based on homgeneous earth?: Yes
Skywave based on homogeneous earth?: Yes
Polarizations: Vertical*
Maximum antenna height: 0 km*
Noise calculations?: Yes/No
Mathematical approach to skywave: Wave-hops (a type of ray theory)
Note: F. Rhodes of the Naval Research Laboratory has started work on a task to make ANIHOP more general. Features being addressed are marked (in the list above) with an asterisk.

NOSC - Developed Skywave-With-Groundwave Models[3-12]

Program names: GRNDMC/ARBNMC
Nominal frequency range: 10-60 kHz
Anisotropic ionosphere?: Yes
Stored model of ionosphere?: No
Ionosphere can vary along path?: Yes
Groundwave based on homogeneous earth?: Heterogeneous
Skywave based on homogeneous earth?: Heterogeneous
Polarizations: Vertical/Arbitrary
Maximum antenna height: 0 km/60 km
Noise calculations?: No
Mathematical approach to skywave: Waveguide modes, with mode conversion between path segments.

3-12 Morfitt, D., "Numerical Modeling of the Propagation Medium at ELF/VLF/LF," in AGARD-CP-305, NATO, Neuilly Sur Seine, France, September, 1981.

3.5 CONCLUDING REMARKS

Measurements not included in this study, that could be used to obtain prediction error statistics for a larger sample of paths, are documented in References 3-3, and 3-10 through 3-16. Guidelines for choosing h and L_1 could be refined as the result of such a study.

Because of the pulsed nature of LORAN-C transmissions, it is possible, and desirable, to distinguish between the pulses that propagate by skywave and the ones that propagate by groundwave. (Figure 3-8, published by the Austron Corporation,[3-17] shows the arrival of the groundwave and the skywave at different times.) Therefore, predicting the signal level of desired LORAN-C signals requires curves or models based only on the groundwave component signal. A set of curves for smooth paths with homogeneous ground constants appears

---

3-13 Bickel, J. E., et al, "Experimental Observations of Magnetic Field Effects on VLF Propagation at Night," Radio Science, Vol. 5, No. 1, January 1970.

3-14 Bain, W.C., "Models of the Ionospheric D Region at Noon," IEE Conference Publication 195, London, April 1981.

3-15 Hildebrand, et al, Examination of VLF/LF Propagation Effects as a Function of Frequency, Naval Weapons Center, Corona Report NWCCL TP 886, December 1969.

3-16 LF-VLF Strengths and Radio Noise at High Latitudes: Comparisons of Measurements and Predictions, DCA Report 960-TP-74-43, 31 December 1974.

3-17 Porter, J. W. et. al., "Design Considerations for a LORAN-C Timing Receiver in a Hostile Signal-to-Noise Environment," 12th Annual Precise Time and Time Interval Applications and Planning Meeting, NASA, Greenbelt, MD, 3 December 1980.

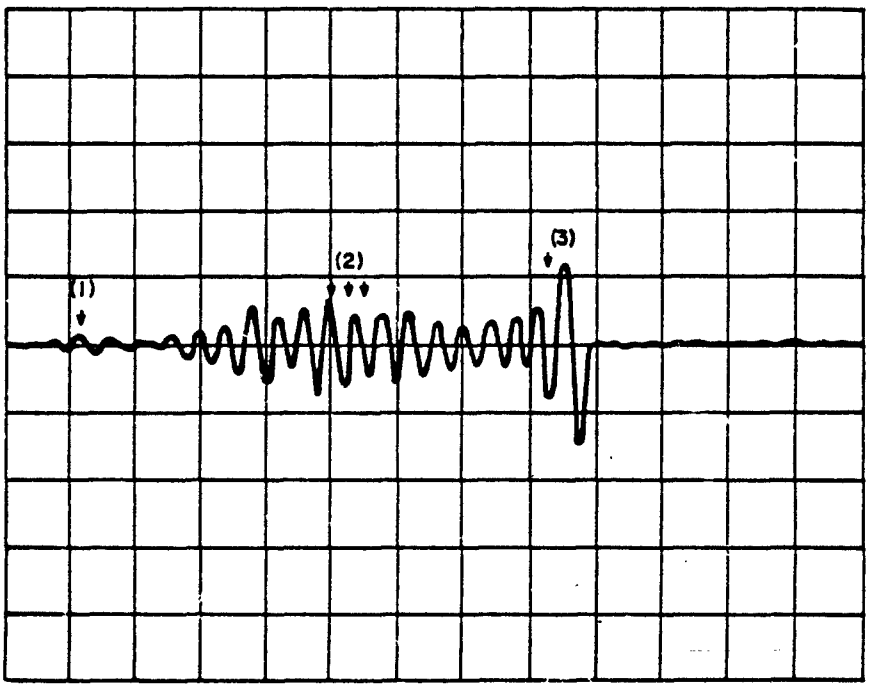

Figure 3-8. Recording of a received LORAN-C signal (from Reference 3-17). Because of the pulsed nature of LORAN transmissions, it is usually practical to distinguish the groundwave from the skywave modes.

Notes:

(1) Groundwave

(2) Skywave, First Hop

(3) Skywave, Second Hop

Path Length: 2665 km, George, WA to Austin, TX.

in Reference 3-18. The Millington-mixed-path procedure, described in subsection 6.2.2 of this Handbook, can be used to adjust this type of prediction so that it applies to paths composed of segments with different ground constants. Computer codes based on the work of R. Ott, e.g., WAGNER[3-19] and IT SNR [3-11], account for the effects of irregular terrain as well as varying ground constants. A quantitative assessment of the increase in accuracy that Ott's models offer relative to the smooth-earth mixed-path procedure with effective antenna heights has not yet been done. The predictions and measurements in Reference 3-19 could be used as the starting point for such a study.

A review of models to predict the phase of LF groundwave signals appears in Reference 3-20.

3-18 Rotheram, S., "Ground-Wave Propagation, Part 2", Proc. IEE, Part F October, 1981.

3-19 Ott, R. H., NTIA Report 79-20, May 1979.

3-20 Samaddar, S. N., "The Theory of Loran-C Ground Wave Propagation -- A Review," Journal of the Institute of Navigation, Vol. 26, No. 3, 1979.

CHAPTER 4

SKYWAVE PROPAGATION, 0.5 - 1.6 MHz

By: M. Weissberger

4.1 INTRODUCTION

Coupling between antennas in this band is similar to that in 10-100 kHz band (discussed in the preceding chapter) in that the groundwave and skywave both provide contributions to the received signal over a wide range of distances. One difference is a more rapid decrease in the magnitude of the groundwave signal with distance in the higher frequency band. The received power will decrease by about 40 dB at 100 kHz if the separation between the transmitting and receiving antennas is changed from 1 to 100 km over average ground. The decrease would be about 55 dB for an 0.5 MHz signal and 80 dB for a 1.5 MHz signal over this distance. A second difference is the pronounced decrease of the skywave signal strength in the higher frequency band during the day. At night, signals in both bands are reflected with low attenuation by the E-layer of the ionosphere (90-130 km above the earth). During the day, the D-layer of the ionosphere (70-90 km) forms, and reflects signals in both bands. The physical composition of the D-layer and the strength of the earth's magnetic field are such, however, that the signals in the lower frequency range undergo relatively low-loss reflection, whereas the 0.5-1.6 MHz signals are highly absorbed as they partly penetrate and are then reflected by this layer. The magnitude of the day-night change for a broadcast-band skywave signal is shown in Figures 4-1 and 4-2, which are taken from a study by Norton.[4-1] The theoretical value of the groundwave attenuation is shown

---

[4-1] Norton, D. A., "Low and Medium Frequency Radio Propagation", Electromagnetic Wave Propagation, edited by M. Desirant and J. L. Michiels, Academic Press, London, 1960.

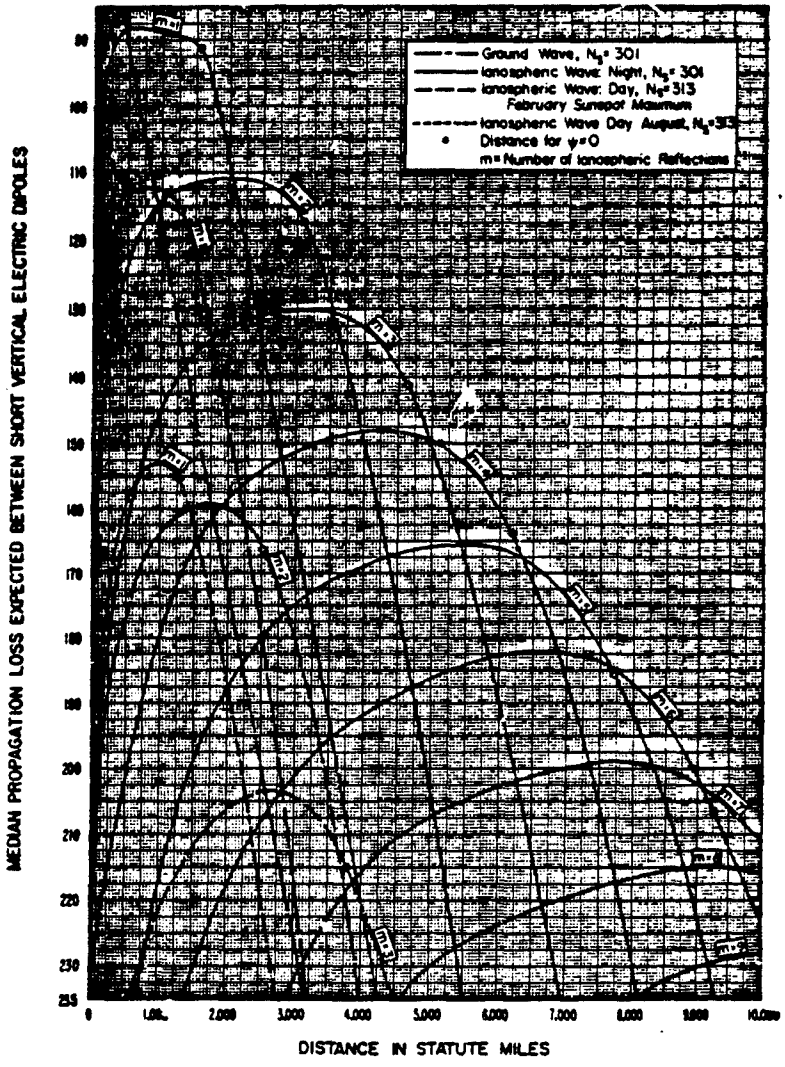

Figure 4-1. Median propagation loss over sea at 500 kHz. σ = 5 mhos/meter; ε = 80; $h_f = h_r$ = 30 feet; Day h = 70 km (D-layer); Night h = 110 km (E-layer).

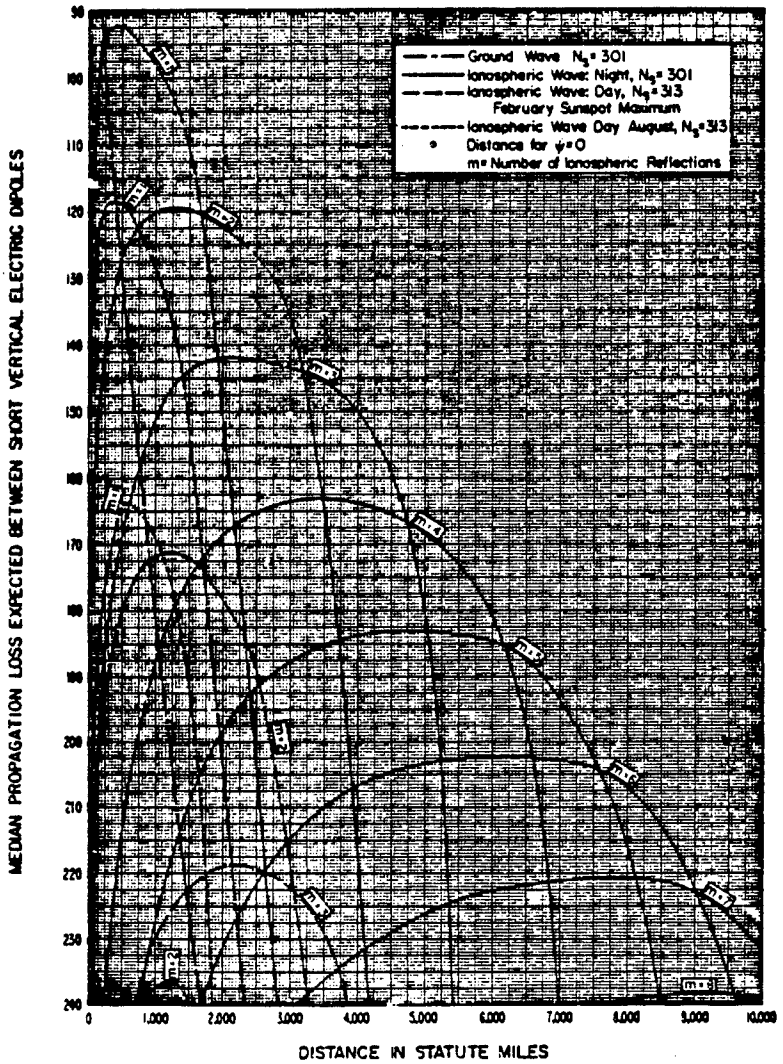

Figure 4-2. Median propagation loss over land at 500 kHz. σ = 0.005 mhos/meter; ε = 15; $h_f = h_r$ = 30 feet; Day h = 70 km (D-layer); Night h = 110 km (E-layer).

for comparison. Measured values of the day-night change have been published by the International Radio Consultative Committee[4-2] and are summarized in TABLE 4-1.

TABLE 4-1

MEASURED INCREASE IN SKYWAVE SIGNAL STRENGTH FROM NOON TO MIDNIGHT

(from Reference 4-2)

FREQUENCY (MHz)	PATH LENGTH (km)	INCREASE (dB)	NOTES
0.750	740	42	Japan, moderate sunspot value
0.845	---	42	Winter
0.845	---	54	Summer
1.160	610	45	Germany
1.538	405	45	Germany
1.466	---	40	Winter
1.466	---	65	Summer

The following subsection contains the recommended model for predicting skywave field strengths in the 0.5-1.6 MHz band as a function of path length and orientation, sunspot number, and effective radiated power. Models for groundwave predictions are documented in Chapter 6.

4-2 CCIR, "Analysis of Sky-wave Propagation Measurements for the Frequency Range 150 to 1600 kHz", Report 431-2, Recommendations and Reports of the CCIR, 1978, ITU, Geneva, 1978.

4.2 A MANUAL METHOD

The procedure presented here is a modification by Wang[4-3] of the CCIR method.[4-4] The modification provides greater accuracy for paths in ITU Region 2, the Americas. The method shown here has several parameter restrictions not in the Wang-CCIR model. These are: $450 < d < 3000$, where d is the great circle distance in km, time is at night (between 4 hours after sunset and 2 hours before sunrise), and the terminals are not close to the sea. The steps are:

a. Compute the cymomotive force, V, dB:

$$V = P + G_V + G_H \qquad (4\text{-}1)$$

where

P = Radiated power, dB above 1 kW.
G_V = Gain in the vertical plane, dB. See Figure 4-3.
G_H = Gain factor due to azimuthal directivity, dB. This is 0 for omnidirectional antennas.

b. Compute the sky-wave path length, p, km:

$$p = [d^2 + (4 \times 10^4)]^{1/2} \qquad (4\text{-}2)$$

d = great circle distance, km.

[4-3] Wang, J. C. H., "Medium Frequency Skywave Propagation in Region 2", IEEE Trans. on Broadcasting, September 1979. (Errata in next issue)

[4-4] CCIR, "Sky-Wave Field Strength Prediction Method for the Frequency Range 150 to 1600 kHz," Recommendation 435-3, Annex 1, op. cit.

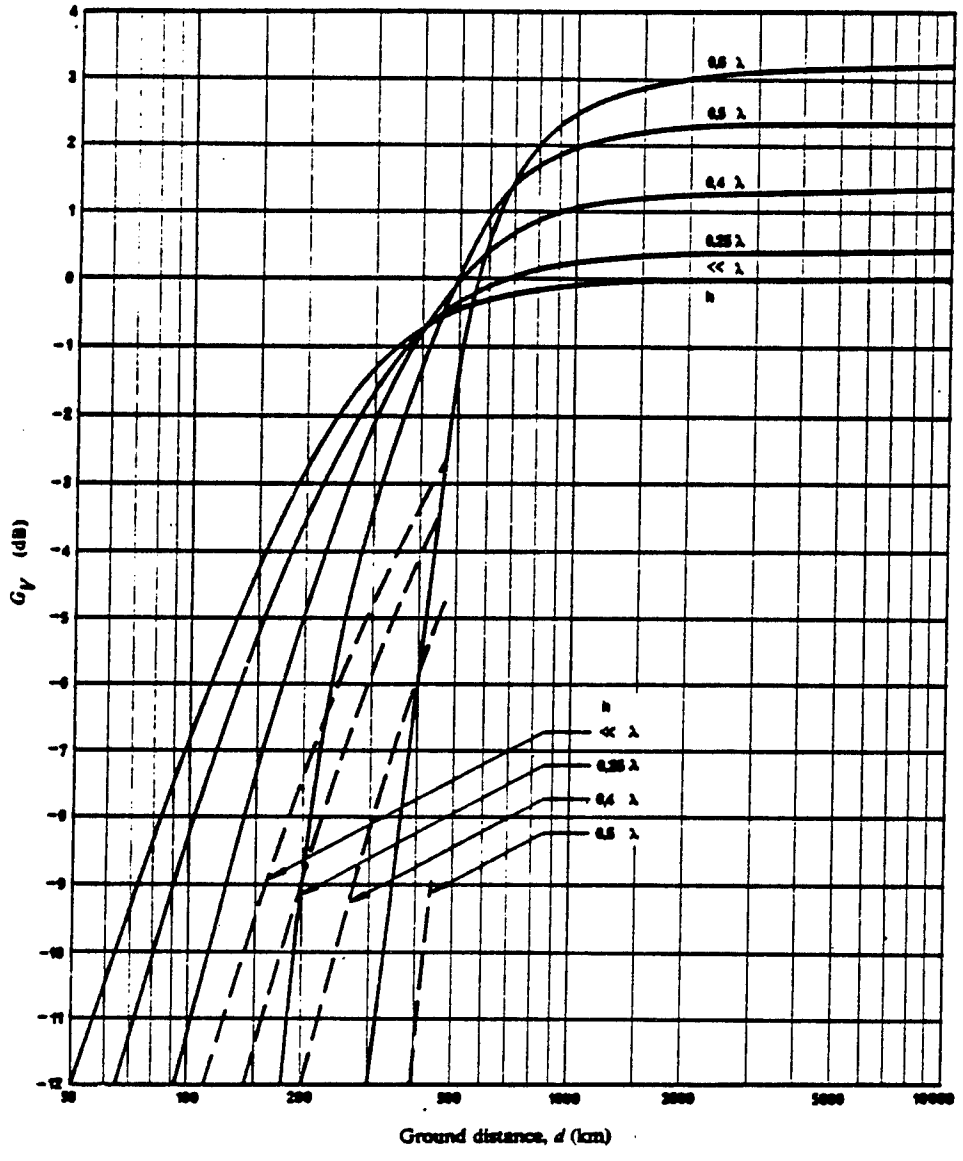

Figure 4-3. Transmitting antenna gain factor for monopoles (G_V) (see Reference 4-4).

h = Antenna height
———— h_r = 100 km (E layer reflection)*
— — — — h_r = 220 km (F layer reflection)

*Applicable to problems involving 0.5 < f (MHz) < 1.6 and d > 450 km.

c. Compute the polarization coupling loss, L_p, dB, for both terminals. For one terminal this is:

$$L_p = 180\ (36 + \theta^2 + I^2)^{-1/2} - 2 \qquad (4\text{-}3)$$

where

θ = Path azimuth relative to magnetic East-West, degrees. $\theta \leq 90°$. From Figure 4-4.

I = Magnetic dip, North or South, at the terminal, degrees. From Figure 4-5. If > 45°, $L_p = 0$.

d. Compute ϕ, the path average geomagnetic latitude, degrees. This is the average of the values for the transmitter and receiver, each read from Figure 4-6. Use positive values for North and negative for South.

e. Compute the Loss Factor, k_r. Wang's value is:

$$k_r = b\ R \times 10^{-2} + k \qquad (4\text{-}4)$$

$$k = (0.0667|\phi| + 0.2) + 3 \tan^2(\phi + 3) \qquad (4\text{-}5)$$

R = Twelve month smoothed sunspot number (see TABLE 5-1 in this Handbook).

$$b = 0.4\ |\phi| - 16 \quad (|\phi| \geq 45°) \qquad (4\text{-}6)$$
$$= 0 \quad (|\phi| < 45°)$$

f. Compute the annual median of half-hourly median field strengths, F (dBμV/m):

$$F = V - L_p + 106.6 - 2 \sin \phi - 20 \log p - 10^{-3} k_r p \qquad (4\text{-}7)$$

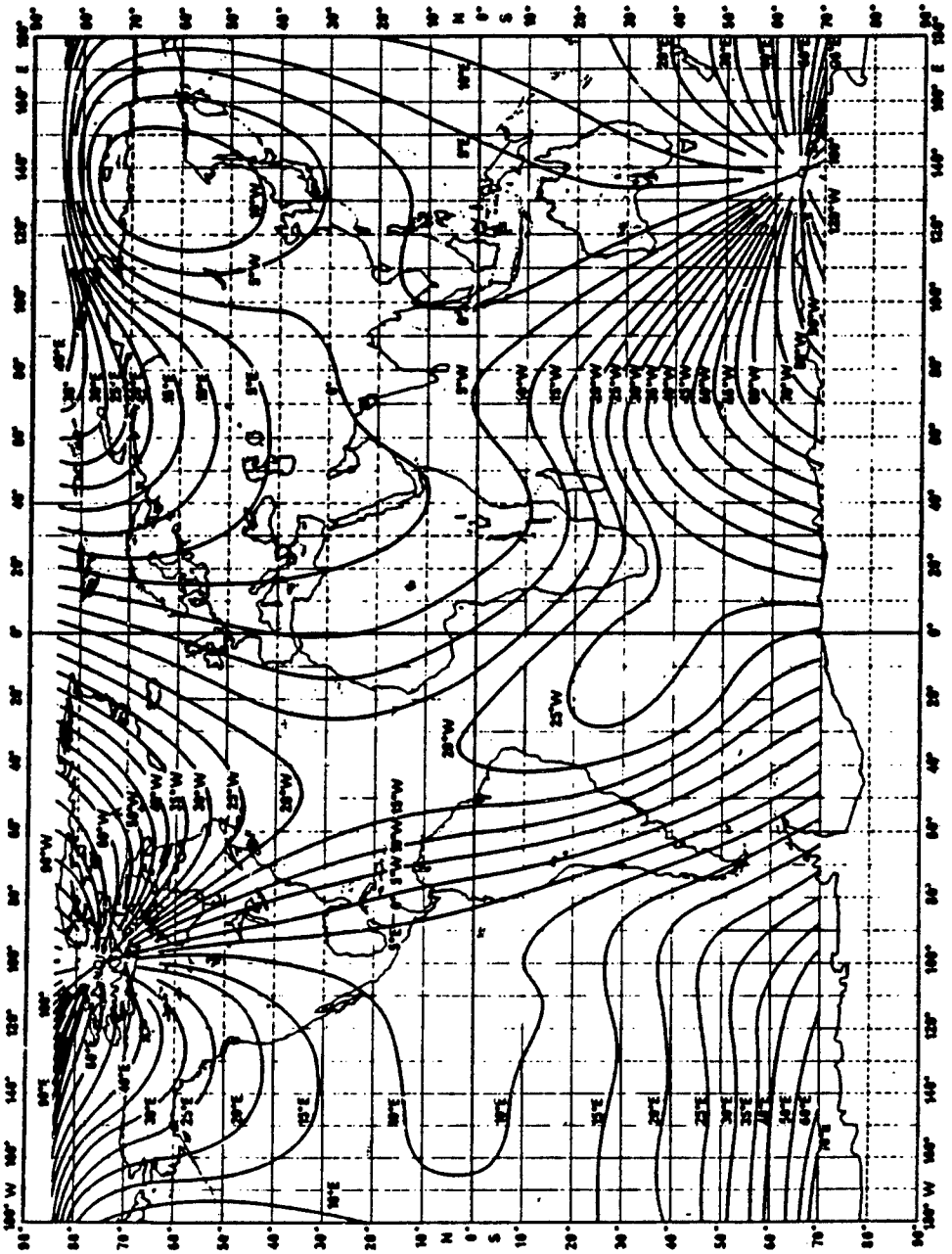

Figure 4-4. Map of magnetic declination (epoch 1975.0) (Reference 4-4).

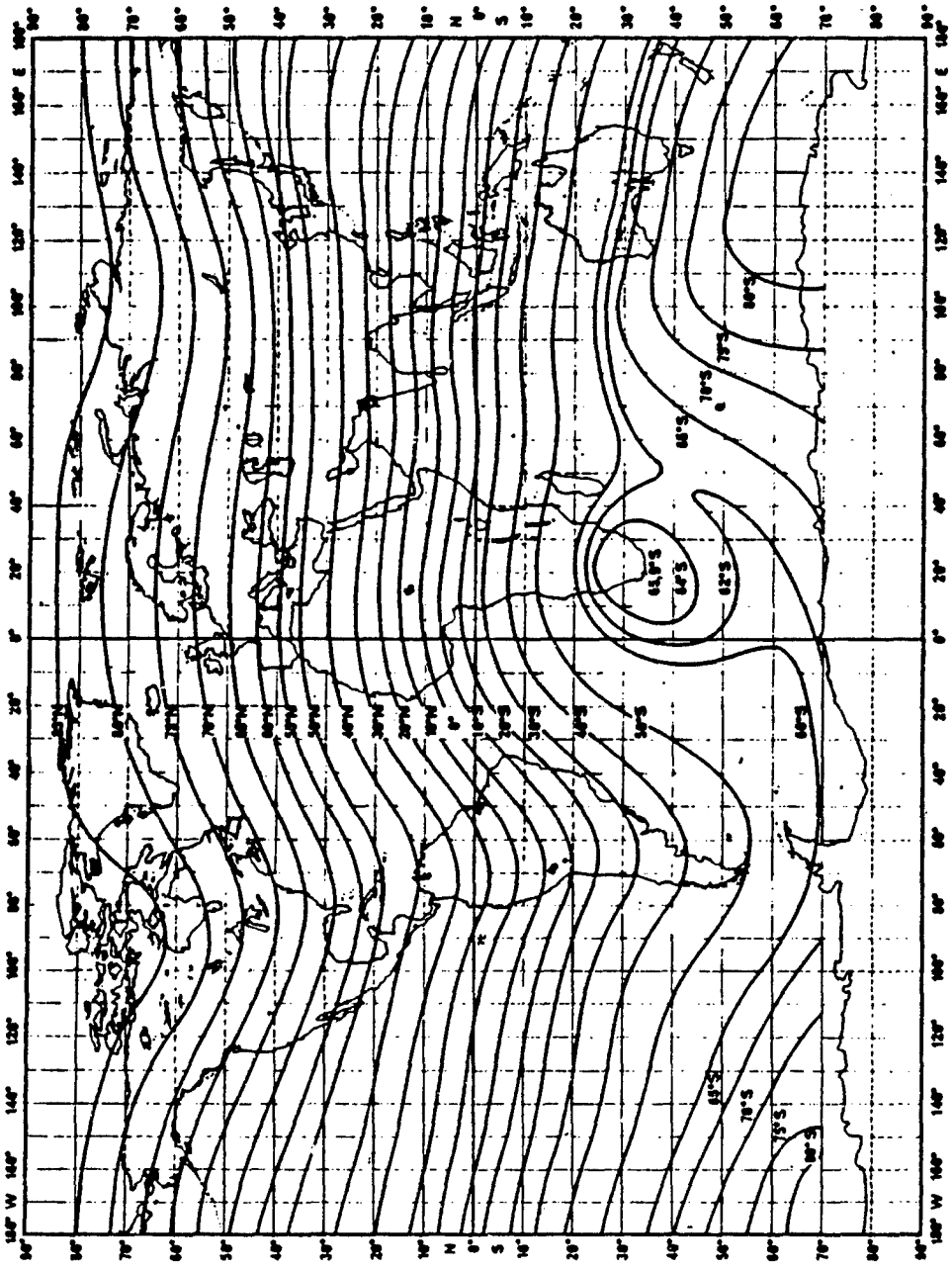

Figure 4-5. Map of magnetic dip (epoch 1975.0) (Reference 4-4).

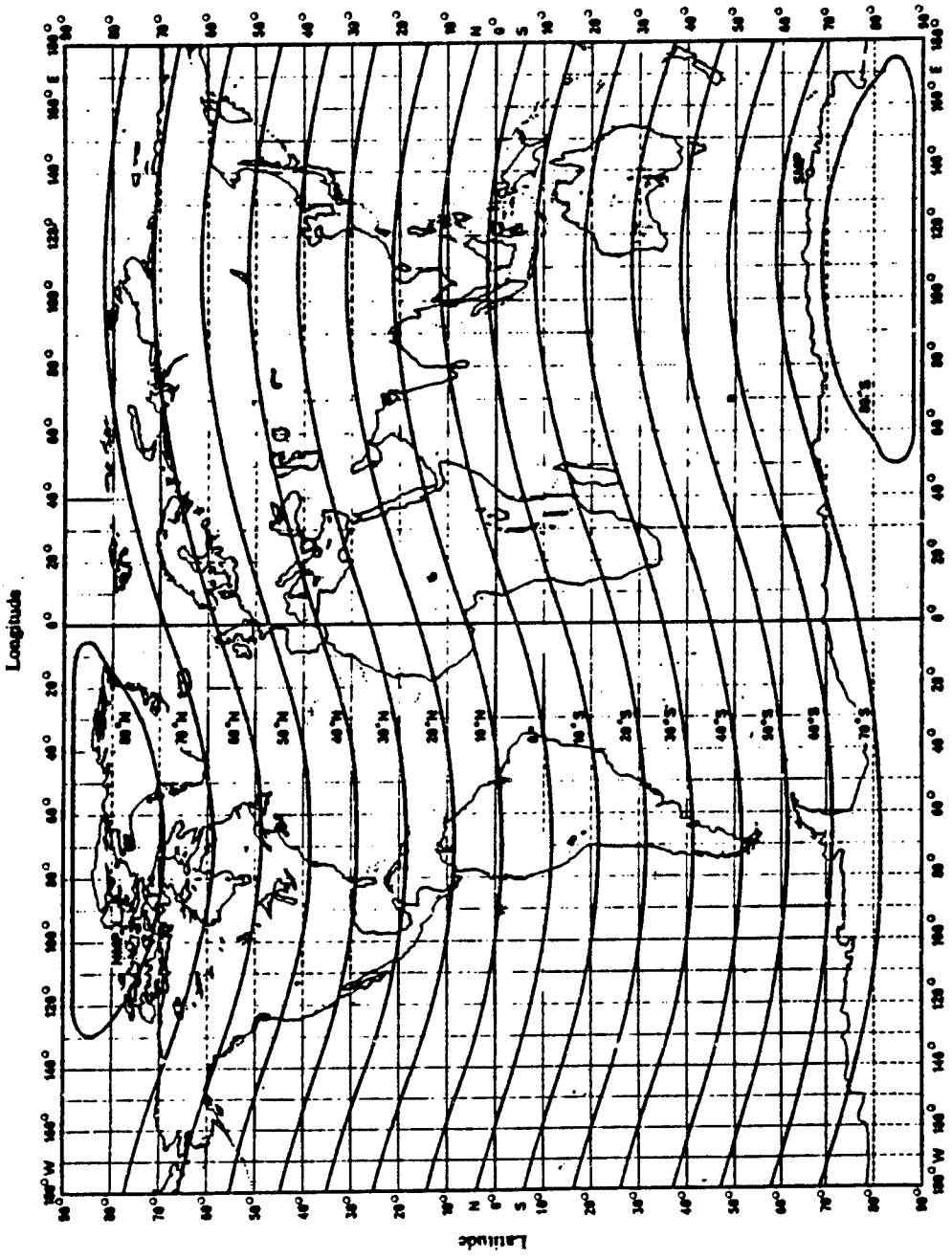

Figure 4-6. Geomagnetic latitudes (Reference 4-4).

4.3 AUTOMATED METHODS

No automated version of this procedure is presently available for general use on the ECAC computer.

4.4 VALIDATION AND COMPARISON WITH OTHER MODELS

In his study, Wang compared the prediction accuracy of the model just described with that of the CCIR (Reference 4-4), FCC "clear-channel",[4-5] and ITU "Cairo" models.[4-6] The comparison involved 13 paths. The rms error for Wang's procedure was 4 dB. For the other procedures, it varied from 7 to 23 dB. This study was done based on the data used by Wang to refine the CCIR model. Thus, comparison of the procedure predictions with other data sets would probably lead to larger deviations.

4.5 CONCLUDING REMARKS

The procedure adopted by the 1980 ITU Regional Administrative MF Broadcasting Conference for Region 2, the Americas, is the FCC "clear channel" model (Reference 4-5). Project engineers should, therefore, coordinate selection of a model with their sponsors.

It is desirable to conduct a more comprehensive validation of Wang's procedure.

4-5 Federal Communications Commission, Rules and Regulations, Part 73, Section 73.190, U.S. Government Printing Office, Washington, DC, 1976.

4-6 ITU, International Radio Conference, Cairo, 1938.

CHAPTER 5

SKYWAVE PROPAGATION, 2-30 MHZ

By: H. Riggins

High frequency (2-30 MHz) systems are used primarily for communications over large distances and for radar detection of targets at very distant points. Typical communication links may be over path lengths of several thousand kilometers or more. The propagation of HF signals over these large distances is facilitated by both mirror-like reflections and incoherent scatter from the ionosphere at heights of 100 to 500 km. Ionospherically propagated signals and their study are referred to as "skywave signals" and "skywave propagation" respectively. Skywave propagation-prediction procedures are complex because of the varying irregular nature of the ionosphere on a global basis and as a function of time. This section discusses the pertinent facts of skywave propagation. For short distances (less than 50 to 300 km, depending on frequency, polarization, ground condition, etc.), groundwave propagation may be important. Chapter 6 contains a general discussion of groundwave propagation.

5.1 BASIC CONCEPTS

In order to understand the propagation of skywave signals, the earth's ionosphere and the various factors that affect its behavior must be appreciated. The following paragraphs briefly discuss some of the basic ionospheric concepts. More in-depth treatments are readily available in the literature.[5-1,5-2,5-3]

[5-1] Rishbeth, H. and Garriott, O. K., Introduction to Ionospheric Physics, Academic Press, New York, NY, 1969.

[5-2] Ratcliffe, J. A., An Introduction to the Ionsophere and Magnetosphere, Cambridge University Press, MA, 1972.

[5-3] Davies, K., Ionospheric Radio Propagation, NBS Monograph 80, U.S. Government Printing Office, 1965.

The ionosphere is an electrically charged region of the earth's atmosphere that begins about 50 km above the surface and extends to thousands of kilometers. The ionospheric heights that are important to HF propagation lie between approximately 50 and 500 km. The ionization is produced by the x-ray and ultraviolet components of solar radiation. The change of atmospheric constituents with altitude and the interaction of these constituents with components of the solar flux give rise to an ionization structure that consists of distinct layers or regions. These layers (regions) are called the D, E, F1, and F2 layers.

In the normal ionosphere, the D-layer usually has significant ionization above 50 km with a maximum at approximately 80 to 90 km. The night-time ionization is insignificant in regard to HF propagation. The D-layer is not dense enough to reflect HF energy. The main influence of the D-region is the absorption of energy from the radio signals passing through it. The D-region absorption is caused by collision of the free electrons, which are set in motion by the passage of the electromagnetic wave, with the neutral constituents of the atmosphere. The lower frequencies are more heavily attenuated than the higher frequencies. This occurs because the wavelength of the lower frequency is longer and, consequently, the motion of the electrons for the lower frequency will be over a larger distance so that the chance of collision with neutral constituents, and resulting attenuation, is larger.

The E-layer is the lowest layer with sufficient ionization to reflect HF signals back toward the earth. In the day-time, the E-layer has a maximum height at about 100 to 110 km. The ionization level of the normal night-time E-layer is insignificant for HF propagation. The behavior of the normal E-layer is a regular function of time of day, solar activity, and season, and hence can be predicted relatively well. In addition to the normal E-layer, there is a more irregular variation known as sporadic-E, E_S. The E_S layer may contain much larger electron densities than the normal E-layer. As its name suggests, the appearance of this ionization is erractic and generally is treated on a statistical basis.

The daytime F-layer consists of two separate layers. The lower layer, called the F1-layer, generally exists in the height region between about 150 and 250 km. The upper layer, called the F2-layer, has a maximum electron density between about 250 and 500 km. At night, the electron density of the F1-layer decreases to a level that is insignificant for HF propagation. However, the electon density of the F2-layer remains sufficiently large so that HF signals may be propagated as sky waves.

The electron density increases with height up to the F-region peak. Hence the D-layer has the lowest electron density and the F2-layer has the highest electron density. Propagation conditions vary according to the electron-density fluctuations. The primary considerations are the concentration of the electrons and the distribution with height (or effective virtual height) of the layers.

Since the electrons are created by the solar flux, the electron density varies as a function of season, time of day, and the 11-year solar cycle. The D, E, and F1 layers are at lower altitudes where the physical processes are reasonably well known and, consequently, can be modeled without too much difficulty. On the other hand, the F2 layer is at very high altitudes in a rarefied environment and its fluctuations are quite complex and difficult to model. The F2 layer has been found to contain a number of irregular variations in addition to the normal expected regular variations, such as time of day and solar cycle, etc. For instance, one anomally is that the F2-layer electron density is less in summer than in winter, which is contrary to what would be expected solely on the basis of solar flux. Most of the long-distance communications are via F2-layer propagation modes; therefore, an understanding of the behavior of this layer is important.

The solar radiation varies in a cycle that has about an 11-year period. The output of the solar radiation over this 11-year period has been found to correlate with the number and grouping of magnetic storms, called sunspots, on the sun's surface. To measure this solar activity, an index is required. The

most common index is the Zurich 12-month running mean sunspot number, R_{12} defined by:

$$R_{12month} = \frac{1}{12} \sum_{k=n-6}^{n+6} R_k \qquad (5\text{-}1)$$

where R_K is the mean value of the sunspot number for the kth month, and n is the month of interest.

The above formula indicates that six months of data following the month of interest is required. Predictions of the appropriate data are available in the ECAC library, as shown in TABLE 5-1 from a monthly publication[5-4].

5.1.1 Propagation Frequency

The ionosphere refracts radio signals propagating through it. If this refraction is large enough, the signals are completely reflected back to the earth. An explanation of the refraction process was developed in 1920 by Sir Edward Appleton.[5-5] In this theory, which assumes the ionosphere electron density varies as a function of altitude only, the refractive index, n, is given by:

$$n = \left(1 - 80.5 \frac{N}{f^2}\right)^{1/2} \qquad (5\text{-}2)$$

5-4 Solar Geophysical Data - Prompt Reports, National Geophysical and Solar Terrestrial Data Center, Boulder, CO, January, 1980.

5-5 Appleton, E. V., URSI Proc., Washington, DC, 1927.

TABLE 5-1

SMOOTHED OBSERVED AND PREDICTED SUNSPOT NUMBERS

CYCLE 21 (see Reference 5-4)

MONTH	JAN	FEB	MAR	APR	MAY	JUN	JUL	AUG	SEP	OCT	NOV	DEC
1976	15.2	13.2	12.2	12.6	12.5	12.2	12.9	14.0	14.3	13.4	13.5	14.8
1977	16.7	18.1	20.0	22.2	24.2	26.3	29.0	33.4	39.1	45.6	51.9	56.9
1978	61.3	64.5	69.6	76.9	83.2	89.3	97.4	104.0	108.4	111.0	113.3	116.7
1979	122.8	130.4	136.1	141.0	147.4	153.7 |	158.7 (2)	162.1 (5)	164.4 (7)	165.7 (10)	166.1 (13)	165.4 (17)
1980	163.4 (20)	161.5 (21)	160.0 (22)	159.5 (26)	158.4 (29)	154.5 (33)	150.1 (37)	146.5 (39)	144.3 (40)	143.2 (41)	141.7 (43)	140.4 (46)
1981	140.5 (48)	140.1 (47)	137.4 (46)	134.2 (44)	131.3 (45)	128.4 (45)	127.2 (43)	127.1 (42)	126.5 (41)	125.1 (41)	122.5 (40)	119.0 (38)
1982	115.4 (36)	111.8 (35)	109.4 (34)	107.4 (33)	104.9 (31)	102.4 (29)	98.4 (27)	93.2 (26)	88.5 (24)	83.4 (22)	79.8 (21)	76.2 (20)
1983	72.1 (20)	69.2 (20)	67.3 (21)	65.3 (21)	63.1 (21)	60.5 (22)	58.4 (24)	56.6 (25)	54.7 (27)	53.6 (29)	52.7 (30)	51.7 (31)
1984	50.3 (31)	48.1 (30)	44.8 (29)	41.0 (29)	38.4 (30)	37.4 (32)	36.5 (32)	35.0 (32)	33.4 (31)	32.0 (29)	30.6 (28)	28.8 (28)
1985	27.7 (27)	27.0 (27)	26.3 (27)	25.8 (27)	25.2 (26)	24.1 (25)	23.2 (24)	22.3 (23)	21.6 (23)	20.8 (24)	19.9 (24)	19.3 (25)
1986	18.8 (25)	17.9 (25)	17.1 (24)	16.0 (23)	14.6 (22)	13.3 (21)	12.4 (20)	11.8 (19)	11.6 (18)	11.3 (16)	11.1 (15)	11.2 (14)
1987	11.6 (12)	12.1 (12)	13.0 (12)	14.1 (12)	15.2 (13)	16.3 (14)	17.5 (15)					

The table gives observed Zurich smoothed sunspot numbers for Cycle 21 up to the one calculated from the latest observed data, marked by a vertical bar. They are based on final Zurich numbers through 1978 and provisional Zurich numbers thereafter. Some of these data after the June 1976 value will change slightly when final data for 1979 are received. The numbers after the vertical bar are predictions by the McNish-Lincoln method (see Explanation of Data Reports, February 1978). Shown in parentheses are the corresponding absolute values of the 90% confidence interval, an indication of the uncertainty above and below the predicted number.

where N is the electron density (electrons/m^3) and f is the frequency in Hz. When a wave enters the ionosphere at vertical incidence, it will be completely reflected back toward the earth at the point where n = 0, which means by the above equation that $f = 9\sqrt{N}$. As long as frequencies are less than or equal to a critical frequency f_c, defined by

$$f_c = 9\sqrt{N_{MAX}} \tag{5-3}$$

where N_{MAX} is the maximum electron density of the ionosphere, the electromagnetic wave will be reflected back to earth. For more realistic cases of interest, where the propagation of the waves is not vertical but subtends an angle of incidence, i, with the vertical, the maximum frequency, f, that may be propagated over the path can be estimated by the simplified formula:

$$f = kf_c \sec i. \tag{5-4}$$

Here k is a factor to account for the spherical geometry and ranges from 1.0 to 1.2, depending on distance and ionospheric height.

The maximum frequency supported by ionospheric propagation is called the maximum usable frequency (MUF). The MUF varies on a daily basis and is generally predicted statistically. The monthly median, upper decile, and lower decile are used to specify the predicted propagation frequencies. The median value is referred to as the predicted MUF, the upper decile as the

highest possible frequency (HPF), and the lower decile as the frequency of optimum traffic (FOT).[5-6, 5-7]

When characterizing the frequencies that will propagate over a circuit, the communication engineer frequently chooses to use the FOT value in a system analysis because it contains a margin for the daily variations. The term "mode" is used to characterize the particular path whereby a signal travels from the transmitting terminal to the receiving terminal. The terminology "one-hop" mode is used to designate when there is one ionospheric reflection, the "two-hop" mode is when there are two ionospheric reflections (with one ground reflection between the two ionospheric reflections), etc. A one-hop E mode is written as 1E, a two-hop E mode as 2E, and a one-hop F1 mode as 1F1, etc. A typical geometry for several ray paths is shown in Figure 5-1.

The arrival of two signals that have traveled over different paths results in different arrival times and phase relationships, which presents a problem of destructive self-interference known as multipath interference. Since the height of the ionosphere is several hundred kilometers, the difference in path length (and thus delay time) for the different modes can be significant, especially for telegraph transmissions. For example, a path length difference of 300 km corresponds to a delay time difference of a millisecond. The undesirable multipath interference problem is minimized by choosing the highest possible frequency that is below the actual MUF. Generally this choice of frequency will also provide the best reliability, as discussed in the following subsection.

5-6 Barghausen, A. F., et al, "Predicting Long Term Operational Parameters of High-Frequency Skywave Telecommunication Systems," ESSA Tech Report ERL 110-ITS-78, Environmental Sciences Services Administration, May 1969.

5-7 Lloyd, J. L., et al., Estimating the Performance of Telecommunication Systems Using the Ionospheric Transmission Channel, Environmental Sciences Administration, Draft report.

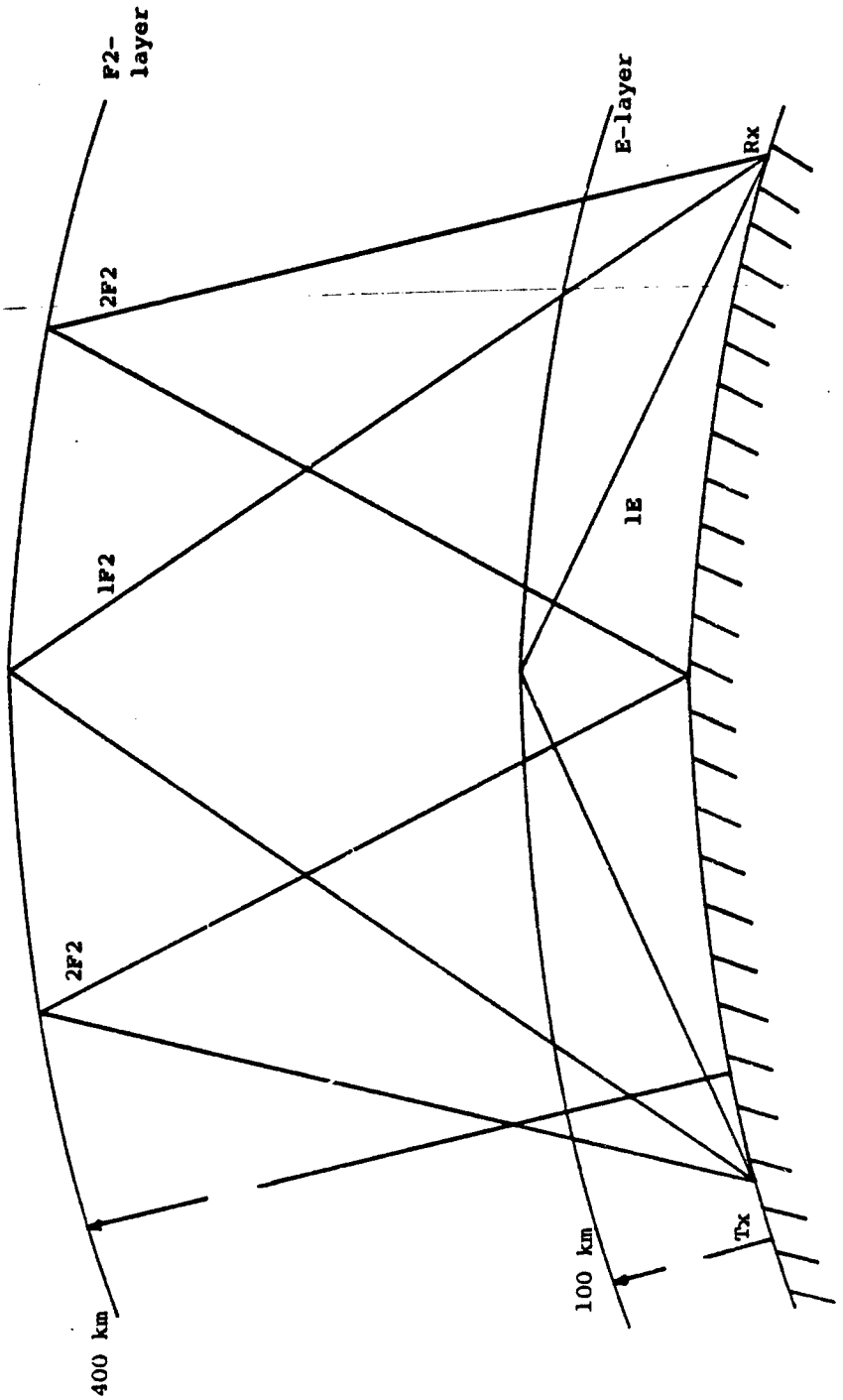

Figure 5-1. Skywave geometry for a typical path.

The characteristics of the different ionospheric layers and their relationship to HF propagation are discussed in documents such as Reference 5-8.

5.1.2 Signal Level and System Performance

The received signal level from a distant transmitter is calculated from the overall transmission loss along the path. The signal level is used with other quantities to estimate the overall system performance of the circuit. The transmission loss is calculated by summing the free-space spreading loss, which is calculated as previously explained, and other loss terms appropriate to skywave propagation. These loss mechanisms include D-region absorption, ground-reflection losses for multiple hop cases, auroral losses, defocusing losses, and sporadic-E obscuration losses.

The D-region absorption loss increases as the frequency decreases, as previously mentioned. This is indicated in a semi-empirical formula derived by Laitinen and Haydon,[5-9] in which the absorption, A, in dB per hop is:

$$A\ (dB) = \frac{615.5\ \sec i\ (1+0.0037R)\ (\cos .881\psi)^{1.30}}{(f + f_H)^{1.98}} \qquad (5\text{-}5)$$

5-8 Betts, J.A., High Frequency Communications, American Elsevier, New York, 1967.

5-9 Laitinen, P. O. and Haydon, G. W., Analysis and Prediction of Skywave Field Intensities in the High Frequency Band, Technical Report 9, U.S. Army Signal Radio Propagation Agency, Fort Monmouth, NJ, revised October 1962.

where

i is the angle of incidence of the wave at the D-region height

R is the 12-month running sunspot number

ψ is the solar zenith angle

f_H is the gyro frequency in MHz and

f is the transmission frequency in MHz.

The dependence of absorption on frequency can be shown by using the above formula for a set of typical parameters. For the case where sec i =3 (approximately a 2500 km path), R = 100, f_H = 1.4, and ψ = 15° (noon in June at 35° N. latitude), the absorption loss will be 5.6 dB at 20 MHz, 19.7 dB at 10 MHz, and 61.8 dB at 5 MHz.

The ground-reflection loss can be calculated with the Fresnel reflection coefficient[5-10] which uses the ground constants. One of the automated computer models used at ECAC also accounts for sporadic-E loss. Explicit auroral loss calculations are available in a special research model. The other loss terms are estimated by adding in an empirically derived correction factor.

The system performance may be calculated when the transmission loss, the noise power, and some receiver performance criteria are specified. The atmospheric noise power at different locations and times is estimated by using the data in CCIR Report 322[5-11] tabulated on the basis of a large set of

---

5-10 Jordan, E. C. and Balmain, K. G., Electromagnetic Waves and Radiating Systems, Prentice Hall, Englewood Cliffs, NJ, 1968.

5-11 CCIR World Distribution and Characteristics of Atmospheric Radio Noise,

worldwide measurements. The data contained in CCIR 322 has been put in numerical form suitable for automation on a large-scale general-purpose computer. Also models of galactic noise and manmade noise are available. The resultant noise calculated on the large scale computer model is the RMS contributions of these three noise types.

As explained, the highest frequency that can be used on a path depends on the ionospheric electron density. The lowest frequency that can be used is determined by the system-performance criteria. The noise generally increases as the frequency decreases. Since the absorption also increases as the frequency decreases, the system performance will decrease as the frequency decreases. On a given circuit, the lowest usable frequency (LUF) that meets operational or system design criteria may be calculated. The range of frequencies that may be used for a given path and time are specified on the lower end by the LUF and on the upper end by the FOT (MUF, or HPF). Recall, however, that the higher frequencies may be more desirable to avoid multipath interference problems.

5.2 HF PROPAGATION MODELS

For many years, numerous organizations have been using the HF spectrum for long distance communications and have studied HF propagation characteristics. The Institute for Telecommunications Sciences (ITS), which was formerly known as the Central Radio Propagation Laboratory (CRPL) of the National Bureau of Standards, has led the way in the development of HF propagation models[5-6, 5-7, 5-12, 5-13] in the United States. Some important

---

5-12 Lucas, D. L. and Haydon, G. W., MUF-FOT Predictions by Electronic Computers, NBS Report 6789, U.S. Dept. of Commerce, Boulder, CO 80303, 1961.

5-13 Central Radio Propagation Laboratory, Ionospheric Radio Propagation, NBS Circular 464, 1948.

early research was also conducted by the U.S. Army Radio Signal Propagation Agency[5-9,5-14] in Fort Monmouth, New Jersey.

The first HF propagation models were manual methods developed in the mid-1940's. In the early 1960's, the first computer programs to calculate HF propagation predictions were developed. Today, HF predictions are routinely done using a computer because of the speed and the convenience, and manual calculations are seldom used. For a scientist familiar with HF propagation, the manual calculation of HF propagation conditions takes 15 to 30 minutes for a single hour on a single path. In contrast, the computerized models require only about 15 seconds of computer time to calculate HF propagation conditions for all 24 hours of the day along a single path.

This subsection describes the manual (e.g., MINIMUF) and computerized (e.g., HFMUFES-4 and IONCAP) HF propagation models generally available and gives detailed information on the models used at ECAC. The project engineer should use the computer models at ECAC for the reasons stated above. The manual methods may be used in special circumstances, such as a one-time training exercise, to provide more in-depth knowledge to the engineer who is especially interested in HF propagation.

HF propagation models are very complex because of the many irregular and anomalous variations of the ionosphere, especially the F-region. The major sources of ionospheric data are ground-based radars called ionosondes that measure the vertical critical frequency and layer heights. The manual methods use a series of global charts of the ionospheric parameters for different conditions, i.e., time of day, season, sunspot number, etc. Consequently, the manual methods require the availability of several large volumes of ionospheric data. The computer model contains the ionospheric data in

---

5-14 U.S. Army Radio Propagation Agency, Calculation of Skywave Field Intensities, Maximum Usable Frequencies, and Lowest Useful High Frequencies, Tech Report No. 6, Fort Monmouth, NJ, Revised June, 1949.

numerical form. The numerical technique used to represent the ionospheric data is based on a least-squares fit to spherical harmonic functions. Over 12,000 coefficients are used to achieve the desired accuracy. Consequently, most computer models are suitable for use only on a large-scale, general-purpose computer. However, one novel model for use on a small desk-top calculator is discussed herein.

5.2.1 Computer Models

Many methods have been developed in different countries, including the United States, U.S.S.R., France, Japan, and India. The differences among these various codes are discussed on pages 66 to 70 of CCIR Report 252-2.[5-15] Two models used at ECAC are HFMUFES-4 and IONCAP both of which were developed in the United States by ITS. The HFMUFES-4 model was originally developed over a decade ago for estimating skywave field strength and transmission loss. In the United States, the ITS models have been traditionally considered to be the "industry standard" model for HF propagation. The IONCAP program is a recently developed model that includes state-of-the-art techniques. It is considered by ITS to be a replacement for the HFMUFES-4 program. IONCAP, HFMUFES-4, and the MINIMUF program are described in the following subsections.

5.2.1.1 IONCAP and HFMUFES-4

Although IONCAP and HFMUFES-4 are two completely different and separate codes, the general engineering features of the two progams are similar in many ways except for some important improvements added to the IONCAP program. Consequently, it is convenient to discuss the basic features of these two models together and to indicate differences in the programs as appropriate. Unless otherwise stated, the basic concepts described in this subsection apply

---

[5-15] CCIR Report 252-2, CCIR Interim Method for Estimating SKYWAVE Field Strength and Transmission Loss at Frequencies Between the Approximate Limits of 2 and 30 MHz, Geneva, Switzerland, 1970.

to both programs. A summary at the end of this subsection indicates the major engineering differences between the two programs.

The IONCAP program and the HFMUFES-4 program both calculate the circuit parameters of a radio signal propagating via the ionosphere. The calculation of the HF propagation conditions essentially involves predicting two quantities, the frequencies that are reflected by the ionosphere and the signal loss over the path. Also the values for loss are used, along with the calculated antenna gains, the noise levels, and other system parameters, to calculate the system performance and other values that are directly usable by an HF operator in establishing and evaluating a communications circuit.

The ionospheric regions used are a D, E, F, and (optionally) sporadic-E (E_s). The models assume all ionospheric absorption is non-deviative and occurs in the D-region. The normal E and F regions are assumed to have a parabolic electron density profile. For a given circuit, these layers are used to calculate the frequencies at which energy will be reflected back to the ground. It should be mentioned that, since signal absorption and signal reflection are controlled by different ionospheric regions, their calculations are independent of each other, and it is necessary to have frequencies that are supported by the ionosphere as well as adequate signal-to-noise ratio to establish a circuit.

Basic ionospheric properties such as F-layer critical frequency, etc., and other geophysical data such as the earth's magnetic field components, median atmospheric radio noise data, and worldwide land-sea boundaries are evaluated by numerical techniques, frequently referred to as 'numerical maps'. In these techniques, large quantities of data collected at worldwide sites are represented by a Fourier-harmonic series expansion or spherical-harmonic series expansion. The coefficients used in the series expansion are evaluated by means of least squares fit to the measured data. The measured data is described as a function of as many as five independent variables, such as latitude, longitude, universal time, day of year, and sunspot number.

The coefficients are stored in a mass-storage device and are read into the computer program during initialization. The measurements on which the ionospheric coefficients are based were taken during both the high (1958) and low (1954) phases of the sunspot cycle. The dependence of the ionospheric parameters on solar activity is accounted for by linear interpolation between coefficients used to describe the above two sets of measurements.

The propagation frequency varies on a daily basis and is predicted on a statistical basis. The probability of signal reflection as a function of frequency is assumed to have a chi-square distribution. The upper and lower deciles, derived from worldwide ionogram data, are used to set the skew property of the distribution. These decile values are computed by a table look-up process. The predictions are made for the median, upper decile and lower decile values -- the "MUF", "HPF" and "FOT" values, respectively.

The mechanisms included in the system-loss computation are free-space spreading along the slant range of the mode geometry, D-region absorption, intermediate ground-reflection loss for multiple-hop modes, transmitter and receiver antenna gain, and an adjustment quantity called excess system loss. The adjustment is a small empirical correction factor, based on measurements, which essentially accounts for complex and time varying loss mechanisms not included in the theoretical model. This factor is a function of geomagnetic latitude and time. The IONCAP program also includes loss factors for sporadic-E obscurations and, above the MUF, scatter loss.

The program assumes that the logarithm of system loss and, therefore, the logarithm of signal strength, is distributed (over a 30-day period for any specific hour) according to a chi-square probability distribution function. The two logarithmic intervals extending from the median loss to the upper standard deviation and from the median to the lower standard deviation are used to adjust the skew property of the distribution. These two intervals are obtained by means of a table look-up procedure. The table is based upon worldwide measurements.

Calculation of the propagation frequencies is based on the assumption of a parabolic ionospheric layer. Ionospheric characteristics, determined from "numerical maps", are used to define the parabolic layer. Path geometry (take-off angle) of F-layer modes is corrected for ray path bending due to its passage through a parabolic E layer.

System performance is based upon an estimate of actual signal-to-noise ratio (SNR) and its comparison with a required signal-to-noise (RSN) value. The RSN is an input parameter to the program, and it can vary depending on the desired quality of radio service and the emission format. The estimates of the system performance are based on the probability that the predicted SNR will exceed the RSN.

Radio noise sources accounted for by the program are of three kinds: atmospheric radio noise, man-made radio noise, and galactic radio noise. Receiver noise is not modeled in the program, since the levels of one or more of the above three types of radio noise are expected to exceed typical HF receiver noise to an extent that receiver noise can be neglected.

Atmospheric radio noise is based on a numerical representation of the noise data contained in CCIR report 322 (see Reference 5-11). Galactic noise estimates are obtained from measurements and also from CCIR Report 322.

The man-made noise environment is highly variable from one location to the next and, in fact, is difficult to represent accurately without measurements or some previous experience. The program addresses this problem by making available four (three in HFMUFES-4) models of man-made noise environments, which are essentially different noise levels. The four models, called industrial, residential, rural, and remote noise, are estimates of the nominal noise levels experienced in these areas.

Frequently, the actual noise environment is altered by the presence of local machinery and equipment, such as dc generators, trucks, jeeps, or shipboard associated noises, so that a simple description of the noise

environment by one of the three above models is frequently not adequate. Hence, there is an option that allows the user to enter the level of man-made noise to be used in the calculations. The value entered is at the reference frequency of 3 MHz.

The accessible antenna package (APACK) program[5-16] has been interfaced with IONCAP. The APACK program models sixteen frequently used antennas such as log periodic, vertical monopole, Yagi, etc. The gain of the antenna is computed as a function of frequency, take-off angle and azimuth.

The HFMUFES-4 program contains a similar antenna package, although it is not as complete as the APACK package. The range of applicability of the IONCAP and HFMUFES-4 models is as follows:

1) In the frequency domain, these programs predict the highest frequency that can be supported by ionospheric propagation, regardless of how high the value may be. However, calculations of antenna gains are made only for frequencies from 2 to 30 MHz. Accordingly, calculations of received power, signal-to-noise ratio, and other system parameters that are a function of antenna gain are also limited to frequencies from 2 to 30 MHz.

2) Program outputs for the point-to-point circuits may be calculated for transmitter-receiver separation distances from a few meters to a maximum distance of 30,000 km. For the area coverage analysis in HFMUFES-4, calculations may be made for ranges up to 20,000 km from the base station. These programs do not include groundwave propagation. For the very short distances, where both skywave and groundwave propagation may be appropriate, the results for the skywave propagation should be obtained from these

---

5-16 Chang, S., APACK - A Combined Antenna and Propagation Model, ESD-TR-80-102, Electromagnetic Compatibility Analysis Center, Annapolis, MD, July 1981.

programs, and the results for the groundwave propagation should be obtained from one of the other appropriate programs discussed in Chapter 6.

3) In the time domain, values of program outputs are useful for any 30-day period centered on any day of any year for which a Zurich sunspot number has been estimated. The ionosphere is an extremely complex medium that is created in part by solar radiation and, accordingly, has regular variations associated with time of day, season, and sunspot cycle. The ionosphere also has irregular and random fluctuations that can be described only by statistical methods. The statistical estimates are based on hourly data gathered over a period of a month. Thus, the SKYWAVE model is typically used to estimate the propagation conditions for each of the 24 hours of the day on a monthly basis. The predictions are a function of sunspot number so that, if predictions are needed for the same month but different years (i.e, different sunspot numbers), it will be necessary to perform separate calculations for each year.

Both the IONCAP and HFMUFES-4 models are very user-oriented, with simplified input card structures and more than eighteen different output formats. The different output formats include both tables and graphs generated on the high speed printer. Instructions on the use of the IONCAP and HFMUFES-4 programs and their output examples are provided in the Propagation User's Manual.[5-17]

The IONCAP program consists of a complete revision of HFMUFES-4 to make the code itself more modern and to change some calculations. Over the years, a number of improvements have been made to the ECAC version of HFMUFES-4. One of the more significant developments was an area-coverage display and interference analysis. Calculations have historically been made for point-to-

---

[5-17] Baker, R. L., Radio Wave Propagation: A User's Manual, for the Computer Codes, ECAC-UM-80-001, Electromagnetic Compatibility Analysis Center, Annapolis, MD, September 1980.

point circuits, i.e., where the location of the transmitting and receiving sites are fixed. The area-coverage displays consist of contour plots about a single fixed location. This capability will be added to the IONCAP program in the future.

The IONCAP program contains the following major improvements or features that are not available in the HFMUFES-4 program.

1) Addition of an F1-layer model

2) Revision of the manner in which sporadic-E is used in the mode calculation

3) Addition of loss terms to account for sporadic-E obscurations.

4) Addition of loss terms to account for scatter propagation at frequencies above the MUF.

5) Revision of the calculations for long-distance circuits to allow for the variation of the ionosphere along the path.

It is recommended that project engineers use IONCAP for routine analyses unless special circumstances require that the HFMUFES-4 program be used (e.g., to obtain map overlays of reliability using ECAC's special driver for HFMUFES-4.)

5.2.1.2 MINIMUF Program

The Naval Ocean Systems Center (NOSC) at San Diego, California, has developed a novel algorithm for estimating the maximum usable frequencies (MUF) for propagation of electromagnetic signals via the ionosphere. This

algorithm has been incorporated into a computer program call MINIMUF.[5-18] The significant feature of the program is its very small size, which allows its use on a small programmable calculator such as the HP-41C. The small size of the program was achieved by using only six constants to represent different ionospheric conditions, including time of day, sunspot number, and season. In comparison, predictions of the MUF using current state-of-the-art techniques in IONCAP and HFMUFES-4 require 12,000 coefficients.

While the small size of the MINIMUF program makes it attractive, the MINIMUF predictions are less accurate than the IONCAP and HFMUFES-4 programs. In a previous ECAC study[5-19] for the Navy Electromagnetic Spectrum Center (NAVEMSCEN), predictions from the MINIMUF program and those from the HFMUFES-4 program were compared. The results of this study indicated that the MINIMUF predictions could result in sizeable errors for certain conditions. Part of the problem with the MINIMUF program is that, with only six coefficients, it fails to account for important anomalous ionospheric behavior such as the seasonal anomaly. Also the program does not include the effect of variations in ionospheric height. For routine project analyses, the IONCAP program should be used rather than the MINIMUF program to make HF propagation predictions. The MINIMUF program is useful in special situations where the user needs timely predictions but does not have access to a large scale computer. The MINIMUF program has been put on the HP-41C and the UNIVAC 1100 at ECAC. If one of the versions is required, DRD should be contacted to identify an appropriate member of the propagation staff to provide assistance.

5-18 Rose, R. B. and Martin, J. N., MINIMUF Tech Document 201, Naval Ocean Systems Center (NOSC), San Diego, CA, October 1978.

5-19 Jones, J. L., Riggins, H. L., and Cameron, S. H., Navy Electromagnetic Spectrum Center Fiscal Year 1979 Support, ECAC-CR-79-076, Electromagnetic Compatibility Analysis Center, Annapolis, MD., September 1979.

5.3 VALIDATION

This subsection summarizes the results of studies in which skywave-model predictions were compared with measurements. Though IONCAP was not always used for the predictions, the studies are still useful in giving analysts the order of magnitude of accuracy that is expected from this model.

CCIR Report 255-4 (Reference 5-20) indicates that the errors in predicting the f_oF2 parameter are 15% or less except in high (i.e., the shaded and cross-hatched areas, except the region near the Equator, shown in Figure 7-5 of this Handbook) latitudes where the inaccuracies may be as high as 40%.

An extensive analysis of the predicted MUF accuracy of the HFMUFES-4 model was made by Gosnell for the Joint Chiefs of Staff.[5-21] Observations were made on 15 paths over a period from 1968 to 1970. The paths were primarily east-west oriented, ranging in length from 8,000 km to 10,000 km. No part of any path extended far enough north to be greatly affected by the auroral zone. The forward oblique sounder made by Barry Research Corporation was used to record the data. This equipment has a frequency range from 2.5 to 27.5 MHz. The MUF during daylight periods was often greater than 27.5 MHz, so that the major results of this data apply to night-time periods. These results are summarized in the form of percentage difference [(predicted MUF - measured MUF)/measured MUF] for each path and each month. The data was tabulated for over 290 different path/months. Generally, the percentage difference for most months was between 5 and 15 percent. The difference exceeded 20% for only five month/path sets of data. In three of these sets,

---

5-20 CCIR Report 255-4, Long-Term Ionospheric Propagation Predictions, Recommendations and Reports of the CCIR, Volume VI, p. 36 XIVth Plenary Assembly, Kyoto, 1978.

5-21 Gosnell, P. C., Comparison of Predicted and Observed MUFS, Joint Chiefs of Staff 208a Working Group, March 1972.

the percentage difference was less than 22. In the other two cases the difference was 49% and 28%.

The ionospheric data contained in the IONCAP and HFMUFES-4 model are based on worldwide, vertical-incidence, ionogram data collected in 1954 and 1958 at over 150 worldwide stations. The numerical technique used involved fitting a set of spherical harmonic curves to these sets of data. The rms error in this curve fitting process was less than 0.5 MHz for each month of the 1954 data and less than 0.7 MHz for each month of the 1958 data.[5-22] This data does not include a significant number of measurements in the polar regions.

A comparison of observed and predicted signal strengths is given in CCIR Report 571-1 for non-polar regions.[5-23] Ninety percent of the measurements were within ± 20 dB of the predictions. A CCIR method was used for the predictions.

Another CCIR study[5-24] shows that rms errors of 13 dB are typical for both IONCAP and HFMUFES-4. This implies that 90% of the measurements were within roughly ± 21 dB of the predictions.

A study of the prediction accuracy in polar regions was made at ECAC using OTH radar data.[5-25] This data was collected over three paths for a

---

5-22 Jones, W. B., et al., Advances in Ionospheric Mapping by Numerical Methods, Tech Note 337, National Bureau of Standards, Washington, DC, February 14, 1965.

5-23 CCIR, Comparisons Between Observed and Predicted Sky-Wave Field Strength and Transmission Loss at Frequencies Between 2-30 MHz, Report 571-1 Documents of the XIVth Plenary Assembly, Kyoto, Japan, 1978.

5-24 CCIR, Comparison of Methods Used to Compute HF Skywave Field Strength, Document F6/4 for the Special Preparatory Meeting, 1978.

5-25 Larson, R., Comparison of Predicted and Measured Sky-Wave Propagation Loss in the Polar Regions, IIT Research Institute, MD, ESD-TR-73-002, Annapolis, MD, August, 1973.

period of nine months. The rms prediction error was between 11 and 19 dB, depending on the path. There was a bias such that the model (an earlier version of HFMUFES-4) predicted an average of 10 dB too little loss.

5.4 CONCLUDING REMARKS

A recent paper discussing the confidence of the knowledge of ionospheric phenomena that affect communications systems was published by Rush.[5-26] Practical advice about choosing an optimum frequency for skywave propagation appears in the text and tables of a handbook prepared by Jacobs and Cohen.[5-27]

[5-26] Rush, C.M., "HF Propagation: What We Know and What We Need to Know," IEE Conference Publication 195, IEE, London, April 1981.

[5-27] Jacobs, G., and Cohen, T.J., The Shortwave Propagation Handbook, Cowan Publishing, Port Washington, NY, 1979.

CHAPTER 6

NON-IONOSPHERIC PROPAGATION, 0.1 - 40.0 MHz

By: M. Weissberger

6.1 INTRODUCTION

This chapter discusses modeling of basic transmission loss, L_b, for signals in the 0.1-40.0 MHz band that are not propagated by reflections or scatter from the ionosphere.

A manual procedure for computing L_b is presented in Subsection 6.2. The status of computer codes for predicting this loss is discussed in Subsection 6.3. Validation of the procedures is shown in Subsection 6.4. Subsection 6.5 contains concluding remarks.

6.1.1 Ionospheric vs. Non-Ionospheric Propagation

The models discussed here account for coupling by waves that are not affected by the ionosphere. Models to predict coupling via waves reflected by the ionosphere are discussed in Chapters 4 and 5 of this handbook. This separate treatment of the two types of coupling is a pattern used in texts such as Terrestrial Radio Waves[6-1] and Electromagnetic Waves and Radiating Systems.[6-2]

Predicting situations in which either the ionospheric or non-ionospheric components can be assumed to be completely dominant, or when both will be of a comparable order of magnitude, is a difficult problem. The solution depends

---

[6-1] Bremmer, H., Terrestrial Radio Waves, Elsevier, NY, 1949.

[6-2] Jordan, E., Balmain, K., Electromagnetic Waves and Radiating Systems, Prentice Hall, Englewood Cliffs, NJ, 1968.

on the frequency, antenna type, time-of-day, season, sunspot number, latitude, earth conductivity and earth dielectric constant.

Figures 6-1 and 6-2 show experimental results for one particular set of parameters. These were measured by Stanford Research Institute (SRI)[6-3].

Reference 6-4 contains an extensive set of measurements of the skywave-groundwave transition in the HF band. Southwest Research Institute workers have also conducted experiments regarding this matter[6-5]. Reference 6-6 shows a typical prediction for the MF band.

The straightforward approach to determining which modes of propagation are significant for a specific set of circumstances is to calculate received power using the techniques outlined in this chapter, do a similar calculation using the models recommended in Chapter 5, and then compare the results.

6-3 Tupper, B. C. and Hagn, G. H., Nap of the Earth Communication Program for U.S. Army Helicopters, AVRADCOM-TR-76-0868-F, June 1978.

6-4 Van der Vis, P. A., Measurements on Short Distance HF Data Links, IR 1979-72, Physics Laboratory of the National Defense Research Organization, TNO, the Hague, the Netherlands, October 1979.

6-5 Hipp, J.E., and Green, P.C., Measured Sea Path Skywave-Groundwave Signal Power Ratios Over the 2-10 MHz Range, Task Report 33, NAVELEX Contract N-0039-72-C-1275, Southwest Research Institute, San Antonio, TX, 23 January 1976.

6-6 Laport, E. A., Radio Antenna Engineering, McGraw-Hill, New York, NY, p. 103, 1952.

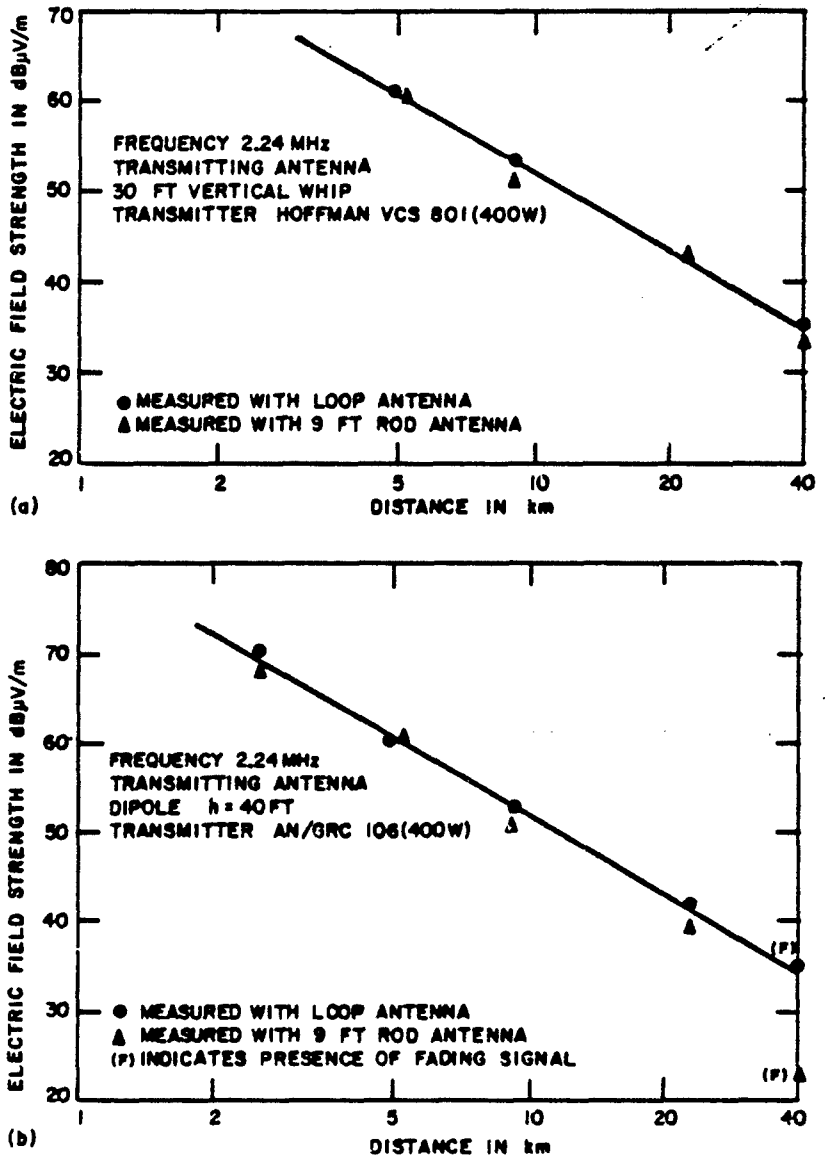

Figure 6-1. Measured examples of the region where skywave field strength begins to be comparable in magnitude to the groundwave field-strength, 2 MHz. This region is indicated by the fading of the received signal. (From measurements at Ft. Hood, TX, Reference 6-3.)

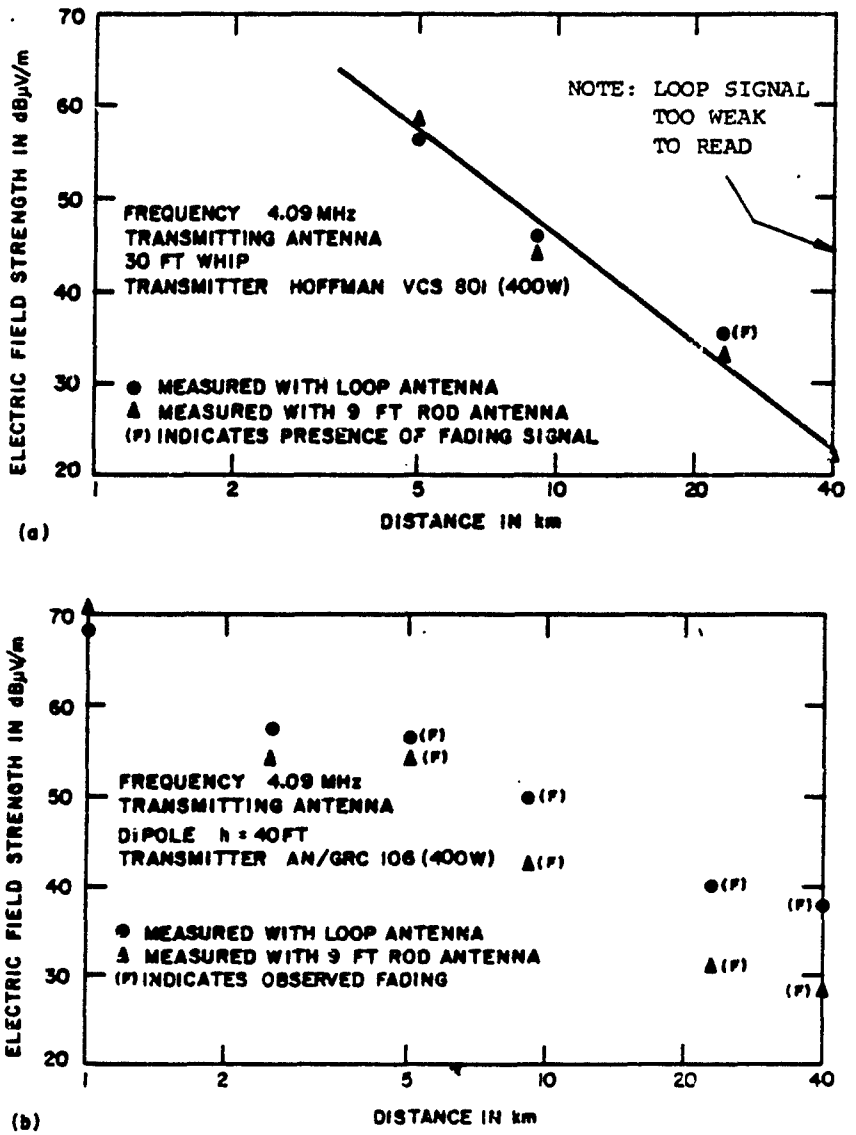

Figure 6-2. Measured examples of the region where skywave field strength begins to be comparable in magnitude to the groundwave field strength, 4 MHz. This region is indicated by fading of the received signal. (From Measurements at Ft. Hood, TX, Reference 6-3.)

6.2 MANUAL PROCEDURES FOR COMPUTING LOSS

Two factors that affect groundwave loss in this band are the constituent parameters (conductivity and dielectric constant) of the surface along the propagation path and the topographic features of the path. The procedures described below will account for the constituent parameters but not the topographic features. The uncertainty caused by not accounting for topographic features is quantified in Section 6.4.

The manual procedures address two types of problems. The first problem is that in which the constituent parameters are relatively constant along the propagation path. The manual procedure is the set of curves presented in Section 6.2.1. The second type of problem is that in which segments of the path have constituent parameters different from the parameters of other parts of the path. The manual procedure is an equation that generates the proper answer as the sum of losses computed for segments with constant parameters.

6.2.1 Curves for Smooth Homogeneous Ground

The basic transmission loss between two antennas, discounting ionospheric effects, is illustrated in the accompanying graphs. Figures 6-3 through 6-9 are for vertically polarized isotropic radiators over typical dry land. Figures 6-10 through 6-16 are for vertically polarized radiators over sea water. The curves are computations of the NLAMBDA[6-7, 6-8] computer code. This model is based on the assumptions that the earth is a smooth sphere and that

---

6-7 Frazier, W. E. and Rutter, J., A Theoretical Ground Wave Propagation Model, Phase I, ECAC-TN-003-269, Electromagnetic Compatibility Analysis Center, Annapolis, MD, January 1967.

6-8 Maiuzzo, M. A. and Frazier, W. E., A Theoretical Ground Wave Propagation Model - Nλ Model, ESD-TR-68-315, Electromagnetic Compatibility Analysis Center, Annapolis, MD, December 1968.

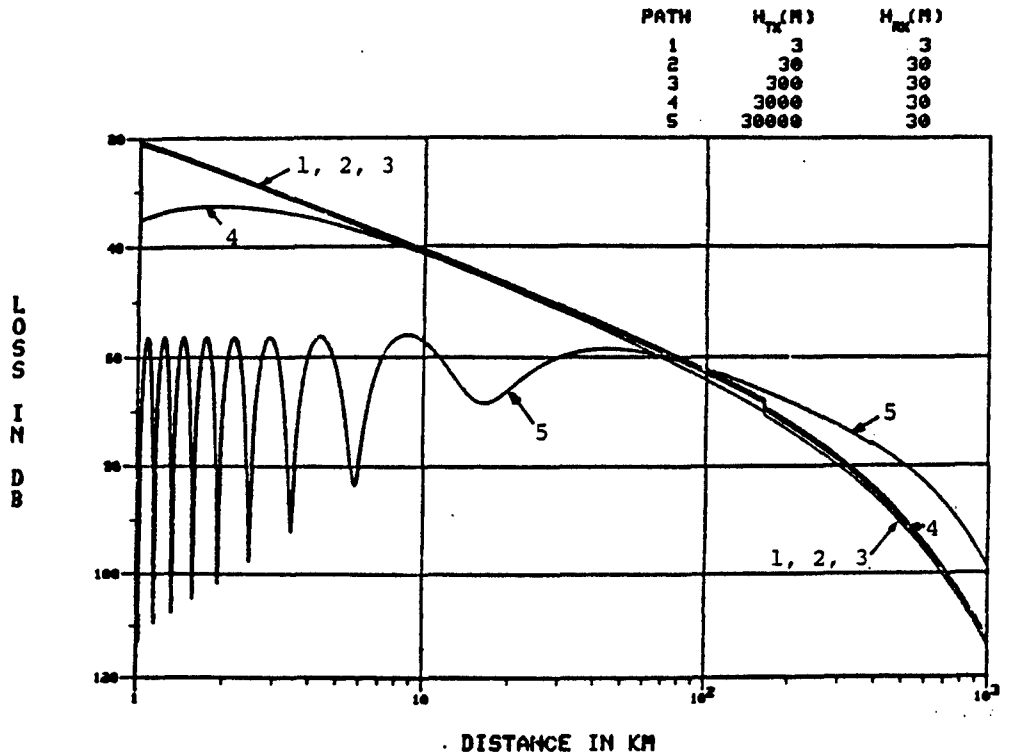

Figure 6-3. Ground wave loss over average earth, 0.5 MHz.

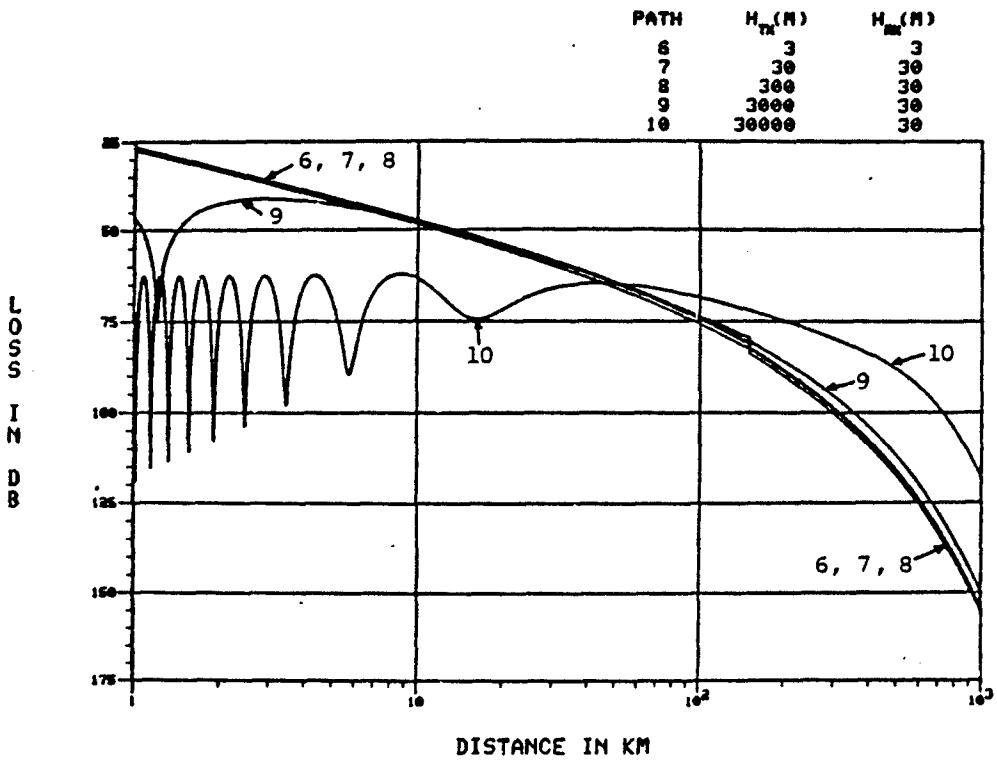

Figure 6-4. Ground wave loss over average earth, 1.0 MHz.

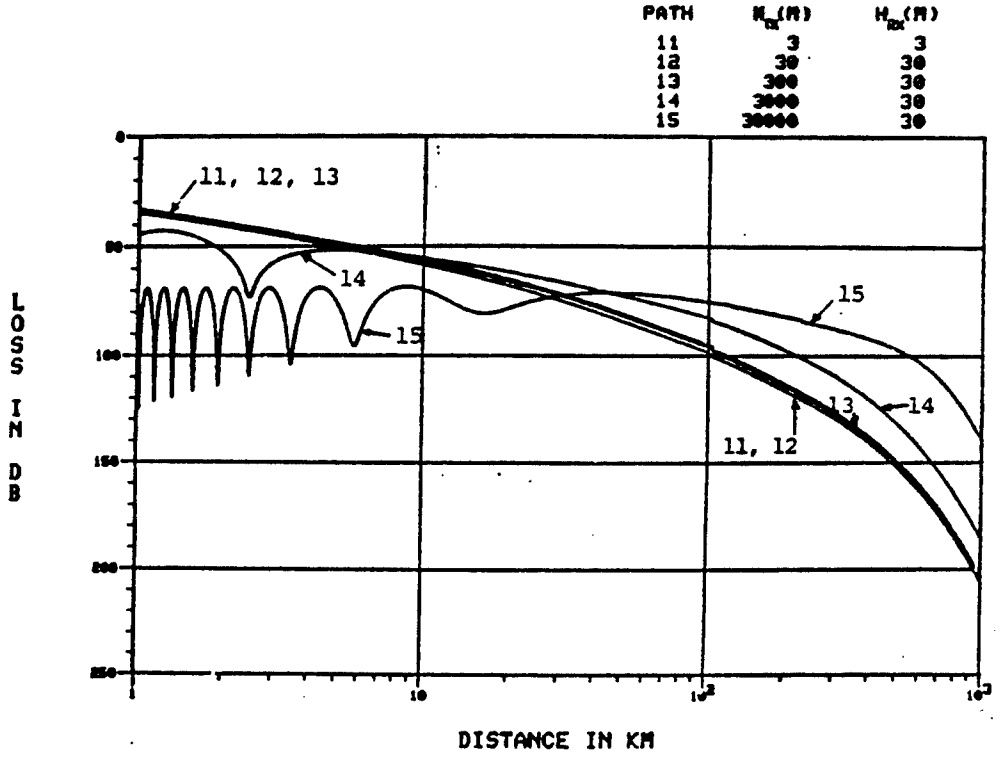

Figure 6-5. Ground wave over average earth, 2.0 MHz.

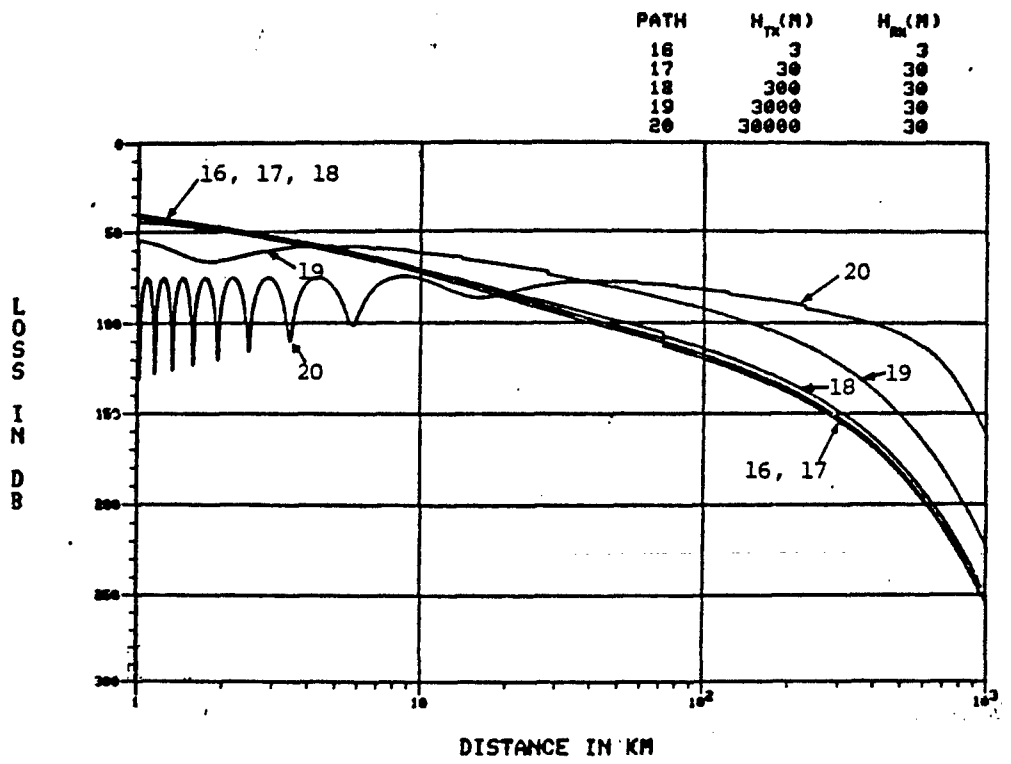

Figure 6-6. Ground wave loss over average earth, 4.0 MHz.

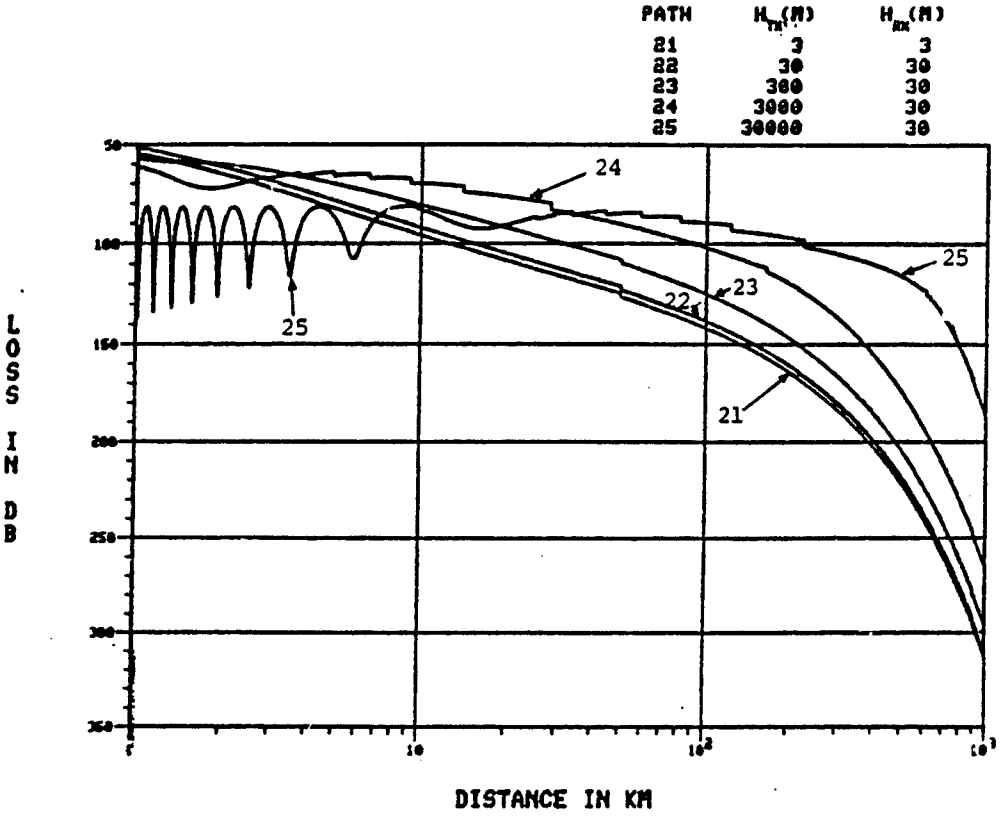

Figure 6-7. Ground wave loss over average earth, 8.0 MHz.

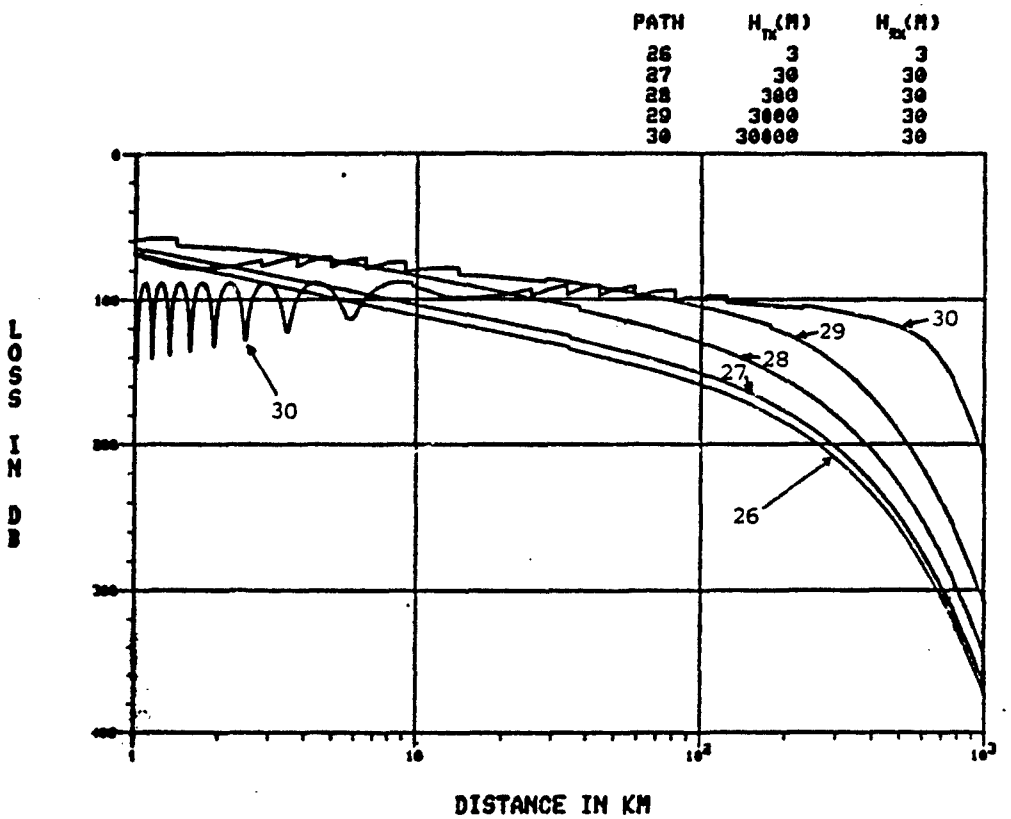

Figure 6-8. Ground wave loss over average earth, 16.0 MHz.

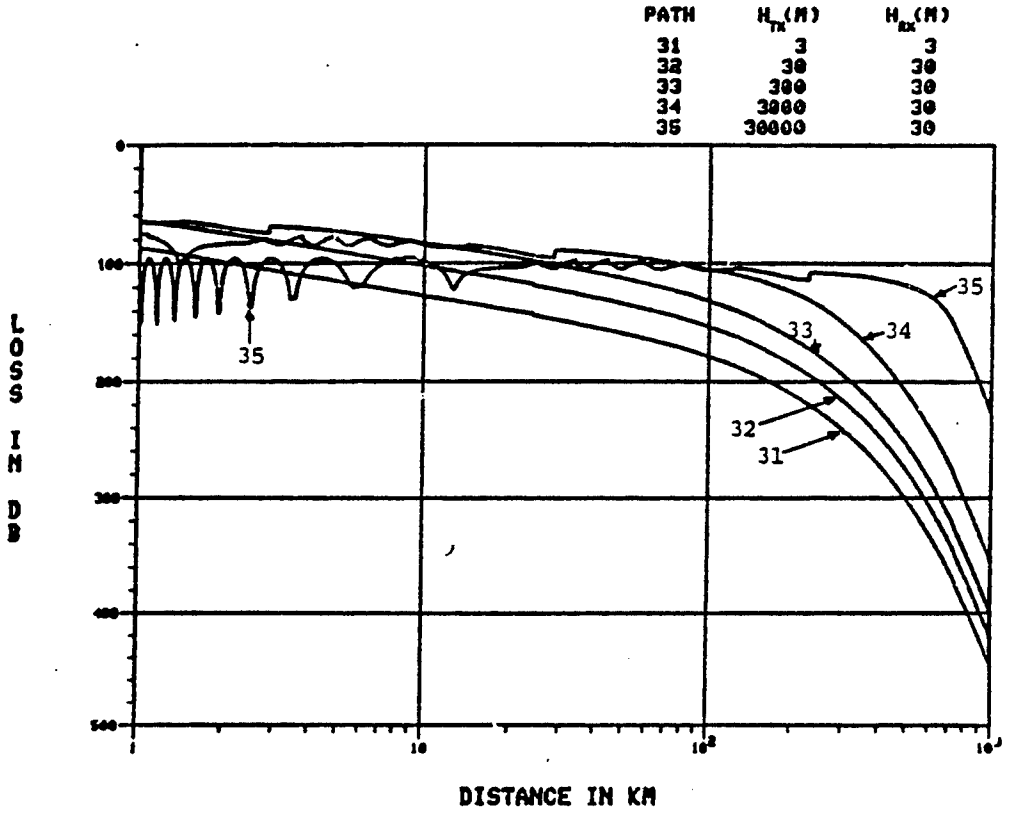

Figure 6-9. Ground wave loss over average earth, 32.0 MHz.

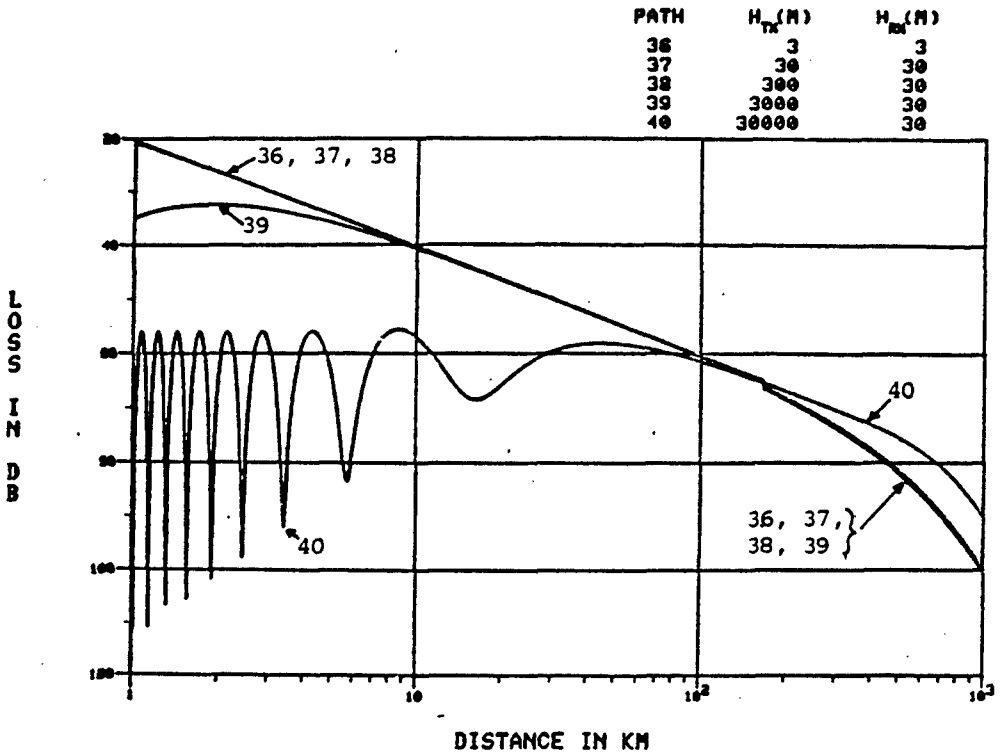

Figure 6-10. Ground wave loss over sea water, 0.5 MHz.

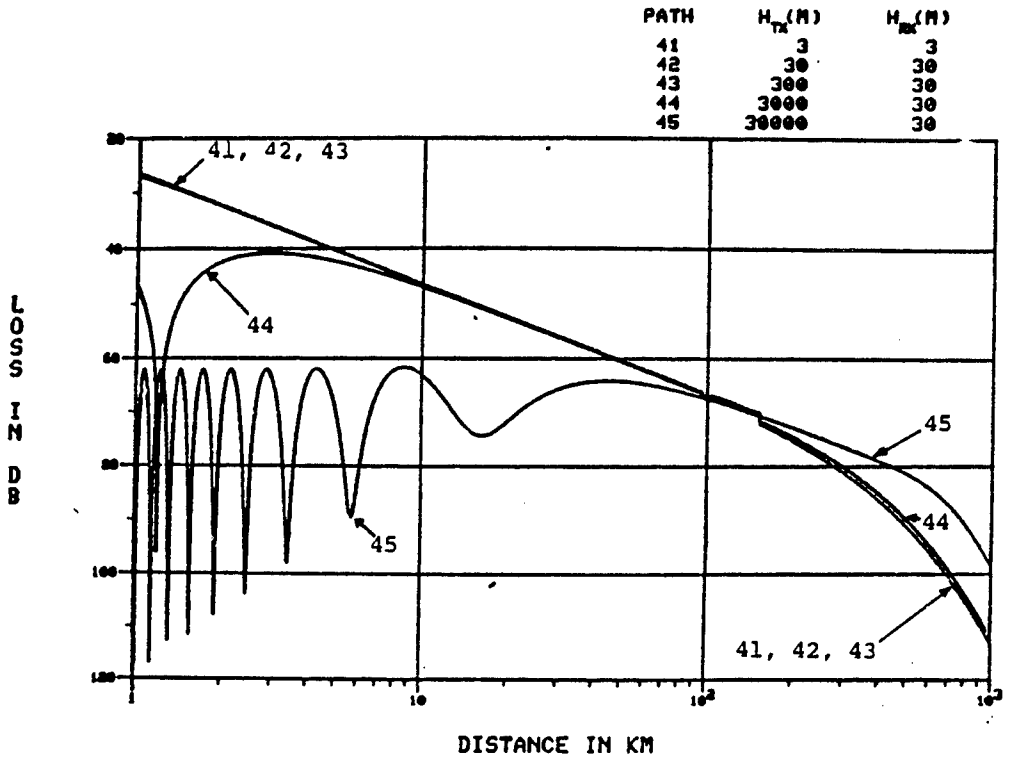

Figure 6-11. Ground wave loss over sea water, 1.0 MHz.

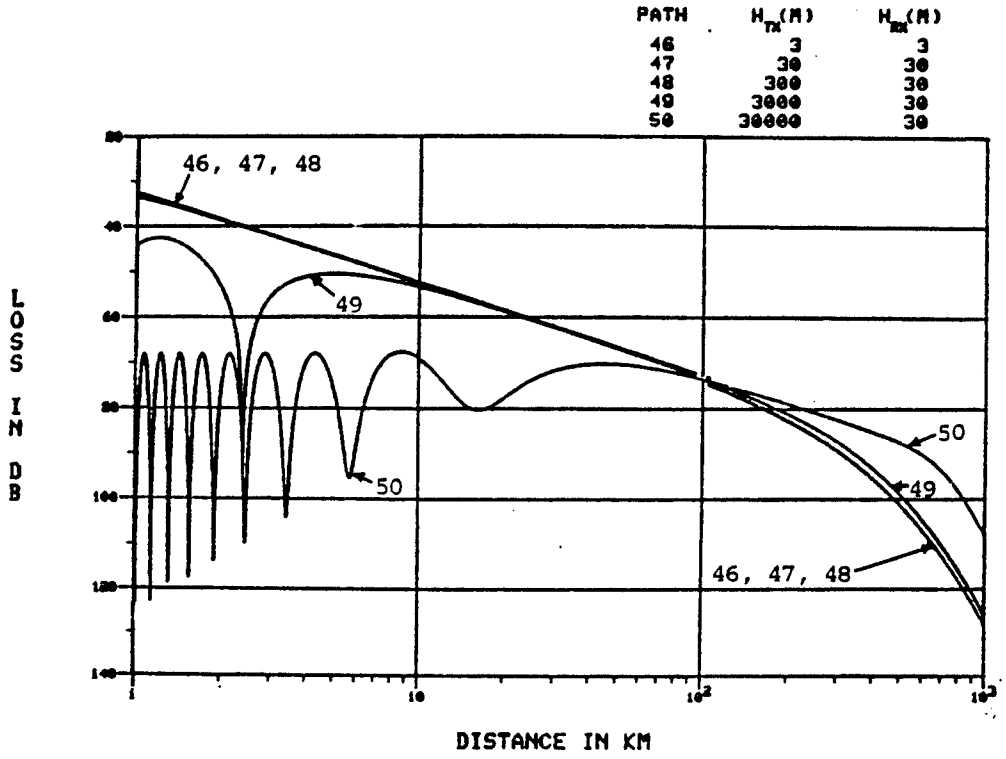

Figure 6-12. Ground wave loss over sea water, 2.0 MHz.

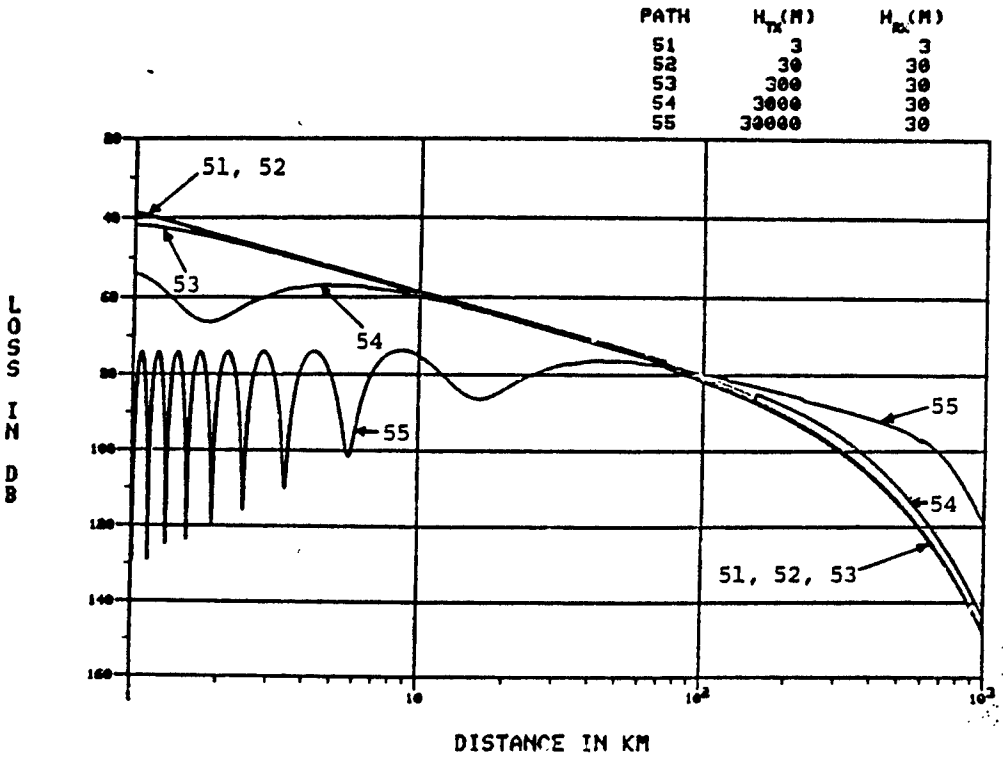

Figure 6-13. Ground wave loss over sea water, 4.0 MHz.

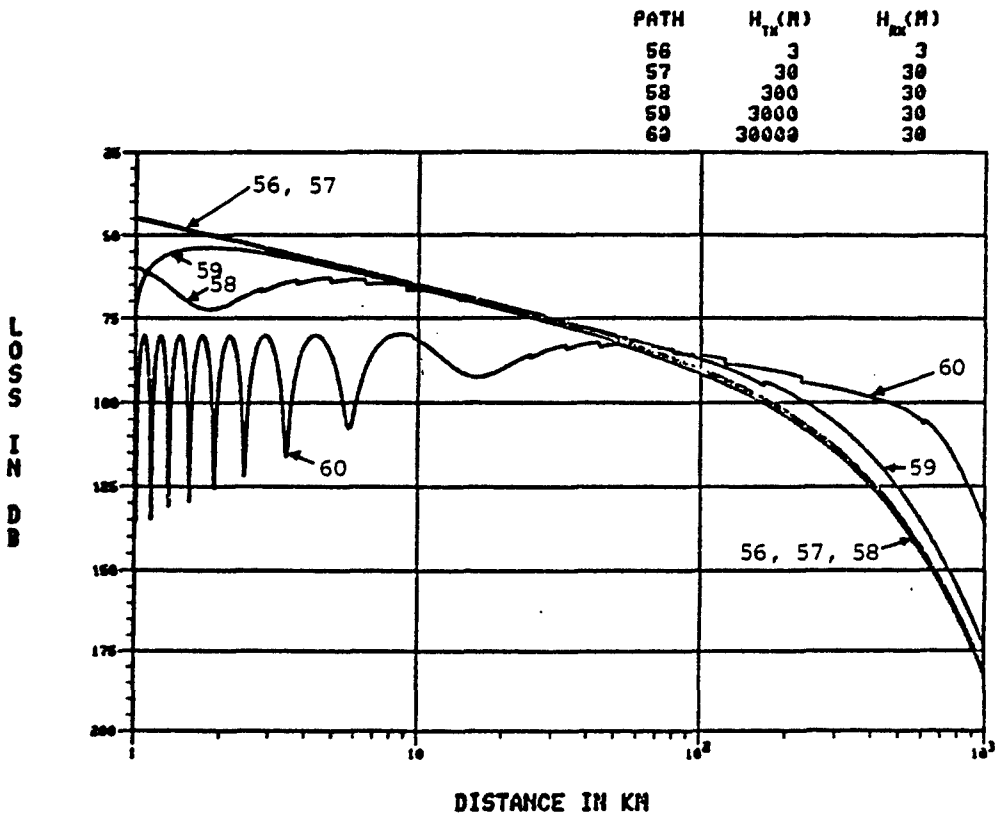

Figure 6-14. Ground wave loss over sea water, 8.0 MHz.

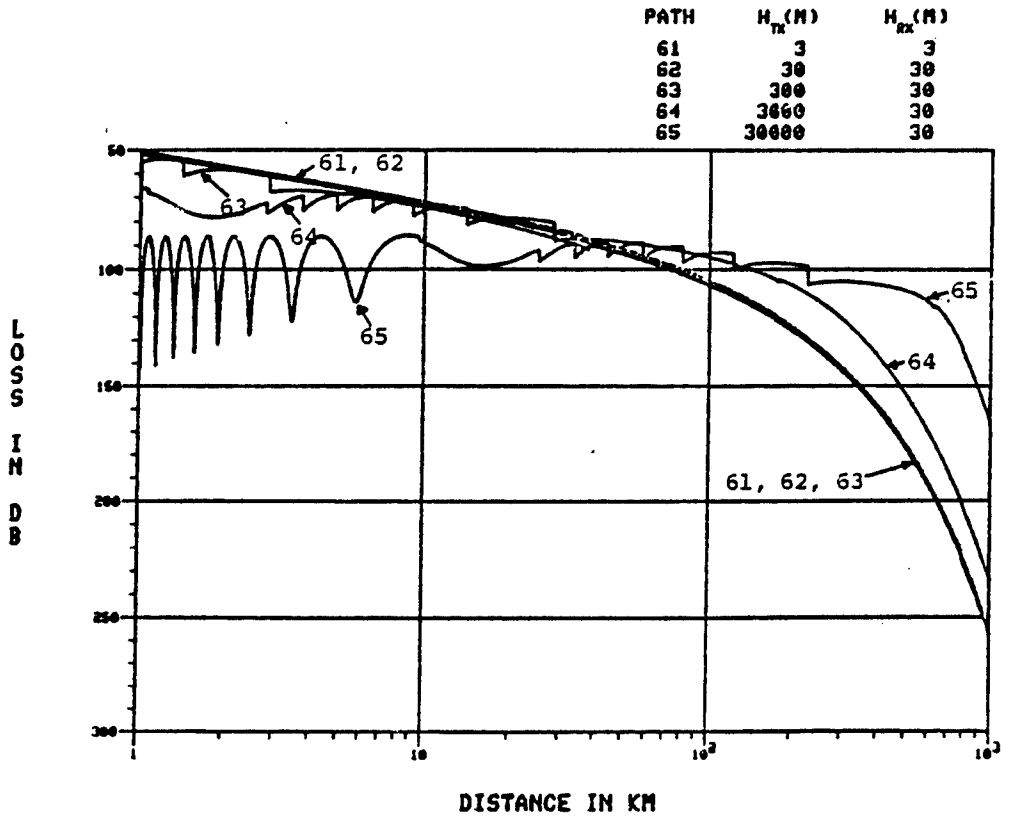

Figure 6-15. Ground wave loss over sea water, 16.0 MHz.

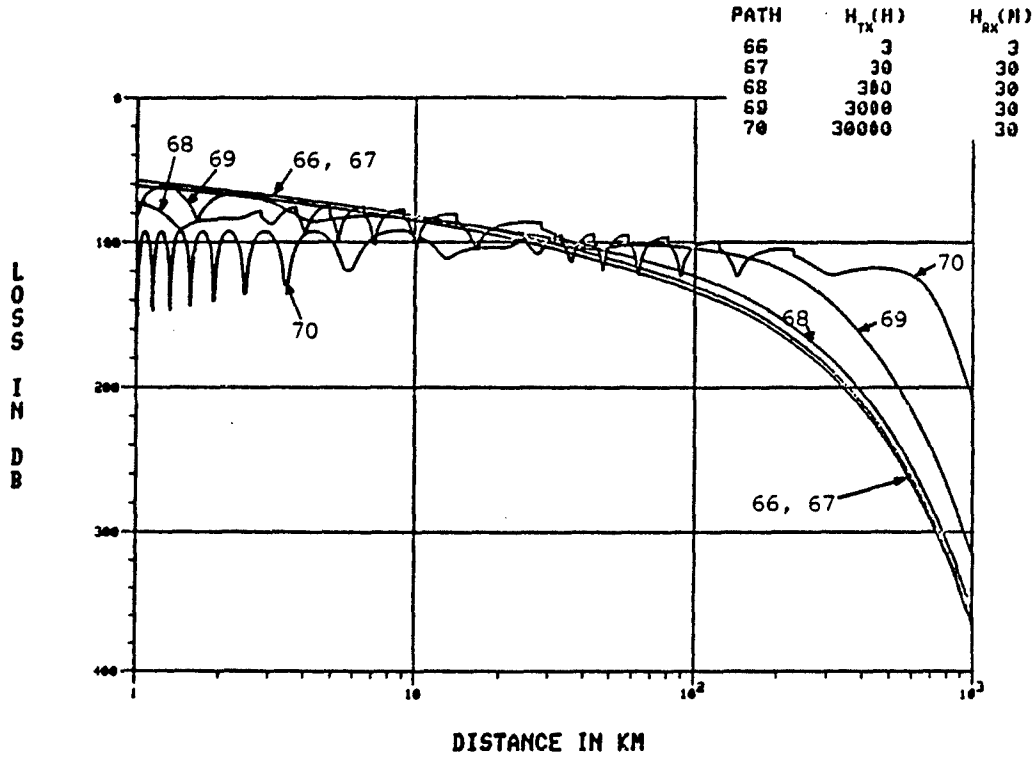

Figure 6-16. Ground wave loss over sea water, 32.0 MHz.

the oxygen and water vapor densities in the atmosphere decrease exponentially with altitude.

Subsection 6.2.3 presents information about adjusting the predictions in Figures 6-10 through 6-16 to account for the roughness of the sea surface.

6.2.2 Mixed-Path Calculations

The preceding subsection showed results that apply to problems in which the constituent parameters are constant along the great circle path between the transmitter and receiver. In this subsection, a formula is presented for computing the loss on "mixed paths," i.e., paths in which there are segments of the surface which have constituent parameters different from the parameters in other parts of the path. A discussion of some typical results[6-9] precedes the formula.

For antennas that are near the earth's surface, increases in the conductivity and dielectric constant of the surface lead to decreases in path loss for signals between about 0.1 MHz and 160 MHz. The magnitude of the change is greatest at 10 MHz. Above 160 MHz, the effect is negligible. At frequencies well below 0.1 MHz [Bremmer (Reference 6-1, p.121) cites an example at 15 kHz], the trend, while not substantial, is opposite to the trend at the higher frequencies.[a]

---

[a] The information in this paragraph was obtained from Reference 6-1, from theoretical predictions using the Nλ model (Reference 6-8), and from Reference 6-10.

6-9 Jablinske, R. J. and Weissberger, M. A., Use of Features Data in ECAC Propagation Loss and Line-of-Sight Prediction Models, ECAC-IN-79-027, Electromagnetic Compatibility Analysis Center, Annapolis, MD, August 1979.

6-10 Bullington, K., "Radio Propagation Fundamentals," Bell System Technical Journal, May 1957.

Figure 6-17 is an illustration of the mixed-path effect measured at 78 MHz.[6-11] As shown, the reduction in path loss due to propagation over sea water ($\sigma = 4.6 \times 10^{0}$ mhos/m, $\varepsilon = 80$), in contrast to propagation over land ($\sigma = 1.0 \times 10^{-2}$ mhos/m, $\varepsilon = 10$), is 20 dB for a distance of only 3 km.

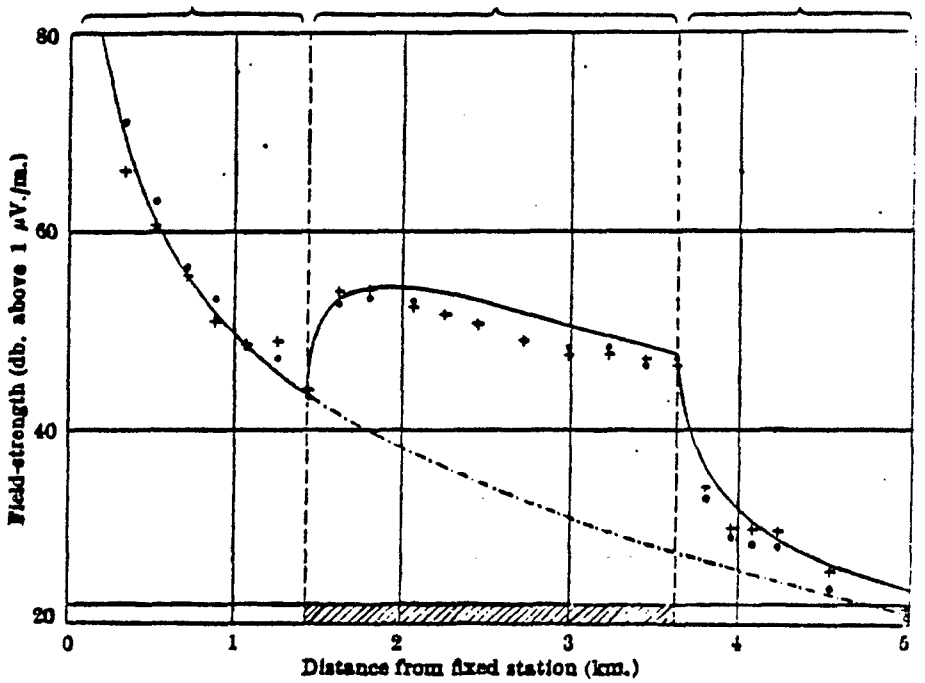

———, Theoretical curve, land and sea; — · — · —, theoretical curve, land only; ⊢, measurements at fixed station; o, measurements at mobile station. $\lambda = 3{\cdot}9$ m.; $P = 10$ watts; vertical polarization, $h_T = h_R = 0$

Figure 6-17. An example of the measured effect of conductivity on propagation loss. The frequency is 78 MHz. The center section of the path (1.4 - 3.6 km) is sea water ($\sigma = 4$ mho/m), the ends are land ($\sigma = 1 \times 10^{-2}$). This is the model discussed in Section 6.2.2. (from Reference 6-11).

6-11 Millington, G., "Ground-Wave Propagation Across a Land/Sea Boundary," Nature, 22 January 1949, p. 128.

Other examples of measurements (collected in a literature search by Riggins)[6-12] show that:

a. On a 200-km path that was 45% over land and 55% over sea, the effect of the sea was 27 dB at 3 MHz (i.e., a 200-km path that was all land would have a loss 27 dB higher than that measured.)

b. On a 215-km path at 0.8 MHz, a 30-km segment of sea reduced the overall path loss by 26 dB.

c. On a 300-km path at 1.2 MHz, differing conductivities resulted in a 23 dB reduction in path loss.

The effects of the differences in the electrical parameters of different types of land will not be as large as the differences between any type of land and sea water. However, the results are still significant. The FCC map of land conductivities for the United States[6-13] shows sectors with $\sigma = 0.03$ mhos/m and $\sigma = 0.004$ mhos/m to be adjacent. The loss at 1 MHz over a 100-mile path (vertical polarization, $H_t = H_r = 0$ ft.) is 23 dB larger for $\sigma = 0.004$ than for $\sigma = 0.03$. The difference is 10.5 dB at 10 MHz, and diminishes to 0 at 100 MHz.[a]

---

[a] Based on theoretical calculations using the NLAMBDA model.

6-12 Riggins, H., "The Mixed Path Model," in Propagation User's Manual, ECAC-UM-78-001, Electromagnetic Compatibility Analysis Center, Annapolis, MD, January 1979.

6-13 FCC Map R-3, Federal Communications Commission, Washington, DC.

Figure 6-18 shows a typical mixed-path geometry. The basic transmission loss for this type of path can be computed using Millington's Method[6-14, 6-15]. The formula for a path with n segments is:

$$L_b = \tfrac{1}{2}(L_f + L_r) \tag{6-1}$$

where L_f and L_r are intermediate parameters defined below:

$$L_f = L_1(d_1) + L_2(d_1 + d_2) + L_3(d_1 + d_2 + d_3) + \ldots + L_n(d_1 + d_2 + \ldots + d_n) - L_2(d_1) - L_3(d_1 + d_2) - \ldots - L_n(d_1 + d_2 + \ldots + d_{n-1}) \tag{6-2}$$

$$L_r = L_n(d_n) + L_{n-1}(d_n + d_{n-1}) + L_{n-2}(d_n + d_{n-1} + d_{n-2}) + \ldots + L_1(d_n + d_{n-1} + \ldots d_1) - L_{n-1}(d_n) - L_{n-2}(d_n + d_{n-1}) - \ldots - L_1(d_n + d_{n-1} + \ldots + d_2) \tag{6-3}$$

6-14 Millington, G., "Ground-Wave Propagation Over an Inhomogeneous Smooth Earth," Proc. IEE, Part III, Vol. 96, 1949.

6-15 CCIR, Ground-Wave Propagation Curves for Frequencies between 10 kHz and 30 MHz," Recommendation 368-3, ITU, Geneva, Switzerland, 1978.

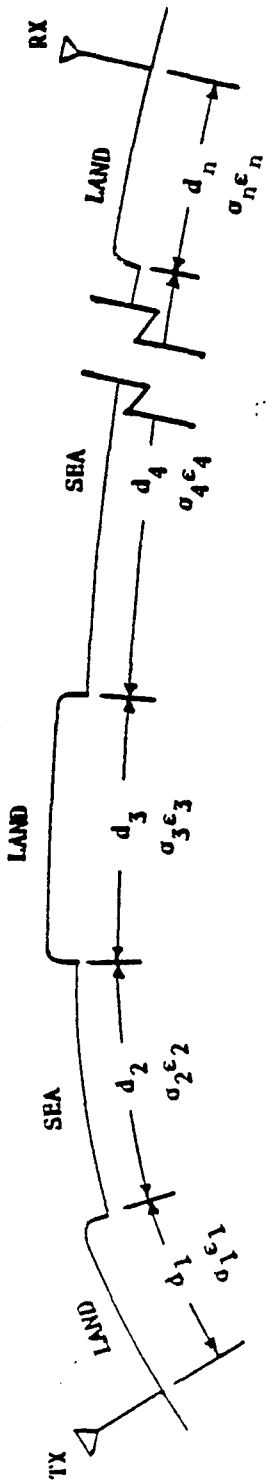

Figure 6-18. A mixed-path geometry for n segments.

L_i (d_j) is the loss over a path of length d_j, computed assuming that this path has the electrical properties of the ith section.

This mixed-path procedure is applicable only when the antennas are within line-of-sight of each other and close enough to the ground or sea so that the surface wave is significant (i.e., within ~ 10 wavelengths over the sea, ~ 1 wavelength over land), or when the antennas are not within line-of-sight but are coupled via diffraction (in contrast to tropospheric scatter or ionospheric reflections). If the antennas are within line-of-sight but are high enough above the ground so that the field strength is due essentially to only the direct and ground-reflected rays, the loss can be predicted using Equation A-15 (in Appendix A) with the reflection coefficient, R, that is appropriate for the surface at the actual point of reflection. Values of R are given in References 6-2 and 6-16. If the antennas are beyond line-of-sight of each other, and elevated, a reasonable procedure for computing the mixed-path loss is to use Equations 6-1 through 6-3, with each of the terms computed as if the antenna heights were zero. The loss is then adjusted for antenna height by using height gains appropriate for antennas over a homogenous path with constituents equal to those in the foreground of each antenna. This last suggestion is based on the technique used in Ott's mixed path model.[6-17]

6-16 Reed, H. R., Propagation Data for Interference Analysis, RADC-TDR-61-313, Vol. II, Rome Air Development Center, NY, January 1962.

6-17 Ott, R. H., "Ground Wave Propagation Over Irregular, Inhomogeneous Terrain: Comparisons of Calculations and Measurements," IEEE Trans. Ant. & Prop., March 1979.

6.2.3 The Effects of the Roughness of the Sea on Basic Transmission Loss

Barrick's theoretical work[6-18, 6-19] indicates that the waves on the surface of the sea can lead to both increases and decreases in the basic transmission loss. His analysis dealt with antennas located close enough to the sea so that the surface wave was significant (i.e., within about 10 wavelengths). His study showed that the effect is most prominent at 10-15 MHz and decreases to zero below about 2 MHz and above approximately 100 MHz. Figure 6-19 shows curves of the difference between loss over a wavy sea and over a smooth sea.

6.3 STATUS OF THE COMPUTER CODES

The ECAC Far-Field Smooth-Earth Coupling Code, EFFSECC, is recommended for computing the power coupled between two antennas located above a smooth earth with homogeneous ground constants. EFFSECC is an extension of Chang's work[6-20, 6-21, 6-22] by Marcus.[6-23] It can be considered as a consolidation and

---

6-18 Barrick, D. E., "Theory of HF and VHF Propagation Across the Rough Sea, 2, Applications," Radio Science, May 1971.

6-19 Barrick, D. E., Theory of Ground-Wave Propagation Across A Rough Sea at Dekameter Wavelengths, Battelle Memorial Institute, AD-865-840, January 1970.

6-20 Chang, S., The Accessible Antenna Package, ECAC-TN-78-011, Electromagnetic Compatibility Analysis Center, Annapolis, MD, Volume 1, October 1978.

6-21 Chang, S., The Accessible Antenna Package, ECAC-TN-78-011, Electromagnetic Compatibility Analysis Center, Annapolis, MD, Volume II, September, 1979.

6-22 Chang, S., " A New Combined Antenna and Propagation Model," IEEE Antennas and Propagation Symposium Record, Quebec, June 1980.

6-23 Marcus, S., Description of the ECAC Far-Field Smooth-Earth Coupling Code (EFFSECC), ECAC-TN-80-014, Electromagnetic Compatibility Analysis Center, Annapolis, MD. August 1980.

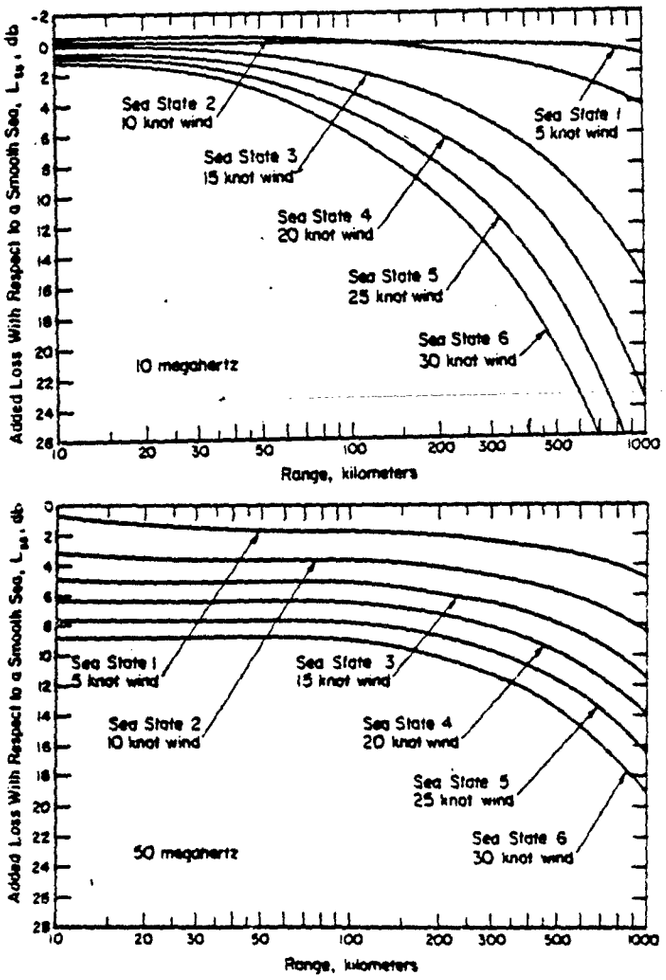

Figure 6-19. The additional loss due to the roughness of the surface of the sea. These are Barrick's theoretical predictions (see References 6-18 and 6-19).

extension of the best features of the NLAMBDA, IPS, and APACK codes. TABLE 6-1 is a simplified comparison of these models. Instructions for using EFFSECC appear in Reference 6-24.

For computing basic transmission loss over a smooth earth with heterogeneous ground constants, the ECAC Mixed Path Model is recommended. Instructions for using it are given in Reference 6-24.

GTE-Sylvania[6-25] has developed a code for predicting the effects of a rough sea on path loss. It gives results similar to Barrick's calculations, but uses simplified formulas. This code is not available at ECAC.

6.4 VALIDATION AND COMPARISON WITH OTHER MODELS

6.4.1 Propagation Over a Homogeneous Earth

Information about the accuracy of NLAMBDA and IPS is summarized here. It may be assumed that the accuracy of EFFSECC is comparable or slightly better than that of IPS and NLAMBDA. (Note: It is emphasized that there are many problems for which EFFSECC will be substantially more accurate than the other models. In particular, EFFSECC will provide better predictions of the off-axis coupling between antennas. However this category of problems was not

---

6-24 Baker, R. L., Radio-Wave Propagation: A User's Manual for the Computer Codes, ECAC-UM-80-001, Electromagnetic Compatibility Analysis Center, Annapolis, MD, September, 1980.

6-25 Kaliszewski, T., "Modifications and Extensions of the CCIR Groundwave Prediction Program for Rough Sea Paths," Program and Abstracts, 1976 National Radio Science Meeting, Amherst, MA, October 1976.

TABLE 6-1

A COMPARISON OF ECAC SMOOTH-EARTH MODELS

Feature	EFFSECC	NLAMBDA	IPS	APACK
Accounts for the effects of antenna pattern on the ratio of direct, reflected and surface wave	X			X
Accounts for horizontal and vertical components, on-axis and off-axis	X			X
Has a tropospheric scatter model that is more accurate than the YEH model	X			
Has an efficient scheme for selecting line-of-sight diffraction and troposcatter calculations	X	X	X	
Accurately accounts for refraction effects when an antenna is at a high altitude	X			
Has the option of accounting for phase interference between direct and ground reflected rays or assuming that it is zero	X		X	
Has the option of assuming that the phase difference between the direct and ground reflected rays is π	X			

examined in the NLAMBDA or IPS studies. Therefore the preceding statement about "comparable" accuracy is reasonable.)

6.4.1.1 The Colorado Plains and Ohio Data. The IPS was compared with measurements collected by the Institute of Telecommunication Sciences at sites in the plains of Colorado. The results of the comparisons are shown in TABLE 6-2.[6-26]

The error-trend analysis in APPENDIX C demonstrates that the data in TABLE 6-2 has the characteristics listed below:

a) The mean errors are normally distributed. Figure 6-20 demonstrates this graphically.
b) The mean errors are not strongly correlated with frequency.
c) The individual errors in each set (e.g., the 393 errors associated with the 393 path measurements in the Colorado Plains at 20.1 MHz) are normally distributed about the mean for the set.
d) The standard deviations listed in each set are strongly correlated with the log of the frequency of the transmissions being measured. Figure 6-21 illustrates this.
e) In view of a and c above, the overall distribution of errors at any frequency may be modeled as a normal distribution that is the sum of two other normal distributions. The mean of this distribution (i.e., the average over-prediction of loss) is 0.8 dB. The standard deviation of the overall distribution of errors is given by:

6-26 Meidenbauer, R., Chang, S., and Duncan, M., A Status Report on The Integrated Propagation System, ECAC-TN-78-023, Electromagnetic Compatibility Analysis Center, Annapolis, MD, September 1978.

TABLE 6-2

IPS PREDICTION ERROR[a]

Freq (MHz)	Location	Number of Paths	Mean Error (dB)	σ of Error (dB)
20.1	Colorado Plains	393	-5.1	6.0
49.7	Colorado Plains	393	-0.6	8.3
101.4	Colorado Plains	447	5.9	9.8
101.5	Colorado Plains	444	5.7	10.1
101.5	Colorado Plains	447	8.1	9.3
101.5	Colorado Plains	444	7.3	11.9
101.8	Northeast Ohio	67	13.5	12.2
101.8	Northeast Ohio	70	7.1	10.5
101.8	Northeast Ohio	70	7.5	11.2
910	Colorado Plains	105	3.8	12.8
910	Colorado Plains	104	3.3	12.2
910	Colorado Plains	148	0.5	13.3
1846	Colorado Plains	115	-2.1	15.8
1846	Colorado Plains	129	-3.6	17.0
1846	Colorado Plains	129	-5.4	15.6
4595	Colorado Plains	176	-2.0	21.2
4595	Colorado Plains	206	-6.4	20.7
4595	Colorado Plains	179	-7.2	20.6
9190	Colorado Plains	213	-1.9	25.3
9190	Colorado Plains	227	-5.1	25.7
9190	Colorado Plains	233	-7.1	23.2

Error = Predicted loss (dB) - Measured loss (dB)

[a]From Reference 6-26.

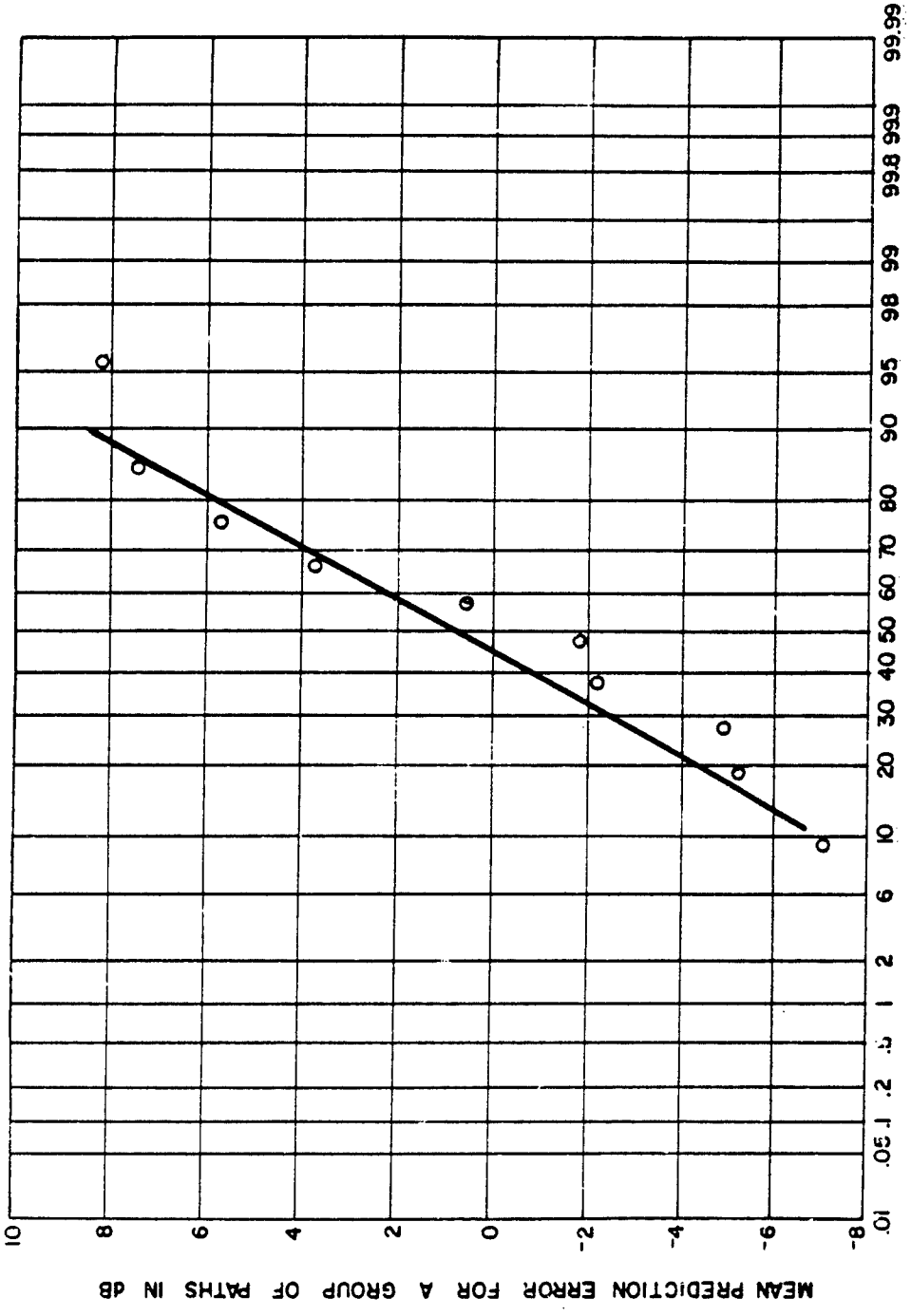

Figure 6-20. Distribution of the mean prediction error for the 21 groups of data. The solid line is the theoretical normal distribution having the same mean and σ. In addition to this graph, Chi-square testing supports the assumption that the distribution is normal.

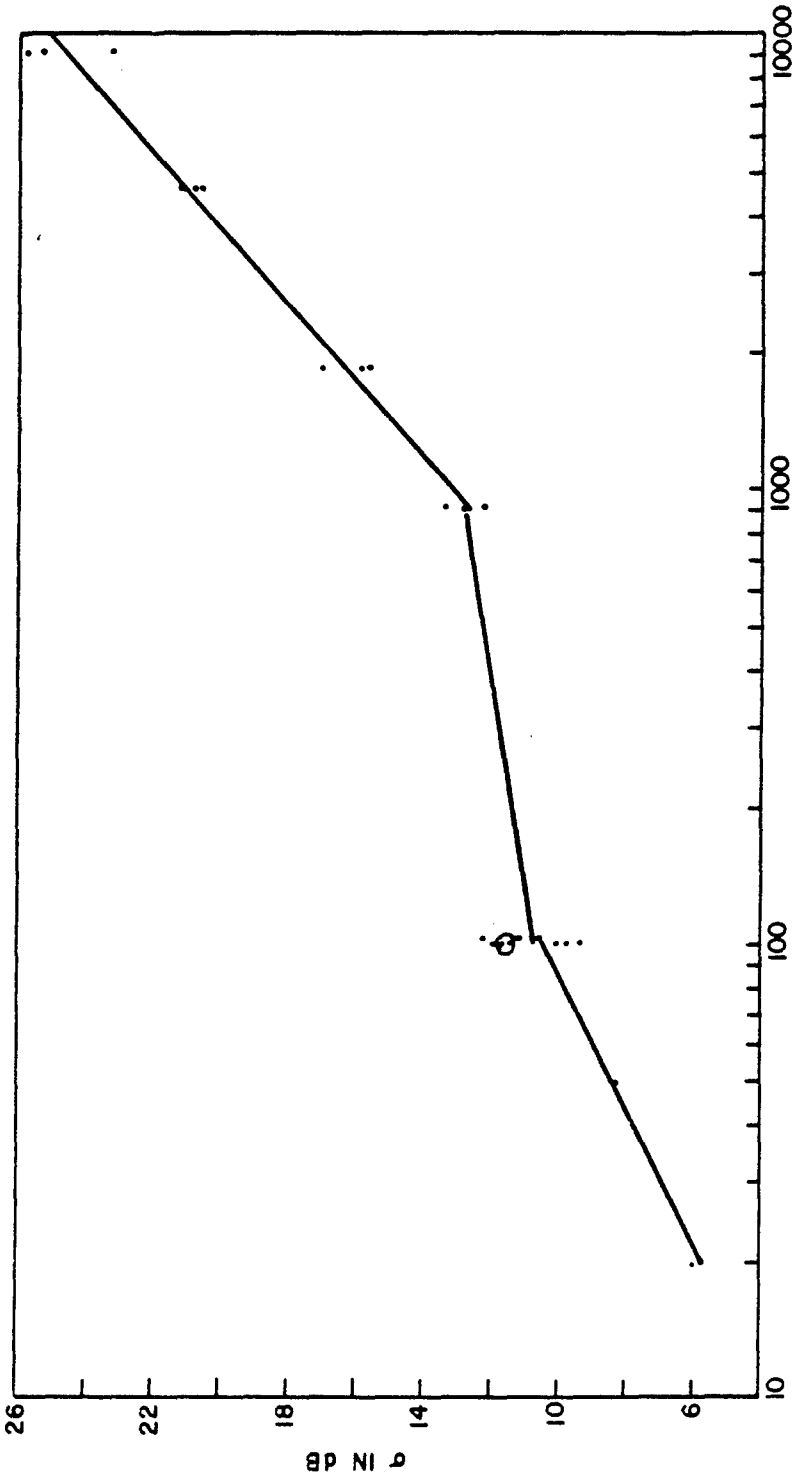

Figure 6-21. The standard deviation of the prediction error vs. frequency for the 23 groups of measurements. The two groups from the Colorado Mountains are circled. The square of the coefficient of linear correlation, ρ^2, excluding the mountain data is 0.89. The straight lines represent the regression fit given by Equations 1a, 1b, and 1c, of APPENDIX C of this Handbook.

$$\sigma = \sqrt{46.32 - 41.76 \log f + 46.02 \log^2 f} \qquad (6\text{-}4)$$

where f is the frequency in MHz and σ is in dB.

Equation 6-4 was based on the subset of measurements taken at frequencies between 20 and 101 MHz. As will be shown in the following subsection, Equation 6-4 is also suitable for use at frequencies as low as 2 MHz. Below 2 MHz, the polynomial used as the basis for the equation yields erroneous results.

Another aspect of the applicability of Equation 6-4 is topography. One scalar descriptor of the topographic features of a region is the terrain irregularity factor, ΔH. This parameter, as defined by Longley and Rice, is the difference between the elevation above which 10% of the terrain features lie and the elevation below which 10% of the terrain features lie. The ΔH for the Colorado Plains and Northeastern Ohio is (per Reference 6-27) 90 meters.

In the following subsections, predictions from smooth-earth propagation models are compared with measurements taken in geographic regions with other values of ΔH. The applicability of Equation 6-4 to these other data sets is noted.

6-27 Longley, A. G. and Rice, P. L., ESSA Technical Report ERL 79-ITS 67, Boulder, CO, July 1968.

6.4.1.2 The Arizona Data. Figures 6-22 through 6-30 (adapted from Reference 6-28) show how smooth-earth model predictions compare with measurements taken over hilly terrain near Flagstaff, Arizona. The limits within which 80% of the predictions should fall if Equation 6-4 is sufficiently universal to cover this type of data are also shown.

Figures 6-22, 6-25, and 6-28 show data taken in a region of Arizona in which the terrain irregularity, ΔH, was 223 meters. Figures 6-23, 6-26, and 6-29 show data taken in a region in which the terrain irregularity was 351 meters. The terrain irregularity for Figures 6-24, 6-27 and 6-30 was 448 meters.

The 80% limits (i.e., $\pm 1.29\sigma$) computed from Equation 6-4 encompass 83% of the 223 meter data, but only 57% of the 351 meter and 69% of the 448 meter data. Therefore, in the 2-32 MHz band, Equation 6-4 provided conservative estimates of the smooth earth model's accuracy for the 223 meter measurements. In the more irregular terrain (ΔH = 351 and 448 meters), the errors were larger than those predicted by Equation 6-4.

Though the mean errors for each of the nine sets of data (3 frequencies at each of the 3 ΔH's) are all different, there is no obviously consistent trend with regard to frequency or ΔH. More research on this matter is needed.

6.4.1.3 The Colorado Mountains Data. Comparisons between predictions of the IPS smooth-earth model and measurements taken at 101 MHz over paths in the Colorado Mountains were also reported in Reference 6-26. In one set of 137 measurements, the mean error was -10.4 dB and the σ was 11.5 dB. In a second

---

6-28 Whiteman, R. A., A Supplement to an Analysis of Bell Aerosystems Co.'s, Flagstaff Propagation Measurements, ECAC-CR-81-029, Electromagnetic Compatibility Analysis Center, Annapolis, MD, December 1981.

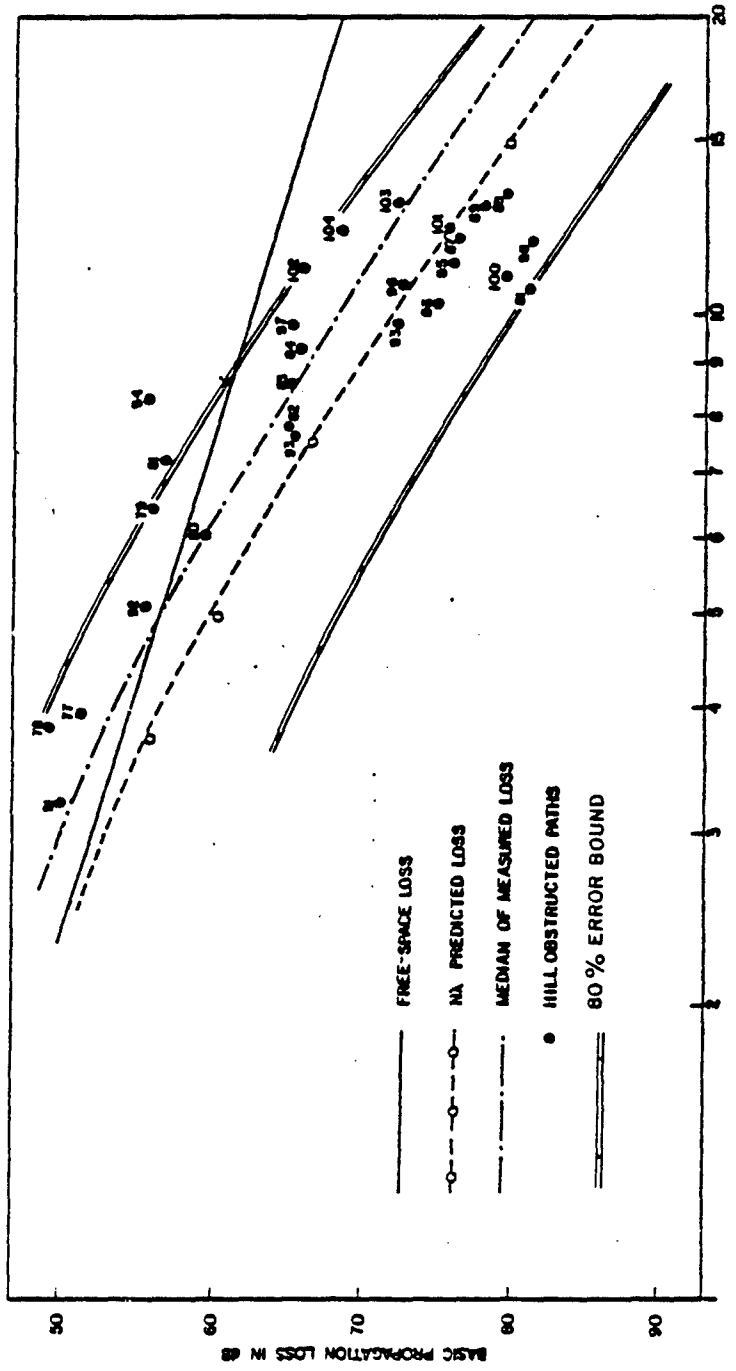

Figure 6-22. A comparison between a smooth-earth model, NA, and the Bell Aerosystems propagation measurements taken near Flagstaff, Arizona, where frequency = 2 MHz, Δh = 221 m, h_t = 5.1 m, and h_r = 3.6 m. (The numbers on the data points identify particular paths. More information about each path can be obtained by consulting Reference 6-28.)

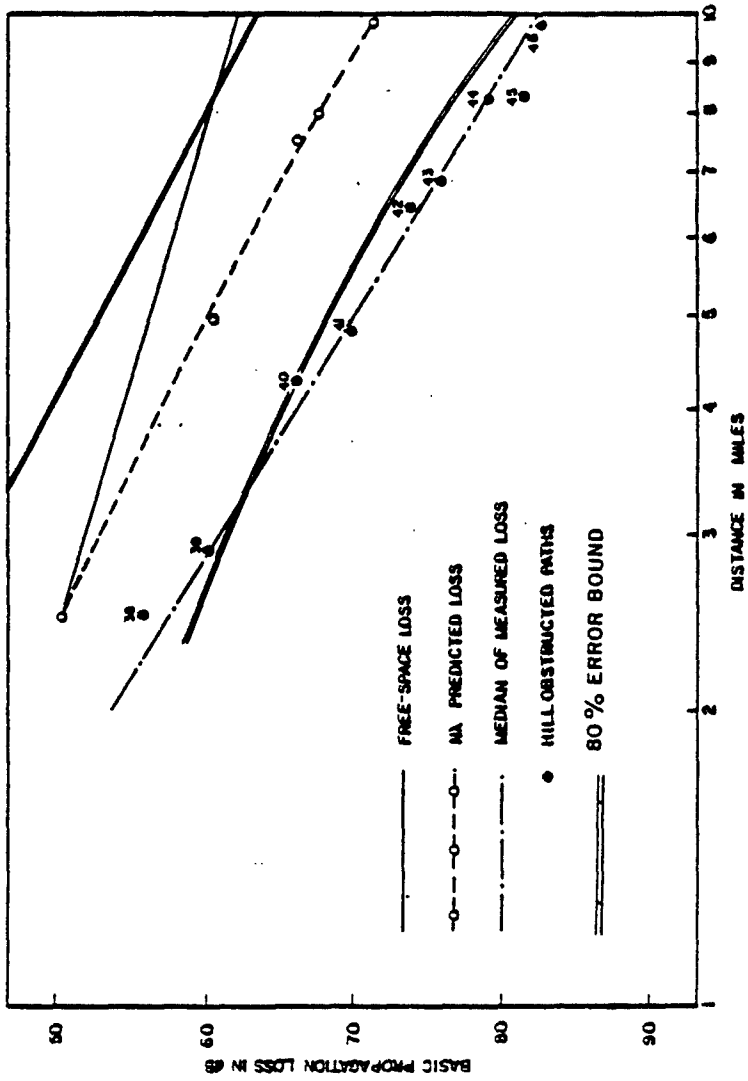

Figure 6-23. A comparison between a smooth-earth model, Nλ, and the Bell Aerosystems propagation measurements taken near Flagstaff, Arizona, where frequency = 2 MHz, Δh = 351 m, h_t = 5.1 m, and h_r = 3.6 m.

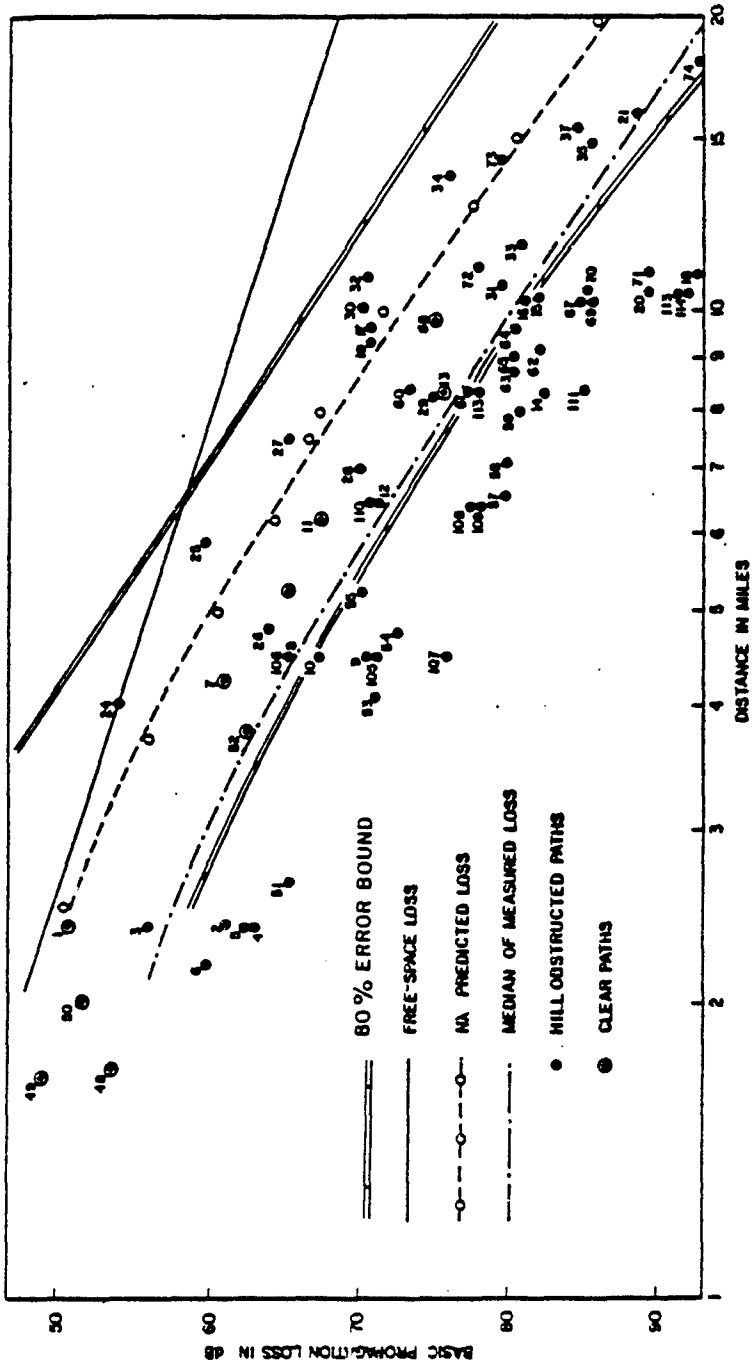

Figure 6-24. A comparison between a smooth-earth model, Nλ, and the Bell Aerosystems propagation measurements taken near Flagstaff, Arizona, where frequency = 2 MHz, Δh = 448 m, h_t = 5.1 m, and h_r = 3.6 m.

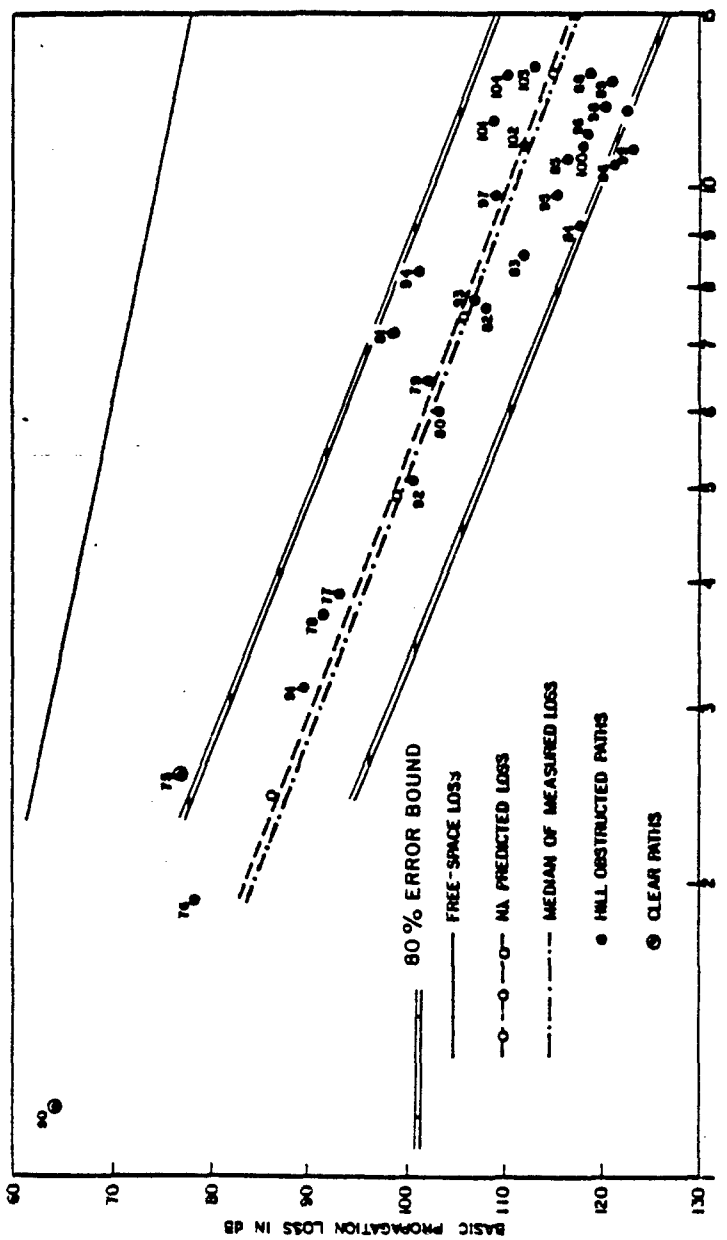

Figure 6-25. A comparison between a smooth-earth model, Nλ, and the Bell Aerosystems propagation measurements taken near Flagstaff, Arizona, where frequency = 8 MHz, Δh = 223 m, h_t = 5.1 m, and h_r = 3.6 m.

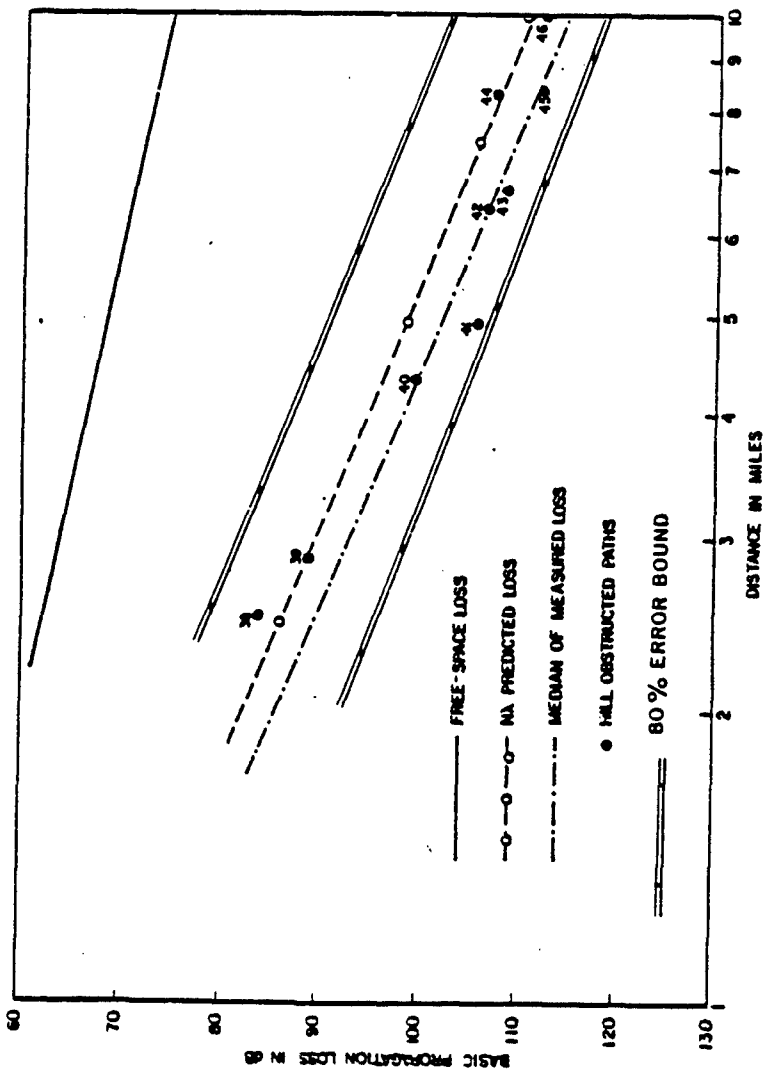

Figure 6-26. A comparison between a smooth-earth model, Nλ, and the Bell Aerosystems propagation measurements taken near Flagstaff, Arizona, where frequency = 8 MHz, Δh = 351 m, h_t = 5.1 m, and h_r = 3.6 m.

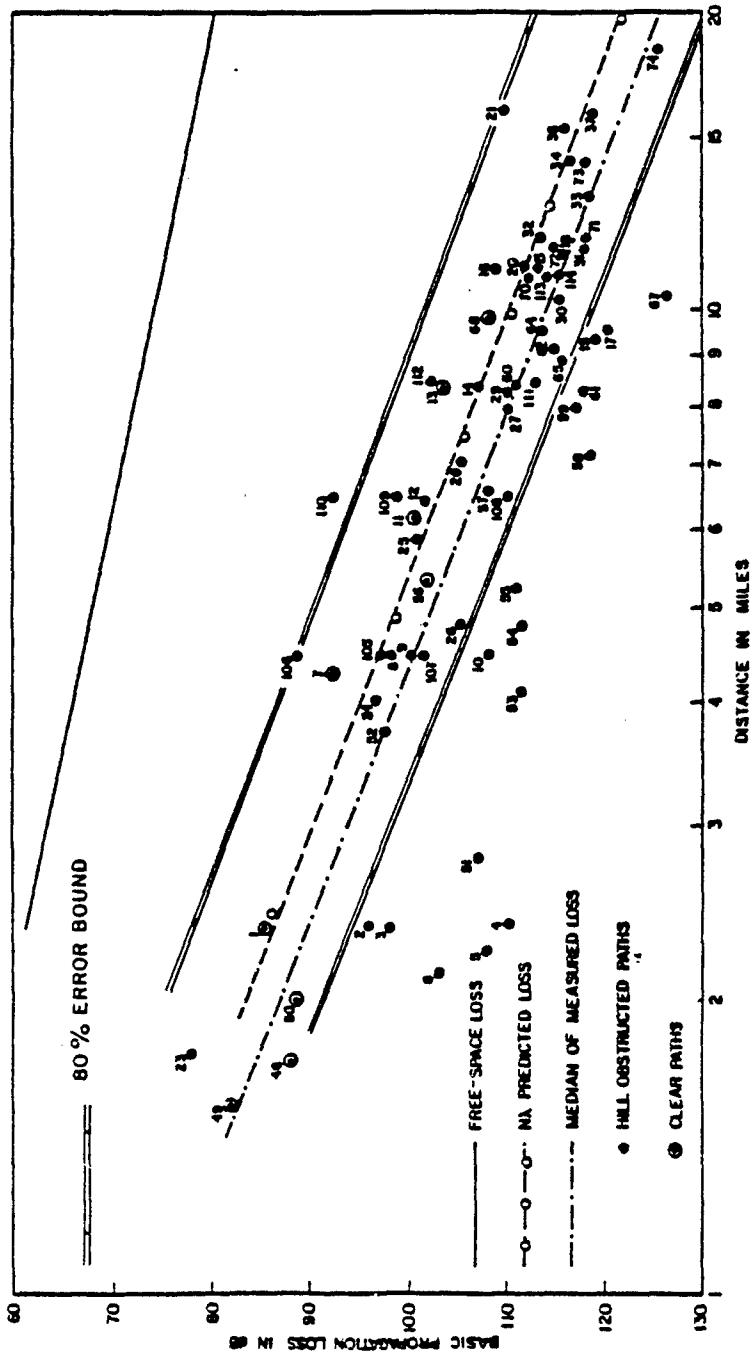

Figure 6-27. A comparison between a smooth-earth model, Nλ, and the Bell Aerosystems propagation measurements taken near Flagstaff, Arizona, where frequency = 8 MHz, Δh = 448 m, h_t = 5.1 m, and h_r = 3.6 m.

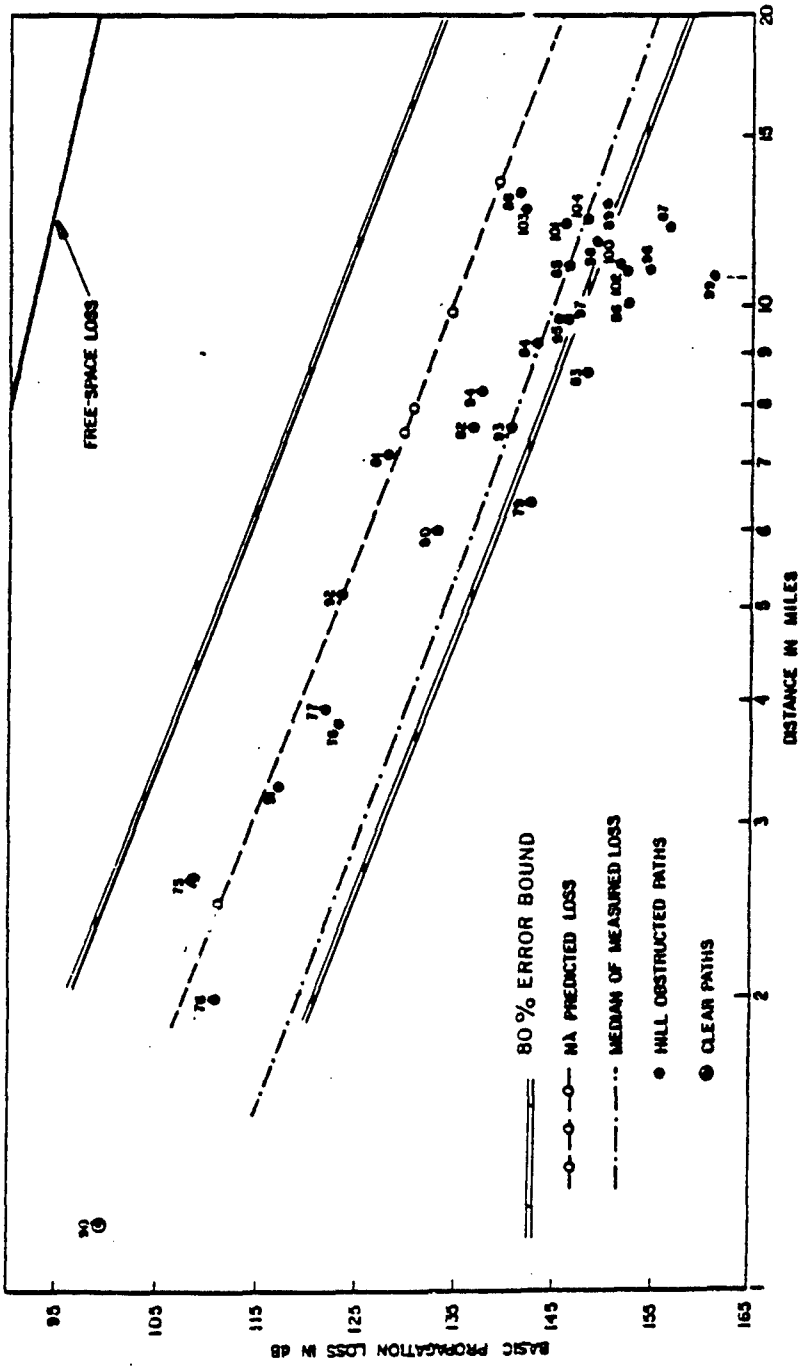

Figure 6-28. A comparison between a smooth-earth model, Nλ, and the Bell Aerosystems propagation measurements taken near Flagstaff, Arizona, where frequency = 32 MHz, Δh = 223 m, h_t = 5.1 m, and h_r = 3.0 m.

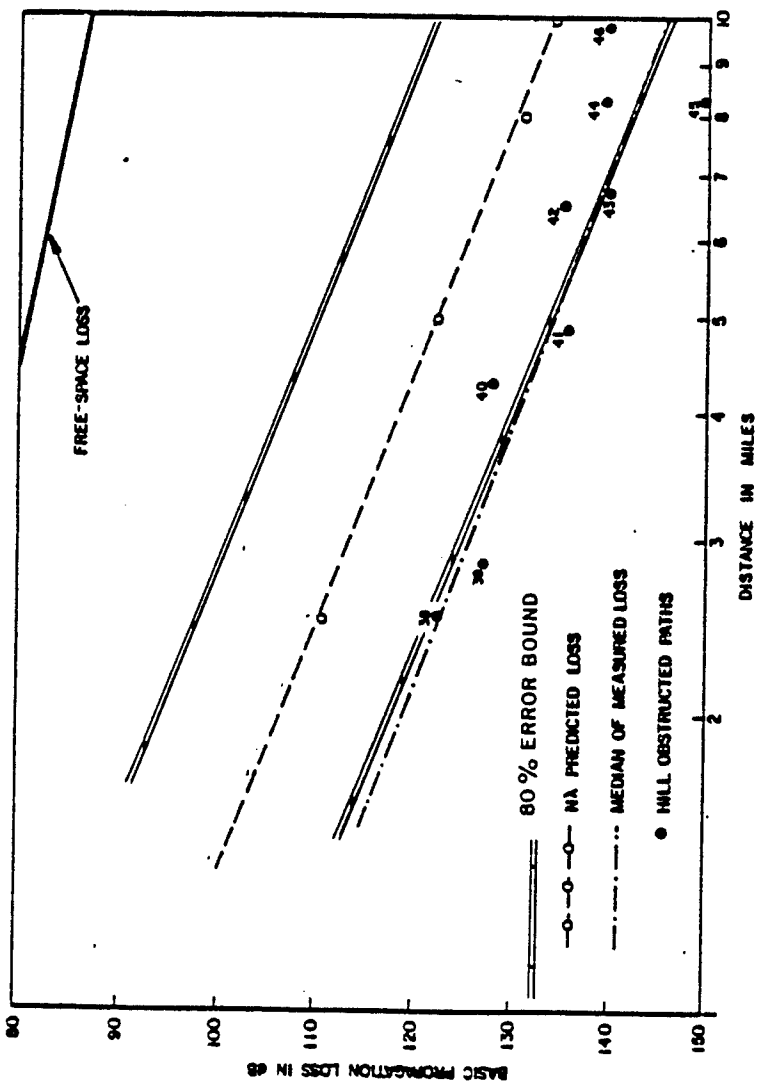

Figure 6-29. A comparison between a smooth-earth model, Nλ, and the Bell Aerosystems propagation measurements taken near Flagstaff, Arizona, where frequency = 32 MHz, Δh = 351 m, h_t = 5.1 m, and h_r = 3.0 m.

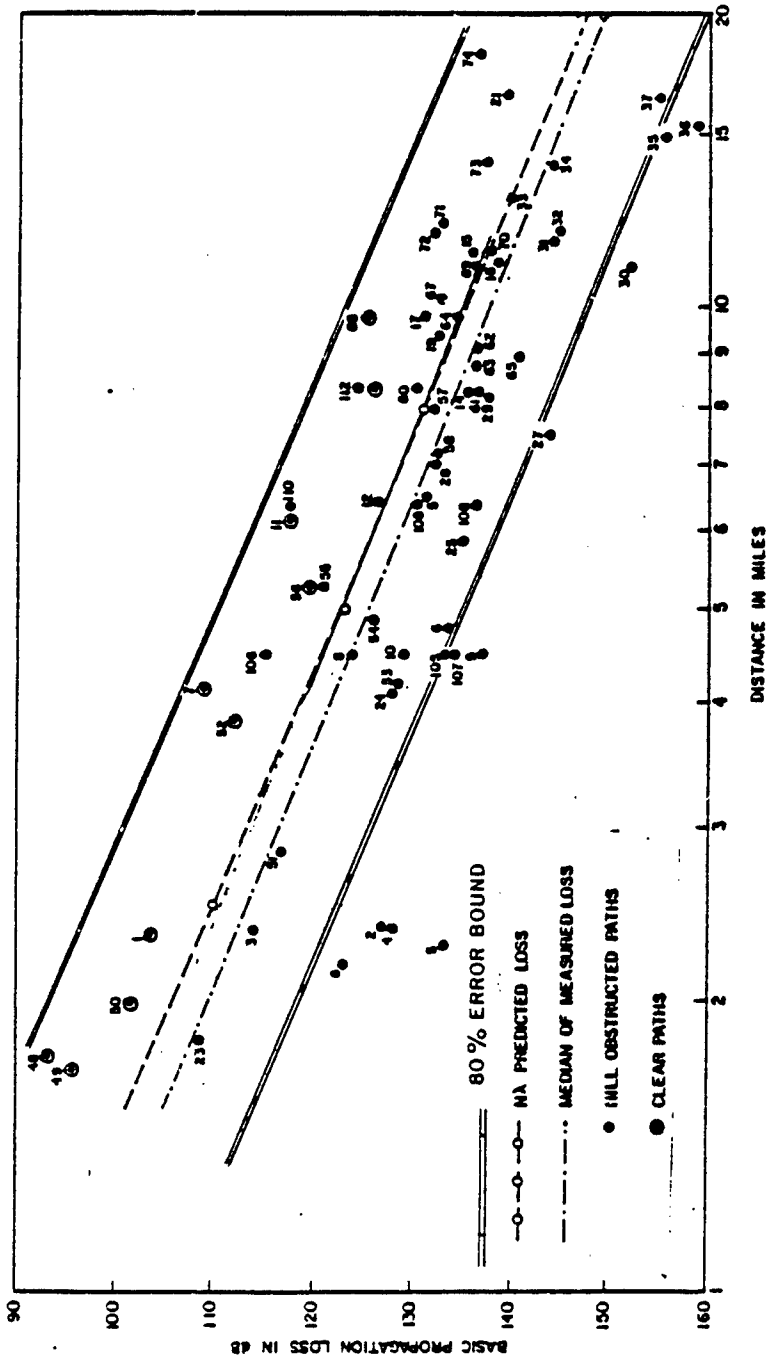

Figure 6-30. A comparison between a smooth-earth model, Nλ, and the Bell Aerosytems propagation measurement taken near Flagstaff, Arizona, where frequency = 32 MHz, Δh = 448 m, h_t = 5.1 m, and h_r = 3.0 m.

set of 137 measurements, the mean error was -13.4 dB and the standard deviation was 11.6 dB. If it is assumed that the distribution of errors about the mean is normal, then only 61% of the errors fall within the 80% limits predicted by Equation 6-4. The terrain irregularity of the Colorado Mountains is 650 meters.

6.4.1.4 The Japanese Data. Figures 6-31 and 6-32 (from Reference 6-29) show the results of a comparison between predictions and measurements taken over paths located near Tokyo, Japan.

The data shown in Figure 6-31 were taken over a fresh-water lake, where ΔH was approximately 0 meters. The 80% error limits computed from Equation 6-4 encompass 100% of the data.

The data shown in Figure 6-32 were taken in a region with a ΔH of approximately 80 meters. 97% of the measured points fall within the 80% limits.

Thus, for these two sets of data, Equation 6-4 was adequate for providing a conservative statistical description of the error limits.

6.4.1.5 The Southern California Over-Sea Data. P. Hansen of NOSC made measurements[6-30] in the 4-32 MHz band for a 24-hour period in June along a 235-km over-sea path off the coast of Southern California. Figure 6-33 illustrates the measured and predicted loss values. The dotted line shows the prediction using a smooth-earth model under the assumption of a standard

---

6-29 Kinase, A., NHK Technical Monograph NO. 14, Japan Broadcasting Corporation, March 1969.

6-30 Hansen, P., "Measurements of Basic Transmission Loss for HF Ground-Wave Propagation Over Sea Water," Radio Science, May 1977.

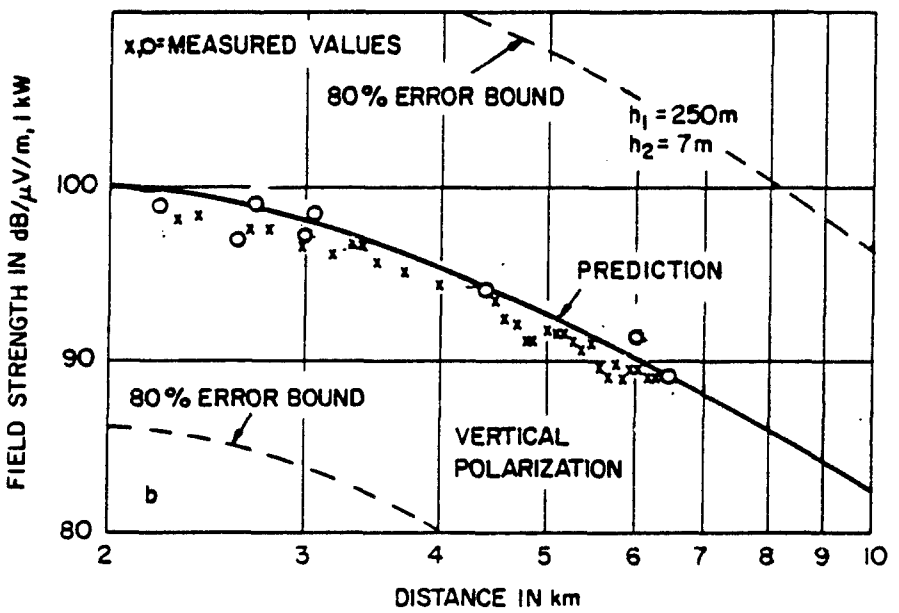

Figure 6-31. Comparisons between measured field strengths and field strengths predicted by a smooth-earth model (like EFFSECC), 91.25 MHz. Surface is a fresh water lake (Reference 6-29). The 80% error limits derived from Equation 6-4 encompass the measurements with a wide margin.

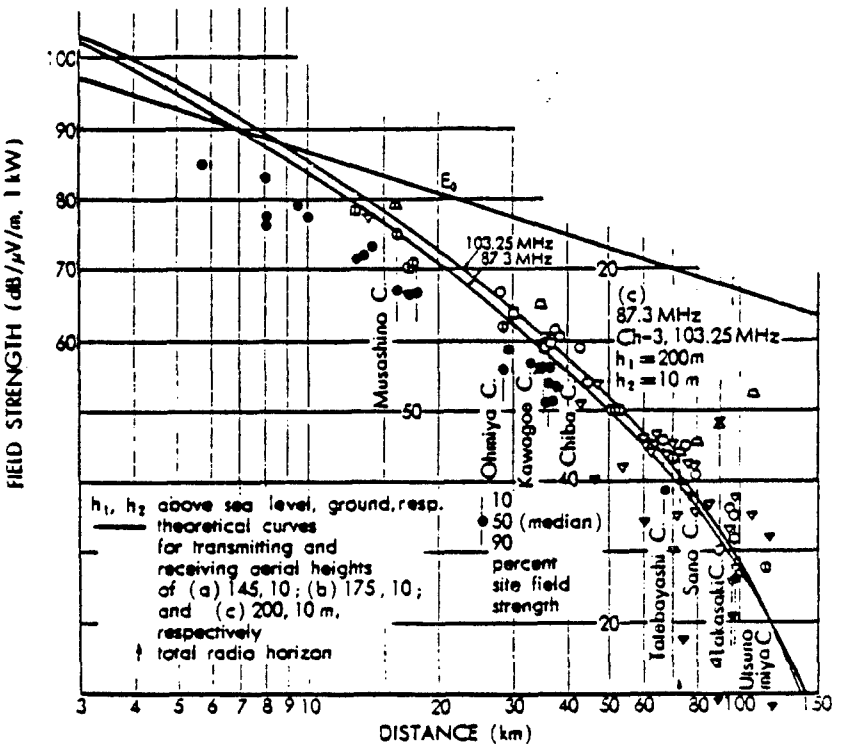

Figure 6-32. Comparisons between measured field strengths and field strengths predicted by a smooth-earth model (like EFFSECC), 87-103 MHz. The surface is a plain near Tokyo with a range of terrain height variations that is less than 100 meters (Reference 6-29). The 80% error limits derived from Equation 6-4 are ±15.6 dB. These bounds (not shown) will encompass more than 80% of this set of measurements.

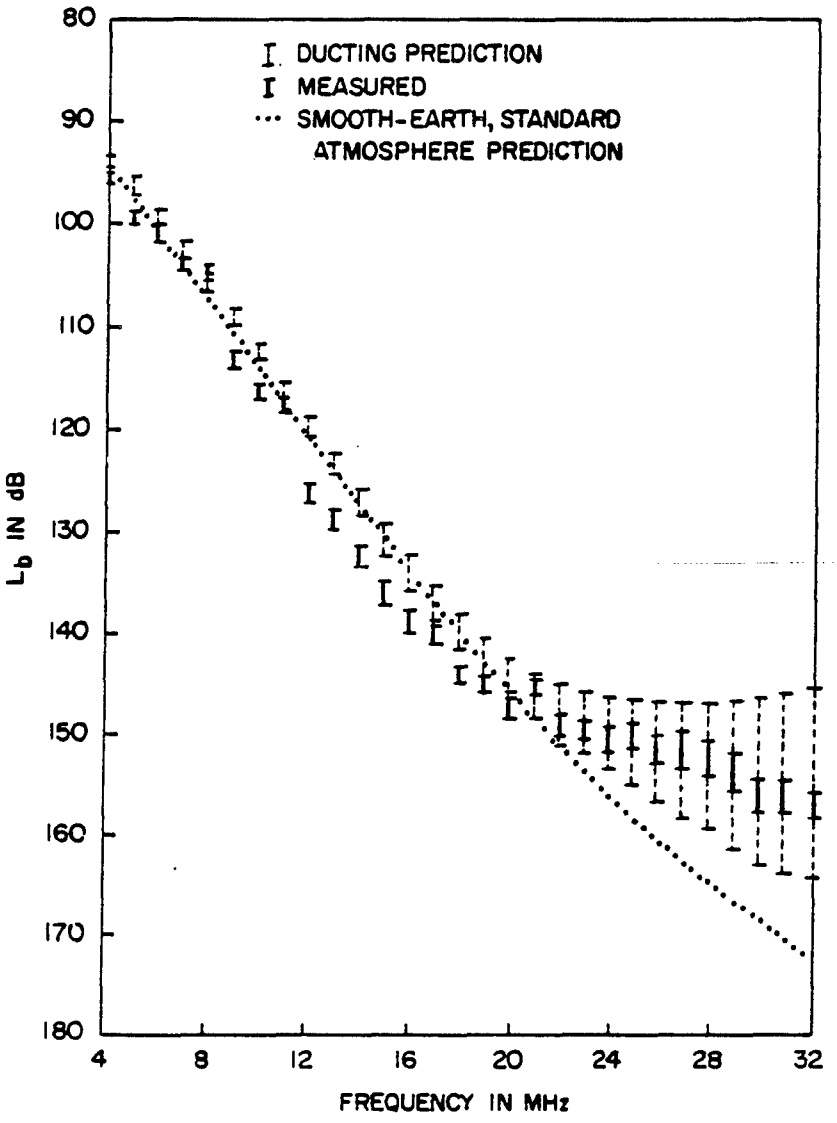

Figure 6-33. Comparison between predicted and measured loss values for a 235-km over-sea path near southern California (Reference 6-30). The data represents a full 24 hour period. The groundwave loss prediction made with a standard atmosphere is 15 dB too high at 32 MHz. Accounting for ducting will reduce the bias in the predictions.

refractive index profile. For frequencies higher than 20 MHz, this model predicted up to 15 dB too much loss for the entire 24 hour period. Pappert and Goodhart[6-31] made predictions in light of the actual measured refractive index profile and were able to encompass the measured values. The actual atmospheric profile allowed ducting above about 20 MHz.

It is to be noted that the predicted (by Pappert) variability of the data is much larger than the observed variability. Thus a steady state phenomenon such as tropospheric scatter may really be the dominant physical effect. The smooth-earth model used in the study did not account for the tropospheric scatter mechanism at these frequencies.

Below 20 MHz, there is a tendency for the smooth-earth, standard atmosphere model to predict approximately 5 dB less loss than was measured. Hansen (Reference 6-30) observed that Barrick's (see Section 6.2.3) rough-sea loss factors were appropriate to make up this difference.

6.4.1.6 The New Hampshire Over-Sea Data. In another Navy-sponsored program, Cullen measured the field strength at 30 MHz over the sea near New Castle Island, New Hampshire.[6-32] Comparisons between predicted and measured loss values are shown in Figure 6-34. At 56 kilometers, the smooth-earth model predicted 9 dB more loss than was measured.

6-31 Pappert, R. A. and Goodhart, C. L., "A Numerical Study of Tropospheric Ducting at HF," Radio Science, September 1979.

6-32 Cullen, F. P., Propagation Measurements for Over-Water Low-Angle and Over-Horizon Communications With Buoys, Sanders Associates, Nashua, NH September, 1969. AD 861 695. Figure 4-13.

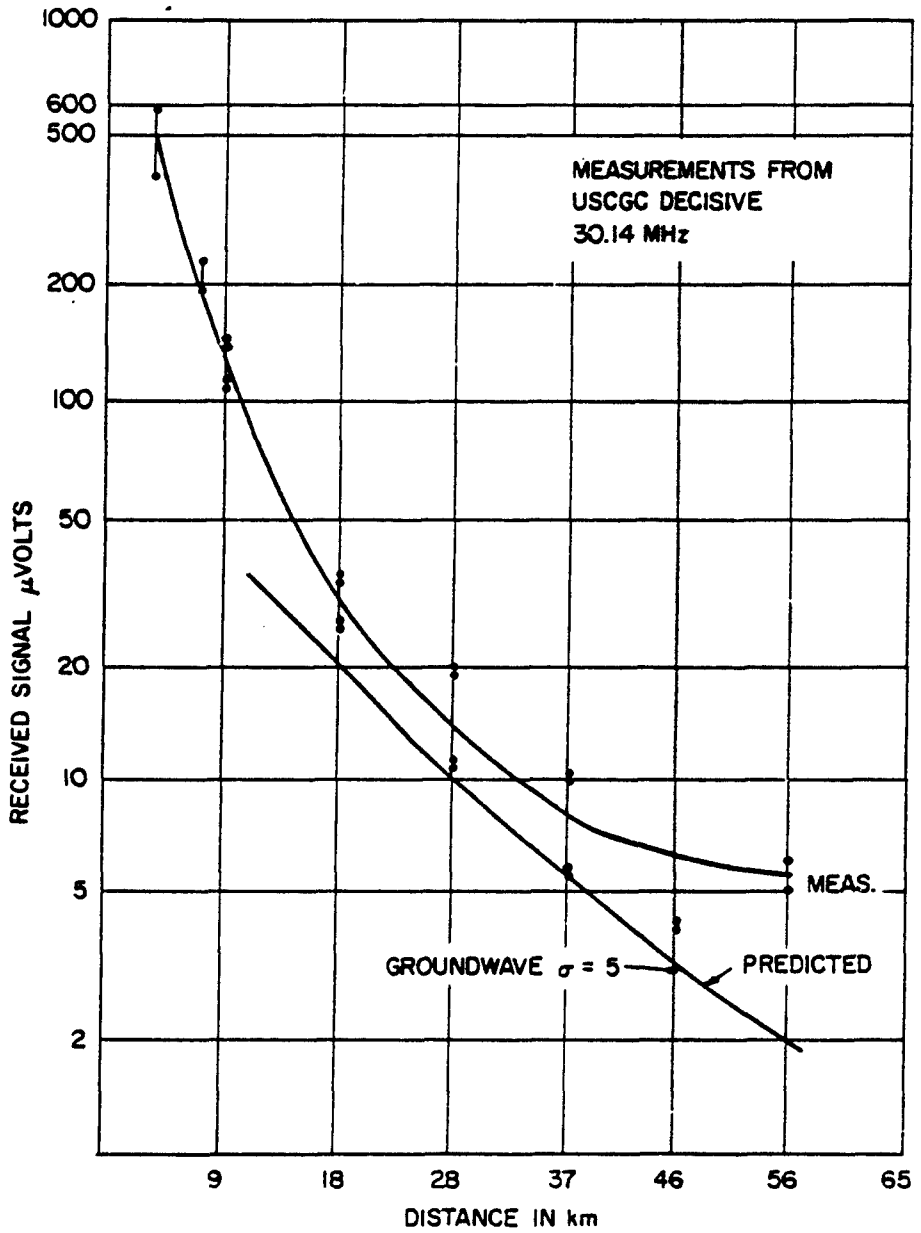

Figure 6-34. A comparison between measured and predicted field strength values for an oversea path at 30 MHz (Reference 6-32). Possible reasons for the bias in the predictions are presented in the text.

A study of Sylvania's duct-occurrence data[6-33] indicates that it is extremely unlikely that a 30-MHz signal will be ducted in the North Atlantic near New Hampshire. Ionospheric reflections at these short distances at 30 MHz are also unlikely. It is possible that tropospheric scatter is the mechanism that produces the discrepancy between the predictions and the measurements. The smooth-earth model used in this study did not account for tropospheric scatter at the measurement frequencies.

6.4.1.7 Summary of the Validation of Smooth Earth Models for Use in Predicting the Loss Over Ground With a Homogeneous Conductivity. Predictions from the IPS smooth earth propagation model were compared with 2700 measurements taken in the 20-100 MHz band over paths in the Colorado Plains and northeastern Ohio. It was found that the mean error was an 0.8 dB overprediction of loss. The standard deviation of the errors was calculated using Equation 6-4. A simplified description of the terrain in these regions of Colorado and Ohio is that 80% of the terrain elevations lie in a range of 90 meters. This range is given the symbol ΔH.

The standard deviation bounds the errors that occurred when smooth earth models were used to predict the losses along paths in Arizona (ΔH = 223 meters) and Japan (ΔH = 0, 80). Observed errors were larger than those predicted by Equation 6-4 when a smooth-earth model was applied to problems in the Colorado mountains (ΔH = 650 meters) and other regions in Arizona (ΔH = 351 meters and 448 meters).

The comparisons between model predictions and measurements taken over sea water paths indicated good agreement below 20 MHz. Hansen (Reference 6-30)

6-33 Ortenburger, L. N., et. al., Radiosonde Data Analysis III, GTE Sylvania, Mountain View, CA, December 1978.

maintains that the use of Barrick's rough sea factors improves the prediction accuracy in this band.

In the two cases examined here, the smooth-earth model with an assumed standard atmosphere overpredicted the loss over sea water in the 20-32 MHz region. Pappert (Reference 6-31) was able to show that ducting conditions could explain the mean error in one case. A possible explanation in both cases is tropospheric scatter. Neither the ECAC nor non-ECAC smooth-earth models used in the study account for this phenomenon at frequencies lower than 40 MHz.

6.4.1.8 Comparisons With Other Models. Section 6 of the Meidenbauer and Chang report (Reference 6-26) shows a comparison between IPS predictions and the CCIR smooth-earth curves that were included in the 1974 plenary report. The largest differences occurred in the troposcatter region. The use of a CCIR-based troposcatter model in EFFSECC should reconcile this discrepancy.

The EFFSECC has greater flexibility than Berry's 1966 model[6-34] because the latter

a) Does not include tropospheric scatter effects

b) Uses an effective-earth's radius to account for refraction effects. Thus, it only accounts for a linear decrease in atmospheric density. EFFSECC accounts for an exponential decrease.

c) Does not apply to elevated antennas that are within line-of-sight of each other.

d) Does not allow prediction of off-axis coupling between antennas.

[6-34] Berry, L. A. and Chrisman, M. E., NBS Report 9178, March 1966.

EFFSECC should be at least as useful as the FCC broadcast model[6-35] because the latter:

a) Is restricted to frequencies in the AM broadcast band

b) Is based on a set of curves that were imperfectly drawn (per Anderson)

c) Does not allow off-axis coupling predictions.

6.4.2 Validation of the Mixed-Path Model and Comparison With Other Models

6.4.2.1 Validation. Riggins (Reference 6-12) compared predictions of the ECAC Mixed-Path Model with measurements. His results are reproduced in TABLES 6-3 and 6-4. The former is a summary of information about the paths over which the measurements were taken. The latter shows the results of comparisons between model predictions and measurements. The errors are all

---

6-35 Anderson, H. R., "A Computer Program System for Predicting and Plotting Mediumwave Broadcast Groundwave Field Strength Contours," IEEE Trans. on Broadcasting, September 1980.

TABLE 6-3
DATA USED IN VALIDATION OF MIXED PATH MODEL[a]

Data Set Number	Frequency (MHz)	Type	Ground		Conductivity (mhos/m)	Reference
			Range (km)	Dielectric Constant		
1	77.575	Land	0-1.4	15	0.01	6-11, P. 128
		Sea	1.4-3.6	80.	4.	
		Land	3.6-5.0	15	0.01	
2	3.13	Land	0-87.5	5	0.01	6-37, P. 215
		Sea	87.5-198.0	80.	4.	
3	1.176	Land	0-76.0	5.	0.01	6-37, P. 210
		Sea	76.0-103.0	80.	4.	
		Land	103.0	5.	0.01	
4	1.122	Land	0-225.3	5	0.01	6-38, P. 115
		Sea	225.3-378.1	80.	4.	
5	0.540	Sea	0-60.0	80.	4.	6-39, P. 372
6	0.800	Land	60.0-162.0	15.	0.003	6-39, P. 373
		Land	162.0-182.0	15.	0.006	
		Sea	182.0-210.0	80.	4.	
		Land	210.0-215.0	15.	0.003	
7	0.540	Land	0.-8.0	15.	0.009	6-39, P. 374
8	0.800	Sea	8.0-78.0	80.	4.	6-39, P. 375
		Land	78.0-180.0	15.	0.003	
		Sea	180.0-205.0	80.	4.	
		Land	205.0-208.0	15.	0.003	
9	1.060	Land	0.-78.0	15	0.01	6-37, P. 220
		Sea	78.0-116.0	80.	4.	
		Land	116.0-154.0	15.	0.002	
		Sea	154.-234.0	80.	4.	
		Land	234.-243.0	15.	0.003	
10	0.537	Sea	0-82.0	80.	4.	6-40, P. 492
11	0.922	Land	82.0-298.0	10.	0.011	6-40, P. 493
12	1.050					6-40, P. 493
13	1.240					6-40, P. 494

[a]From Reference 6-12.

TABLE 6-4
COMPARISON OF MEASURED DATA WITH MIXED PATH MODEL PREDICTIONS[a]

Data Set No.	Frequency (MHz)	Number of Measurements Along Path	Path Loss Difference (Measured, dB, - Predicted Mixed Path Model, dB)			Absolute Value of Maximum Difference Between Predicted Loss, dB, For Mixed Path Model and homogeneous-ground-constant Model (Using Ground Type of First Segment)
			Mean	Standard Deviation	R.M.S.	
1	77.575	33	0.74	1.26	1.46	20.4
2	3.13	20	0.06	0.81	0.81	27.1
3	1.176	14	0.15	0.37	0.40	6.0
4	1.122	25	3.00	1.14	3.21	19.1
5	0.540	6	0.92	0.58	1.09	14.9
6	0.800	7	-0.81	3.14	3.24	25.6
7	0.540	7	-3.27	1.55	3.62	13.9
8	0.800	6	-1.42	1.46	2.04	18.6
9	1.060	12	-4.83	2.30	5.35	14.7
10	0.537	30	1.03	1.13	1.53	11.9
11	0.922	34	0.66	1.83	1.95	20.5
12	1.050	31	-0.01	1.36	1.37	21.6
13	1.240	36	0.52	1.56	1.65	22.9

[a]From Reference 6-12.

well within the bounds predicted by Equation 6-4. The measurements used in the study were taken from Reference 6-11 and References 6-36 through 6-39.

More measurements are available[6-40,6-41] should a more comprehensive study be desired.

6.4.2.2 Comparison of the ECAC Mixed Path Model With Other Models. Ott has developed the Wagner model, which accounts for both the inhomogeneity of ground constants and the irregularity of the terrain surface.[6-17, 6-41, 6-42] The model was improved with funding by ECAC. Though the model has been shown to be occasionally suitable for use at frequencies as high as 60 MHz (Reference 6-17), it is not clear that it will consistently converge to an accurate result for frequencies higher than 2 MHz (Reference 6-41).

6-36 Millington, G. and Isted, G., "Groundwave-Wave Propagation Over An Inhomogeneous Smooth Earth," Proceedings of the IEE, Vol. 97. Part III (Radio and Communication Engineering), No. 48, July, 1950.

6-37 Elson, N., "Ground-Wave Propagation Across A Land/Sea Boundary," Nature, Vol. 164, July 16, 1949.

6-38 CCIR, Doc. 148E (Denmark), Fifth Meeting, Stockholm, Sweden, July 1948.

6-39 Kirke, H. L., "Calculation of Ground-Wave Field Strength Over A Composite Land and Sea Path," Proceedings of the IRE, May, 1949.

6-40 Damboldt, T., "HF Groundwave Field-Strength Measurements on Mixed Land-Sea Paths," IEE Conference Publication 195, London, April 1981.

6-41 Ott, R. H., NTIA Report 79-20, May 1979.

6-42 Ott, R. H., "An Alternative Integral Equation for Propagation Over Irregular Terrain," Radio Science, Vol 6, No. 4, 1971.

6.4.3 Validation of Barrick's Model for Propagation Over a Rough Sea

Hansen's report demonstrated that, for his one path, Barrick's rough-sea factors were valid in the 4-18 MHz band (Reference 6-31).

6.5 CONCLUDING REMARKS

1. Subsection 6.4.1 shows that, even though the effects of terrain on path loss diminish with decreasing frequency (per Equation 6-4), they are still substantial below 40 MHz. Available techniques (e.g., the WAGNER model) are not fully satisfactory for modeling phenomena in this range.

2. The time variability of signals in this band (0.1-40 MHz) has not been modeled. Figures 6-1 and 6-2 show that ionospheric effects can cause fading even at short transmitter-receiver distances. Recent Navy studies show that tropospheric anomalies cause substantial signal fluctuations (Reference 6-31) at frequencies as low as 20 MHz. Present time-variability models do not address behavior below 40 MHz.

3. For the region in which interference between the direct and ground-reflected waves is substantial (e.g., distances in the 1-20 km range for curve 10 in Figure 6-4), statistical representations appear to be desirable and should be investigated. The IF-77 model (discussed in Chapter 8) of this handbook represents one embodiment of this technique that should be studied.

4. The effect of tropospheric scatter as a non-anomalous propagation mechanism at frequencies below 40 MHz is not included in this chapter's curves. This phenomenon may be responsible for the discrepancies between the over-sea measurements and smooth-earth groundwave-model predictions shown in Sections 6.4.1.5 and 6.4.1.6. The Longley-Rice empirical model (Reference 6-28) accounts for troposcatter at frequencies as low as 20 MHz. The importance of this phenomenon at these frequencies should be reviewed.

5. Studies by several other authors confirm the acceptability of a smooth-earth model for predicting the median strength along radials at frequencies as low as 40 MHz:

a. The Fine-Egli Model,[6-43,6-44] based on broadcast data, predicts that a bias from smooth-earth predictions will not be observed below 40 MHz. A range of terrain irregularities was represented in the data.

b. Saxton and Harden[6-45] showed good agreement along two radials at 62 and 103 MHz. The terrain irregularity was about 250 meters.

c. Brown's study of two radials,[6-46] one with a ΔH of about 75 m, the other with ΔH about 250 m, showed good median agreement with smooth-earth predictions at 67 MHz.

d. Dyer[6-47] observed that this type of model accurately described measurements over sea water paths at 30 MHz on the east coast of Florida.

6-43 Fine, H., UHF Propagation Within Line of Sight, T.R.R. Report No. 2.4.12, Federal Communications Commission, Washington, DC, June, 1951.

6-44 Egli, J., "Radio Propagation Above 40 MHz Over Irregular Terrain," Proc. IRE, October 1957.

6-45 Saxton, J.A., and Harden, B.N., "Ground-Wave Field Strength Surveys at 100 and 600 MHz," Proc. IEE (London), Vol. 101, Part III, 1956, p. 215.

6-46 Brown, G.H., Epstein, J., and Peterson, D.W., "Comparative Propagation Measurements; Television Transmitters at 67.25, 288.510 and 910 Megacycles, RCA Review, June 1948.

6-47 Dyer, F.B., et al, "Radio-Wave Propagation Measurements Over Sea Water," IEE Conference Publication 169, Antennas and Propagation, 1978.

Thus there is further support for the premise of this Chapter that smooth-earth models, with confidence limits, are a reasonable approach to predicting basic transmission loss for groundwave-coupled links at frequencies below about 40 MHz.

6. The FCC also estimated a variability of the data about the predicted median value. Their σ was about 6 dB at 40 MHz (see Reference 6-44, Figure 4). Equation 6-4 leads to a σ of 10 dB at this frequency. The restriction of the FCC data to line-of-sight circuits with one very high antenna may be partly responsible for this difference.

7. A recent study by S. Rotheram indicates that, at frequencies below 10 MHz, increased theoretical accuracy is obtained by a more rigorous accounting for the non-linear change in the refractive index of the earth's atmosphere with height. His curves, which are for a zero-height antenna, appear in Reference 6-48.

6-48 Rotheram, S., "Ground-Wave Propagation, Part 2: Theory for Medium and Long Distances and Reference Propagation Curves," Proc. IEE, Part F, October, 1981.

CHAPTER 7

EARTH-SPACE PROPAGATION, 100 MHz - 100 GHz

By: M. Weissberger

7.1 INTRODUCTION

This chapter presents a model (SATPROP) that can be used to predict propagation loss over line-of-sight satellite-to-ground links. The prediction consists of both a median loss and the time variability statistics expected over the period of one year. Section 7.2 contains formulas and graphs that can be used to calculate predictions manually. Section 7.3 describes the status of the SATPROP computer code of this procedure. Section 7.4 compares this model's predictions with measurements and with the predictions of other models. Section 7.5 provides concluding remarks.

7.2 A MANUAL METHOD FOR LOSS PREDICTIONS

This procedure is based on References 7-1 and 7-2. The formula for the basic transmission loss is:

$$L_B(P) = L_{BFS} + A_{OW} + A_S(P) + A_R(P) \qquad (7\text{-}1)$$

7-1 Weissberger, M. A. and Duncan, M. S., Propagation Factors in Satellite-to-Ground Communications, ECAC-TN-77-004, Electromagnetic Compatibility Analysis Center, Annapolis, MD, September 1977.

7-2 Weissberger, M. A. and Meidenbauer, R. H., Modeling Rain Attenuation on Earth-Space Microwave Links, IEEE International Antennas and Propagation Symposium Digest, Quebec, Canada, June 1980.

where

$L_B(P)$ = basic propagation loss not exceeded P% of the year, in dB

L_{BFS} = basic free-space propagation loss, in dB

A_{OW} = attenuation due to oxygen and water-vapor absorption, in dB

$A_S(P)$ = attenuation due to ionospheric scintillation not exceeded P% of the year, in dB

$A_R(P)$ = attenuation due to rain not exceeded P% of the year, in dB.

L_{BFS} can be computed using Equation 2-6. The other terms are described in the following subsections.

7.2.1 Attenuation Due to Oxygen and Water Vapor Absorption

Absorption by oxygen and water vapor molecules will increase the median satellite-to-ground loss to a value greater than the free-space value. Incident RF energy excites a certain fraction of the molecules to higher rotational energy states. Part of the absorbed energy is reradiated isotropically; another part is converted to kinetic energy (heat). The result is a reduction of the power of the signal flowing through the medium.[7-3] The zenith and tangent attenuations for the 1-150 GHz band are shown in Figure 7-1. More detail for the 60 GHz band is shown in Figure 7-2. (As noted in

---

7-3 Straiton, A. W., "The Absorption and Reradiation of Radio Waves by Oxygen and Water in the Atmosphere," IEEE Trans. on Antennas and Propagation, July 1975.

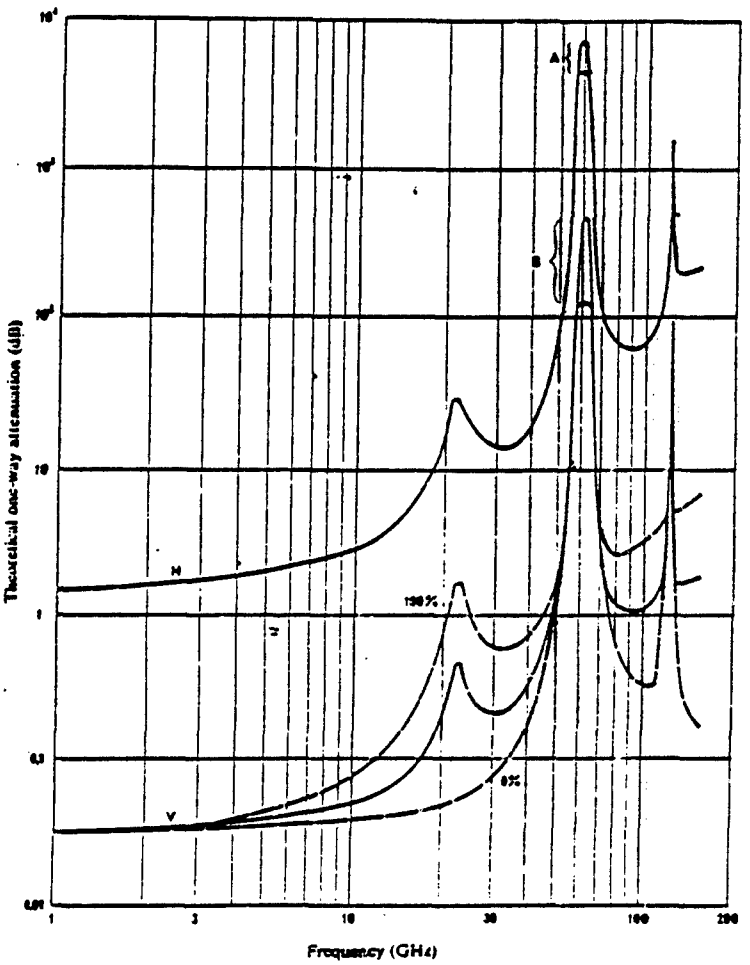

Theoretical one-way attenuation for vertical and horizontal paths through the atmosphere (calculated using the United States standard atmosphere for July at 45° N latitude). Solid curves are for a moderately humid atmosphere (7.5 g/m^3 at the surface); dashed curves for vertical path represents dry atmosphere. (SATPROP uses the solid curves.)

A: Range of values
B: Range of values
H: Horizontal
V: Vertical (Zenith)

Figure 7-1. Attenuation due to atmospheric constituents (from Reference 7-4).

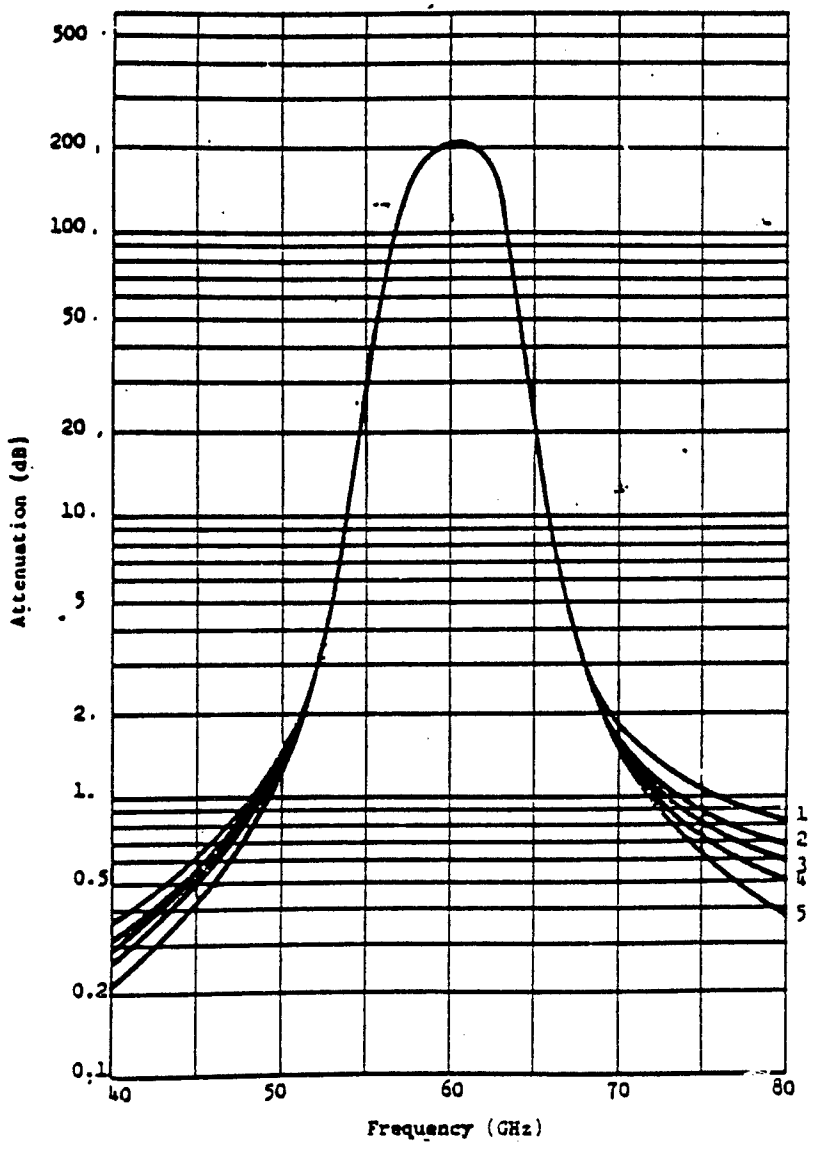

Curve #	Water Vapor Concentration
1	15 g/m^3
2	10
3	8 (SATPROP uses this curve)
4	5
5	0

Figure 7-2. Zenith attenuation due to atmospheric constituents (from Reference 7-4).

subsection 7.4, there are details in the 60 GHz band which this degree of resolution still does not reveal. Engineers needing this higher resolution should study the publications cited in TABLE 7-10 of the subsection). The values at other angles are computed using this approximation:[7-4, 7-5]

$$A_{OW} = \begin{cases} \text{Min} & A_{OW}(V)/\text{SIN}(E_{RS}) \\ & A_{OW}(H) \end{cases} \qquad (3\text{-}2)$$

where

$A_{OW}(E_{RS})$ = absorption due to water vapor and oxygen at the radio elevation angle to the satellite relative to the horizontal, dB.

$A_{OW}(V)$ = absorption along the zenith angle path, dB.

E_{RS} = radio elevation angle to the satellite. (Degrees above the horizontal).

$A_{OW}(H)$ = absorption along a ray path that is tangent to the earth's surface.

Figures 7-3 and 7-4 indicate typical world-wide humidity values. These were taken from Reference 7-6.

7-4 CCIR, Conclusions of the Interim Meeting of Study Group 5, Doc. 5/142-E, Report 234-3 (Rev. 76), April 1976.

7-5 Hill, D. A., A Survey of Earth-to-Satellite Propagation Factors Between 2.5 and 275 GHz, OT Report 74-43, Office of Telecommunications, Boulder, CO, July 1974. COM-75-10792.

7-6 Bean, B. R. and Dutton, E. J., Radio Meteorology, NBS Monograph 92, National Bureau of Standards, Boulder, CO, 1966.

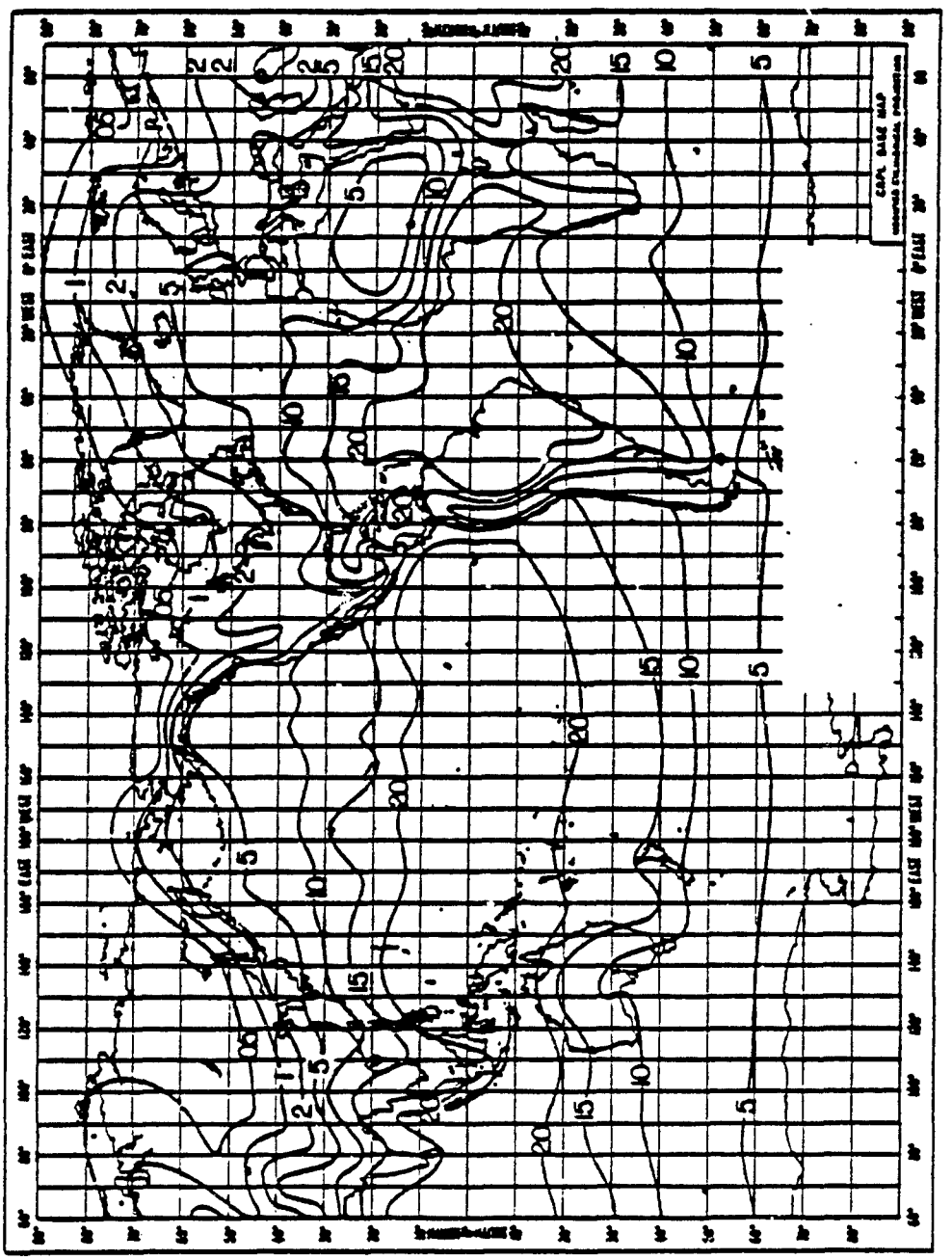

Figure 7-3. Average absolute humidity (g/m^3), February (Reference 7-6).

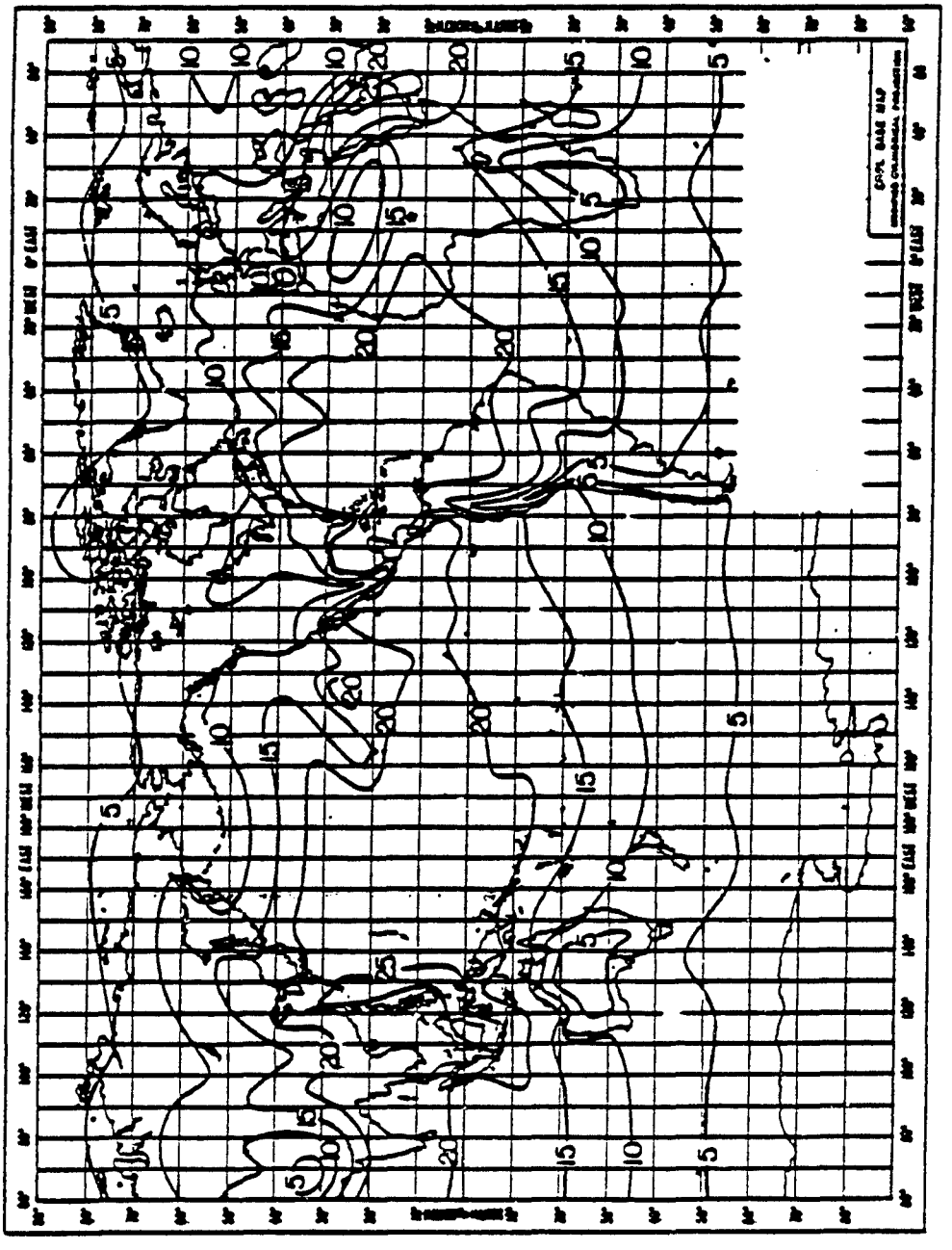

Figure 7-4. Average absolute humidity (g/m^3), August (Reference 7-6).

7.2.2 Signal Variability Due to Ionospheric Scintillation (7-7, 7-8, 7-9, 7-10)

Signals passing through the ionosphere can undergo rapid variations in amplitude, phase, and angle of arrival. These fluctuations are known as scintillations.

Scintillation is caused by irregularities in the electron density of the F-layer. The received signal is the sum of rays coming from nearby parts of the ionosphere with different electron densities. The rays can combine so as to enhance or cancel one another. The resultant amplitude varies with time. The variation is at one rate if the irregularities move across the ray path (geostationary satellites) and at a faster rate if the ray path moves across the irregularities (non-geostationary satellites).

The phenomenon is most prevalent for signals that traverse the F-layer (225-400 km above the earth) in the auroral latitudes or near the geomagnetic equator. Figure 7-5 illustrates these regions.

The magnitude of the amplitude variations decreases as signal frequency increases. TABLE 7-1 provides data for three frequencies. These data can be considered to be worst-case annual statistics: they are based on measurements

---

7-7 Aarons, J., Whitney, H. E. and Allen, R. S., "Global Morphology of Ionospheric Scintillations," Proc. IEEE, February 1971.

7-8 Giordano, J. A., "Ionospheric Scintillations," MITRE Technical Report 6559, December 1973.

7-9 Taur, R. R., "Ionospheric Scintillation at 4 and 6 GHz," COMSAT Technical Review, Spring 1973.

7-10 CCIR, Conclusions of the Interim Meeting of Study Group 6, Dec. 6/177-E, Report 263-3 (Rev. 76), May 1976.

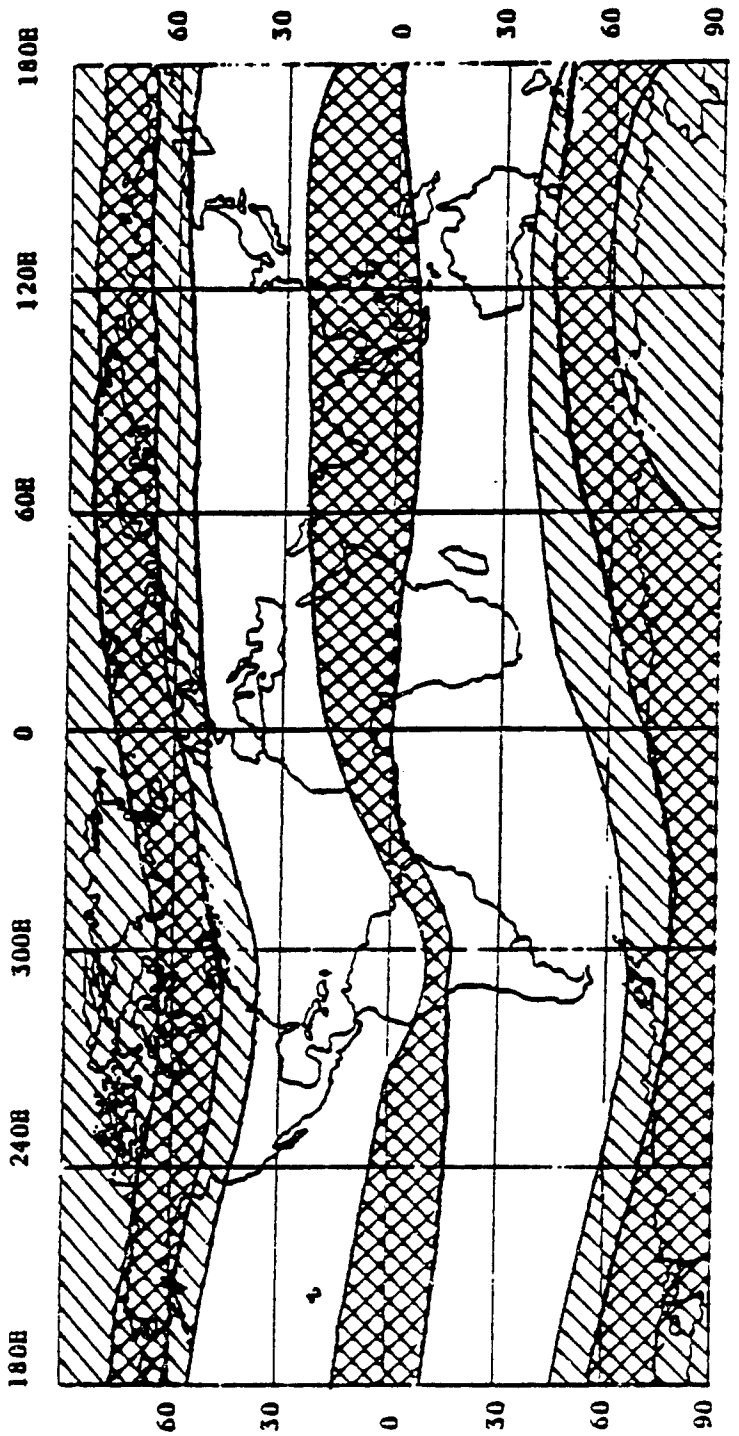

Figure 7-5. Regions of frequency scintillation activity. Ray paths intersecting the cross-hatched regions at altitudes of 250-400 km are susceptible to the most severe scintillation (Reference 7-8). This scintillation is characterized by amplitudes shown in Figures 7-6 and 7-7. Ray paths through the regions with light shading or no shading experience progressively less severe scintillation.

TABLE 7-1

ANNUAL SCINTILLATION STATISTICS

Percent of Time Value Is Not Exceeded	Change in Loss, dB		
	136 MHz[a]	4000 MHz[b]	6000 MHz[c]
.1 (d)	-8.4	-3.1	-2.0
1 (d)	-4.5	0.0	0.0
5 (d)	-2.0	0.0	0.0
50	0.0	0.0	0.0
95 (e)	2.2	0.0	0.0
99 (e)	5.8	0.0	0.0
99.9 (e)	11.8	3.1	2.0

[a]From Reference 7-7, Figure 13.
[b]From Reference 7-9, Figure 3. The ordinate and abscissa were divided by two.
[c]From Reference 7-9, Figure 4. The ordinate and abscissa were divided by two.
[d]Signal enhancements.
[e]Signal fades.

from sites in the auroral or equatorial zones, and they were taken during periods of high sunspot numbers. The user is cautioned that data from any one month or hour can be worse than these annual data.

The values from TABLE 7-1 are plotted in Figures 7-6 and 7-7. These curves are used in SATPROP. For a specified probability, the model allows scaling as a function of frequency. In theory, there is a variation with

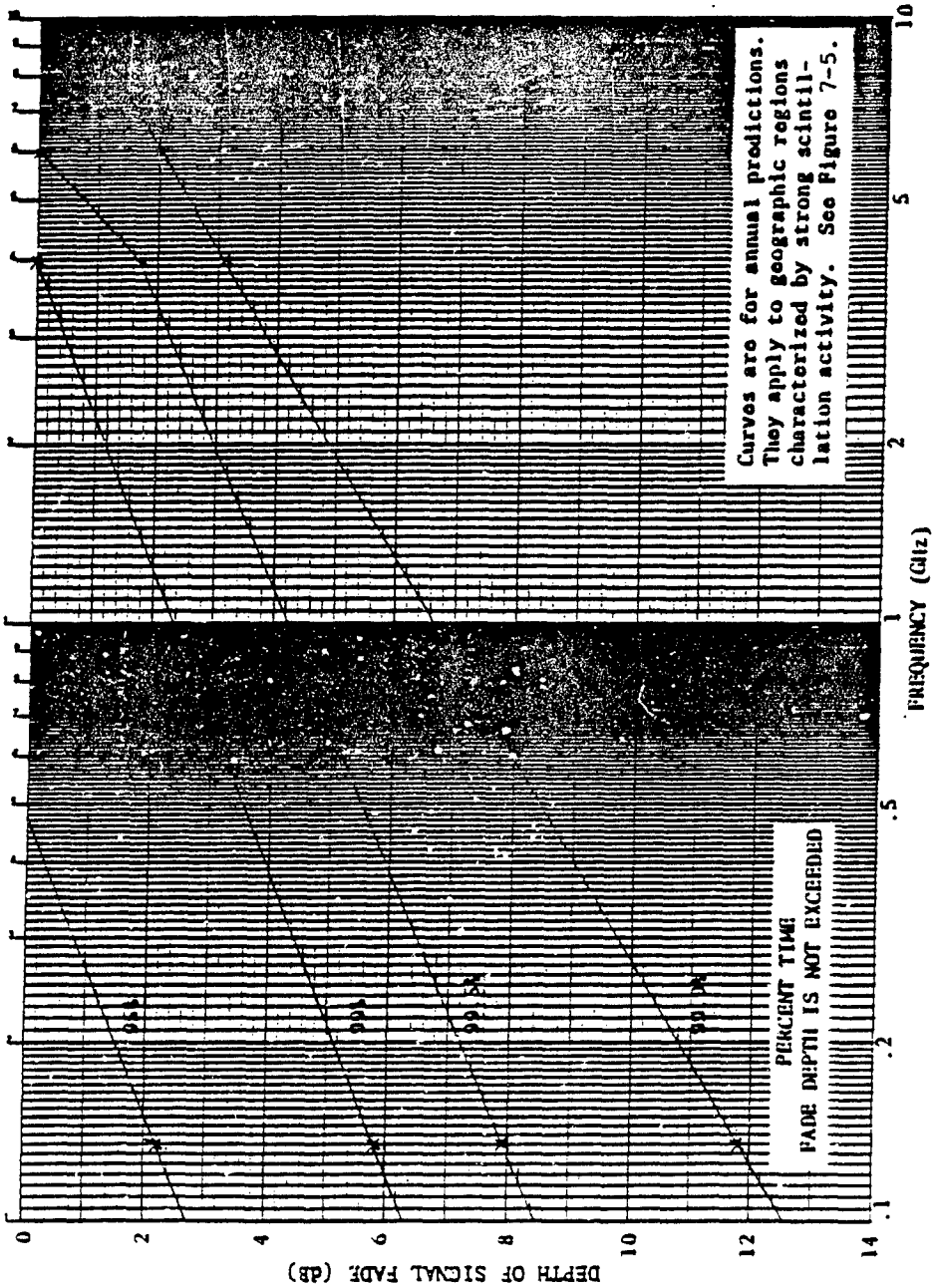

Figure 7-6. Fades due to scintillation (Reference 7-1).

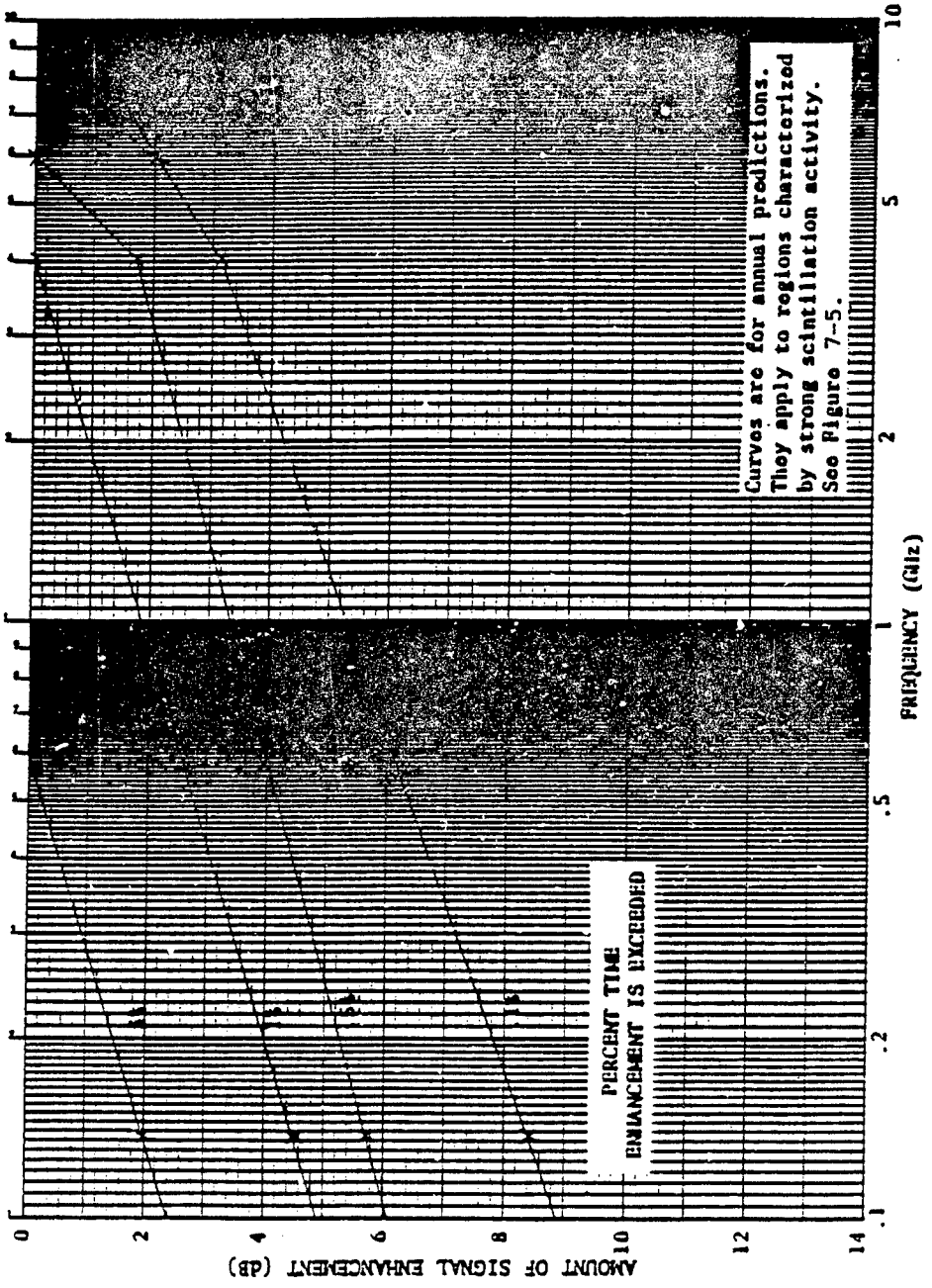

Figure 7-7. Enhancements due to scintillation (Reference 7-1).

elevation angle.[7-11, 7-12] However, analysis of Taur's and Paulson's[7-13] measurements shows that, at least in these instances, there is no definite trend.

7.2.3 Rain Attenuation on Earth-Space Links

In the 10-30 GHz band, rain attenuation causes the largest difference between measured and free-space transmission loss on earth-space line-of-sight links. TABLE 7-2 shows some values of fade depths that were observed on actual links by researchers from Bell Telephone Laboratories and GTE Laboratories. This subsection describes a procedure that can be used to predict the attenuation statistics. The procedure is designated SATPROP-80 and was devised by M. Weissberger and E. Cerezo as an improvement to the SATPROP-79 procedure, which is documented in the Antennas and Propagation Symposium Digest (Reference 7-2). It also supersedes the SATPROP-78 (References 7-14, 7-15) and SATPROP-77 (Reference 7-1) models.

7-11 Briggs, B. H. and Parkin, J. A., "On the Variation of Radio Star Scintillations With Zenith Angle," Journal of Atmos. and Terrest. Physics, Vol. 25, 1963, pp. 339-350.

7-12 Crane, R. K., "Ionospheric Scintillation," Proc. IEEE, February 1977.

7-13 Paulson, M. R. and Hopkins, R. U. F., Effects of Equatorial Scintillation Fading on SATCOM Signals, NELC-TR-1875, Naval Electronics Laboratory Center, San Diego, CA, May 1973.

7-14 Weissberger, M. A., Studies of the Prediction Accuracy of Effective Path-Length Rain Attenuation Models for Satellite-to-Ground Circuits, ECAC-TN-78-015, Electromagnetic Compatibility Analysis Center, Annapolis, MD, October 1978.

7-15 Weissberger, M. A., Meidenbauer, R. H., Baker, R. L., and Billings, T. Abstracts of the National Radio Science Meeting, Electromagnetic Compatibility Analysis Center, Annapolis, MD, November 1979.

TABLE 7-2

OBSERVED FADE MARGINS (dB) REQUIRED FOR 99.99% ANNUAL RELIABILITY

Site	Frequency (GHz)				Years	Take-Off Angles
	12	14	19	29		
Georgia		9+	18+	22+	1977	30°
New Jersey	18		23	44	1977, 78	27°, 39°
Massachusetts	10		15+	26+	1977, 78	24°, 35°
	Margins (dB)					

+ means that the actual margin is even greater than the value listed.

The procedure is based on these assumptions:

1. The attenuation through a region with a uniform rain rate (R) is given by:

$$A = \alpha R^{\beta} \cdot L \qquad (7\text{-}3)$$

where

A = the attenuation in dB

R = the rain rate in millimeters/hour

L = the length of the region

α and β = constants shown in TABLE 7-3.

These values are recommended by Lin[7-16].

[7-16] Lin, S. H., "Rain Attenuation on Earth-Satellite Paths-Summary of 10-Year Experiments and Studies," Bell System Technical Journal, February 1980.

TABLE 7-3

VALUES OF α and β

F(GHz)	6.0	11.0	16.0	18.5	30.0	60.0	100.0
α	.001968	0.01545	0.04726	0.06769	0.1961	0.6860	1.138
β	1.239	1.220	1.115	1.089	1.002	0.8310	0.7382

Olsen[7-17] shows that Equation 7-3 is a close approximation to the theoretical (Mie-scatter) prediction of the loss caused by propagation through a region filled with dielectric spheres.

2. Rainfall with an intensity of more than 10 mm/hour usually occurs in cells that are surrounded by regions of less intense rain. For predicting attenuation, an effective description of this structure is that 20% of the ray path will be through the intense rain (rate R) and 80% through a reduced intensity of rate, $R' = 4.57R^{0.34}$. This lateral structure model was developed by Persinger and Stutzman[7-18] and was later validated by Lane and Stutzman.[7-19]. The effective lateral size of the entire rain storm was found to be 10.5 km.

7-17 Olsen, R. L., et al., "The aR^b Relation in the Calculation of Rain Attenuation," IEEE Trans. Antenna and Propagation, March 1978.

7-18 Persinger, R. R. and Stutzman, "Millimeter Wave Attenuation Prediction Using Piecewise Uniform Rain Rate Model," IEEE Trans. Antenna and Propagation, March 1980.

7-19 Lane, S. O. and Stutzman, W. L., "Spatial Rain Rate Distribution Modeling for Earth-Space Link Propagation Calculations," Abstracts of the North American Radio Science Meeting, Quebec, Canada, June 1980.

3. The attenuation is significant only in the region in which there is liquid water.[7-20] When rainfall is not intense (R < 7mm/hr) liquid is found up to the 0° isotherm. This is located at:[7-21]

7.8 - (0.1 x Latitude°),

km above sea level for latitudes greater than 30° and at 7.8 km for latitudes closer to the equator.

4. When the rain rate increases above 7mm/hr, atmospheric turbulence carries rain to heights above the 0° isotherm. The increase in altitude observed by Goldhirsh[7-22] at Wallops Island, VA, was 1.82 log (R/7).

5. The total effective height of the attenuating layer is the height of liquid water above sea level minus the height of the earth station antenna (in km) above sea level (Reference 7-21).

7-20 Crane, R. K., "Propagation at Centimeter and Millimeter Wavelengths," Proc. IEEE, 1971.

7-21 Crane, R. K., EASCON '78 Record, September 1978.

7-22 Goldhirsh, J., Radio Science, September 1977.

These assumptions result in this equation for the rain attenuation not exceeded P% of a year:

$$A_R(P) = \alpha \left(0.2\ R(P)^{\beta} + 0.3\ R'(P)^{\beta}\right) \cdot L \qquad (7\text{-}4)$$

where

α, β = Constants from TABLE 7-3. The values of α and β for frequencies not in TABLE 7-3 may be obtained by linear interpolation.

$R(P)$ = Rain rate averaged over 1 minute that is not exceeded for P% of the year. The values of $R(P)$ may be obtained from TABLE 7-4 (from Reference 7-23). The rain climate regions are shown in Figures 7-8, 7-9, and 7-10.

$$R' = 4.57\ (R(P))^{0.34} \qquad (7\text{-}5)$$

$$L = \text{MIN} \begin{cases} (H_I - H_A + H(R))/\sin\theta \\ 10.5/\cos\theta \end{cases} \qquad (7\text{-}6)$$

$$H_I = 7.8 - 0.1\ \text{LAT}° \quad (\text{LAT} > 30°) \qquad (7\text{-}7)$$

$$= 7.8 \quad (\text{LAT} \leq 30°) \qquad (7\text{-}8)$$

H_A = Height of the earth station antenna above sea level, km

$$H(R) = 1.82\ \text{LOG}\ (R(P)/7) \quad (R(P) > 7)$$
$$= 0 \quad (R(P) \leq 7)$$

7-23 Crane, R. K., Prediction of Attenuation by Rain, Environmental Research and Technology Incorporated, Concord, MA, August 1979.

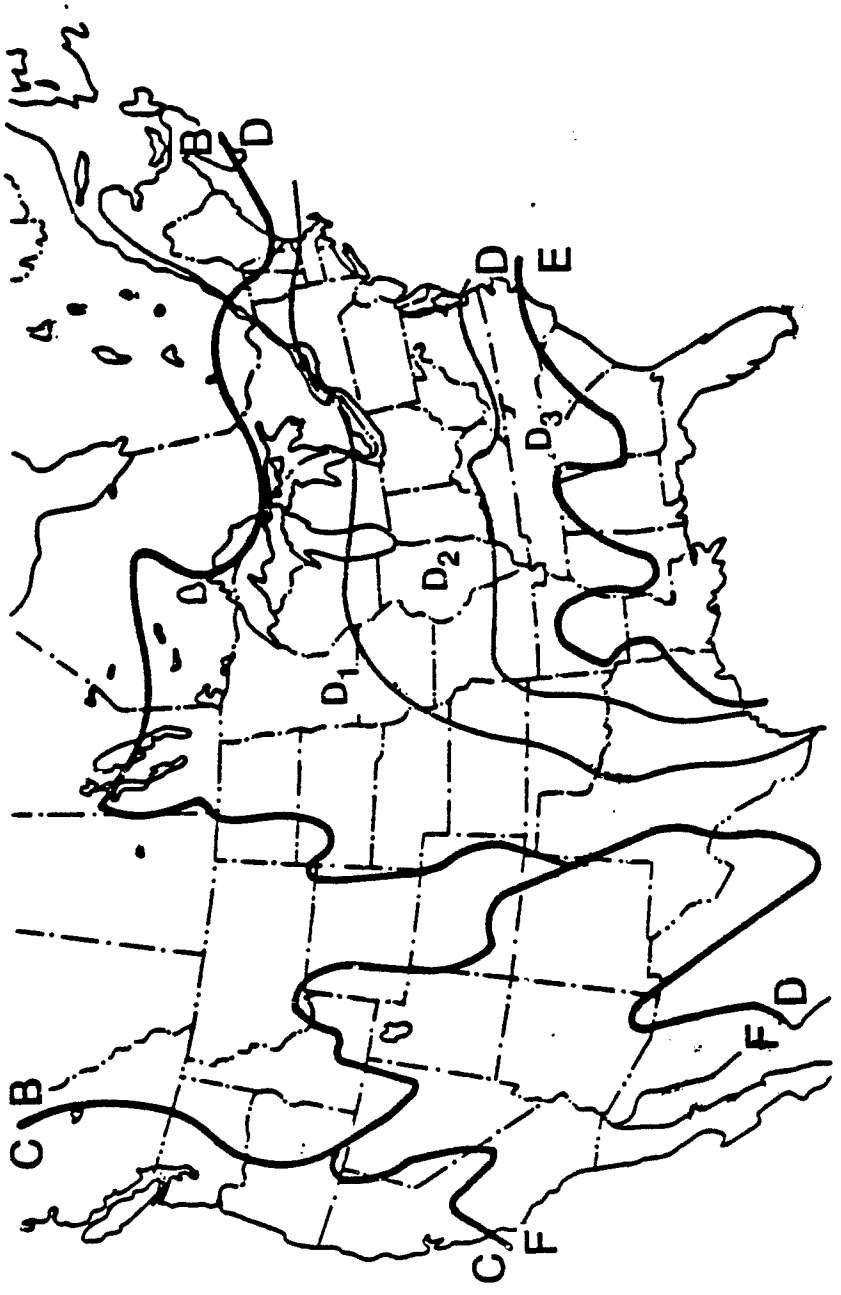

Figure 7-8. Rain-rate climate regions for the continential United States showing the subdivision of Region D (Reference 7-23).

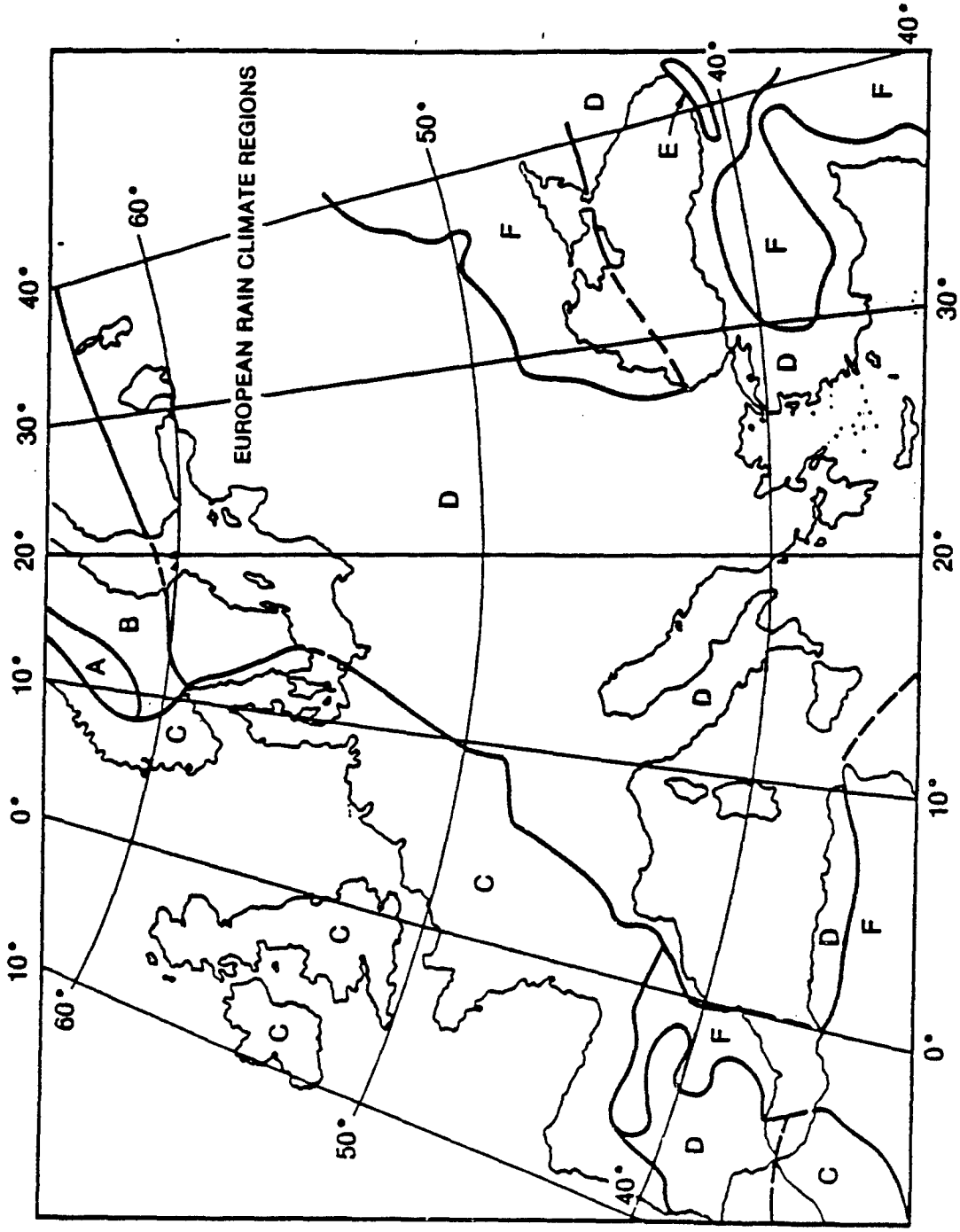

Figure 7-9. Rain climate regions for Europe (Reference 7-23).

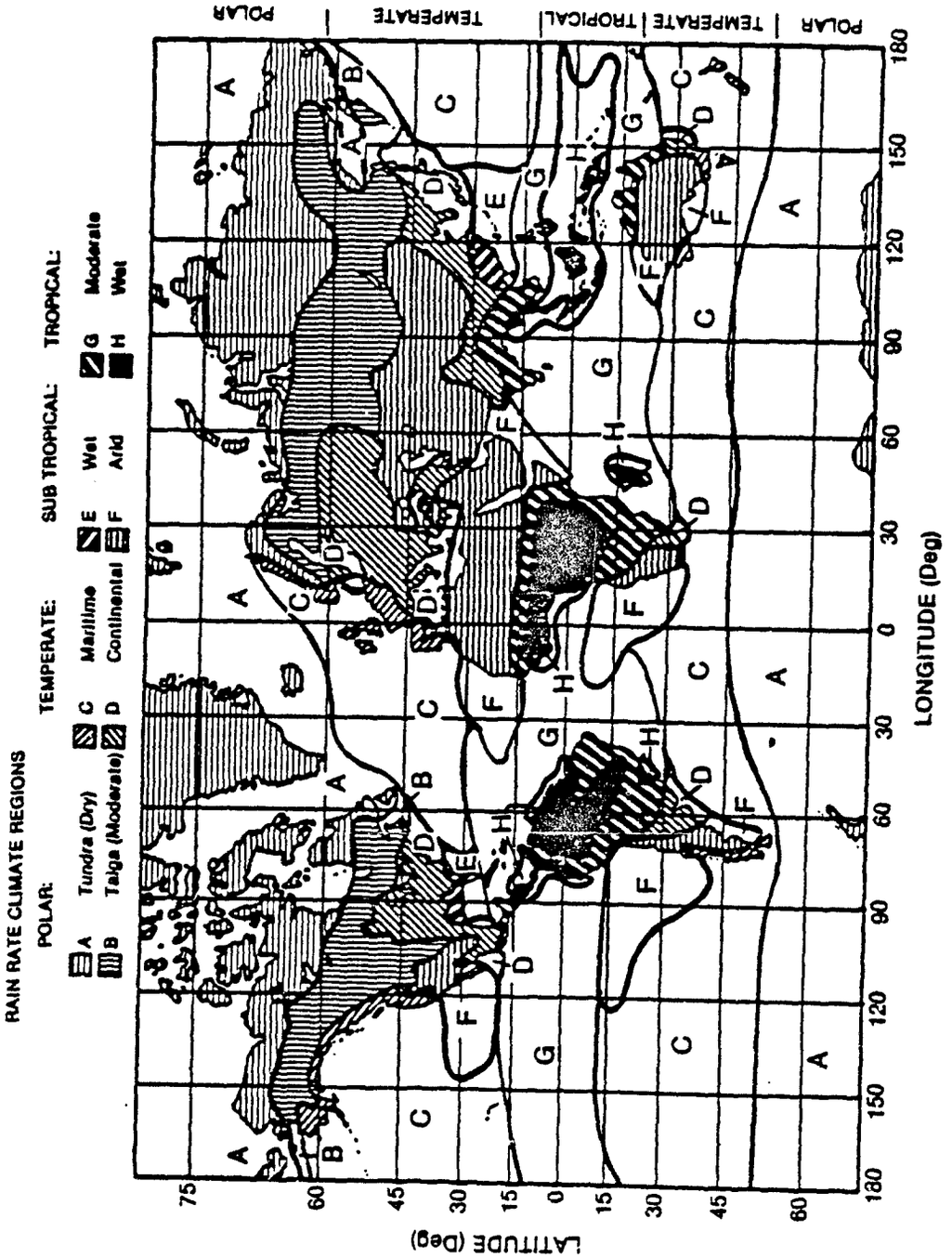

Figure 7-10. Global rain rate climate regions including the ocean areas (Reference 7-23).

TABLE 7-4

POINT RAIN-RATE DISTRIBUTION VALUES (mm/hr)

VERSUS PERCENT OF YEAR RAIN RATE IS EXCEEDED[a]

Percent of Year	Rain Climate Region:										Minutes Per Year	Hours Per Year
	A	B	C	D_1	D_2	D_3	E	F	G	H		
0.001	28	54	80	90	102	127	164	66	129	251	5.3	0.09
0.002	24	40	62	72	86	107	144	51	109	220	10.5	0.18
0.005	19	26	41	50	64	81	117	34	85	178	26	0.44
0.01	15	19	28	37	49	63	98	23	67	147	53	0.88
0.02	12	14	18	27	35	48	77	14	51	115	105	1.75
0.05	8	9.5	11	16	22	31	52	8.0	33	77	263	4.38
0.1	6.5	6.8	72	11	15	22	35	5.5	22	51	526	8.77
0.2	4.0	4.8	4.8	7.5	9.5	14	21	3.8	14	31	1052	17.5
0.5	2.5	2.7	2.8	4.0	5.2	7.0	8.5	2.4	7.0	13	2630	43.8
1.0	1.7	1.8	1.9	2.2	3.0	4.0	4.0	1.7	3.7	6.4	5260	87.66
2.0	1.1	1.2	1.2	1.3	1.8	2.5	2.0	1.1	1.6	2.8	10520	175.3

[a]1-minute average (see Reference 7-23).

7.3 COMPUTER MODEL FOR LOSS PREDICTIONS

A computer program for the procedure described in Section 7.2 is available for use at ECAC. Instructions for using it appear in Reference 7-24. The program, called SATPROP, incorporates the formulas presented in Section 7.2.

7-24 Baker, R. L., Radio Wave Propagation: A User's Manual for the Computer Codes, ECAC-UM-80-001, Electromagnetic Compatibility Analysis Center, Annapolis, MD, September, 1980.

7.4 VALIDATION AND COMPARISON WITH OTHER MODELS

7.4.1 Validation of the Rain Attenuation Algorithm

SATPROP-80 predictions were compared with 25 path-years of data taken at earth stations along the east coast of the United States. The parameters are summarized in TABLES 7-5 and 7-6. The results are shown in TABLE 7-7. The statistics are of the quantity called "prediction error", which is defined by the following convention (also used elsewhere in this Handbook):

Prediction Error (dB) = Predicted Loss (dB) - Measured Loss (dB) (7-9)

TABLE 7-7 shows values of the mean (M), standard deviation (σ), and root mean square (RMS) of the prediction errors. These were each computed from the set of errors that fell into the bins defined by frequency (F) and percent-of-the year (P) that the loss was not exceeded. When the published data permitted, the prediction error was calculated at 0.1, 0.05, 0.01, 0.005 and 0.001% of the year. Figures 7-11 and 7-12 show the maximum errors in relation to the mean measured value. The mean prediction is also shown. In this type of figure, the mean observed error at any percent of the year can be determined by measuring the distance (in dB) between the mean measurement line and the mean prediction line. The observed largest errors can be determined by measuring the distance (in dB) between the error-limit curve and the mean-measurement curve. Thus in the 11-16 GHz band, the mean prediction error for losses not exceeded for 0.01% of the year is -0.8 dB, with individual errors ranging from -7.2 to +2.1 dB.

Comparisons with the accuracy of other state-of-the-art prediction models were made. The other models studied included the CCIR model documented by the 1978 Plenary Assembly (Reference 7-25), a proposed revision to the CCIR model

---

7-25 International Radio Consultative Committee, CCIR Report 564-1 Propagation Data Required for Space Telecommunication Systems, XIVth Plenary Assembly, ITU, Geneva, Switzerland, 1978.

TABLE 7-5

MEASUREMENTS 11-16 GHz

Location	Freq. (GHz)	θ (Deg)	Dates	Source	Measured Rain?
Greenbelt, MD	11.7	29	1/77-1/78	NASA	Yes
Greenbelt, MD	11.7	29	1/78-1/79	NASA	Yes
Blacksburg, VA	11.7	33	1/78-1/79	VPI	Yes
Waltham, MA	11.7	24	6/77-1/78	GTE	Yes
Waltham, MA	11.7	24	2/78-1/79	GTE	Yes
Holmdel, NJ	11.7	27	4/76-4/77	BTL	No
Holmdel, NJ	11.7	27	5/77-5/78	BTL	No
Holmdel, NJ	11.7	27	5/78-5/79	BTL	No
ETAM, WV	11.7	18	10/77-10/78	COMSAT	Yes
Palmetto, GA	13.6	38	1/70-1/72	BTL	Yes
Palmetto, GA	13.6	30	6/76-7/77	BTL	No
Palmetto, GA	13.6	50	8/77-8/78	BTL	No
Rosman, NC	15.3	42	1/70-1/71	NASA	Yes
Clarksburg, MD	15.3	38	7/70-7/71	COMSAT	No

TABLE 7-6

MEASUREMENTS 19-29 GHz

Location	Freq. (GHz)	θ (Deg)	Dates	Source	Measured Rain?
Blacksburg, VA	19.0	45	1/78-1/79	VPI	Yes
Holmdel, NJ	19.0	39	5/77-5/78	BTL	No
Holmdel, NJ	19.0	19	6/76-6/77	BTL	No
Palmetto, GA	19.0	30	6/76-6/77	BTL	No
Palmetto, GA	19.0	50	8/77-8/78	BTL	No
Holmdel, NJ	28.6	39	5/77-5/78	BTL	No
Wallops Is, VA	28.6	42	4/77-3/78	JHU	Yes
Blacksburg, VA	28.6	45	1/78-1/79	VPI	Yes
Palmetto, GA	28.6	30	6/76-6/77	BTL	No
Palmetto, GA	28.6	50	9/77-9/78	BTL	No

TABLE 7-7

PREDICTION ERROR STATISTICS (dB)

TYPICAL REGIONAL DISTRIBUTIONS OF RAIN USED AS INPUT

$0.01 \leq P\% \leq 0.1$

	GLOBAL-78	VPI-79	SATPROP-80	CCIR	5/10T	F(GHz)	# of Paths
M	-0.04	-2.17	0.04	-2.18	0.26		14
σ	2.47	2.90	2.52	2.87	2.50	$11 \leq F \leq 16$	
RMS	2.47*	3.59	2.49	2.57	2.48		
M	-2.54	-3.80	0.25	-2.57	5.86		10
σ	4.19	5.33	3.44	4.22	7.30	$19 \leq F \leq 29$	
RMS	4.81	6.45	3.37*	4.86	9.23		

$0.001 \leq P\% \leq 0.01$

	GLOBAL-78	VPI-79	SATPROP-80	CCIR	5/10T	F(GHz)	# of Paths
M	-2.04	-6.63	-1.49	-6.94	0.47		9
σ	5.05	5.18	4.43	5.48	5.08	$11 \leq F \leq 16$	
RMS	5.33	8.33	4.57*	8.76	4.97		
M	6.10	-8.46	-0.07	-4.94	15.07		4
σ	8.41	9.43	7.34	8.32	11.29	$19 \leq F \leq 29$	
RMS	9.89	12.15	6.80*	9.15	18.35		

*Lowest RMS error in data bin.

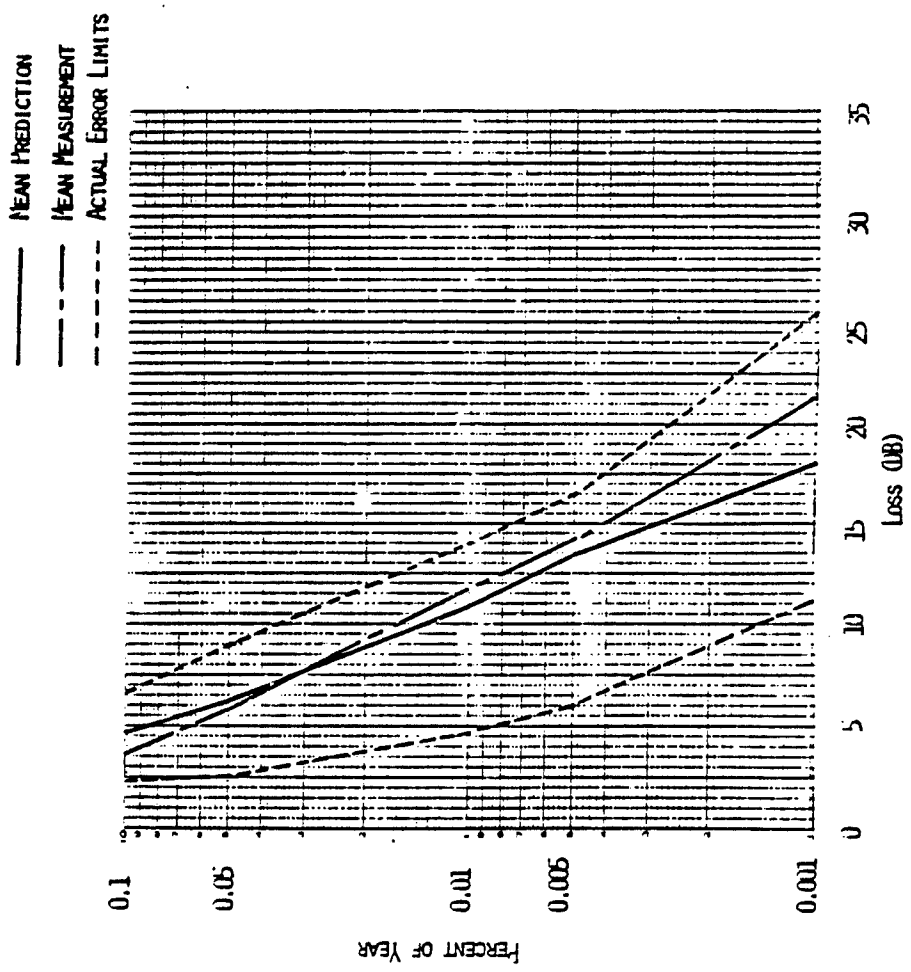

Figure 7-11. Error limits: SATPROP-80, 11-16 GHz.

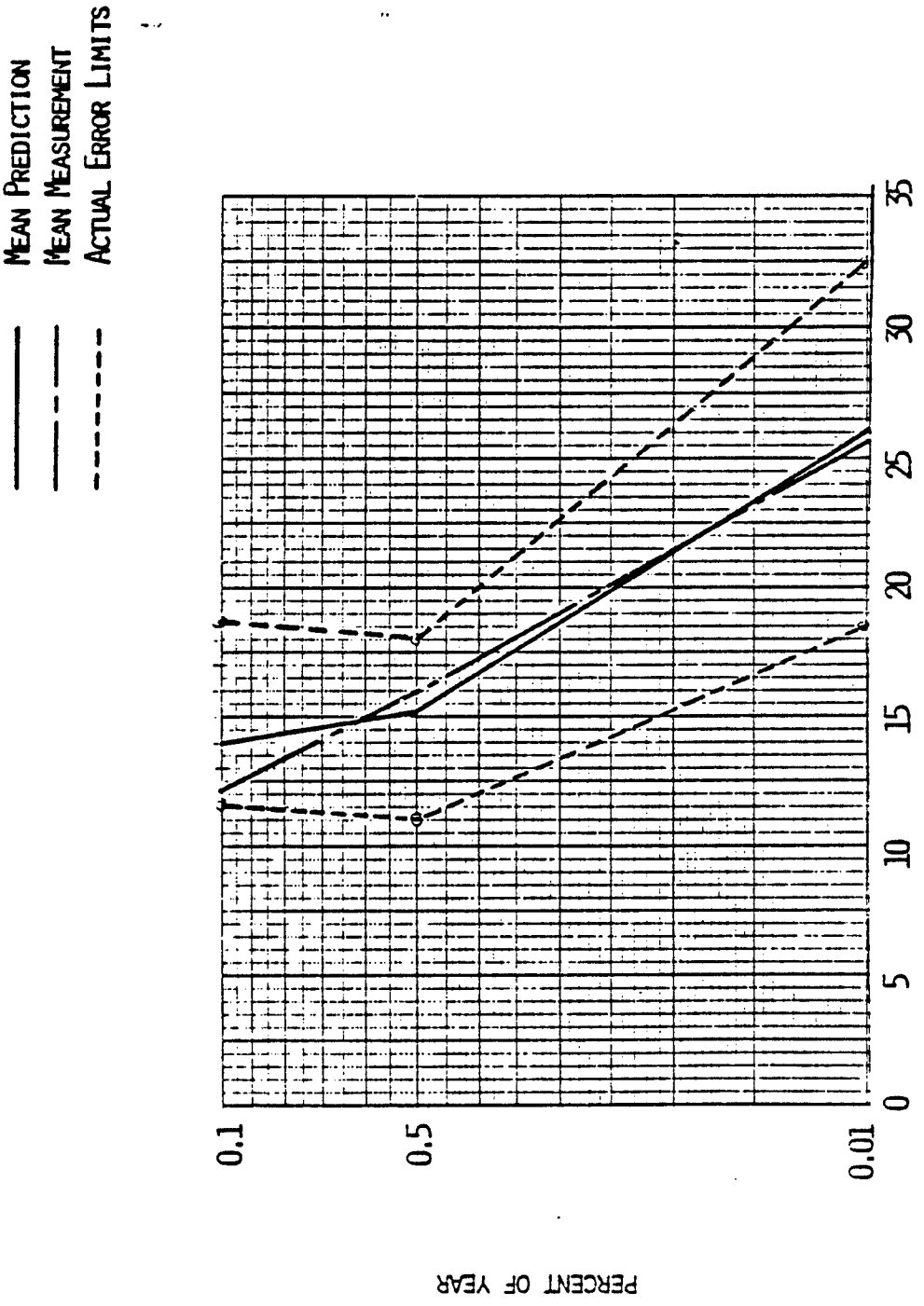

Figure 7-12. Error limits: SATPROP-80, 19-29 GHz.

(References 7-23 and 7-26), the Global Model (Reference 7-21), and the VPI (1979) Model (Reference 7-18). TABLE 7-7 shows the accuracy of these models when they are used to perform regular predictions, i.e., with input values of R(P) coming from TABLE 7-4 and Figures 7-8, 7-9, and 7-10. The data in TABLE 7-7 show that SATPROP-80 has the lowest RMS error for 3 of the 4 bins of data, and is within 0.02 dB of the Global Model in the 4th bin.

The error results discussed so far include the effects of model inaccuracy and input data inaccuracy. Again, these are the results that will be encountered in practice. The model comparison was extended, however, to show error trends when the input data errors were further reduced. This was done by entering rain rate statistics measured at the earth station sites during the time periods when the loss statistics were measured. The resulting model errors are shown in TABLE 7-8. Here again SATPROP has the lowest RMS error in 3 of the 4 data bins and is within 0.55 dB of the CCIR model in the 4th bin.

TABLE 7-9 summarizes the RMS errors for all of the tests.

7-26 CCIR Doc. USSG 5/10T and 5/6T, November 1979. By R. Crane (see Reference 7-23).

TABLE 7-8

ERROR STATISTICS

MEASURED RAINRATES USED AS INPUT

$0.01 \leq P\% \leq 0.1$

	GLOBAL-78	VPI-79	SATPROP-80	CCIR	5/10T	F(GHZ)	# of Paths
M	0.91	-1.22	0.92	-1.63	1.51		8
σ	3.68	3.56	2.90	2.85	3.76	$11 \leq F \leq 16$	
RMS	3.72	3.69	2.98*	3.23	3.98		
M	-0.61	-3.73	-1.49	-3.49	2.26		3
σ	3.62	2.99	2.52	2.98	6.51	$19 \leq F \leq 29$	
RMS	3.44	4.66	2.79*	4.47	6.50		

$.001 \leq P\% \leq 0.1$

	GLOBAL-78	VPI-79	SATPROP-80	CCIR	5/10T	F(GHZ)	# of Paths
M	-2.21	-7.08	-1.71	-7.57	0.33		6
σ	4.89	5.09	4.07	5.77	4.72	$11 \leq F \leq 16$	
RMS	5.22	8.62	4.29*	9.40	4.57		
M	6.58	-3.85	1.85	-1.75	14.15		2
σ	4.99	1.21	2.25	1.42	8.66	$19 \leq F \leq 29$	
RMS	7.87	3.99	2.69	2.14*	16.01		

*Lowest RMS error in data bin.

TABLE 7-9

SUMMARY OF RMS ERRORS

F (GHz)	P(%)	Rain Input	GLOBAL	VPI	SATPROP	CCIR	5/10T
11 < F < 16	.01-.1	Measured	3.72	3.69	2.98*	3.23	3.98
		Typical	2.47*	3.59	2.49	2.57	2.48
	.001-.01	Measured	5.22	8.62	4.29*	9.40	4.57
		Typical	5.33	8.33	4.57*	8.76	4.97
19 < F < 29	.01-.1	Measured	3.44	4.66	2.79*	4.47	6.50
		Typical	4.81	6.45	3.37*	4.86	9.23
	.001-.01	Measured	7.87	3.99	2.69	2.14*	16.01
		Typical	9.89	12.15	6.80*	9.15	18.35
	Overall		5.34	6.43	3.74*	5.57	8.26

*Lowest RMS error in data bin.

Two models (the ITS model and Lin's model) were not included in this most recent validation study. ECAC did not compare SATPROP and ITS model [7-27] predictions for the full 25 path-years of data, but a comparison was made in January, 1980, for 17 path-years of data. The prediction accuracy computed from this set of data is shown in Reference 7-2. The RMS errors for the ITS model are larger than those reported in this Handbook for SATPROP-80.

Lin's model (Reference 7-16) was not studied because it requires as input a distribution of the 5-minute average of rain-rates expected during the year. No source of such data was readily available. The distributions shown in TABLE 7-4 are for 1-minute averages. The use of 1-minute averages instead of 5-minute averages could result in substantial over-prediction of losses.

[7-27] Dutton, E., NTIA Report 78-10, ITS Boulder, CO, October 1978.

7.4.2 Validation of the Oxygen and Water-Vapor Attenuation Algorithm

Validation of the oxygen and water-vapor absorption subroutines of SATPROP was shown in the original documentation (Reference 7-1). The summary is reproduced here as TABLE 7-10. It is seen that the SATPROP predictions (based on Reference 7-4) generally are as accurate as other procedures[7-28, 7-29, 7-30] when compared with Thompson's measurements.[7-31] Potential problems arise at the family of oxygen absorption lines near 60 GHz. The detailed calculations done by Welch and Liebe (Reference 7-32) show that there is a great variation within the 55-65 GHz range. The loss varies between 130 and 380 dB, depending on the specific frequency being used. Thus the CCIR (and SATPROP) estimates can only be considered as nominal values in this band.

7-28 CCIR, XIIIth Plenary Assembly, Volume 5, Report 233-3, Geneva, Switzerland, 1974.

7-29 Rice, P. L., Longley, A. G., Norton, K. A., and Barsis, A. P., Transmission Loss Predictions for Tropospheric Communication Circuits, NBS TN101, National Bureau of Standards, Boulder, CO, January 1967. AD 687820.

7-30 Lukes, G. D., Penetrability of Haze, Fog, Clouds, and Precipitation by Radiant Energy Over the Spectral Range 0.1 Micron to 10 Centimeters, Center for Naval Analysis, Arlington, VA, May 1968. AD 847658.

7-31 Thompson, W. I., A Survey of Electromagnetic Wave Transmission in the Earth's Atmosphere over the Frequency (Wavelength) Range 3 kHz (100 km) 3,000 THz (0.1 μm), DOT-TSC-NASA-71-6, Transportation Systems Center, Cambridge MA, February 1971. N71-20121.

7-32 Liebe, H. J. and Welch, W. M., Molecular Attenuation and Phase Dispersion Between 40- and 14- GHz for Path Models from Different Altitudes, OT Report 73-10, Office of Telecommunications, Boulder, CO, May 1973.

TABLE 7-10

A COMPARISON AMONG PREDICTED AND MEASURED VALUES OF ZENITH ATTENUATION (dB) FOR DRY DAYS

	SOURCE[a]						
Freq. (GHz)	1	2	3	4	5	6	7
.8-1.5	.06	.016	.022	.1			.03-.07
9.-10.	.06	.068	.066	.15	.01		.05-.15
22.23	.5	.536	.448	.60	2.0		.85-.9
30	.3	.340	.296	.45	.25		.336
59-61	205	62.24	62.19	150	200	130-380	
100	1.2	1.54	1.32	1.4	1.4		.6-2.0

[a]SOURCE CODE:

1. CCIR Report 234-3. These are computed zenith values. They are the values used in SATPROP. (Reference 7-4).
2. CCIR Report 233-3 (Van Vleck sea level differential absorption x an effective path length) (Reference 7-28).
3. NBS TN 101 (Van Vleck sea level differential absorption values x an effective path length) (Reference 7-29).
4. Lukes (Computed zenith values) (Reference 7-30).
5. Straiton (Reference 7-3).
6. Welch and Liebe (Considers oxygen only) (Reference 7-32).
7. Thompson (Collected measurements) (Reference 7-31).

7.5 CONCLUDING REMARKS

The scintillation estimates described in Section 7.2 are based on the interpretation of only a small set of measurements. Twenty-six papers containing the results of recent measurement and modeling programs appear in References 7-33 through 7-36. Reference 7-37 contains data that could be used to refine the estimates for frequencies above 10 GHz.

Data that would allow a more extensive validation of the SATPROP rain-attenuation algorithm appears in References 7-38 through 7-40.

7-33 Proceedings of the 1981 Symposium on the Effect of the Ionosphere on Radiowave Systems, Naval Research Laboratory, Washington, D.C., 14-16 April 1981.

7-34 Fang, D. J., and Pontes, M. S., "4/6 GHz Ionospheric Scintillation Measurements During the Peak of Sunspot Cycle 21," COMSAT Technical Review, Autumn, 1981.

7-35 Aarons, J., "Global Morphology of Ionospheric Scintillation," Proc. IEEE, April 1982.

7-36 Yeh, K. C., and Liu, C. H., "Radio Wave Scintillations in the Ionosphere," Proc. IEEE, April 1982.

7-37 Awaka, J., et al., "ETS-II Experiments Part V: Effect of the Ionosphere," IEEE Trans. on Aerospace and Electronic Systems, September 1980.

7-38 Ippolito, L. J., Kaul, R. D., and Wallace, R. G., Propagation Effects Handbook for Satellite Systems Design, NASA Reference Publication 1082, Second Edition, December 1981.

7-39 Antennas and Propagation, IEE Conference Publication 195, London, April 1981.

7-40 Fujita, M., et al., "ETS-II Experiments Part IV: Characteristics of Millimeter and Centimeter Wavelength Propagation," IEEE Trans. on Aerospace and Electronics Systems.

A review of the depolarization effects of rain and ice has been prepared by Cox.[7-41]

[7-41] Cox, D. C., "Depolarization of Radio Wave by Atmospheric Hydrometeors on Earth Space Paths: A Review," Radio Science, September, 1981.

CHAPTER 8

AIR-TO-AIR AND AIR-TO-GROUND PROPAGATION, 100 MHz - 16 GHz

By: M. Weissberger

8.1 INTRODUCTION

This chapter describes manual and automated procedures for predicting basic transmission loss for air-ground circuits in the 100 MHz - 15,000 MHz frequency range. It applies to problems in which at least one of the antennas is 1 km or higher above the ground. The recommended model is IF-77.[8-1] The model should be used in the smooth-earth mode rather than the terrain - sensitive mode.

8.2 A MANUAL METHOD

This subection is based on a report submitted by Gierhart and Johnson to the CCIR.[8-2]

Figures 8-1 through 8-6 show values of the basic transmission loss, L_b, for frequencies of 125, 300, 1200, 5100, 9400, and 15,500 MHz.

Each figure consists of three curve sets, where the upper, middle and lower sets provide $L_b(0.05)$, $L_b(0.5)$, and $L_b(0.95)$, respectively. These correspond to time availabilities of 0.05, 0.5, and 0.95. For example,

---

8-1 Johnson, M. E. and Gierhart, G. D., (1978) Applications Guide For Propagation and Interference Analysis Computer Programs (0.1 to 20 GHz) DOT-Report FAA-RD-77-60, National Technical Information Service, Springfield, VA, U.S.A., March 1978, ADA 053242.

8-2 CCIR Doc. USSG 5/D-3, (by Gierhart and Johnson), 5 November 1979.

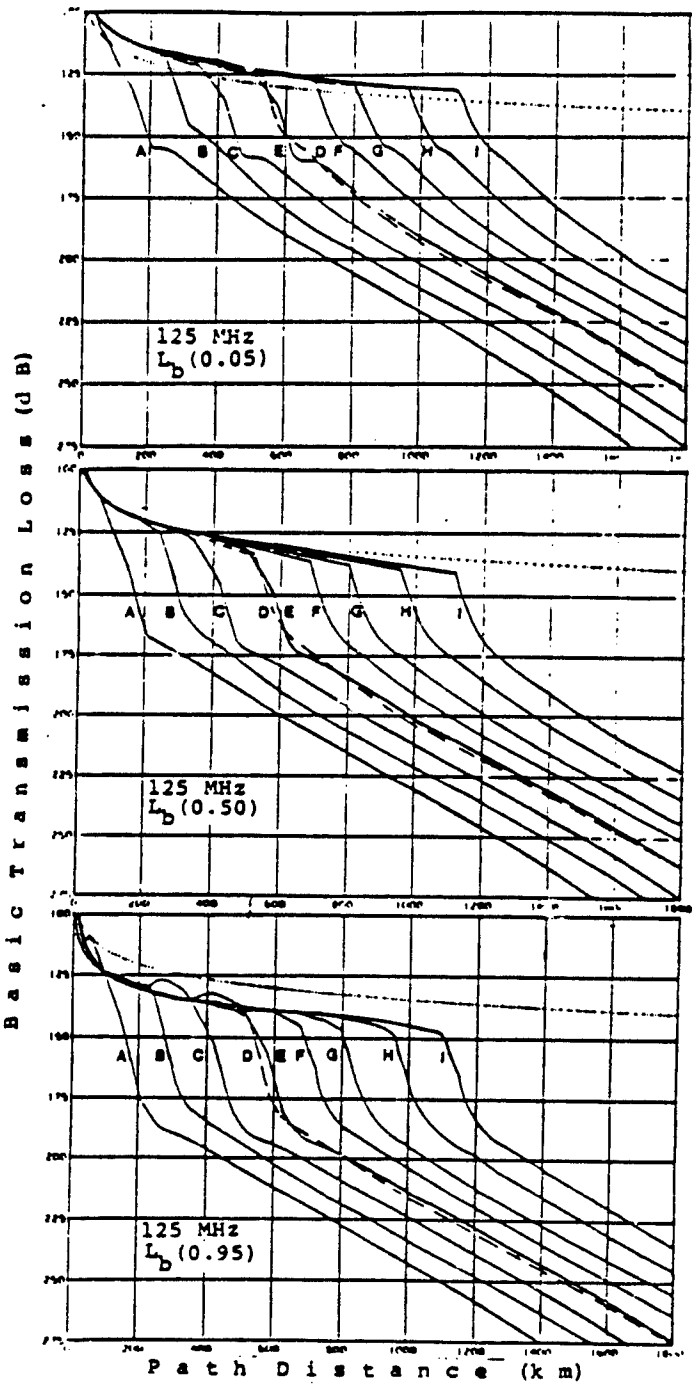

Antenna heights as indicated.

Code	H_1 (m)	H_2 (m)
A	15	1000
B	1000	1000
C	15	10000
D	1000	10000
E	15	20000
F	1000	20000
G	10000	10000
H	10000	20000
I	20000	20000

.....Free space

Continental temperate climate.
N_s=301 (k=4/3).
smooth earth (Δh=0).
horizontal polarization.
average ground.
and isotropic antennas.

Time availability on graph.

Figure 8-1. Basic transmission loss, 125 MHz.

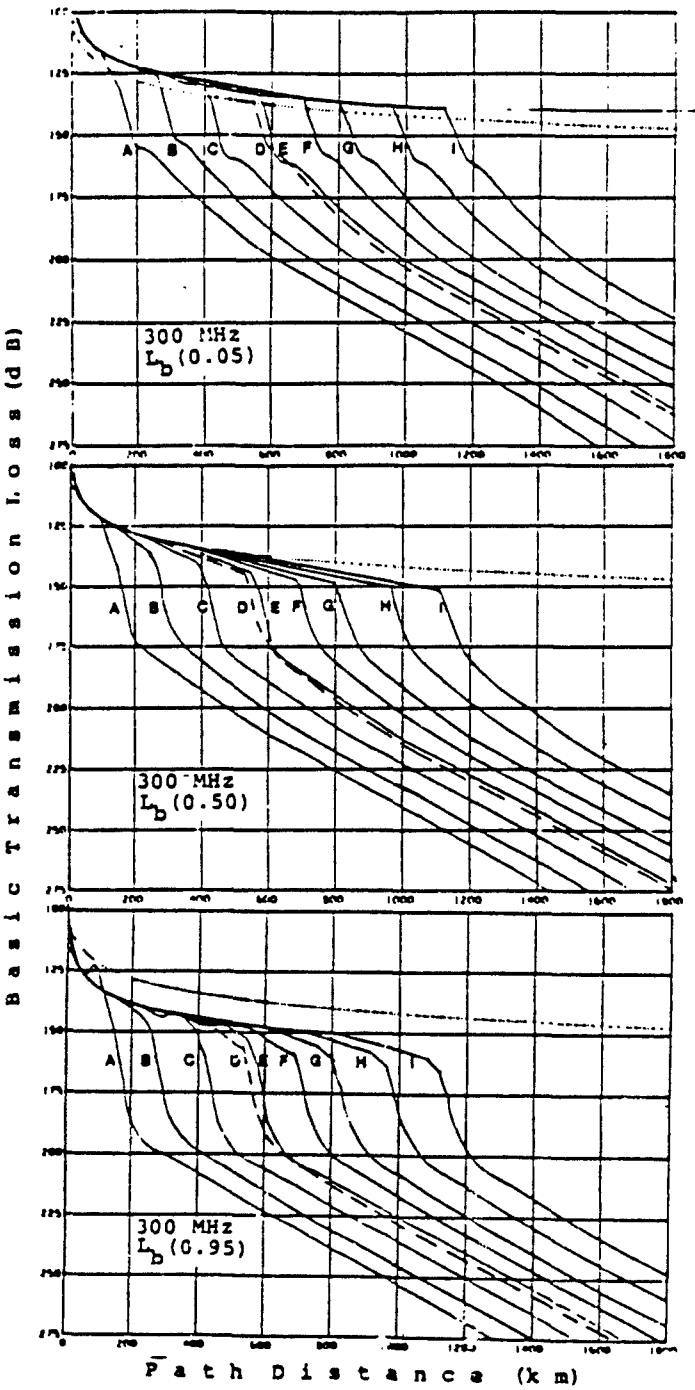

Antenna heights as indicated.

Code	H_1 (m)	H_2 (m)
A	15	1000
B	1000	1000
C	15	10000
D	1000	10000
E	15	20000
F	1000	20000
G	10000	10000
H	10000	20000
I	20000	20000

.....Free space

Continental temperate climate,
N_s=301 (k=4/3),
smooth earth (ih=0),
horizontal polarization,
average ground,
and isotropic antennas.

Time availability on graph.

Figure 8-2. Basic transmission loss, 300 MHz.

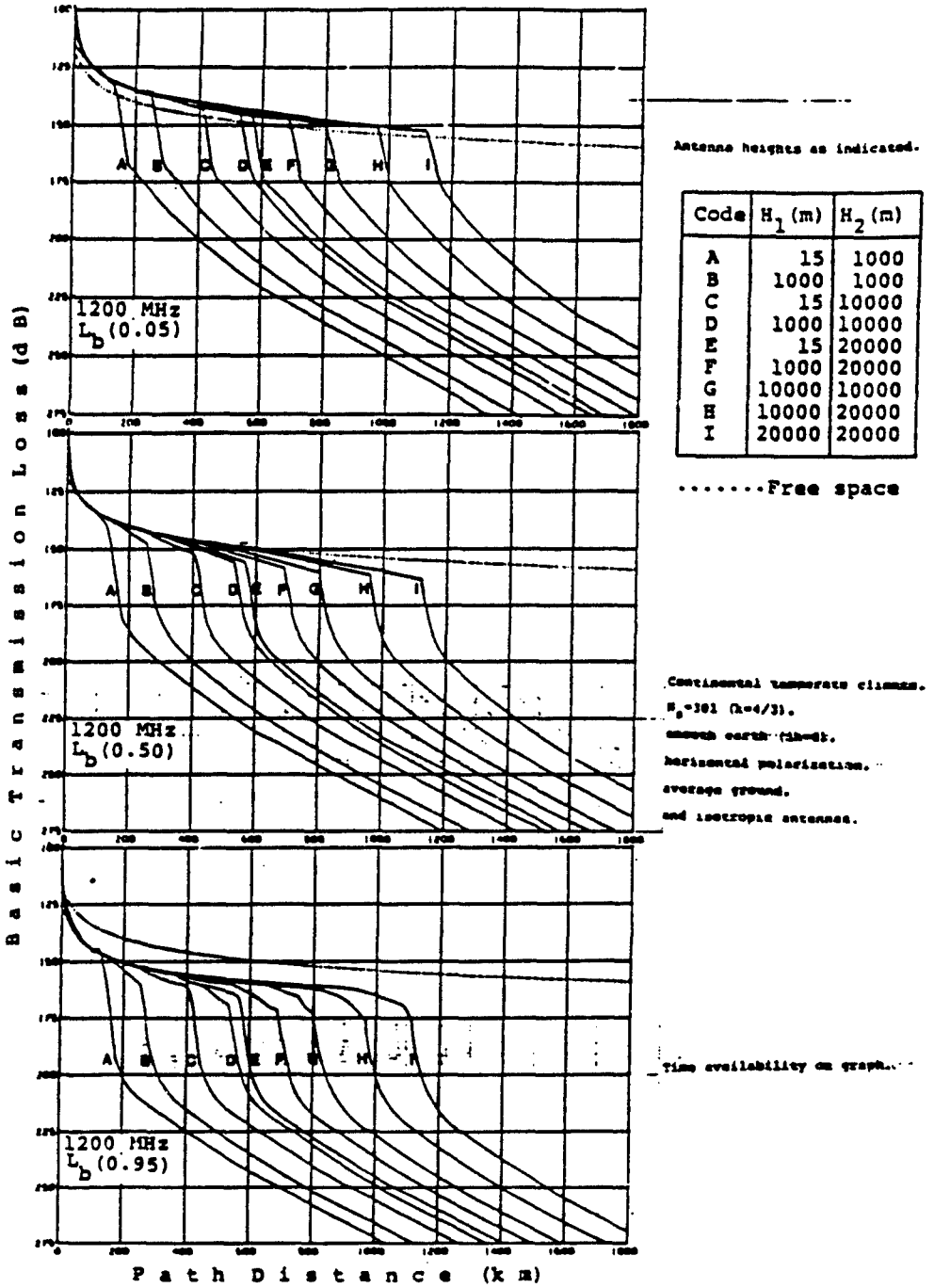

Figure 8-3. Basic transmission loss, 1200 MHz.

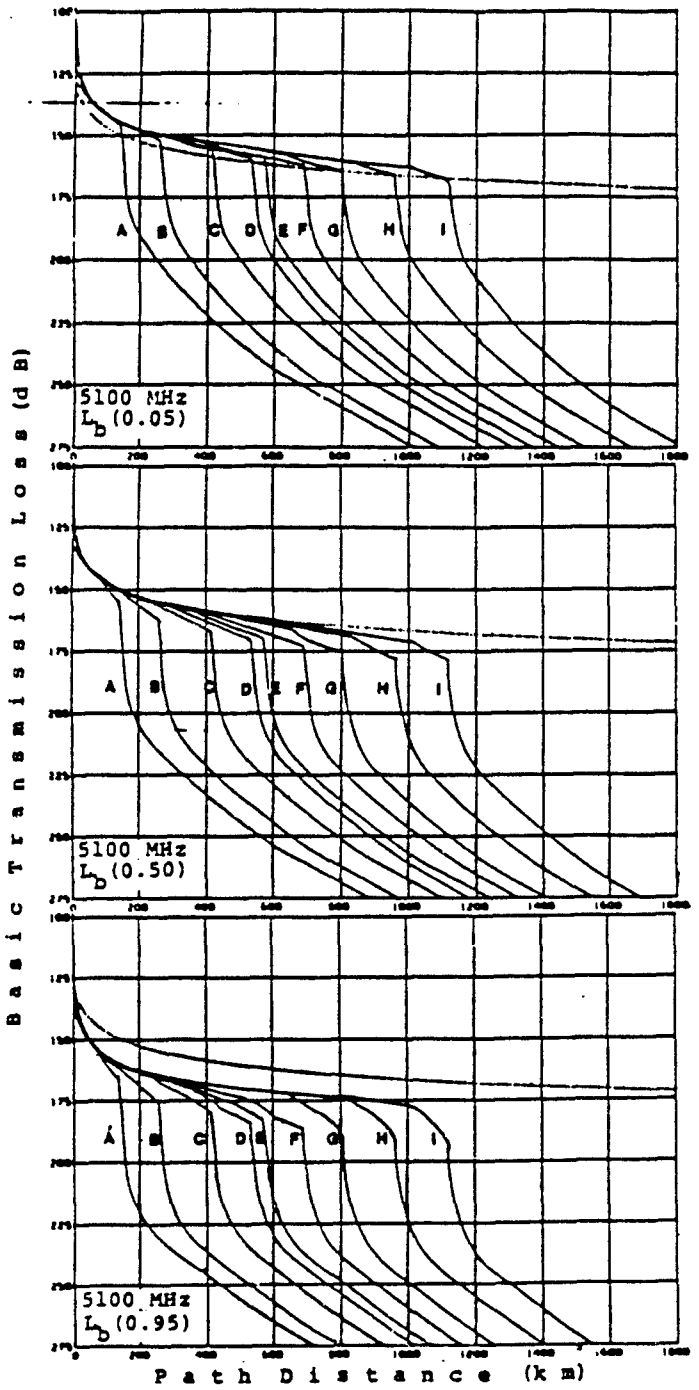

Antenna heights as indicated.

Code	H_1 (m)	H_2 (m)
A	15	1000
B	1000	1000
C	15	10000
D	1000	10000
E	15	20000
F	1000	20000
G	10000	10000
H	10000	20000
I	20000	20000

.....Free space

Continental temperate climate.
N_s=301 (k=4/3).
smooth earth (Δh=0).
horizontal polarization.
average ground.
and isotropic antennas.

Time availability on graph.

Figure 8-4. Basic transmission loss, 5100 MHz.

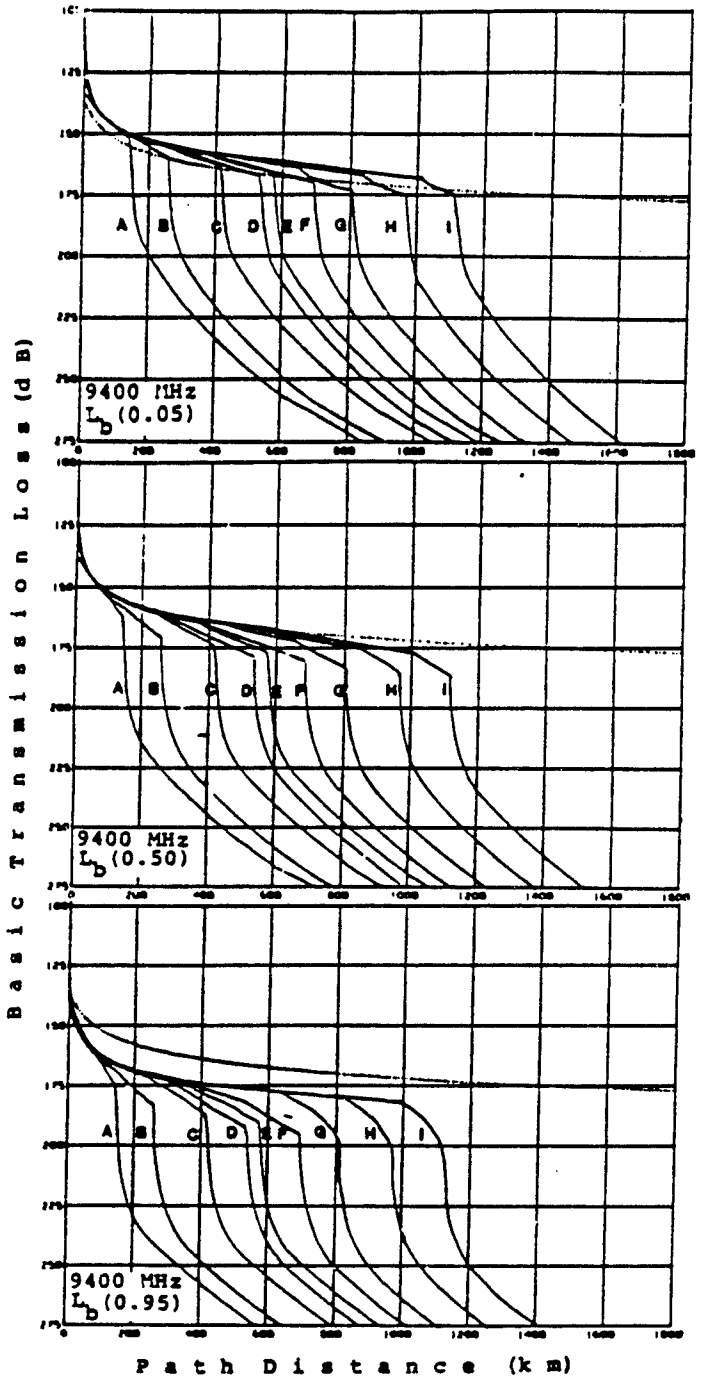

Antenna heights as indicated.

Code	H_1 (m)	H_2 (m)
A	15	1000
B	1000	1000
C	15	10000
D	1000	10000
E	15	20000
F	1000	20000
G	10000	10000
H	10000	20000
I	20000	20000

.....Free space

Continental temperate climate.
N_s=301 (k=4/3),
smooth earth (Δh=0),
horizontal polarisation,
average ground,
and isotropic antennas.

Time availability on graph.

Figure 8-5. Basic transmission loss, 9400 MHz.

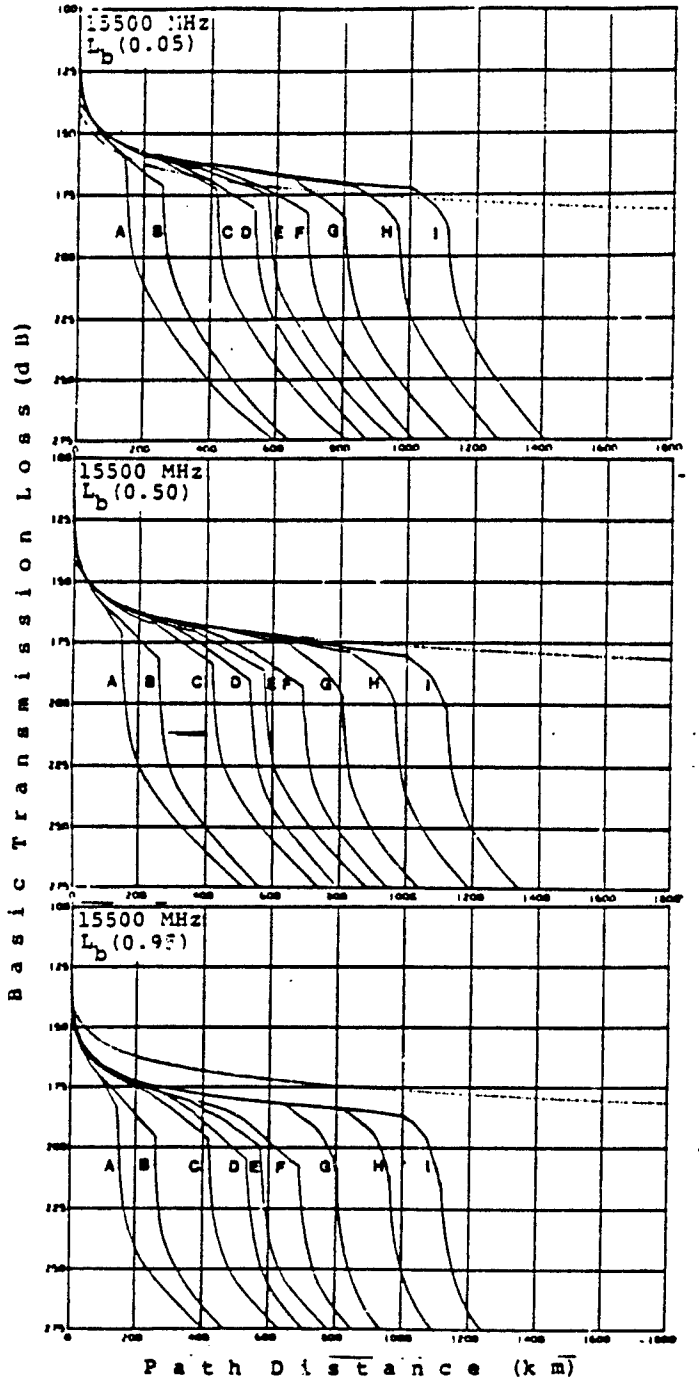

Antenna heights as indicated.

Code	H_1 (m)	H_2 (m)
A	15	1000
B	1000	1000
C	15	10000
D	1000	10000
E	15	20000
F	1000	20000
G	10000	10000
H	10000	20000
I	20000	20000

.....Free space

Continental temperate climate,
N_s=301 (k=4/3),
smooth earth (Δh=0),
horizontal polarization,
average ground,
and isotropic antennas.

Time availability on graph.

Figure 8-6. Basic transmission loss, 15,500 MHz.

$L_b(0.95)$ = 200 dB means that the basic transmission loss would be 200 dB or less during 95% of the time. The antenna heights shown vary from 15 m to 20,000 m, covering both ground station and aircraft heights.

8.3 THE COMPUTER MODEL

The computer code for IF-77 is operational at ECAC. Documentation of operating instructions has not yet been completed.

8.4 VALIDATION AND COMPARISON WITH OTHER MODELS

Validation of IF-77 appears in References 8-3 and 8-4. The computer program can be used in two modes of operation: smooth-earth and terrain-sensitive. Studies in Reference 8-3 indicate that the smooth-earth mode has greater prediction accuracy.

A short study was conducted in FY-81. TABLE 8-1 lists the RMS errors presented in the output of this effort.[8-5]

8-3 Smith, R. D., A Comparison of Measured Data and ITS Model Predictions: VOR and TACAN Signal Strengths, FAA-RD-77-106, Federal Aviation Administration, Washington, DC, January 1978.

8-4 Johnson, M. E. and Gierhart, G. D., Comparison of Measured Data with IF-77 Propagation Model Predictions, FAA-RD-79-9, Federal Aviation Administration, Washington, DC, August 1979.

8-5 Weissberger, M. A., and Powell, J. R., Results of the FY81 Study to Determine the Feasibility of Improving the Procedure for Predicting VHF Communications/Navigation Coverage, Memorandum to FAA-RD-450, November 1981.

TABLE 8-1

COMPARISON BETWEEN IF-77 SMOOTH-EARTH MODEL PREDICTIONS AND MEASURED LOSSES ON AIR-GROUND LINKS

Data Description	Type of Path	Number of different paths	RMS PREDICTION ERROR (dB)
Cliff-Ground Golden, Colorado Frequency: 230 MHz Great circle Distance: 10-80 km Altitude: 500 m Terrain irregularity: 125 m	LOS	27	12.0
	Non LOS	8	7.9
Air-Ground Chickasha, Oklahoma 110 MHz 40 - 80 km Altitude: 150-1500 m Terrain irregularity: 0 m	LOS	33	4.7
	Non LOS	7	5.1

LOS: Line-of-Sight

Non LOS: Beyond Line-of-Sight

Extensive comparisons between ECAC's models and IF-77 have not yet been done. The current recommendation that the smooth-earth mode of IF-77 be used at ECAC for air-ground predictions in the 100 MHz < f < 15,000 MHz range is based on:

1. The acceptance of IF-77 by the FAA and the CCIR.
2. The availability of published comparisons between IF-77 predictions and air-ground measurements.
3. The fact that IF-77 contains algorithms which allow a statistical treatment of the interference pattern caused by the interaction between the direct and ground-reflected rays. ECAC smooth-earth codes do not have this option presently.

8.5 CONCLUDING REMARKS

1. The consistent ability of the IF-77 code to accurately account for terrain irregularity has not been demonstrated yet.
2. Potential biases are introduced by using the present IF-77 troposcatter subroutine instead of the validated[8-6] NBS TN101 algorithm. (This will only be significant for paths well beyond the radio horizon.)

[8-6] Longley, A. G., Reasoner, R. K., and Fuller, V. L., OT/TRER 16, ITS, Boulder, CO, 1971.

CHAPTER 9

SURFACE-TO-SURFACE PROPAGATION IN THE 40 MHz - 20 GHz BAND: MEDIAN LOSS

PART 1: STATISTICAL AND POINT-TO-POINT MODELS

By: M. Weissberger

9.1 INTRODUCTION

Part 1 of this chapter provides a brief overview of the types of models available for predicting the basic transmission loss between two antennas located on or above the earth's irregular surface. Section 9.2 contains a description of statistical models. These were developed to predict the median loss value for a set of circuits with the same lengths, antenna heights, frequency, and polarization. Because each circuit in a set will usually pass over a different topographic profile, and because the profile is one factor that determines the loss, a set of circuits will have a range of losses rather than a single value. The statistical models use a probability distribution (usually a normal distribution of decibel values) to describe this range of losses. They do not use the details of a specific path profile to predict the loss for an individual circuit in a set. Statistical models include those which:

a. Utilize no information about the geographical area for which the predictions are being made, e.g., Egli's model.

b. Are intended only for one geographical region, e.g., the British Aircraft Corporation's Federal Republic of Germany statistical model.

c. Utilize a terrain irregularity factor to adapt the model to different geographical areas and a qualitative description of how well the two antennas are sited with regard to the terrain, e.g., the Longley-Rice model.

d. Utilize a terrain irregularity factor to adapt the model to different geographical areas and a quantitative description of how high the

transmitting antenna is above the foreground in a particular sector, e.g., the FCC R6602 model.

e. Utilize a qualitative description of the degree of urbanization, e.g., Okumura's model.

f. Utilize a quantitative description of the degree of urbanization, e.g., Kinase's model.

Section 9.3 is an overview of the second type of model used to compute median loss in this band. These are the "point-to-point" models which utilize the details of the terrain profile between a specific transmitting location and a specific receiving location in the process of computing the basic transmission loss for a radio circuit between these two points. (Both statistical and point-to-point models should account for time variability and the magnitude of the model's inaccuracy. Both types of models rely on statistics for these purposes. Thus, the method of accounting for the effects of profiles is the only difference between the two categories of models described in this chapter. Note also that an accurate point-to-point model, with accurate topographic input data, could be used to predict the distribution of losses for any arrangement of paths in any geographical area. Thus, in principle, a point-to-point model can be used to synthesize a statistical model. A study of the accuracy of these synthesized statistical models in comparison with that of statistical models derived through other means was initiated in FY82.)

Section 9.4 provides examples of the increase in prediction accuracy that has been observed when a statistical model was replaced by a point-to-point model.

Part 2 of ths chapter provides a description of the point-to-point model that is recommended for use at ECAC. This is TIREM, the Terrain Integrated Rough Earth Model.

9.2 STATISTICAL MODELS

9.2.1 Published Formulas

The overall thrust of this chapter of the Handbook is to recommend use of point-to-point models whenever possible. However, because of the large number of statistical-model development efforts that have been reported, it is desirable to at least acquaint the reader with them. Further, there may be occasions when an analyst finds one statistical model based on data that are very similar to the type that would help him to estimate system performance in a particular environment.

Equation 9-1 will be used as a universal formula for a quantitative description of the models:

$$L_b = a_1 + a_2 \log f + (a_{3a} + a_{3b} \log f) \log d + a_4 \log h_t + a_5 \log h_r. \quad (9\text{-}1)$$

where

L_b = Basic transmision loss, dB
f = Frequency, MHz
d = Path length, km
h_t = Transmitting antenna height, m
h_r = Receiving antenna height, m
$a_1 - a_5$ = Constants obtained from theory or by curve fitting of measurements.

The use of separate coefficients for the transmitting and receiving antennas does not represent a violation of reciprocity. It is a format used by some model developers to describe the fact that the functional dependence of loss on antenna height is different for antennas near the earth than it is for antennas well above the earth. Several statistical models were developed to predict the performance of circuits consisting of a central broadcasting

transmitting antenna located more than 100 meters above the surrounding terrain and remote receivers located no more than about 10 meters above the surface. Therefore, these models generally have different coefficients for the transmitting and receiving antenna heights. The 1951 FCC model[9-1] represents one of the earlier examples of this approach.

The fact that many statistical models can be represented by Equation 9-1 is related to the starting point of these models -- the theoretical equation for the basic transmission loss between two antennas over a plane earth. (This is derived in APPENDIX A of this Handbook.) Other models (e.g., EPM-73,[9-2]) were developed by modifying relations for propagation over a smooth spherical earth. Another model (Longley-Rice,[9-3,9-4]) is based on a combination of the smooth-sphere and double-knife-edge obstruction relations. The models without the plane-earth starting point generally have functional forms different from Equation 9-1. To provide insight into the general nature of differences between all of the formulas, a set of results of the non-plane-earth-based equations was generated, and least-squares curve fitting was done to obtain values of a_i for these equations. Because this procedure was carried out for a very narrow parameter range, the agreement between the values obtained from the original published versions of the equations and the values obtained from the transformed equations is very good. Values of a_i that were obtained from equations originally published in another form are annotated.

9-1 Fine, H., UHF Propagation Within Line-of-Sight, T.R.R. Report 2.4.12, Federal Communications Commission, Washington, DC, June 1951.

9-2 Lustgarten, M. N., and Madison, J. A., "An Empirical Propagation Model (EPM-73)," IEEE Trans. on Electromagnetic Compatibility, August 1977.

9-3 Longley, A. G., and Rice, P. L., Prediction of Tropospheric Radio Transmission Loss Over Irregular Terrain -- A Computer Method 1968, ESSA Tech. Report 148-ITS 97, ITS, Boulder, CO, 1968.

9-4 Hufford, G. A., Longley, A. G., Kissick, W. A., A Guide to the Use of the ITS Irregular Terrain Model in the Area Prediction Mode, NTIA Report 82-100 ITS, Boulder, CO, April 1982.

Eleven statistical models are described on the following pages. The labels "data" and "application" are used, when necessary, to distinguish between the parameter range of the measurements used to develop a model and the parameter range over which the model's author reports the equation applicable. A table of values of a_i follows the descriptions.

Egli (References 9-5 and 9-1)

Frequencies: 40-910 MHz. Notes below apply to the data above 288 MHz.

Path Lengths: 8-48 km.

Antenna Height: Transmitter - Generally greater than 100 m above the foreground terrain. Receiver - 2-10 m above the ground.

Locale: Smooth and hilly, urban and rural in the United States (data). No limits are prescribed for the areas of application.

Reported Standard Deviation: 8.3 dB at 128 MHz; 11.6 dB at 510 MHz.

Notes: The best understanding of this model is obtained by reading both Egli's and Fine's reports since Egli borrowed heavily from Fine. Most of Fine's data were for line-of-sight paths, but he noted similar behavior on one transhorizon path. The model was derived from observation of the deviations of the measured loss from the theoretical plane-earth loss. Fine's model was derived using values of antenna height measured relative to the terrain stretching from 2 to 10 miles in front of the transmitter. Egli claims that antenna heights "above the surface" can be used in the equation with acceptable results.

Saxton,[9-6] reported a model similar to Egli's in 1954. It was based on a collection of data that overlapped Egli's.

[9-5] Egli, J. J., "Radio Propagation Above 40 MC Over Irregular Terrain," Proc. IRE, October 1957.

[9-6] Saxton, J. A., "Basic Ground-Wave Propagation Characteristics In the Frequency Band 50-800 Mc/s," Proc. IEE, (London), Vol. 101, Part III, 1954, p. 211.

Longley-Rice (References 9-3 and 9-4)

Frequencies: 20-600 MHz (most of data). 20-20,000 MHz (application).

Path Lengths: 5-50 km (data in the 20-100 MHz band) 5-160 km (data in the 60-600 MHz band). Data at much longer distances were used to develop the tropospheric scatter model. 1-1,000 km (application)

Antenna Height: 1-9 m above the ground, transmitter and receiver (data in the 20-100 MHz band.) 10-1500 m above the foreground terrain (transmitter) and 3-9 m above local terrain (receiver) (data in the 60-600 MHz band.) 0.5-3,000 m (application).

Locale: Wide range of terrain types. Most of the measurements used to develop the model were for paths on which the antenna foregrounds were clear. Vegetation and buildings tended to be sparse.

Reported Standard Deviation: 10 dB at 100 MHz for rough or moderately rough terrain.

Notes: One input parameter is ΔH, the interdecile range of terrain elevations for the area in which predictions are desired. Another is a code to describe each antenna's siting as being either random, careful, or very careful. In the diffraction region, the predictions are a weighted combination of smooth-sphere and double-knife-edge results. A preliminary version of the model is documented in Annex 1 of a report by Rice.[9-7] For a period of time, this model was called "ARPROP" (Area Propagation Model) and recent ITS reports use the name "ITS Irregular Terrain Model". There is an option to use the model to obtain point-to-point predictions when profile information for a path is available.

[9-7] Rice, P. L., Transmission Loss Predictions for Tropospheric Communication Circuits, NBS Technical Note 101, ITSA, Boulder, CO, revised, January 1967.

The accuracy of the model's statistical (area) mode has been questioned in studies of the loss on certain types of paths (line-of-sight[9-8,9-9] and single knife-edge[9-9]), of circuits at frequencies above 400 MHz[9-10], and of paths in certain geographical areas.[9-11,9-12] Potential users of the model should review References 9-8 through 9-12, since the latest version of the code (Reference 9-4) does not appear to have been modified as a result of these questions. A comprehensive validation effort in which the new code is used with input parameters chosen according to the principles outlined in Reference 9-4 would be informative, but has not yet been conducted.

9-8 Longley, A. G., and Reasoner, R. K., Comparison of Propagation Measurements With Predicted Values in the 20 to 10,000 MHz Range, ESSA Tech Report ERL 148-ITS 97, ITS, Boulder, CO, January 1970.

9-9 Longley, A. G., et al., Measured and Predicted Long-Term Distributions of Tropospheric Transmission Loss, OT/TRER 16, ITS, Boulder, CO, July 1971.

9-10 Barsis, A. P., "Radio Wave Propagation Over Irregular Terrain in the 76-9200 MHz Range," IEEE Trans. on Veh. Tech., August 1971.

9-11 Whiteman, R. A., An Analysis of Bell Aerosystem Co.'s Propagation Measurements, ECAC-CR-79-014, ECAC, Annapolis, MD, March 1978.

9-12 Whiteman, R. A., A Supplement to an Analysis of Bell Aerosystems Co.'s Flagstaff Propagation Measurements, ECAC-CR-81-029, ECAC, Annapolis, MD, December 1981.

Okumura (References 9-13 and 9-14)

Frequencies: 150-2000 MHz.

Path Lengths: 1-100 km.

Antenna Heights: Transmitting: 30-1000 m above foreground terrain. Receiving: 2-7 m above ground.

Locale: Urban, suburban, open; smooth, hilly, isolated mountain, gently sloping, and land-sea; near Tokyo, Japan.

Reported Standard Deviation: 8.5 dB, 2000 MHz, hilly suburban locale.

Notes: The core of the model is a set of curves of data taken in a dense, level, urban area. Then corrections for other levels of urban buildup and terrain types were developed. Hata (see Reference 9-14) developed analytical expressions for Okumura's curves.

9-13 Okumura, Y., et al, "Field Strength and its Variability in VHF and UHF Land Mobile Service," Review of the Tokyo Electrical Communication Laboratory, September-October, 1968.

9-14 Hata, M., "Empirical Formula for Propagation Loss in Land Mobile Radio Services," IEEE Trans. on Veh. Tech., August 1980.

EPM-73 (see Reference 9-2)

Frequencies: 20-10,000 MHz (data). 1-10,000 MHz (application).

Path Lengths: 1.6 - 480 km (application). 0.5-965 km (data).

Antenna Height: 1-3000 m (application). 1-400 m (data).

Locale: Primarily rolling plains. Long distance troposcatter measurements were from a wide range of areas (data). Terrain that is not mountainous (application).

Reported Standard Deviation: 10 dB at 100 MHz. 14 dB at 400 MHz.

Notes: Derived from smooth-earth theory. Separate models for high and low values of (antenna height/wavelength).

Malaga (Reference 9-15)

Frequencies: 3-450 MHz.

Path Lengths: 0.1-4 km (data). 0.1-10 km (application).

Antenna Height: 1.5 meters above ground (transmitter and receiver data).

Locale: Separate equations were developed for an urban area, Boston, MA, and a suburban area (residential and shopping districts), Lexington, MA.

Reported Standard Deviation: 7.7 dB for urban area, 3-450 MHz. 7.3 dB for the suburban area, 3-450 MHz.

Notes: Regression fit of data. Uses a non-zero value of a_{3b}. Recommends use of Okumura's data to adjust results for different antenna heights ("height gain.") Appears to be the only statistical model for urban propagation based on data in the 3-50 MHz band.

9-15 Malaga, A., "An Empirical Path Loss Model for HF/VHF Propagation in Urban Areas," Radio Science, May 1981.

Kinase (Reference 9-16)

Frequencies: 90-770 MHz (data). 3-1000 MHz (application).

Path Lengths: 2-100 km

Antenna Height: Transmitting antennas: 90-300 m above receivers. Receiving antennas: 3-20 m.

Locale: Smooth and hilly terrain, urban, suburban and rural clutter. Near Tokyo and Osaka, Japan.

Reported Standard Deviation: Data are given, but the emphasis is on the deviation of the effects of buildings and trees, not deviation of the overall prediction method.

Notes: The main statistical prediction is of the effects of clutter (i.e., buildings and trees) on the loss that would be expected for the same terrain profile with no clutter. Graphs of Kinase's clutter correction appear in Chapter 11 of this Handbook.

9-16 Kinase, A., Influences of Terrain Irregularities and Environmental Clutter Surroundings on the Propagation of Broadcasting Waves in the UHF and VHF Bands, Japan Broadcasting Corporation (NHK) Technical Monograph 14, March 1969.

British Aircraft Corporation Statistical (Reference 9-17)

Frequencies: 40-110 MHz.

Path Lengths: 2-60 km.

Antenna Heights: Transmitter: 13 m above ground. Receiver: 3 m above ground.

Locale: West Germany. Transmitter was carefully sited. Along one radial it was 200 meters above the foreground. Topography included high ground with heavy woods.

Reported Standard Deviation: 13.3 dB.

Notes: Regression fits were done for the complete set of paths as well as for these categories of paths: line-of-sight, one obstacle, multiple obstacles. Author observes similarities of results for all paths with Egli's model. In the comparison, only the structural height of the transmitting antenna was used.

9-17 Lee, B. K., "VHF Propagation Predictions With Path Profile Methods," AGARD Conference Proceeding No. 244, NATO, France, September 1978.

AMSAA (Reference 9-18)

Frequencies: 50-450 MHz.

Path Lengths: 1-15 km (radial data). 1-10 km (tactical data).

Antenna Height: 1 meter (transmitter and receiver).

Locale: Harford County, MD. Rolling hills, ridges, heavy woods. The "radial" data involved a transmitter with random siting relative to the terrain along some radials and careful siting with regard to the terrain along others. The "tactical data" involved transmitters and receivers in various locations - except hilltops.

Reported Standard Deviation: 9.3 dB for radial data.

Notes: Regression of data used to obtain values of a_1, a_2, and a_{3a}. Separate models for radial data, tactical data, and obstructed tactical paths. Author notes similarities between terrain of measurement area and terrain in portions of FRG.

9-18 Stratton, S., and Prichard, D., Measured Propagation Ioss Data at 50, 150, and 450 MHz, Interim Note C-100, U.S. Army Materiel Systems Analysis Activity (AMSAA), Aberdeen Proving Ground, MD, May 1981.

NBS TN 101, Annex 1 (Reference 9-7)

Frequencies: See notes below.

Path Lengths:

Antenna Heights:

Locale:

Reported Standard Deviation:

Notes: TN 101 is known chiefly as a reference for formulas used in point-to-point models. In Annex 1 of the report, however, there are descriptions of the three statistical models listed below.

i) A predecessor of the Longley-Rice model.

ii) A smooth-earth model with troposcatter calculations.

iii) A very simple empirical model using only a_1, a_2, and a_{3b}, developed for (primarily) beyond line-of-sight links with carefully sited antennas.

Rice recommends use of point-to-point models when knowledge of the terrain is available. For other cases, he recommends "i" as being the best of the statistical models. Since this has been updated (References 9-3 and 9-4) over the years and is now called "Longley-Rice", readers should see the separate entry under this name.

Arctic (Reference 9-19)

Frequencies: 150-450 MHz

Path Lengths: 1-100 km.

Antenna Heights: Transmitting: 7-17 m. Receiving: 1.5-3.0 m.

Locale: Canadian North West Territories. Separate models for these two cases:

1. Well-sited transmitter, ground flat and hilly, sparse vegetation, 69° latitude.
2. Random-sited transmitter, flat-topped hills, salt water, 75° latitude.

Reported Standard Deviation: 10 dB for area 1, 15 dB for area 2.

Notes: Regression fitting was done to obtain a_1, a_2, a_{3a}, a_4, and a_5. Separate values were determined for summer and winter. Notes on the effects of fresh-water and salt-water ice are presented.

9-19 Palmer, F. H., "Measurements of VHF/UHF Propagation Characteristics Over Arctic Paths," IEEE Trans. on Ant. and Prop., November 1980.

Modified Plane Earth[9-20,9-21]

Frequencies: 20-100 MHz

Path Lengths: 5-80 km

Antenna Heights: 1-9 m

Locale: Colorado plains, forested hills outside of Cleveland, OH.

Reported Standard Deviation: Hufford reported that the standard deviation of the plains data at 100 MHz, at fixed antenna heights, was about 9 dB. Therefore, the σ of the model errors has to be at least this large.

Notes: In the "Modified Plane Earth Model", the coefficients a_i are the same as in the theoretical equation for a plane earth as listed in the second line of TABLE 9-1. (A derivation of this is shown in APPENDIX A.) The terms h_i, however are replaced by:

$$h_i' = h_i + h_e \qquad (9\text{-}2)$$

where h_e is the effective antenna height. This is a mathematical device used by Bullington to account for the surface wave. Hufford estimated h_e to be 150/f for vertical polarization and 50/f for horizontal. He reported that the resulting L_b equation gave a reasonable approximation to the mean of the data described above. In TABLE 9-1, the values of a_4 and a_5 were derived from this equation:

$$20[\log (9 + h_e) - \log (1 + h_e)] = a_{4,5} (\log 9 - \log 1) \qquad (9\text{-}3)$$

9-20 Bullington, K., "Radio Propagation Fundamentals," Bell System Technical Journal, May 1957.

9-21 Hufford, G. A., and Montgomery, J. L., On the Statistics of VHF Field Strength Measurements Using Low Antenna Heights - I, NBS Report 9223, National Bureau of Standards, Boulder, CO, May 1966.

TABLE 9-1 contains values of the coefficients for Equation 9-1 for the statistical models.

9.2.2 Supplementary Data Involving Coupling Between Two Low Antennas Over Irregular Terrain at UHF

Figure 9-1 illustrates several sets of measured basic transmission loss values for these parameters: f = 300 MHz, $h_t = h_r$ = 1-3 m, $1 \leq d(km) \leq 20$. An equation showing the corresponding values of a_1 and a_{3a} also appears on the figure. The figure and equation are not intended to be a model. They are presented to alert analysts to more sets of data which may be directly applicable to a task at hand. The source documents are References 9-18, 9-11, and 9-22.

TABLE 9-2 contains some additional measured values of a_2 (loss vs distance). TABLE 9-3 contains some additional measured values of a_5 (loss vs antenna height). The Barsis report cited in the TABLE is Reference 9-23.

9-22 Hause, L. G., UHF Radio Propagation Data For Low Antenna Heights, ERL 134-ITS 93-1, ITS, Boulder, CO, November 1969.

9-23 Barsis, A., et al, Analysis of Propagation Measurements Over Irregular Terrain, ERL 114-ITS 82, ITS, Boulder, CO, March 1969.

TABLE 9-1

TYPICAL VALUES OF COEFFICIENTS FOR EQUATION 9-1

Model	Parameter Restrictions Other Than Those Noted In Text	a_1	a_2	a_{3a}	a_{3b}	a_4	a_5
Free Space		32	20	20	0	0	0
Plane Earth Theory		120	0	40	0	-20	-20
Modified Plane Earth		120	0	40	0	-13	-13
Egli[a]	$h_r \leq 10$ m	78	20	40	0	-20	-10
Egli[a]	$h_r > 10$ m	88	20	40	0	-20	-20
British Aircraft	All paths	70	10	37	0	--	--
Malaga	Suburban	-63	30	35[b]	1.53[b]	--	--
AMSAA	Radial	57	31	26	0	--	--
Okumura[c]	Urban, h_r = 1.5 m D = 1-20 km h_t = 30-200 m	70	26	(45-6.6 log h_t)	0	-14	--
Longley-Rice[d]	f = 300 MHz $h_t = h_r$ = 2 m D = 5-20 km (ΔH = 100 m)	108	--	33	--	--	--
EPM-73[d]	As above	108	--	33	--	--	--
Spherical Earth Theory[d,e]	As above	103	--	46	--	--	--
Arctic	Area 2, winter	96	8	31	0	-7	-16
Arctic	Area 2, summer	89	8	31	0	-7	-16

Note: In this table, "--" in a coefficient column means that the parameter restrictions of the model or the parameter restrictions of the portion of the model presented here are such that the coefficient is not applicable. In contrast, "0" in a coefficient column means that the model developer believes that the parameter does not play a significant role in determining loss.

[a]Coefficients derived from Fine, Equation 4, Reference 9-1.

[b]For D in meters.

[c]Hata's description.

[d]Coefficients derived from curve fitting of other expressions.

[e]Based on predictions from the NA computer model (see Maiuzzo and Frazier, Reference 6-8).

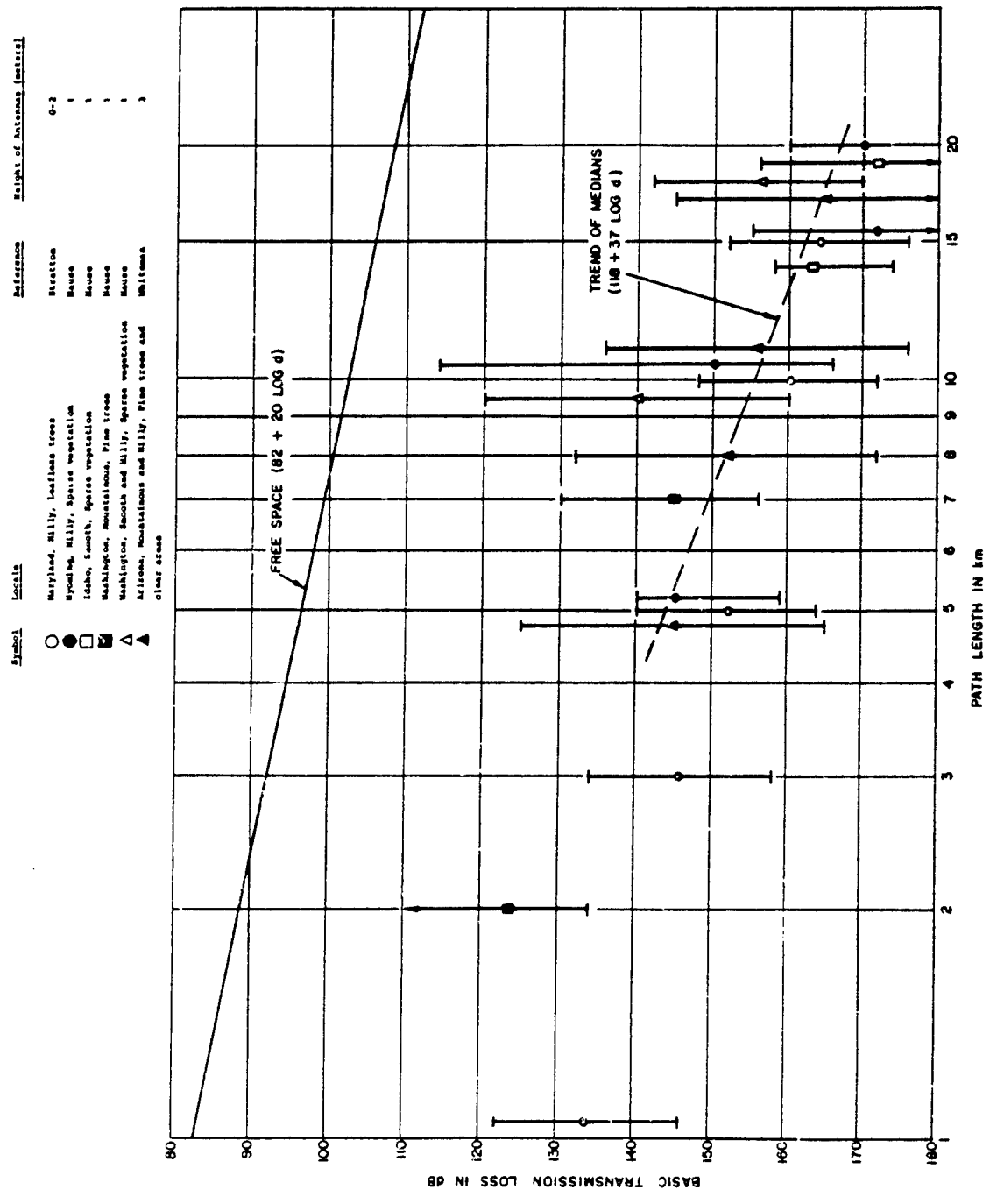

Figure 9-1. Measured values of basic transmission loss on paths with low antennas, Vertical Polarization. Vertical lines denote range that encompasses 80% of the measurements at a locale.

TABLE 9-2

OBSERVED INCREASE IN LOSS (dB)

WHEN FREQUENCY INCREASES FROM 300 MHz (ANTENNAS NEAR THE EARTH)

Measurement Locale	Final Frequency (MHz)		Reference
	1000	3000	
Colorado Plains	8 (15)	20 (20)	Barsis (9-23)
Colorado Mountains	24 (46)	44 (44)	Barsis (9-23)
Virginia Hills	12 (23)	30 (30)	Barsis (9-23)
Maryland Hills	16 (31)[a]	--	Stratton (9-18)
Arizona Hills and Mountains	8 (15)	--	Whiteman (9-11)
Median of Above	12 (23)	30 (30)	

[a]Projected from 450 MHz.

Note: The number in parentheses is the effective value of a_2.

TABLE 9-3

OBSERVED DECREASE IN LOSS

WHEN ONE ANTENNA HEIGHT INCREASES

FROM 1 METER TO 3 METERS (Barsis, Reference 9-23)

Measurement Locale	Δ Loss (dB)	a_5[a]
Colorado Mountains	14	-29
Colorado Plains	6	-13
Idaho Plains	9	-19
Washington Hills	8	-17
Wyoming Hills	6	-13
Median of Above	8	-17

[a] This is the value of a_4 also, if the transmitting antenna is at a low height.

9.3 POINT-TO-POINT MODELS

In a sense, the history of point-to-point models extends back to a date no later than 1933. This was the year of the Bell System Technical Journal article[9-24] that contained a user-oriented procedure for predicting the field strength due to a transmitter in the presence of a knife-edge obstacle located on an otherwise smooth earth. The prediction depended on the specific height of the obstacle and its location in reference to the transmitter and point of observation. The colleagues of the authors of that article also described an application of the procedure to an analysis of air-ground measurements in the 60 - 80 MHz range in 1933.[9-25] A point-to-point procedure for predicting UHF television field strengths, involving iterative knife-edge calculations and empirical adjustments for manmade structures, was published by Epstein and Peterson of RCA in 1953.[9-26]

Accomplishing a point-to-point prediction procedure by hand for a large number of circuits is not practical, particularly when it is appropriate to supplement knife-edge nomograms with calculations involving, for example, Norton's four-arc diffraction equation.[9-27] Therefore, computer-automated means of extracting parameters for the basic transmission loss equations from digitized representations of topographic profiles and for computing the loss were developed, as will be noted, no later than about 1964. This subsection

---

[9-24] Schelleng, J. C., Burrows, C. R., and Ferrell, E. B., "Ultra-Short Wave Propagation," Bell System Technical Journal, April 1933.

[9-25] Englund, C. R., Crawford, A. B., and Mumford, W.W., "Some Results of a Study of Ultra-Short Wave Transmission Phenomena," Proc. IRE, March 1933.

[9-26] Epstein, J., and Peterson, D., "An Experimental Study of Wave Propagation at 850 MC," Proc. IRE, May, 1953.

[9-27] Norton, K. A., Rice, P. L., and Vogler, L. E., "The Use of Angular Distance in Estimating Transmission Loss and Fading Range for Propagation Through a Turbulent Atmosphere Over Irregular Terrain," Proc. IRE, October, 1955.

addresses only these computer-automated point-to-point models. A brief description of several typical examples follows.

TIREM. The Terrain Integrated Rough Earth Model, TIREM, was developed at ECAC in the early 1960's and has been upgraded in the ensuing years.[9-28-9-33] TIREM utilizes a digitized terrain profile supplied by the analyst or one derived from a grid of elevations from Defense Mapping Agency tapes or other sources. The model is applicable from 40 - 20,000 MHz. It can be used for line-of-sight, diffraction and tropospheric-scatter paths. The primary validation efforts have involved antenna heights in the 3 - 500 m range, although air-ground studies are being conducted presently (see Reference 8-5). The propagation calculations are outlined in Part 2 of this Chapter.

9-28 Anderson, D., Automatic Extraction of Propagation Parameters From Profile Data, ASA-40, ECAC, Annapolis, MD, June, 1963.

9-29 Frazier, W., First Extension of Automatic Propagation Parameter Extraction Routine, MD-106, ECAC, Annapolis, MD, January 1964.

9-30 Plack, L., Terrain Integrated Rough Earth Model (TIREM), TN-011-187, ECAC, Annapolis, MD, January 1964.

9-31 Madison, J., TIREM Mode Selection Definition, Validation, and Proposed Model Improvement Efforts, ECAC-TN-73-06, ECAC, Annapolis, MD, July 1973.

9-32 Boldissar, F., An Analysis of Field Strength Contours for Public Broadcasting Stations, ECAC-PR-78-010, ECAC, Annapolis, MD, March 1978.

9-33 Meidenbauer, R., Powell, J., and Stuart, W., "TIREM Improvement Status," memo to XM/Janoski, September 1981.

POPROP. The Institute for Telecommunication Sciences (ITS) summarized many of the algorithms used in their own and in other point-to-point models in NBS TN-101 (Reference 9-7). The latest ITS point-to-point model, POPROP,[9-34] represents somewhat of a departure from the earlier work. The user can supply a digitized profile or the model can derive one from a grid of Defense Mapping Agency data. Paths are categorized as being either line-of-sight or beyond-line-of-sight. The former are handled by a combination of free-space spreading loss, ground-proximity loss at each terminal, and a line-of-sight obstacle-diffraction loss. Beyond-line-of-sight losses are covered by a troposcatter calculation in conjunction with either a rounded obstacle or double-knife-edge obstacle diffraction calculation. The troposcatter routine is a new development by Hufford. POPROP applies to problems in the 20 - 20,000 MHz range. Antenna heights may vary from 0.5 m to essentially infinity. The Longley-Rice model (References 9-3 and 9-4) is another ITS computer program that can be used to generate point-to-point predictions.

University of Manchester Service Area Model.[9-35] This code was developed for predicting the coverage of transmitters for a VHF mobile radio network. It accesses a stored grid of terrain elevations with a 500-meter lateral spacing. Propagation calculations include free-space, plane-earth, line-of-sight with a knife-edge diffraction loss, beyond-line-of-sight with 1, 2, or 3 knife-edges, and Bullington's effective knife-edge loss for paths with more than three discrete obstructions. The main application is for terrestrial antennas in the VHF band.

9-34 Hufford, G. W., and Longley, A. G., A Computerized Radio Propagation Model for Point-to-Point Applications, NTIA Technical Memorandum, June 1978, ITS, Boulder, CO, (not published).

9-35 Edwards, R., and Durkin, J., "Computer Prediction of Service Areas for VHF Mobile Radio Networks," Proc. IEE (London), Vol. 116, No. 9, September, 1969.

Directorate of Radio Technology Land Mobile Services Code[9-36] This uses the same profile extraction system devised by Edwards and Durkin (see Reference 9-35). The propagation model involves the theoretical loss over a smooth, spherical earth for line-of-sight links, and a weighted combination of smooth-sphere and knife-edge-diffraction losses for beyond-line-of-sight links. This beyond-line-of-sight method was described by Longley and Rice (see Reference 9-3). It differs from the statistical Longley-Rice model cited in Subsection 9.2 in that it takes into account the locations of the horizons resulting from the specific terrain profile between the transmitter and the assumed receiver location. The model is used in the VHF and UHF bands for terrestrial antennas. Like the code described earlier (see Reference 9-35), its applicability for interference calculations appears limited because there is no tropospheric scatter subroutine to predict propagation at long distances.

British Aircraft Corporation Empirical Path Profile Method. This was developed by BAC from their measurements in the 40 - 110 MHz band in FRG (see Reference 9-17). It differs from the statistical model described in subsection 9.2 in that it utilizes a grid of terrain elevations with either a 250-meter (smooth terrain) or a 125-meter (hilly terrain) lateral interval. Each path is categorized as to either line-of-sight, single-obstacle, or multiple-obstacle. Regression of measured values was used to determine coefficients for a loss equation that includes terms for path length, frequency, obstacle width, number of trees near an antenna, height of trees, distance between the horizons of the transmitter and receiver and other geometrical factors. The model's applicability to other locales is not clear.

9-36 Durkin, J., "Computer Prediction of Service Areas for VHF and UHF Land Radio Services," IEEE Transactions on Veh. Tech., November, 1977.

The BBC Co-Channel Interference Model[9-37] This model accesses a terrain data base for Great Britain, Ireland and Northwestern Europe. Profile points have a 500-meter lateral separation for Great Britain and Ireland and a larger spacing for Europe. Building and tree information is in the data bank. The model applies to frequencies from about 470 to 960 MHz, and to path lengths up to 1000 km. Loss calculations involve smooth spherical-earth diffraction, wedge diffraction, multiple-knife-edge diffraction, a four-arc diffraction model, and tropospheric scatter. Interference fields are estimated for 5% and 1% of the year.

Terrain.[9-38] This is computer program applicable to line-of-sight paths for which the field strength can accurately be represented by the sum of the direct and ground-reflected rays. The algorithm involves dividing the digitized terrain profile into a string of piecewise linear segments. Each segment is examined to determine if it is visible to the transmitter and receiver. Those that are visible are then are examined to determine which one is at the angle closest to the optimum for specular reflection. The effects of this segment are then determined using the amplitude and phase appropriate for rough-earth reflection. Limited validation in the UHF and SHF bands is reported in Reference 9-38. Some comparisons with air-ground measurements are reported in an ECAC study for the FAA (see Reference 8-5 in Chapter 8 of this Handbook). The model can access either user-supplied terrain profiles or an automated grid of values such as the one ECAC derived from Defense Mapping Agency tapes.

9-37 King, R. W., and Causebrook, J. H., Computer Programs for UHF Co-Channel Interference Prediction Using a Terrain Data Bank, BBC RD 1974/6, British Broadcasting Corporation, U.K., February, 1974.

9-38 Kuebler, W., and Leggett, R., "Deterministic Calculation of Terrain Dependent Propagation Loss," National Telecommunications Conference, Washington, DC, 1979.

Ohio University.[9-39,9-40] The Ohio University geometric-theory-of-diffraction (GTD) point-to-point models use both plane-surface reflection coefficients and edge-diffraction coefficients to predict field strengths in the line-of-sight region. The effects of the pattern of the transmitting antenna and of vegetation on the reflecting surfaces are taken into account. The main application of this code has been for predicting air-ground coupling in the VHF band. An ECAC-funded study of the applicability of the model to higher frequencies and to beyond-the-horizon paths will be published in late 1982. Some preliminary results will appear in the November 1982 IEEE Transactions on Antennas and Propagation.

Wagner.[9-41] The Wagner model is an extension to Hufford's 1952 integral approach. It has been applied successfully to one circuit at 60 MHz, but its consistent accuracy at frequencies of 20 MHz or higher has not been demonstrated.

[9-39] Chamberlin, K. A., Investigation and Development of VHF Ground-Air Propagation Computer Modeling Including the Attenuating Effects of Forested Areas for Within Line-of-Sight Propagation Paths, EER 51-1, Ohio University, Athens, Ohio, March 1981.

[9-40] Luebbers, R., et al., "GTD Terrain Reflection Model Applied to ILS Glide Slope", IEEE Trans. on Aerospace and Electronics Systems, January 1982.

[9-41] Ott, R. H., NTIA Report 79-20, ITS, Boulder, CO, May, 1979.

Other Point-to-Point Models

Other recent point-to-point modeling efforts are discussed in References 9-42 through 9-45.

9-42 Meeks, M. L., VHF Propagation Over Hilly, Forested Terrain, Project Report CMT-19, MIT Lincoln Laboratory, Lexington, MA, April 1982.

9-43 de Mercado, J., "Microcomputers for Spectrum Management", Telecommunications Journal, April 1982.

9-44 Lorenz, R. W., "Field Strength Prediction Method for a Mobile Telephone System Using a Topographical Data Bank", IEE Conference Publication # 188, IEE, London, 1980.

9-45 Terrain Profile and Contours in E. M. Propagation, AGARD Conf. Proc. 269-17, Oslo-Spatind, 1979.

9.4 THE ACCURACY OF POINT-TO-POINT MODELS IN COMPARISON WITH STATISTICAL MODELS, WHEN BOTH MODELS ARE USED TO PREDICT THE LOSS ON A SINGLE CIRCUIT[a]

One early comparison of the accuracy of the two types of models was reported by Rice in 1967 (Reference 9-7). The statistical model used in the comparison was a regression fit to measurements taken on 200 beyond line-of-sight links with carefully sited antennas. (See item "iii" on Page 9-15 of this Handbook). The point-to-point model was based on algorithms described in Reference 9-7. The statistical model was observed to have errors greater than ± 15 dB for about 13% of the paths. The point-to-point model had such errors for only 1% of the paths.

The original (1968) report on the Longley-Rice model (Reference 9-3) contained a comparison between the statistical and point-to-point modes of operation of that model. In this quite influential document, the point-to-point mode was described (through graphs) as being less accurate than the statistical mode. One factor contributing to this result may have been an inaccurate point-to-point algorithm for line-of-sight paths[b]; another factor was that the data shown in the comparison was part of the set used to develop the empirical factors in the statistical algorithms. In a subsequent report (Reference 9-9), an independent data set was examined, and Longley reported the need to isolate specific path types (such as those in which the transmitter and receiver have a common horizon) and then use prediction

---

[a] An error is defined here as the difference between the predicted median loss for a circuit and the observed loss, with both values in dB. Thus, this subsection does not address the ability of any model's published confidence limits to encompass the observed data. Rather it is concerned with the question of which type of model requires the user to add or subtract the smallest number of decibels to the model's median prediction to get a desired percentile of confidence for a circuit. This will generally be the model with the lowest rms error.

[b] The ECAC point-to-point model, TIREM, does not use this algorithm. See part 2 of this Chapter.

equations uniquely suited to these path types. This is essentially a point-to-point procedure, since the path profile must be used to determine which paths require the special treatment.

In 1978, Boldissar (see Reference 9-32), working with this author, compared the accuracies of the ECAC point-to-point model, TIREM, with that of three statistical models -- Longley-Rice (with the 1972 updates), EPM-73, and the current FCC model for VHF and UHF broadcasting coverage.[9-46] One phase of the comparison was concerned with measurements taken by ITS in the Colorado Plains, Colorado Mountains, and North East Ohio (all in the 50 - 100 MHz band) and at the Gunbarrel Hill, Fritz Peak, and Golden sites in Colorado (in the 230 - 751 MHz band). TABLE 9-4 shows the RMS error of the TIREM in comparison with the RMS error for the best of the three statistical models. TABLE 9-5 displays the results of this study in terms of the percentage of the predictions with errors greater than 10, 15, and 20 dB.

In another phase of the comparison effort, the accuracies of TIREM and the FCC R-6602 (statistical) model were compared with regard to predicting measured values of television field strengths. The measurements were primarily those collected by A.D Ring and Associates for the Television Allocation Study Organization, TASO. Measurement sites included Baton Rouge, LA, Lincoln, NB, Buffalo, NY, Wilkes-Barre, PA, Fresno, CA, Columbia, SC, and Columbus, OH. Frequencies ranged from 55 to 790 MHz. The results are shown in TABLE 9-6. It is seen that TIREM's RMS error is less than 19 dB in all cases, and it is less than 15 dB in most cases. The statistical model has errors of 21, 22, 28, and 54 dB. It is seen that, while this R-6602 model is quite accurate when compared with the measurements used in its development, its performance is less accurate when predicting other data sets. The table also shows a shortcoming of TIREM -- it does not presently account for foliage

---

9-46 Damelin, J., Daniel, W. A., Fine, H., and Waldo, G. V., Development of VHF and UHF Propagation Curves for TV and FM Broadcasting, FCC Report No. R-6602, Federal Communications Commission, Washington, DC, September, 1966.

TABLE 9-4

COMPARISON BETWEEN A POINT-TO-POINT MODEL, TIREM, AND THE BEST OF THE THREE STATISTICAL MODELS: RMS ERRORS (Reference 9-32)

Frequency Band	RMS Error (dB)	
	TIREM	Area Model
LVHF (54-108 MHz)	13.10	15.53
HVHF (174-216 MHz)	13.59	17.91
UHF (470-890 MHz)	15.31	21.15
MEAN	14.39	19.15

TABLE 9-5

COMPARISON BETWEEN A POINT-TO-POINT MODEL, TIREM, AND THE BEST OF THE THREE STATISTICAL MODELS: DISTRIBUTION OF ERRORS (see Reference 9-32)

Model	Percent of Paths With Errors Greater Than:		
	10 dB	15 dB	20 dB
TIREM	49%	30%	16%
Area Model	60%	43%	30%

attenuation automatically. Thus, while its mean error is near zero for paths in open areas with sparse vegetation (note the UHF ITS measurements in Colorado and the UHF TASO measurements in Fresno), it underpredicts the UHF fields in areas where vegetation is more prominent. Chapter 11 of this Handbook contains techniques that can be used to account for the additional attenuation due to obstruction by foliage or manmade structures. These techniques should be used to supplement TIREM predictions.

TABLE 9-6

COMPARISON OF TIREM AND THE R-6602 STATISTICAL MODEL WITH MEASUREMENTS

	Model	LVHF (54-88 MHz)				HVHF (174-216 MHz)				UHF (470-890 MHz)			
			#	m	σ	RMS	#	m	σ	RMS	#	m	σ	RMS
Meas. used to develop the FCC Model	T[a]	TASO/ Baton Rouge	97	-3.04	5.47	6.26					TASO/ Buffalo, Wilkes-Barre, Baton Rouge, Columbia	263	-15.11	10.97	18.67
	F[b]			0.07	2.67	2.67							-1.13	12.69	12.74
Meas. not used to develop the FCC Model	T	ITS/ Colo.	3591	-0.49	13.08	13.09	ITS/ Colo.	4218	2.32	13.39	13.59	ITS/ Colo.	8121	-0.56	15.30	15.31
	F			-14.92	23.84	28.12			3.42	20.40	20.68			7.87	20.52	21.98
	T						Neb.	62	2.53	7.00	7.44	TASO/ Fresno	153	1.95	11.82	11.98
	F								5.19	5.11	7.28			50.08	22.37	54.85
	T											OETMC/ Ohio	71	-8.56	11.62	14.43
	F													1.16	11.60	11.66

[a]TIREM.

[b]R-6602 (FCC) model.

The British Aircraft Corporation's model development effort (see Reference 9-17) also included a comparison between statistical and point-to-point models. In the 40 - 110 MHz band, it was found that the standard deviation of prediction errors could be reduced from 13.3 dB to 7.3 dB by utilizing a point-to-point model. This means that the probability of, for example, an error greater than ± 15 dB was reduced from about 26% to about 4%.

In summary, well-designed point-to-point models have been demonstrated to be more accurate than statistical models for predicting the basic median transmission loss at frequencies of 40 MHz or higher. Part 2 of this chapter presents greater detail about the ECAC point-to-point model, TIREM.

CHAPTER 9

SURFACE-TO-SURFACE PROPAGATION

IN THE 40 MHz - 20 GHz BAND: MEDIAN LOSS

PART 2: THE TERRAIN INTEGRATED ROUGH EARTH MODEL (TIREM)

By: R. Meidenbauer

The Terrain Integrated Rough Earth Model (TIREM) evaluates the profile between two sites and, based on the geometry of the profile, selects a mode of propagation. Appropriate formulations are then applied to compute the basic transmission loss.

The actual terrain profiles must be represented by a set of discrete points. The position of each point along the profile is described by a distance and an elevation above sea level as shown in Figure 9-2. This set of terrain points may be generated from a topographic data file or read from a set of input cards.

TIREM is applicable to problems in the 40 MHz to 20 GHz band. Both ground-wave and tropospheric-scatter modes of propagation are considered; ionospheric models are not treated.

9.5 SYNOPSIS OF MODEL THEORY (see Reference 9-32)

TIREM computes the median basic transmission loss in three steps. First, the model obtains the required terrain profile either by reading the appropriate input cards or by generating it from a topographic data base. Next, the terrain profile is examined, and an initial mode of propagation is selected based on the path geometry. The model then branches to the appropriate subroutines that actually compute the loss.

The parameter extractor processes the terrain profile to derive the information needed for primary mode selection. These parameters include radio horizon distances, effective antenna heights, and path angular distances.

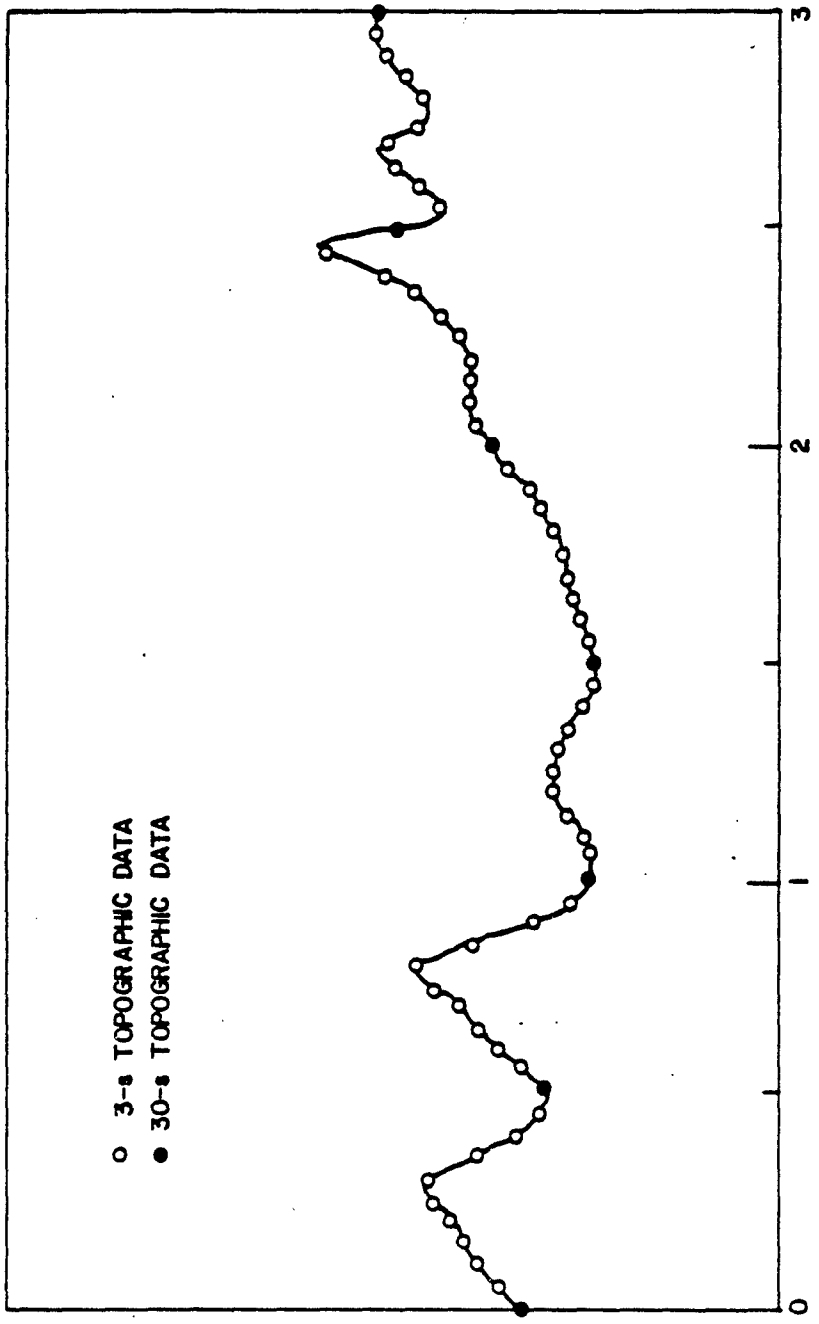

Figure 9-2. A terrain profile represented by discrete points. The points shown are at the interval in which they are stored. In the TIREM model, an interpolation is done to add points at half of the file spacing, i.e., every 15 seconds for 30-second data, every 2 seconds for 3-second data.

Refractive effects of the earth's atmosphere are accounted for by using an effective earth's radius (see Reference 9-7) at heights below 1 kilometer and the CRPL exponential reference atmosphere[9-47] at greater heights.

The radio horizon distances calculated by the parameter extractor are used to select an inital mode, based on whether the given path is within the horizon or beyond it. The final determination of propagation mode is based on a number of parameters (such as Fresnel clearance). Each of the 12 different modes of TIREM is briefly described below. A flow chart for the model is provided in Appendix B.

9.5.1 Line-of-Sight-Modes

If the propagation path is within the radio horizon, the loss is computed by one of three line-of-sight (LOS) modes. The selection of modes is based on the ratio of the minimum ray clearance above the terrain, h, to the width of the first Fresnel zone at that point, r (see Figure 9-3).

Model 8 LOS-FS (line-of-sight, free space): If h/r is greater than 1.5, the ray is well above the terrain and free-space loss is used.

Model 7 LOS-RE (line-of-sight, rough earth): If h/r is less than 0.5, the ray is very near the earth's surface, and an empirical, rough-earth formulation[9-8, 9-3] is used to compute the loss.

Model 5 LOS-TR (line-of-sight, transition): If h/r is between 0.5 and 1.5, a weighted combination of the free-space and rough-earth losses is used.

9-47 Bean, B. R., and Thayer, G. D., CRPL Exponential Reference Atmosphere, NBS Monograph 4, October 1959.

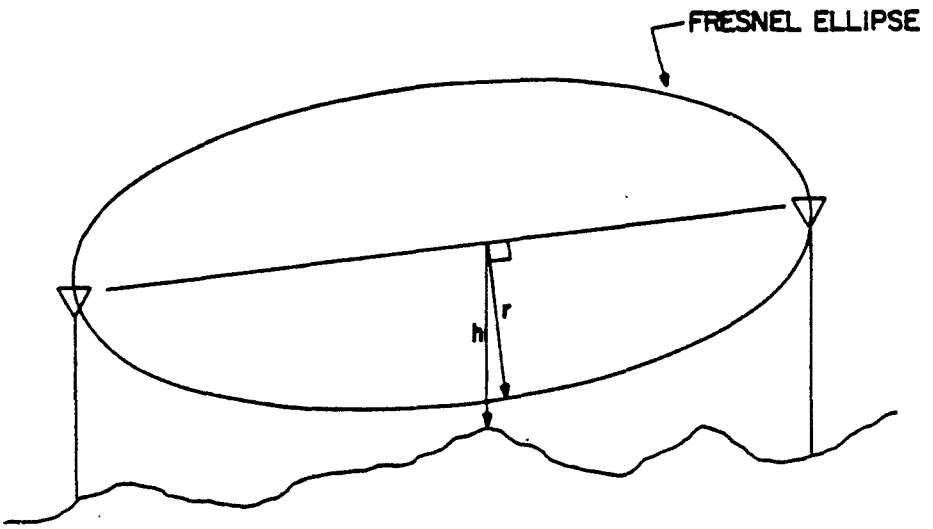

$\frac{h}{r}$ = minimum ratio of h to r along the entire path

If $\frac{h}{r} > 1.5$, use free-space loss (LOS-FS mode)

If $\frac{h}{r} < 0.5$, use empirical rough-earth loss (LOS-RE mode)

If $0.5 < \frac{h}{r} < 1.5$, use weighted combination (LOS-TR mode)

Figure 9-3. Line-of-sight propagation modes in TIREM.

9.5.2 Beyond Line-of-Sight Modes

If the propagation path extends beyond the horizon, the wave can reach the receiving antenna by diffracting around the terrain or by scattering from the troposphere. TIREM has four diffraction modes and one tropospheric-scatter mode.

Model 2 KEBLS (knife-edge diffraction, beyond line-of-sight): If the transmitting antenna and the receiving antenna have a common radio horizon along the great-circle terrain profile (see Figure 9-4), the propagation path can be characterized by a single diffracting knife-edge. Fresnel-Kirchoff diffraction theory is used to compute the loss due to diffraction of the wave around the obstacle. If the paths of the radio rays on either side of the obstacle are near the terrain, the effects of ground reflections are also included (see Reference 9-27).

Model 6 RED (rough-earth diffraction): This mode is based on Norton's work as detailed in APPENDIX I of Reference 9-27. It involves fitting four smooth curves to the terrain, as shown in Figure 9-5, and applying smooth-earth diffraction theory modified to accommodate the four different effective earth radii. Approximations introduced in the diffraction theory limit this mode to propagation paths with large angular distances (θ_{oo} in Figure 9-5).

Model 1 EFFKE (effective knife-edge diffraction): If there are two distinct radio horizons and the angular distance is too small to use the RED mode, a recovery procedure is used.

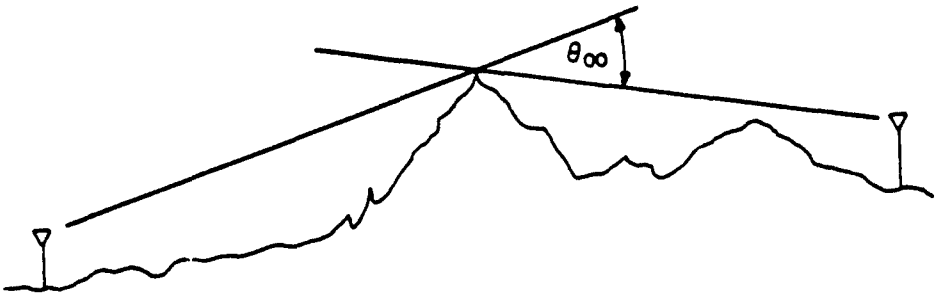

Figure 9-4. Single knife-edge diffraction geometry (KEBLS mode).

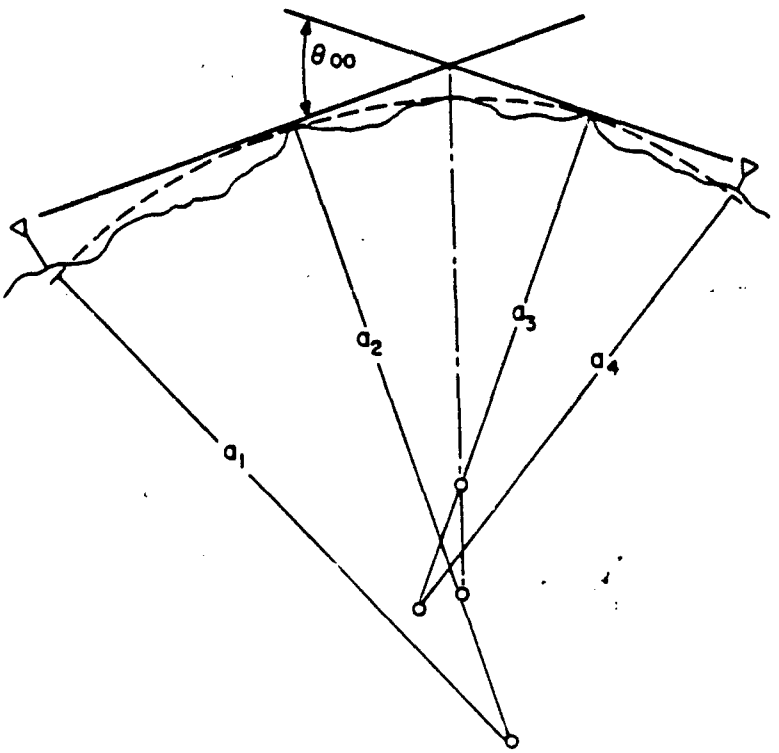

Figure 9-5. General rough-earth diffraction geometry (RED mode).

Following Bullington,[9-48] the propagation path is modeled with an equivalent knife-edge as shown in Figure 9-6. The same formulations that are applied in the KEBLS mode are used to compute the loss.

Model 4 EFFRED (effective knife-edge/rough-earth diffraction): A study of the selection processes in the KEBLS mode and the RED mode showed that abrupt transitions sometimes occur when the mode selector switches between them.[9-49] Therefore, a weighted combination of EFFKE and RED calculations is used when the radio horizons are less than two statute miles apart.

Model 9 TROSC (tropospheric scatter): Transhorizon propagation via forward scattering in the troposphere is usually dominant for paths that extend well beyond the radio horizon. TIREM calculates long-term median values of troposcatter loss using methods based on a very large sample of experimental data.[9-50]

Model 12 EFFDBL (effective double knife-edge): EFFDBL is a double knife-edge diffraction formulation used as a troposcatter recovery mode. Comparisons with measured data (see Reference 9-31) showed that the TROSC mode gave poor results for propagation paths that were very asymmetric

---

9-48 Bullington, K., "Radio Propagation at Frequencies Above 30 Megacycles," Proc. IRE, Vol. 35, October 1947, pp. 1122-1136.

9-49 Madison, J. A., Program Change Request, February 1976.

9-50 International Radio Consultative Committee, CCIR, Tropospheric Wave Transmission Loss Prediction, CCIR Doc. V/23-E, March 1962.

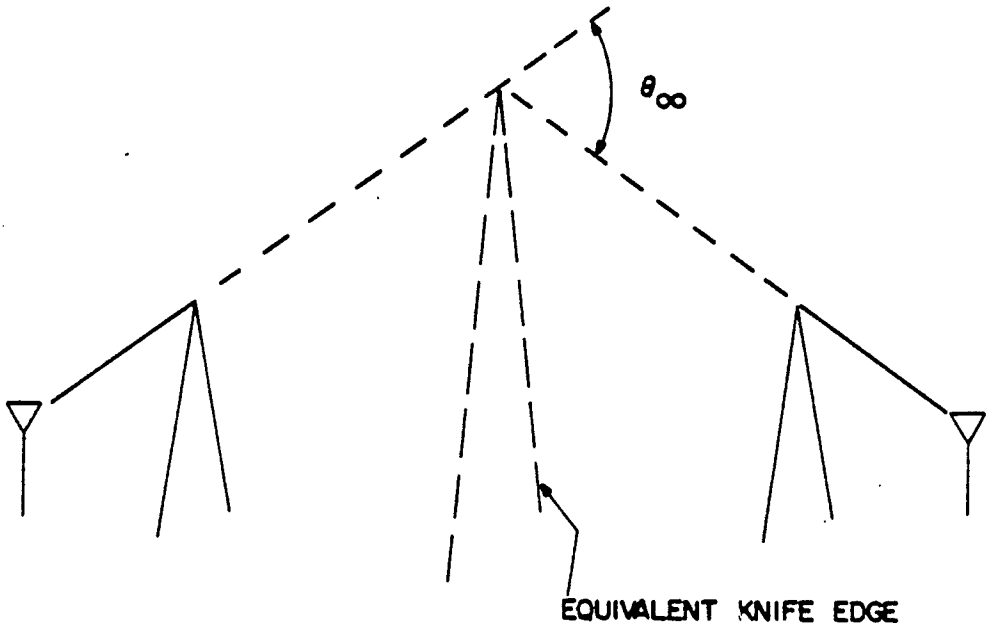

Figure 9-6. Effective knife-edge diffraction geometry (EFFKE mode).

(paths where one radio horizon had a short, steep rise). The comparisons also showed that the double knife-edge model of Sacco[9-51] gave better results for the same paths. Thus, this diffraction loss is used in place of the TROSC loss when the path becomes very asymmetrical.

9.5.3 Combination Modes

Since the main mode of propagation for beyond-the-horizon paths can be diffraction, troposcatter, or a combination of both, weighting schemes are used to combine the losses. Modes are also combined to eliminate discontinuties encountered when switching between modes.

Model 10 DIFSC1 (diffraction-scatter 1): If the diffraction and troposcatter losses are within 18 dB of each other, neither mechanism dominates. This mode follows the procedure from Reference 9-7 to combine the losses for the DIFSC1 loss.

Model 11 DIFSC2 (diffraction-scatter 2): This mode combines the DIFSC1 loss with the EFFDBL loss to eliminate large discontinuities at points of transition between the modes (see Reference 9-49).

Model 11 DIFSC3 (diffraction-scatter 3): This mode is similar to the DIFSC2 mode except that the TROSC and EFFDBL losses are combined.

9.5.4 Atmospheric Absorption

For frequencies greater than 1 GHz, attenuation due to absorption by atmospheric oxygen and water vapor is computed and included in the prediction

---

[9-51] David, P. and Voge, J., Propagation of Waves, Pergamon Press, 1969, p. 111.

of median path loss.[9-52] The absorption model uses a profile of atmospheric temperature, pressure, and water vapor content to determine differential absorption coefficients, which are numerically integrated over the path.

9.5.5 Rain Scatter Coupling

The HYDRO subroutine[9-53] is used to compute non-great-circle coupling due to scatter from columns of rain. HYDRO is based on the program of this name that L. Burch of COMSAT developed. The present version uses the equations from CCIR Report 448-1 (1974).

9.5.6 FY-81/FY-82 TIREM Improvement Tasks

Tasks were initiated in FY-81 to upgrade both the engineering formulations (TIREM Improvement Task) and the computer coding (TIREM Upgrade Task) of the TIREM model. The coding upgrade task was completed in FY-81. The TIREM Improvement Task is being continued through FY-82.

During the FY-81 portion of the TIREM Improvement task, four improvements were evaluated:

1. Multiple knife-edge diffraction
2. Rounded knife-edge diffraction
3. Effects of nearby terrain obstacles
4. Geometrical Theory of Diffraction

The results of this evaluation are described in Reference 9-33. None of these modifications were included as part of the FY-81 TIREM revision.

9-52 Boldissar, F., ECAC Program Change Request, February 1978.

9-53 Snyder, S., Predicting Interference in the 1-40 GHz Band Due to Scatter from Rain, ECAC-TN-77-009, ECAC, Annapolis, MD, June 1977.

In addition to evaluating the proposed improvements noted above, several additional modifications were investigated as possible corrections for errors and problems encountered by project engineers using TIREM. The specific modifications incorporated into TIREM were:

1. Modification of the LOS-RE mode to correct for discontinuities caused by a switch between the 1972 Longley-Rice procedure and the 1970 Longley-Reasoner procedure, which occurred when the smooth-earth horizon distance limitation was violated.

2. Correction of an error in the height-gain clearance calculations in the EFFKE mode.

3. Inclusion of a height-gain interpolation routine to ease abrupt changes in the loss predicted by the KEBLS, EFFKE, and EFFDBL modes.

Ongoing FY-82 work should result in the inclusion of routines to handle multiple knife-edge diffraction effects and the effects of nearby terrain obstacles. Another improvement being studied is the inclusion of additional terms in the Bremmer series in the RED mode. HYDRO is also being updated. The FY-81 evaluation revealed that no improvement in TIREM predictions was obtained by including a rounded knife-edge diffraction calculations and hence this mode will not be added to TIREM. Through an FY-82 external support task, ECAC has funded Ohio University personnel to extend their FAA-sponsored GTD model for ECAC use. It is expected that the inclusion of this GTD model in TIREM will be investigated in a future task.

9.6 COMPARISON OF TIREM PREDICTIONS WITH MEASUREMENTS[a]

TIREM predictions were compared with measured data in the Propagation Measurement Retrieval System (PMRS) for a wide variety of path parameters. The results of this comparison are shown in TABLE 9-7. The mean, standard deviation, and RMS values are shown for the set of prediction errors formed by subtracting the measured values of basis transmission loss from the predicted values.

[a]The error statistics given in this report were generated before the inclusion of the FY-81 improvements. An overview of the improvement in model accuracy after the inclusion is given in Reference 9-33.

TABLE 9-7

TIREM VALIDATION
(Page 1 of 5)

	FREQ. (MHz)	TRANSMITTING ANTENNA HEIGHTS (ft.)	RECEIVING ANTENNA HEIGHTS (ft.)	POL	PREDICTION ERROR STATISTICS				NUMBER OF MEASUREMENTS
					PATH DISTANCES (miles)	$\overline{\delta L}$ (dB)	$\sigma_{\delta L}$ (dB)	δL_{RMS} (dB)	
COLORADO	49.7	13	2,6	V	.5 - 31.4	- 8.51	13.48	15.94	786
PLAINS	101.5	10	10, 20, 30	H	.5 - 50.3	- 4.42	11.60	12.41	1338
AREA A	101.5	10	10, 20, 30	V	.5 - 50.3	- 1.07	12.39	12.43	1338
COLORADO	49.7	13	2, 6	V	3.2 - 31.2	- 5.40	14.16	15.12	240
MOUNTAINS	101.5	10	10, 20, 30	H	3.2 - 31.2	- 3.61	21.21	21.49	409
AREA B	101.5	10	10, 20, 30	V	3.2 - 31.2	.76	19.61	19.60	411
NE OHIO	49.7	9, 14	2, 6	V	6.1 - 31.9	4.36	11.95	12.72	1015
	101.8	10, 13	10, 20, 30	H	6.1 - 31.9	- 1.49	10.47	10.57	1608
AREA C	101.8	10, 13	10, 20, 30	V	6.1 - 31.9	.51	10.96	10.97	1618
R1: GUNBARREL	230	22	3 - 43	H	.3 - 73.8	6.34	7.99	10.20	1742
HILL	407, 410	22	3 - 43	H	1.9 - 74.4	5.55	9.81	11.27	1928
COLORADO	751	22	3 - 43	H	.3 - 73.8	4.82	9.96	11.07	2165
PLAINS	910	24	3 - 43	H	.3 - 73.8	4.70	7.32	8.70	1918
AREA D	1846	24	3 - 43	H	.3 - 73.8	- 3.13	10.17	10.64	2112
	4595	24	3 - 43	H	.3 - 73.8	- 3.60	10.95	11.52	3136
	9190	24	3 - 43	H	.3 - 73.8	- 1.58	10.70	10.82	3700
R2: FRITZ	230	22	3 - 43	H	1.7 - 74.7	- 6.49	18.26	19.37	1218
PEAK	407, 410	22	3 - 43	H	1.7 - 74.7	- 9.97	19.49	21.88	1197
COLORADO	751	22	3 - 43	H	1.7 - 71.5	-18.38	20.37	27.43	927
MOUNTAINS	910	24	3 - 43	H	1.7 - 35.3	- 20.27	22.00	29.90	1012
AREA E	1846	24	3 - 43	H	1.7 - 71.5	- 26.08	22.46	34.41	1003
	4595	24	3 - 43	H	1.7 - 71.5	- 34.22	23.80	41.68	1642
	9190	24	3 - 43	H	1.7 - 49.4	- 37.51	21.91	43.43	830

TABLE 9-7

TIREM VALIDATION
(Page 2 of 5)

	FREQ. (MHz)	TRANSMITTING ANTENNA HEIGHTS (ft.)	RECEIVING ANTENNA HEIGHTS (ft.)	POL	PREDICTION ERROR STATISTICS				NUMBER OF MEASUREMENTS
					PATH DISTANCES (miles)	δL (dB)	$\sigma_{\delta L}$ (dB)	δL_{RMS} (dB)	
R3: GOLDEN	230	22	3 - 51	H	.3 - 49.6	6.97	8.10	10.68	1521
	410	22	3 - 51	H	.3 - 49.6	5.70	7.99	9.81	1497
COLORADO[a]	751	22	3 - 51	H	.3 - 49.6	3.39	7.79	8.49	1909
AREA F	910	24	3 - 49	H	.3 - 49.9	2.95	8.27	8.78	2591
	1846	24	3 - 49	H	.3 - 49.9	.95	8.53	8.59	3318
SITE CODE: O, Z	4595	24	3 - 49	H	.3 - 49.9	- 1.62	12.15	12.26	3229
	9190	24	3 - 49	H	.3 - 49.9	- 2.94	10.20	10.62	3300

[b]

[a] A recent study by Weissberger and Powell revealed that the receiver site elevation was substantially underestimated when determined using an interpolation of the TOPFAS data.

[b] These statistics may be slightly in error due to one bad data point in R-3.

TABLE 9-7

TIREM VALIDATION
(Page 3 of 5)

	FREQ. (MHz)	TRANSMITTING ANTENNA HEIGHTS (ft.)	RECEIVING ANTENNA HEIGHTS (ft.)	POL	PREDICTION ERROR STATISTICS				NUMBER OF MEASUREMENTS
					PATH DISTANCES (miles)	$\overline{\delta L}$ (dB)	$\sigma_{\delta L}$ (dB)	δL_{RMS} (dB)	
KLIR - COLO. PLNS. AREA H	100	225	10, 20, 30	H	3.9 - 75.3	- 4.09	10.47	11.24	1147
KLIR - COLO. MTNS. AREA I	100	225	10, 20, 30	H	10.0 - 57.2	- 3.29	15.28	15.61	403
WYOMING	230	2, 10	2, 3, 7, 10	V	2.2 - 26.8	- 6.85	14.57	16.08	348
AREA J	416	2, 10	2, 3, 7, 10	V	2.2 - 26.8	-5.43	14.55	15.51	356
IDAHO	230	2, 10	2, 3, 7, 10	V	6.7 - 24.7	- 10.07	17.09	19.81	232
AREA K	416	2, 10	2, 3, 7, 10	V	6.7 - 24.7	- 8.92	17.65	19.74	203
WASHINGTON (PT. 1)	230	2, 10	2, 3, 7, 10	V	5.6 - 36.2	2.75	13.07	13.34	404
AREA L	416	2, 10	2, 3, 7, 10	V	5.6 - 36.2	- .38	13.45	13.44	312
WASHINGTON (PT. 2)	230	2, 10	2, 3, 7, 10	V	.9 - 7.1	12.64	18.52	22.33	84 [a]
AREA M	416	2, 10	2, 3, 7, 10	V	.9 - 9.0	12.14	13.43	18.05	92

[a] May be slightly in error due to one bad data point.

TABLE 9-7

TIREM VALIDATION
(Page 4 of 5)

	FREQ. (MHz)	TRANSMITTING ANTENNA HEIGHTS (ft.)	RECEIVING ANTENNA HEIGHTS (ft.)	POL	PROFILE INTER-POLATION?	PREDICTION ERROR STATISTICS				NUMBER OF MEASUREMENTS
						PATH DISTANCES (miles)	$\overline{\delta L}$ (dB)	$\sigma_{\delta L}$ (dB)	δL_{RMS} (dB)	
OT 16	-	-	-	-	NO	-	-	-	-	-
U.S.[a]	-	-	-	-	YES	-	-	-	-	-
CONT. TEMP										
OT 16	41.5 -	16.0 -	6.0 -	V	NO	11.1 -	- 6.22	10.18	11.90	133
U.K.	9640.0	1096.0	194.0	V	YES	397.6	- 6.05	10.11	11.75	133
MTOL										
OT 16	42.0 -	70 -	30 -	V	NO	48.0 -	- 7.34	16.22	17.33	16
U.K. & W.G.	1898.0	700	56	V	YES	491.6	- 1.31	8.39	8.23	16
MTOS										
OT 16	48.7 -	13 -	10 -	V	NO	6.4 -	- 5.48	9.34	10.76	61
JAPAN	7273.4	1304	607	V	YES	499.8	- 5.31	9.26	10.61	61
CONT. TEMP										
OT 16	90.7 -	13 -	3 -	V	NO	59.7 -	- 5.79	7.61	9.48	39
W.G.	9339.5	443	213	V	YES	674.3	- 4.63	7.01	8.33	39
CONT. TEMP.										

[a]Measured profiles not available for U.S. OT-16 paths.

TABLE 9-7

TIREM VALIDATION
(Page 5 of 5)

	FREQ. (MHz)	TRANSMITTING ANTENNA HEIGHTS (ft.)	RECEIVING ANTENNA HEIGHTS (ft.)	POL	PROFILE INTER-POLATION?	PREDICTION ERROR STATISTICS[b]				NUMBER OF MEASUREMENTS
						PATH DISTANCES (miles)	$\overline{\delta L}$ (dB)	$\sigma_{\delta L}$ (dB)	δL_{RMS} (dB)	
OT 16	-	-	-	-	NO	-	-	-	-	-
U.S.[a]	-	-	-	-	YES	-	-	-	-	-
CONT. TEMP										
OT 16	41.5 -	16.0 -	6.0	V	NO	11.1 -	- 6.92	10.30	12.38	133
U.K.	9640.0	1096.0	194.0	V	YES	397.6	- 6.75	10.26	12.25	133
MTOL										
OT 16	42.0 -	70 -	30 -	V	NO	48.0 -	- 11.13	15.62	18.78	16
U.K. & W.G.	1898.0	700	56	V	YES	491.6	- 5.00	8.33	9.49	16
MTOS										
OT 16	48.7 -	13 -	10 -	V	NO	6.4 -	- 7.70	9.43	12.11	61
JAPAN	7273.4	1304	607	V	YES	499.8	[c]	[c]	[c]	61
CONT. TEMP										
OT 16	90.7 -	13 -	3 -	V	NO	59.7 -	- 7.38	7.60	10.53	39
W.G.	9339.5	443	213	V	YES	674.3	- 6.21	7.18	9.43	39
CONT. TEMP.										

[a] Measured profiles not available for U.S. OT-16 paths.

[b] $L_B(50)$ values used.

[c] Values not available.

CHAPTER 10

TIME VARIABILITY OF LOSS ON TERRESTRIAL PATHS AT FREQUENCIES HIGHER THAN 40 MHz

By: M. Weissberger

The preceding chapter was a description of models that can be used to predict the median loss of signals at frequencies greater than 40 MHz. The magnitude of such signals can vary substantially from the median value as the result of changes in the structure and content of the troposphere and, below about 100 MHz, the ionosphere.

Given the task of determining if a communications system will satisfy a relation such as this:

$$(S/I)(t) > (S/I)_{th} \qquad (10\text{-}1)$$

where $(S/I)(t)$ is the signal-to-interference ratio (non-logarithmic units) at time t and $(S/I)_{th}$ is the threshold S/I ratio needed for a particular quality of circuit, the engineer must know the statistics of the fades of S and the enhancements of I that occur during a particular interval of time.

A great deal of research is being conducted on this important subject. Until an adequate summary can be prepared, the following annotated bibliograpy is presented to guide self study of the subject.

BIBLIOGRAPHY

CCIR, "The Evaluation of Propagation Factors in Interference Problems Between Stations on the Surface of the Earth at Frequencies Above About 0.5 GHz", Draft Report 569-1, 9 September 1981. Contains the CCIR's most up-to-date models for ducting end rain-scatter coupling. To be used for interference analyses rather than cull analyses. Will be published in the 1982 Plenary Assembly Reports.

Dougherty, H. T., and Dutton, E. J., The Role of Elevated Ducting for Radio Service and Interference Fields, NTIA-Report-81-69, ITS, Boulder, CO, March 1981. Summarizes the Sylvania duct occurrence data that applies to the 48 states. Presents analytic expressions for the loss in a duct.

Dougherty, H. T., A Survey of Microwave Fading Mechanisms, and Applications, ESSA Tech Report ERL 69-WPL 4, Wave Propagation Laboratories, Boulder, CO, March 1968. Emphasis on the physical basis for different types of fading on line-of-sight links. Tutorial style.

Norton, K. A, et. al., "The Use of Angular Distance in Estimating Transmission Loss and Fading Range", Proc. IRE, October 1955. Gives some physical insight into the shape of the long-term time variability curves published later in NBS TN-101 and in NTIA-TM-79-28.

Kuhn, U., "Propagation Measurements Beyond Line-of-Sight During Thunderstorms", Proc. IEE, June 1968. Observes that a thunderstorm caused enhancements of the received signal by 40 dB. This provides a caution to those who are ready to build a ducting model with the intention of explaining all beyond-line-of-sight signal enhancements.

Dougherty, H. T., "Recent Progress in Duct Propagation Predictions", IEEE Trans. Ant. and Prop., July 1979. Discusses theoretical modeling and states results of personal reviews of measurements.

CCIR, "Propagation Data Required for the Evaluation of Coordination Distance in the Frequency Range 1 to 40 GHz", Draft Report 724, 9 September 1981. Contains a ducting model and a rain-scatter coupling model suitable for a cull procedure. Will be published in the 1982 Plenary Assembly Reports.

Crane, R. K., "A Review of Transhorizon Propagation Phenomena", Radio Science, September 1981. A discussion of the phenomena that cause enhancements of fields beyond the radio horizon. Emphasis is on ducting and rain-scatter coupling.

Longley, A. G., and Hufford, G. A., The Long-Term Variability of Radio Signals - A New Empirical Study, NTIA-TM-79-28, ITS, Boulder, CO, December 1979. Reviews the accuracy of the NBS TN 101 method for predicting long-term enhancements. Finds the method satisfactory for 10% of the year, but

recommends use of models based on specific physical mechanisms for smaller percentages of time. Study was funded by ECAC.

Wheeler, M. S., "Microwave Relay Fading Statistics as a Function of Terrain Clearance Factor", IEEE Trans. on Ant. and Prop., March 1977. Relates the Bell Labs (Barnett-Vigants) model to work by Morita and Battesti. Shows that ray-path clearance is a key parameter. (It is possible that angle and length are more important and that ray path clearance is frequently correlated with these.)

Vigants, A., "Microwave Radio Obstruction Fading", Bell System Technical Journal, July 1981. Discusses a method for determining the antenna heights needed to prevent obstruction of the ray path during unusual refractive-index structures.

Ruthroff, C. L., "Multiple-path Fading on Line-of-Sight Microwave Radio Systems as a Function of Path Length and Frequency", Bell System Technical Journal, Vol. 50, No. 7, 1971. Shows how the Barnett-Vigants empirical-fading-statistics model is explained by atmospheric multi-path rather than ground-reflected multi-path.

Troitsky, V. N., "A Method for Determining Statistical Characteristics of SHF, UHF, and VHF Interfering Signals over Long Distances in Land and Coastal Areas", 4th Symposium and Technical Exhibition on Electromagnetic Compatibility, Zurich, March 10-12, 1981. A straightforward graphical procedure for estimating enhancements. Supported by data in the USSR and other parts of the world.

Sasaki, O., et. al., "Multipath Delay Characteristics on Line-of-Sight Microwave Radio System" (sic) IEEE Trans. on Communications, December 1979. Reviews theory and measurements of the atmospheric structure that causes multipath on line-of-sight systems.

Vigants, A., "Space Diversity Engineering", Bell System Technical Journal, January 1975. Empirical model for fading statistics for line-of-sight systems in the 2-11 GHz band. Update of the "Barnett" and "Lenkurt" models.

Damossi, E., et. al., "A Systematic Comparison of Rain Attenuation and Prediction Methods, for Terrestrial Paths", URSI Commission F Open Symposium, Pre-prints of Papers, Lennoxville, Canada, May 1980. Compares several types of predictions with 11-18 GHz data from Italy.

Crane, R. K., A Two-Component Rain Model for the Prediction of Attenuation and Diversity Improvement, Thayer School of Engineering, Dartmouth College, NH, February 1982. Model for predicting the attenuation statistics due to rain on terrestrial and earth-space paths. Includes validation and comparisons with the CCIR model.

Lin, S. H. "Nationwide Long Term Rain Rate Statistics and Empirical Calculations of 11 GHz Microwave Rain Attenuation", Bell System Technical Journal, November 1977. The Bell Labs method. Used in the ITS ADSEM

model. Should be used with 5-minute average rain data, which is not readily available.

Ince, A. N., et. al., "A Review of Scatter Communications", AGARD Conference Proceedings No. 244, NATO, Neuilly Sur Seine, France, October 1977. Contains information of the short-term fading characteristics of beyond line-of-sight links. Also presents meteor-scatter data for the lower VHF frequencies.

Bullington, K. "Radio Propagation Fundamentals", Bell System Technical Journal, May 1957. Contains a means for estimating fading on line-of-sight links at frequencies below 2 GHz.

Weissberger, M. A., "Documentation of the Propagation Models and Data for the Air Force Simulation Support (AFSIMS) Task", ECAC memorandum to AF/SAGR, December 1980. Discusses method of accounting for short-term and long-term time variability in a Monte Carlo simulation.

Marcus, S, et. al., A Model to Compute EM Fields in Tropospheric Duct Environments at Frequencies Through SHF, ESD-TR-81-102, ECAC, Annapolis, MD, September 1981. A theoretical duct model developed at ECAC. Overcomes mathematical limitations of previous solutions. Requires knowledge of refractive index structure. Validated.

Proceedings of Conference on Atmospheric Refractive Effects Assessment, NOSC TD 260, Naval Ocean Systems Center, San Diego, CA, June 1979. Includes discussion of models such as the Navy's Integrated Refractive Effects Prediction System (IREPS). Addresses the collection and use of both real-time and historical meteorological data. Contains an overview of the GTE Sylvania ducting statistics data base.

Palmer, F. H., Report on the Great Lakes Propagation Measurements Program: Comparisons of the Canadian Data with Predictions of FCC R-6602, CRC Report 1332, Communications Research Centre, Ottawa, Canada, February, 1980. Discusses seasonal and diurnal variations of signal strengths measured on long (160 km) paths in the Great Lakes area. The circuits involved one high and one low antenna. Frequencies were in the 50-900 MHz band.

Hause, L. G., and Wortendyke, D. R., Automated Digital System Engineering Model, NTIA Tech Report 79-18, ITS, Boulder, CO, 1979. Includes short term multipath and rain attenuation models for line-of-sight terrestrial links. Has a procedure for relating worst month statistics to annual values. See also the article by Bursis and the Wortendyke in the May, 1982 Transactions on Antennas and Propagation.

CCIR, "VHF Propagation by Regular Layers, Sporadic-E, or Other Anomalous Ionization", Report 259-4, Recommendations and Reports of the CCIR, 1978, ITU, Geneva, 1978. Presents an overview of Sporadic-E and other ionospheric propagation mechanisms that can cause signal enhancements at frequencies below about 100 MHz.

Hauber, J., Exercise Support Program User's Manual, ECAC-UM-79-002, ECAC, Annapolis, MD, March 1979. Documents a version of TIREM that contains short-term fading statistics. Used for computing reliability of tactical links in the 4400-5000 MHz band. Uses Vigants' equations as published by Lenkurt.

Weissberger, M. A., et al., "Estimating Outage Time in Terrestrial Microwave Systems Caused by Mobile or Stationary In-Band Interference Sources," 1975 IEEE Electromagnetic Compatibility Symposium Record, San Antonio, TX, October, 1975. Provides a technique for integrating time variability models into a band sharing study. (This publication is presented as Appendix D herein.)

CHAPTER 11

OBSTRUCTION BY VEGETATION AND

MAN-MADE STRUCTURES

By: M. Weissberger

11.1 INTRODUCTION

This chapter contains formulas and graphs that can be used to determine the effects of vegetation and man-made structures on basic transmission loss. The chapter summarizes work contained in References 11-1 and 11-2, and updates material in Reference 11-3. Sections 11.2 through 11.6 deal with vegetation; Section 11.7 with man-made structures.

Section 11.2 presents the Modified Experimental Decay (MED) model. This can be used to predict the attenuation caused by propagation through (in contract to over) groves of trees in a temperate forest. Comparisons with measurements in the 230 MHz to 95 GHz frequency range are presented.

Section 11.3 shows how to apply the diffraction model to problems in which the antennas are far enough from the trees so that the radiation propagates over the forest, rather than through it. Examples in the 25 MHz to 5 GHz range are presented.

11-1 Weissberger, M. A., An Initital Critical Summary of Models for Predicting the Attenuation of Radio Waves by Trees, ECAC-TR-81-101, Electromagnetic Compatibility Analyis Center, Annapolis, MD, July 1982.

11-2 Weissberger, M. A., and Hauber, J., "Modeling the Increase in Loss Caused by Propagation Through a Grove of Trees," Abstracts of the North American Radio Science Meeting, Quebec, Canada, June 1980.

11-3 Weissberger, M. A., Jablinski, R., "Examples of Models to Account for the Effects of Man-made Structures on Path Loss and Radio Line of Sight", in ECAC-TN-79-027, Electromagnetic Compatibility Analysis Center, Annapolis MD, August 1979.

Section 11.4 contains a description of Kinase's model[11-4] for predicting the loss that occurs when one antenna is elevated well above the forest and the second antenna is located in a region, η% of which is covered with vegetation or man-made structures. The basis for the model is data in the 80-700 MHz band.

Section 11.5 is a description of the Jansky & Bailey empirical model[11-5] for computing the basic transmission loss between two low (2 - 7 m) antennas immersed in a tropical jungle. Path lengths can vary from 0.08 to 1.6 km. The model applies to the 25-400 MHz band.

Section 11.6 is a summary of data about the variation of signal strength with position that occurs when an antenna is moved through a forest. This variability can affect system performance as much as the mean attenuations predicted by the models in Section 11.3, 11.4 and 11.5.

Section 11.7 describes models of the effects of urban structures on basic transmission loss.

11.2 THE MODIFIED EXPONENTIAL DECAY (MED) MODEL (see References 11-1 and 11-2)

11.2.1 General Discussion and a Manual Model

This model applies to problems in which at least one of the antennas is close enough to a grove of trees so that the majority of energy transmitted or received by the antenna flows through the trees, rather than over them.

11-4 Kinase, A., Influences of Terrain Irregularities and Environmental Clutter Surroundings on the Propagation of Broadcasting Waves in the UHF and VHF Bands, NHK Technical Monograph NO. 14, Japan Broadcasting Corporation, Tokyo, Japan, March 1969.

11-5 Jansky & Bailey Engineering Department, Tropical Propagation Research, Final Report, Volume 1, Atlantic Research Corporation, Alexandria, VA, 1966.

Applicability is best determined on a case-by-case basis by comparing MED predictions with knife-edge diffraction calculations (Section 11.3.1). The model that predicts the lower loss will be the model that is best suited to the actual problem. A preliminary estimate of the result can be obtained by examining the distance to the trees from the antenna that is nearest the trees. One measure of this distance is the take-off angle from the antenna that is nearest the trees to the tops of the trees. When one of the antennas is immersed in the foliage, for example, this angle will be 90°. As both antennas are moved very far from the forest, this angle will approach 0°. The MED model was found to be applicable to all of the cases examined in Reference 11-1 for which the takeoff angle was greater than 26°. It was also applicable to some of the examples with takeoff angles as small as 8°.

Information regarding the frequencies and depths of trees for which the model was found to be applicable are shown in Figure 11-1.

The Equations for predicting received power using the MED model are:

$$P_R = P_T + G_T + G_R - L_{bo} - \alpha d_f \qquad (11\text{-}1)$$

with

$$\alpha = 1.33\, F^{0.284} d_f^{-0.412} \qquad 14 \leq d_f \leq 400 \qquad (11\text{-}2a)$$

$$= 0.45\, F^{0.284} \qquad 0 \leq d_f < 14 \qquad (11\text{-}2b)$$

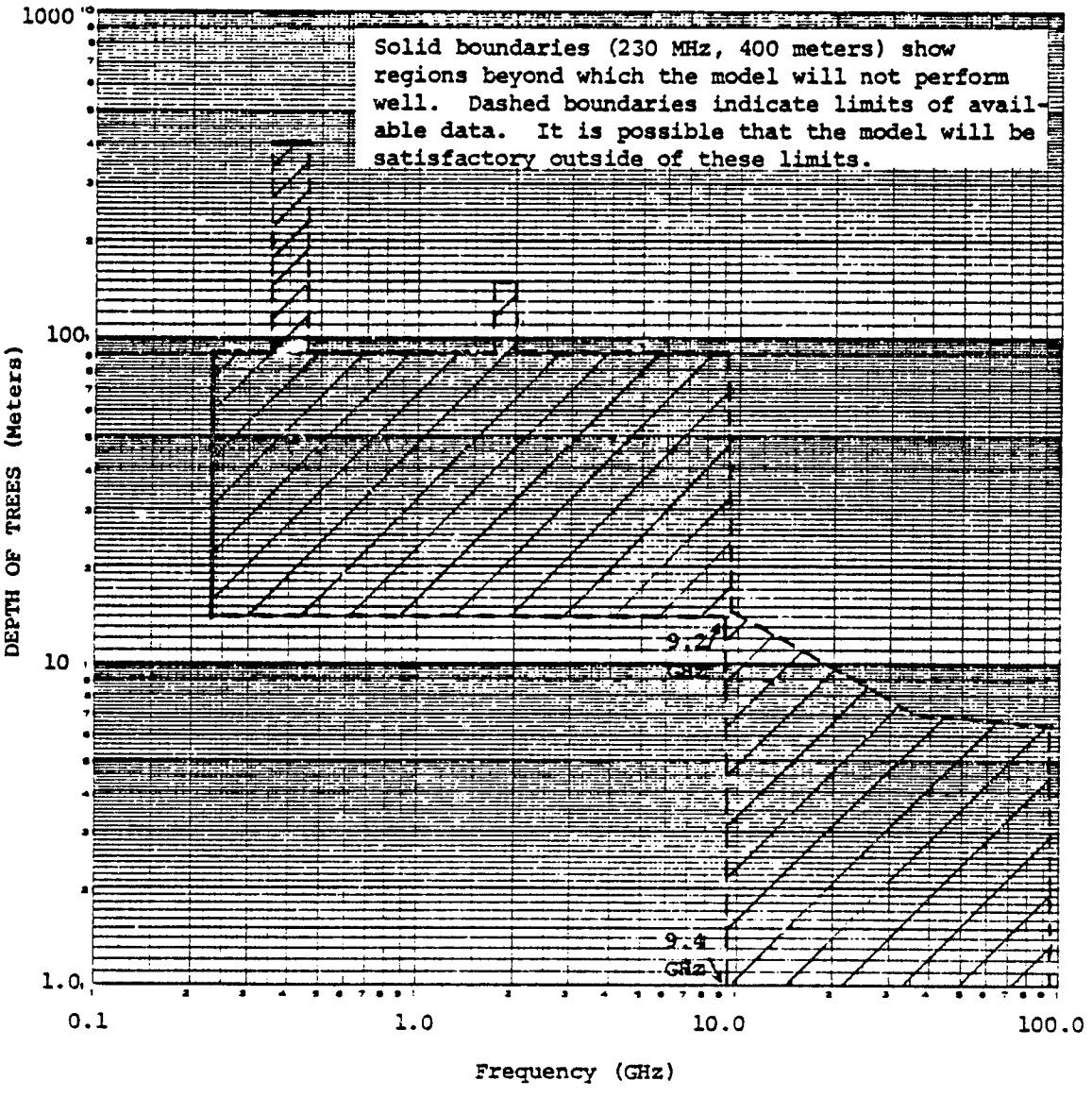

Figure 11-1. Observed range of applicability of the MED model for temperate forests (see Reference 11-1).

where

P_R = received power, in dBm
P_T = transmitted power, in dBm
G_T = transmitter antenna gain, in dBi
G_R = receiver antenna gain, in dBi
L_{bo} = basic transmission loss in the absence of foliage, in dB
d_f = depth of the grove of trees, meters
F = frequency, GHz
α = differential attenuation, in dB/m
($L_{bo} + \alpha d_f = L_b$ as previously defined).

Equation 11-2a was developed by organizing a large set of measurements taken by McQuate[11-6] in Colorado. Equation 11-2b was developed to extend Equation 11-2a to values of d_f small enough so that α does not decrease with distance.

11.2.2 Status of the Computer Model

At the present time, this model is not implemented on the UNIVAC computer at ECAC. If stored data about the location of foliage is added to ECAC's Topographic Data Base, the model could be used as a TIREM subroutine.

11.2.3 Validation and Comparison with other Models

In this subsection, predictions from the MED model are compared with measurements and with predictions from the Exponential Decay (EXD) model. Greater detail on this subject can be found in Section 2 and Appendix A of Reference 11-1.

11-6 McQuate et al., Tabulations of Propagation Data Over Irregular Terrain in the 230-9200 MHz Frequency Range, Part I; Gunbarrel Hill Receiver Site, ESSA-TR-ERL-65-ITS 58-1, Boulder, CO, March 1968.

11.2.3.1 Qualitative Contrasts with the Exponential Decay (EXD) Model

The EXD model is the traditional means of estimating the additional loss caused by propagation through vegetation.[11-7, 11-8, 11-9, 11-10, 11-11, 11-12, 11-13] Equation 11-1 is used to compute received power, but α, unlike α from the MED model, is not a function of distance. One widely used EXD expression for α is:

$$\alpha = 0.26\, F^{0.77} \qquad (11\text{-}3)$$

This was documented by LaGrone (see Reference 11-8) and is based on the data of Saxton and Lane (see Reference 11-7). (This type of expression is called an Exponential Decay model because, if it is inserted in Equation 11-1 and the

---

11-7 Saxton, J. A. and Lane, J. A., "VHF and UHF Reception, Effects of Trees and Other Obstacles," Wireless World, May 1955.

11-8 LaGrone, A. H., "Forecasting Television Service Fields," Proc. IRE, June 1960.

11-9 Currie, N. C., Martin, E. E., and Dyer, F. B., Radar Foliage Penetration Measurements at Millimeter Wavelengths, ESS/GIT-A-1485-TR-4, Georgia Institute of Technology, Atlanta, GA, 31 December 1975, ADA023838.

11-10 International Radio Consultative Committee (CCIR), "Influence of Terrain Irregularities and Vegetation on Tropospheric Propagation," Report 236-4, XIV Plenary Assembly, International Telecommunications Union, Geneva, Switzerland, 1978.

11-11 Krevsky, S., "HF and VHF Radio Wave Attenuation Through Jungle and Woods," IEEE Transactions on Antennas and Propagation, July 1963.

11-12 Frankel, M. S., L-Band Forest Experiments, Packet Radio Temporary Note 254 SRI International, Menlo Park, CA, 19 May 1978.

11-13 Kivett, J. A. and Deiderichs, P. J., PLRS Ground-to-Ground Propagation TES Technical Report (Draft), FR-80-14-6, Hughes Aircraft Company, Fullerton, CA, January 1980.

antilog is taken of the result, then it is seen that the additional reduction of received power due to the foliage has the form $e^{-\alpha' d_f}$.)

The empirical Modified Exponential Decay model describes a slower increase in attenuation with distance -- $e^{-\alpha'' d_f^{(1 - 0.412)}}$. In terms of decibels, the difference can be appreciated by noting that if the loss due to propagation through x meters of trees is 10 dB, then the EXD model predicts that the loss due to 2x meters of trees is 20 dB -- i.e., the average number of decibels of loss added by each meter of trees, α, remains constant regardless of d_f. Equation 11-2a of the MED model predicts that the loss through 2x meters of trees will be only 15 dB -- i.e., the average number of decibels of loss, α, decreases as the depth of the trees increases. Figure 11-2 illustrates a comparison between the measured values of α and the MED and EXD predictions. It is seen that the MED model predicts the measured trend more accurately. The measurements shown are from a Hughes Aircraft study (see Reference 11-13) and are independent of those used to develop the MED model.

The EXD model is consistent with the theoretical result obtained when one analyzes propagation through an infinite medium, whether it is filled with discrete scatterers (see, e.g., Ishimaru's text[11-14]) or a lossy-dielectric continuum. A plausible physical interpretation of the behavior described by the MED model is based on the observation that the forest is not an infinite, uniform medium. In many instances it can be described in terms of three vertical layers -- bare trunks, trunks with branches and leaves or needles, and air. The MED model applies to cases in which the direct ray between the transmitter and receiver is through the middle layer, which is also the layer with the greatest attenuation. For small values of d_f, almost all of the energy propagates through the highly attenuating region. As d_f grows larger,

---

[11-14] Ishimaru, A., Wave Propagation and Scattering in Random Media, Academic Press, New York, NY, 1978.

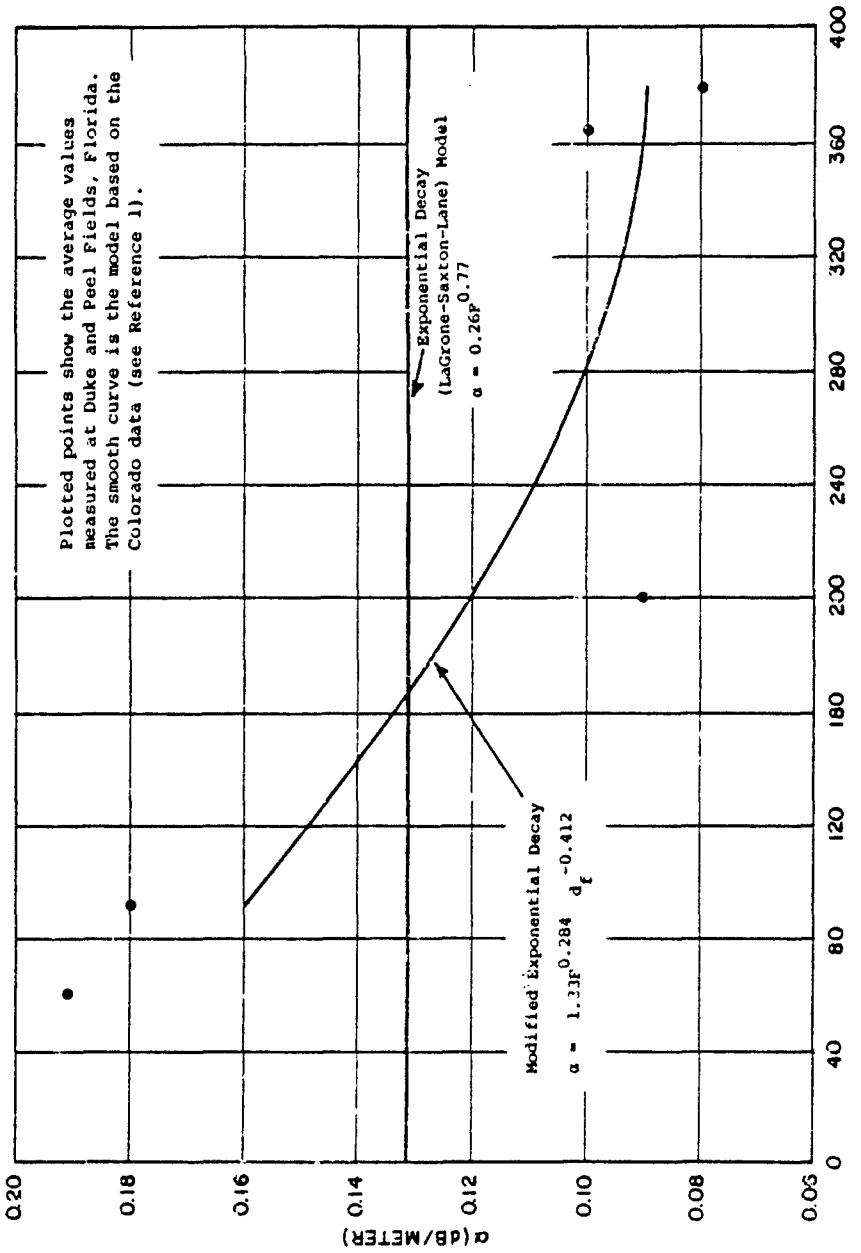

Figure 11-2. Trend of α vs depth of trees for the Florida data and the EXD and MED equations.

an increasing fraction of the energy begins to propagate through the other two regions. Since these regions cause less attenuation per meter, the average α for the entire path begins to decrease.

The MED model predicts a different frequency dependence of α than EXD-model Equation 11-3 predicts -- $F^{0.284}$ versus $F^{0.770}$. The magnitude of the difference between these relations can be better appreciated by noting that the MED equation predicts that the loss due to foliage at 4000 MHz will be 130% larger than the loss at 200 MHz. The EXD equation predicts that the increase will be 900%. In Reference 11-1, data from three geographical areas are shown in comparison with MED and EXD predictions. It is seen that the MED predictions are more accurate. (A more recent comparison of the model predictions with another set of data[11-15] also supports the relative accuracy of the MED frequency trend.) Because the EXD model is also based on measurements it is at first puzzling that it should predict such a different trend. As is explained in Reference 11-1, the problem is probably traceable to the particular set of measurements on which the EXD model is based. These measurements represent a variety of frequencies and a variety of values of d_f. However, there is a correlation between these two parameters -- in general, the higher frequency data was measured through smaller tree depths than was the lower frequency data. The effective α's computed from this data are larger at the high frequecies for two reasons. First, the loss due to a fixed amount of foliage becomes greater, in general, as frequency increases. Second, at a fixed frequency, the dB/meter due to a small grove of trees is more than the dB/meter due to a large grove. This is because, as has just been suggested, when the tree depth increases, a higher percentage of energy propagates outside the highly-attenuating branchy region. Thus, since tree depth was not considered in the development of EXD Equation 11-3, the empirically-determined exponent of F carries the weight of two different phenomena. It appears that the developers of Equation 11-3 would have arrived

---

11-15 Violette, E. J., et. al., SHF-EHF Propagation Through Vegetation on Colorado East Slope, CECOM-81-CS020, Institute for Telecommunication Sciences, Boulder, CO, June 1981, TABLE 4-3.

at a smaller (and more generally applicable) value of the exponent of F if they had had access to measurements of signals at many frequencies propagating through a single depth of trees.

(Another contributing factor to the discrepancy between the two relationships is the fact that they were developed from data in different frequency ranges. The EXD relationships were developed from data at frequencies as low as 100 MHz. The MED relation is based on data at 230 MHz and above.)

11.2.3.2 Quantitative Comparisons Between the MED, EXD and Measured Loss Values.

The rms errors of the two models are shown in TABLE 11-1. The MED model is consistently more accurate. An examination of individual measurements shows that very often the accuracy of the two models is comparable when the product $F \cdot d_f$ (GHz . m) is less than about 100. The errors of the EXD model tend to be a substantial overprediction of loss when $F \cdot d_f$ is larger than 100. Figures 11-3 and 11-4 depict examples of this.

The 9.6 - 57.6 GHz data for $d_f \geq 10$ m in Reference 11-15 were, on the average, 13 dB higher than the MED predictions. Therefore, one should be cautious in using the model for large depths of trees at frequencies greater than about 10 GHz. The EXD model predicts an average of 31 dB too much loss for this data set.

Other remarks regarding observed constraints on use of the MED model are:

a. The model will generally predict too much loss when the frequency is less than 200 MHz or the depth of trees is greater than 400 meters.

b. The model applies to dense groves of in-leaf (or with-needle) trees. Some data for leafless trees is summarized in subsection 2.7.2 of Reference 11-1. The model will predict too much loss for propagation through sparse groves of trees, but no means of quantifying this loss are available.

c. The model predictions are for situations in which the exteriors of the trees are not wet from a recent rain. Some data applicable to wet trees appear in subsection 2.7.3 of Reference 11-1 and in Reference 11-15.

d. The model applies to propagation in temperate latitude woods. The measurements used to develop and validate the model were taken in Colorado, California, Florida, Pennsylvania, Georgia, and England. Models applicable to tropical forests, such as in Thailand and Panama, are discussed in subsection 11.5 of this Chapter.

TABLE 11-1

COMPARISON OF THE RMS PREDICTION ERRORS

OF THE MED AND EXD MODELS

Data Description				RMS Errors (dB)	
Reference	Frequency (GHz)	d_f (m)	Tree Type	EXD	MED
11-1	0.5 - 3.3	24 - 152	Deciduous	3	2
11-6	0.2 - 9.2	14 - 15	Deciduous	10	10
11-6	0.2 - 9.2	45	Deciduous	13	7
11-6	0.2 - 9.2	60	Deciduous	27	9
11-6	0.2 - 9.3	91	Deciduous	37	6
11-12	1.9	50 - 150	Mixed	24	7
11-13	0.4	100 - 400	Coniferous	15	8
11-9	9.4 - 95.0	5 - 14	Mixed	14	2

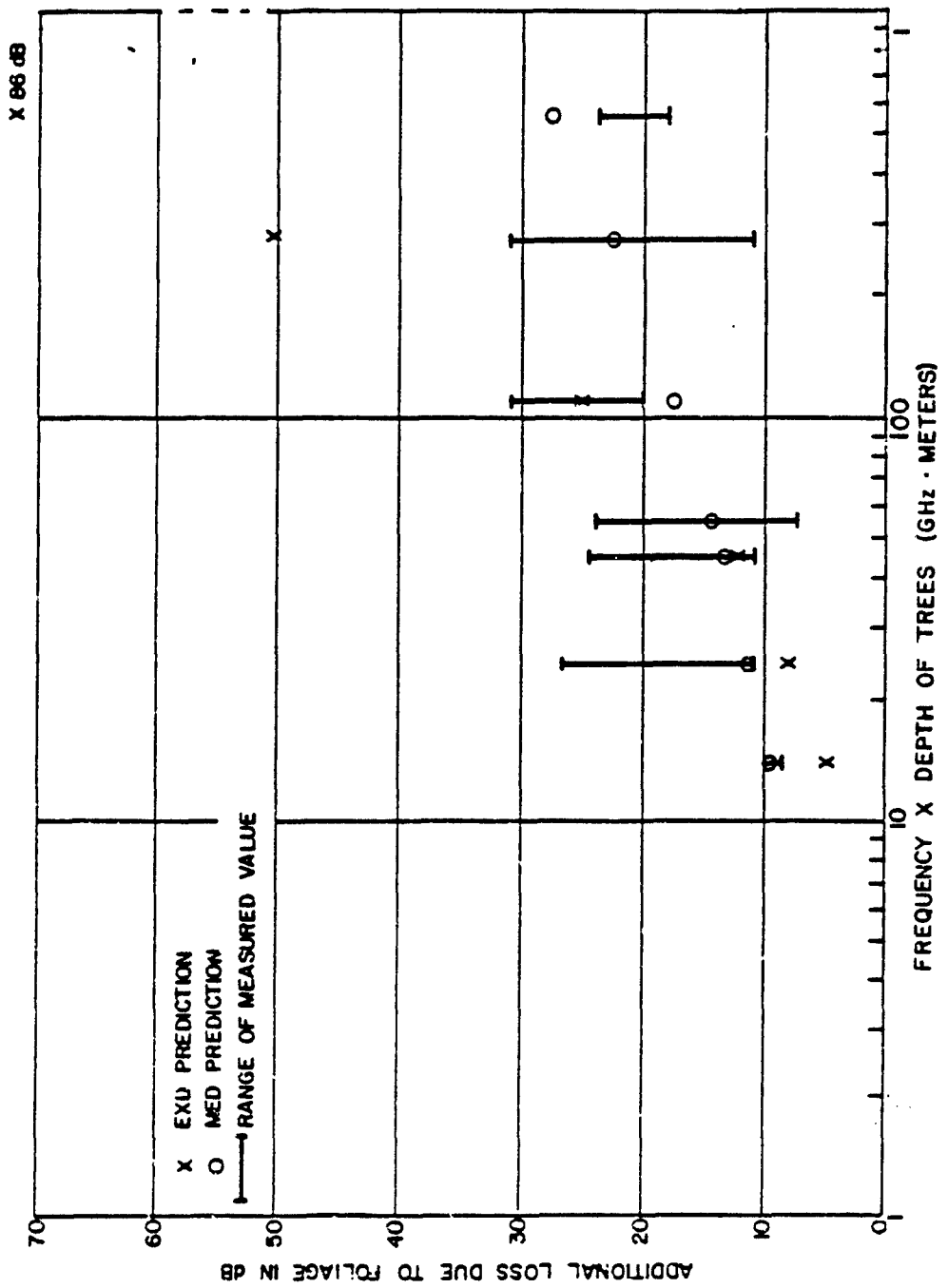

Figure 11-3. Predicted and measured losses for the Colorado (Reference 11-6) data. The depth of the trees is 60 meters, $0.23 < F\ (GHz) < 9.19$.

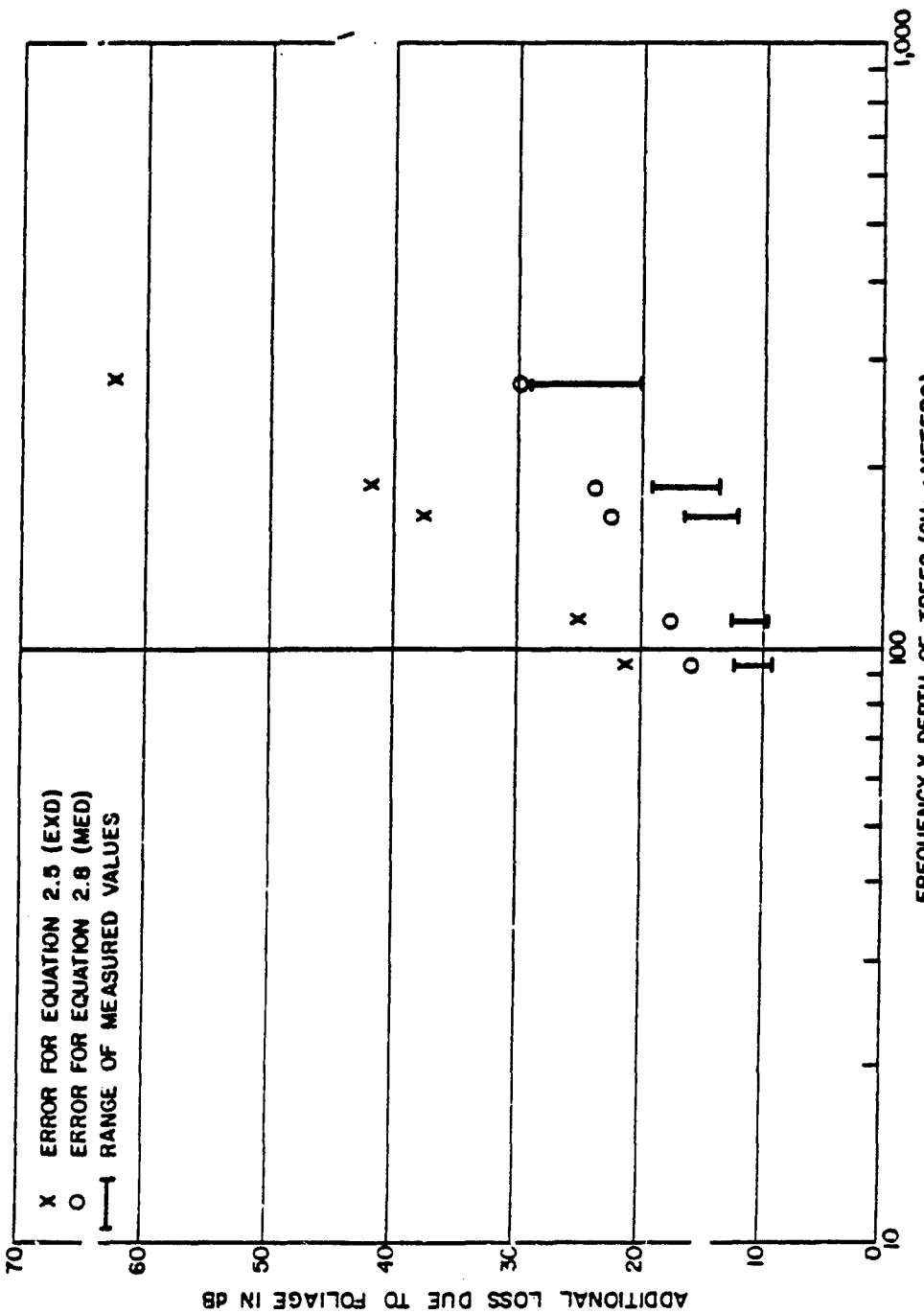

Figure 11-4. Predicted and measured losses for the California data (Reference 11-12). F = 1.85 GHz.

e. The MED model applies to geometries in which the flow of power is, at least initially, through the forest rather than over the forest. Diffraction models, which are discussed in subsection 11.3 of this Chapter, apply to the other type of problem.

The general guidance for predicting which algorithm should be used is this: the MED model will be applicable to problems in which one or both antennas are very near to groves of trees that are less than 400 meters deep. The diffraction model will be applicable to problems in which both antennas are separated by a large clearing from a large grove of trees.

The most accurate approach to determine applicability is to compute the loss using both methods. The more appropriate method is that which results in the lower estimated loss for the particular problem.

For completeness, it is noted that there are cases where combinations of propagation through, and diffraction over, the trees both take place. In fact, the diffraction model procedures described in Section 11.3 are really combination models. They use effective antenna heights which are less than the physical tree heights to account for the fact that there is some propagation through the upper parts of the trees at the edge of the clearing. Longley[11-16] and the Hughes researchers[11-17] proposed their own techniques for combining propagation-over and propagation-through models. Studies have not yet been conducted to determine which of the two models is more accurate.

[11-16] Longley, A. G. and Hufford, G. A., Sensor Path Loss Measurements - Analysis and Comparison With Propagation Models, OTR-75-74, Institute of Telecommunications Science, ITS, Boulder, CO, October 1975.

[11-17] Hughes Aircraft Company, Final Report - JTIDS Ground Foliage Propagation Tests, Technical Report FR-80-16-503, Fullerton, CA, April 1980.

11.3 DIFFRACTION CALCULATIONS

11.3.1. General Discussion and Prediction Formula

This model applies to problems in which both antennas are far enough from the intervening grove of trees so that the majority of the energy transmitted or received by the antenna flows over the trees rather than through them. Applicability is best determined on a case-by-case basis by computing both the MED model loss (Section 11.2.1) and the diffraction loss. The model that predicts the lower loss will be the model best suited to the particular problem.

Reference 11-1 indicates that two forms of the diffraction model have been reported as being successful for predicting the effects of obstruction by trees. Since no clear-cut criterion could be determined for choosing between the two types, this Handbook will describe only the type for which more extensive validation has been reported. This is the knife-edge diffraction model used by LaGrone.[11-18]

Figure 11-5 can be used to determine the additional loss caused by knife-edge diffraction over a grove of trees. This representation was developed by Bullington[11-19] (though not for foliage problems). The curve

---

[11-18] LaGrone, A. H., (1977), "Propagation of VHF and UHF Electromagnetic Waves Over a Grove of Trees in Full Leaf", IEEE Transactions on Antennas and Propagation, November 1977.

[11-19] Bullington, K., "Radio Propagation Fundamentals," Bell System Technical Journal, May 1957.

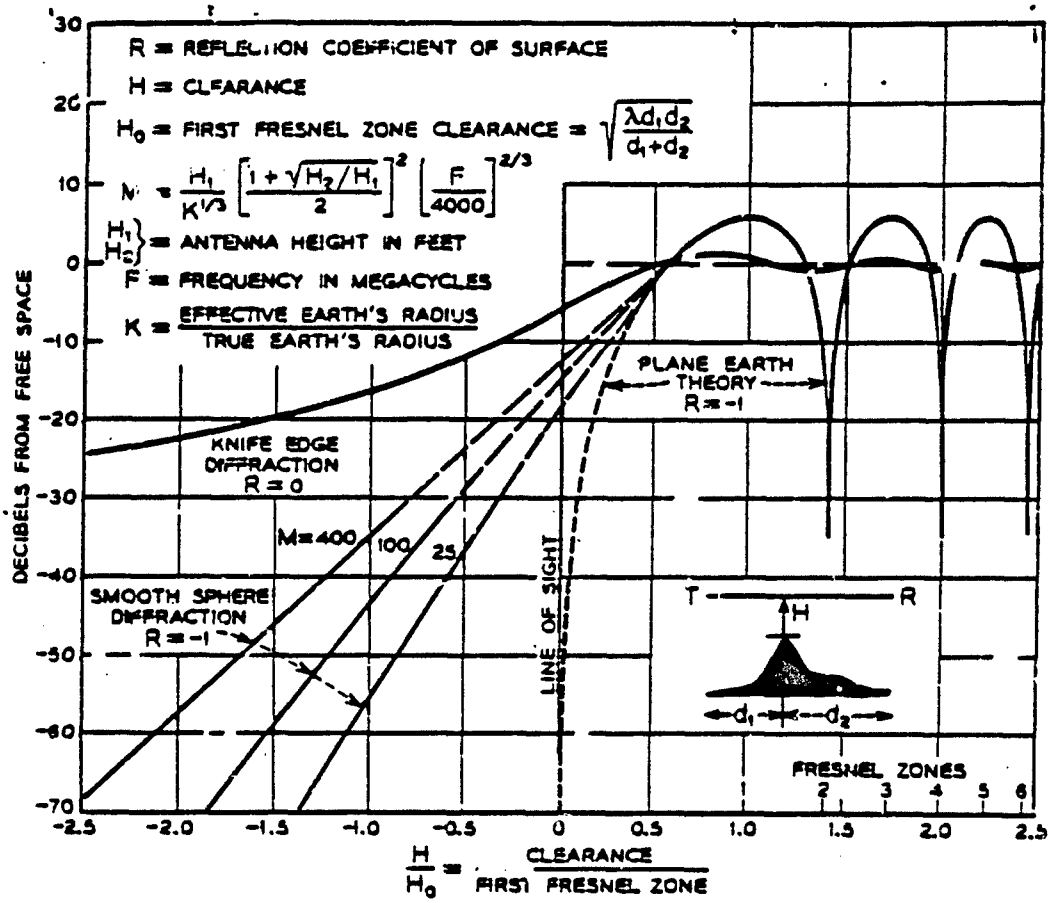

Figure 11-5. The additional loss due to knife-edge diffraction over obstacles (Reference 11-19).

recommended is labeled R=0. The location of the knife edge is assumed to be the edge of the grove that is nearest to one of the antennas. The height of the obstruction should, in general, be less than the height of the trees. Figure 11-6 shows the magnitude of the reduction observed by LaGrone.

11.3.2 A Computer Method

The TIREM program can be used to obtain diffraction calculations. This is done by increasing the assumed elevation of foliated terrain by the height of the trees minus the height reduction shown in Figure 11-6. The "H" card can be used to accomplish this (see ECAC UM 80-001).

11.3.3 Validation and Comparison With other Procedures

LaGrone (see Reference 11-18) demonstrated that the technique was useful for problems in the 82-2950 MHz band. Meeks reported accurate results for a problem at 1090 MHz.[11-20] ECAC engineers have used the TIREM-modification approach and have achieved qualitative success for problems at 5 GHz[11-21]. In another study, good agreement was found between diffraction predictions and measurements at 25 MHz (see Figure 25 in Reference 11-1).

11.4 KINASE'S MODEL FOR TRANSMISSION FROM AN ELEVATED ANTENNA

By combining theoretical analysis with observed loss behavior at 80, 150, and 700 MHz, Kinase (see Reference 11-4) developed a model for computing the loss due to obstructions in the foreground of one antenna. The model assumes

---

[11-20] Meeks, M. L., "A Low-Angle Propagation Experiment Combining Reflection and Diffraction," 1979 International Antennas and Propagation Symposium Digest 18-22 June 1979.

[11-21] Tactical Performance Assessment Program Report, Gallant Eagle 79, Patrick AFB, FL, December 1978.

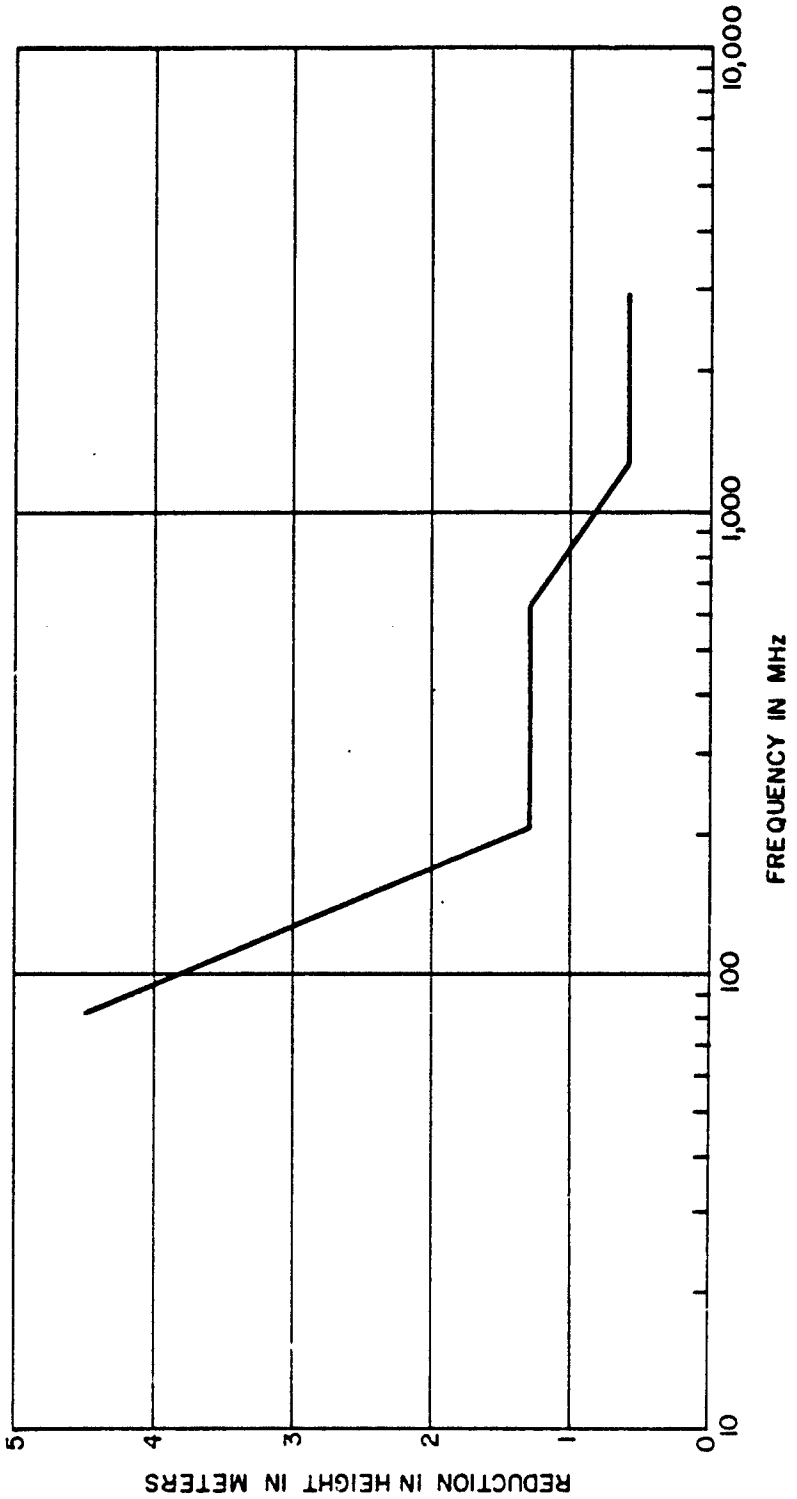

Figure 11-6. True-tree height minus effective obstacle height required to obtain accurate diffraction loss calculation (Based on Reference 11-18).

that the second antenna is elevated well above the clutter. The obstructions that were involved in the measurements were both foliage and man-made structures.

A key input to Kinase's model is η, which is defined as the percent of the land in a 2 km square around the "randomly sited" terminal that is covered by vegetation. It is reasonable to assume that better results could be achieved by considering only the 1 km x 2 km rectangle in front of this terminal.

Figures 11-7 and 11-8 show the loss predicted by Kinase's model.

Head [11-22] also developed an area model that solves the same type of problem as the Kinase model, i.e., one antenna elevated above the clutter and the other in a region where only the percentage of forest cover is defined. However, the Head model is probably less precise than the Kinase model because it does not use the take-off angle from the randomly sited terminal to the base station as a parameter. For cases in which diffraction is the dominant mechanism, this is a shortcoming because the angle through which the rays must diffract will be lower (and the loss lower) for higher take-off angles. For cases in which most of the energy propagates through the trees, the same trends are also true -- higher take-off angles will mean shorter path lengths through the foliage and lower losses. Thus, excluding this parameter represents a shortcoming of the Head "percent cover" model.

Further evaluation of these procedures is desirable. An interim recommendation is that the Kinase model be used for this type of problem. An automated version of the model is not presently available at ECAC.

[11-22] Head, H. R., "The Influence of Trees on Television Field Strengths at Ultra-High Frequencies," Proc. IRE, June 1960, and A Method of Predicting Average Field Strengths at Television Broadcast Frequencies, for the Television Allocation Study Organization (TASO), 1960.

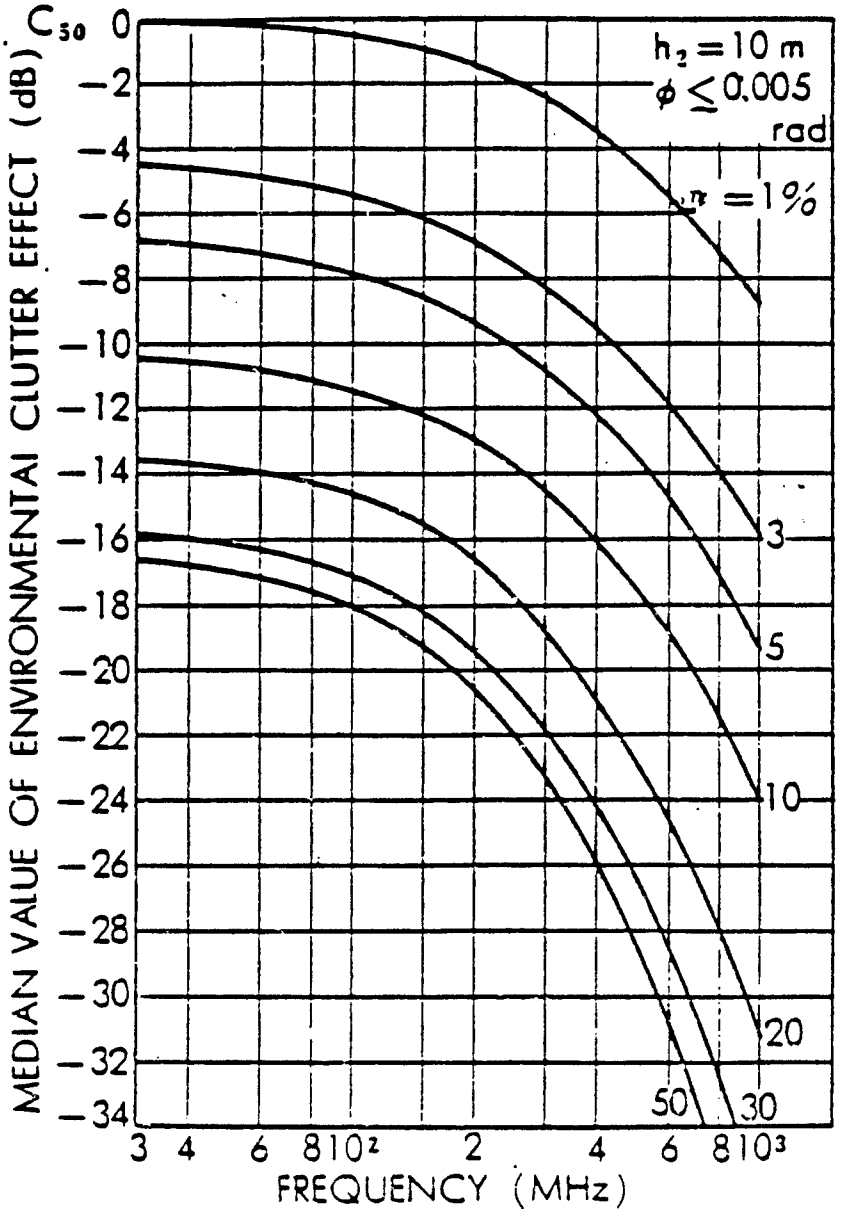

Figure 11-7. The additional loss due to foliage and man-made structures that cover η% of the surface area. ϕ is the takeoff angle from the randomly sited terminal to the base-station antenna (Reference 11-4).

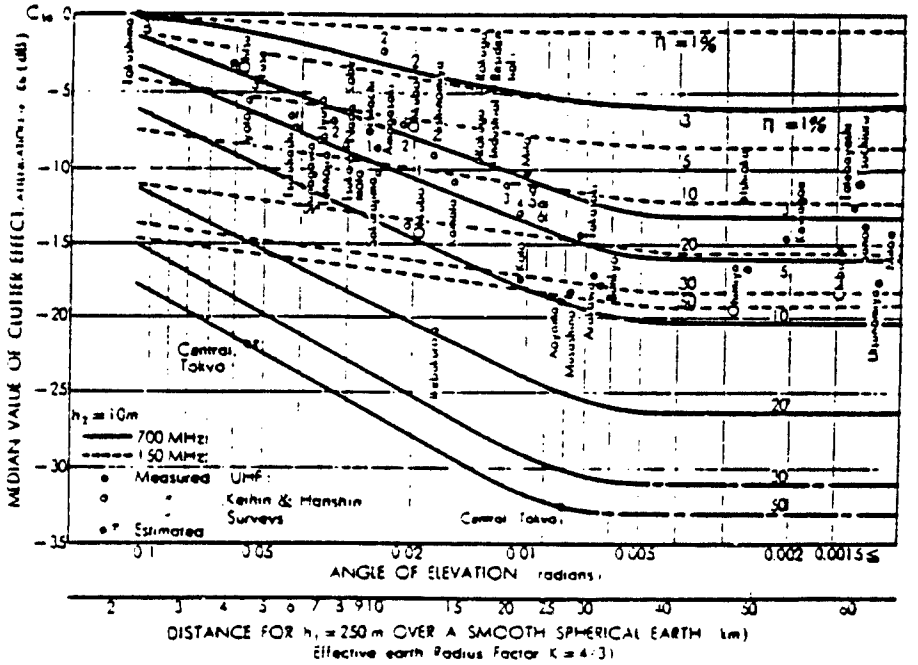

Figure 11-8. Kinase's model for clutter due to man-made obstructions and vegetation (Reference 11-4).

11.5 THE JANSKY AND BAILEY EMPIRICAL MODEL FOR LOSS IN A TROPICAL FOREST

11.5.1 General Discussion and Prediction Formula

This model applies to cases in which both antennas are immersed in foliage and separated by distances from 8 to 1600 meters (0.005 to 1.0 mile). Frequencies can range from 25 to 400 MHz. The model can be adapted to either polarization. Antenna heights can range from 2 to 7 meters. The model was developed by Jansky and Bailey researchers from measurements in the Pak Chong, Thailand, wet-dry, semi-evergreen tropical forest (see Reference 11-5 p. 93).

The equation for calculating loss is:

$$L_b = 36.57 + 20 \log f - 20 \log \left[\frac{Ae^{-1609\alpha d}}{d} + \frac{B}{d^2} \right] \qquad (11\text{-}4)$$

where

L_b = basic transmission loss, in dB

F = frequency, in MHz

α, A, B = empirical constants listed in TABLE 11-2

d = path length, in statute miles.

TABLE 11-2

CONSTANTS FOR THE JANSKY AND BAILEY EMPIRICAL MODEL

Frequency (MHz)	Polarization	α	A	B
25	V	0.0	0.0	0.00212
50	V	0.0	0.0	0.00106
100	V	0.045	0.615	0.000529
250	V	0.050	0.759	0.000443
400	V	0.055	1.02	0.000523
25	H	0.0	0.0	0.00424
50	H	0.0	0.0	0.00424
100	H	0.020	0.472	0.00551
250	H	0.025	0.774	0.000588
400	H	0.035	1.11	0.000598

For distances less than 80 meters, the loss trend follows that of the EXD model. For distances greater than about 160 meters, the loss increases as 40 log d.

11.5.2 Status of a Computer Method

ECAC has no computer program for the JB equation.

11.5.3 Validation and Comparision with Other Models

11.5.3.1 Low Antenna Height Data - The Accuracy of the Jansky and Bailey Model

Predictions of the Jansky and Bailey empirical model were generated for comparison with published measurements that had been taken at five sites. The sites, each containing a different type of tropical foliage, were:

a. Pak Chong, Thailand - A wet-dry semi-evergreen forest. Median tree height is 9.1 meters, median trunk diameter is 0.1 meters. The Jansky and Bailey empirical model is based on this data.

b. Songkhala, Thailand - A tropical rain forest. Median tree height is 18.3 meters, median trunk diameter is 0.3 meters.

c. Panama - Median tree height is estimated (per T. Doeppner) to be 11.6 meters. Trunk diameter is 0.2 meters.

d. Chumphon, Thailand - A fresh-water swamp forest. Median tree height is 11.9 meters. Median trunk diameter is 0.1 meters.

e. Ban Mun Chit - A dry evergreen forest. Median tree height is 6.1 meters. Median trunk diameter is 0.1 meters.

All measurements were made on circuits with antenras that were between 2 and 7 meters above the ground.

The predictions and measurements are listed in TABLE 11-3. It is seen that the rms errors of the Jansky and Bailey empirical model lie between 5 and 14 dB.

TABLE 11-3

COMPARISON BETWEEN PREDICTED AND MEASURED VALUES OF THE TOTAL BASIC TRANSMISSION LOSS BETWEEN ANTENNAS SEPARATED BY TROPICAL FOLIAGE

(Page 1 of 4)

$90 \leq$ FREQUENCY (MHz) ≤ 100

HORIZONTAL POLARIZATION

Distance (km)	Basic Transmission Loss (dB)			Location
	Measured	Jansky and Bailey Empirical Model	Theoretical Model	
1.60	118	122	NA[a]	Pak Chong
1.60	122	122	NA	Songkhala
1.60	139	122	NA	Panama
0.80	119	110	NA	Panama
0.70	114	107	NA	Chumphon
0.40	98	98	143	Ban Mun Chit
0.40	100	98	151	Chumphon
0.20	78	84	133	Ban Mun Chit
0.20	72	84	140	Chumphon
0.16	79	79	NA	Panama
0.10	74	69	130	Chumphon
0.10	64	69	122	Ban Mun Chit
	Rms error (dB)	7.5	55.9	

[a]Not available.

TABLE 11-3 (Continued)

(Page 2 of 4)

90 ≤ FREQUENCY (MHz) ≤ 100

VERTICAL POLARIZATION

Distance (km)	Basic Transmission Loss (dB)			Location
	Measured	Jansky and Bailey Empirical Model	Theoretical Model	
1.6	132	142	NA[a]	Pak Chong
1.6	139	142	NA	Songkhala
1.6	142	142	NA	Panama
0.8	129	130	NA	Panama
0.4	125	118	147	Chumphon
0.2	112	106	137	Chumphon
0.2	88	101	NA	Panama
0.1	86	89	126	Chumphon
	Rms Error (dB)	6.8	30.0	

[a]Not available.

TABLE 11-3 (Continued)

(Page 3 of 4)

40 ≤ FREQUENCY (MHz) ≤ 50

HORIZONTAL POLARIZATION

Distance (km)	Basic Transmission Loss (dB)			Location
	Measured	Jansky and Bailey Empirical Model	Theoretical Model	
1.6	106	118	NA[a]	Pak Chong
1.6	121	118	NA	Songkhala
0.4	94	94	NA	Chumphon
0.4	96	94	118	Ban Mun Chit
0.2	78	82	96	Chumphon
0.2	78	82	107	Ban Mun Chit
0.1	68	70	84	Chumphon
0.1	64	70	95	Ban Mun Chit
	Rms error (dB)	5.4	23.9	

[a]Not available.

TABLE 11-3 (Continued)

(Page 4 of 4)

40 ≤ FREQUENCY (MHZ) ≤ 50

VERTICAL POLARIZATION

Distance (km)	Basic Transmission Loss (dB)			Location
	Measured	Jansky and Bailey Empirical Model	Theoretical Model	
1.60	118	130	NA[a]	Pak Chong
1.60	141	130	NA	Songkhala
1.60	149	130	NA	Panama
0.80	125	118	NA	Panama
0.16	92	90	NA	Panama
0.10	101	82	72	Chumphon
	Rms errors (dB)	13.2	29.0	

[a]Not available.

11.5.3.2 Low Antenna Height Data - Comparisons with the Theoretical Lateral-Wave Model

A lateral-wave mechanism has been proposed by several authors[11-23,11-24, 11-25, 11-26, 11-27] as a means of explaining the observed loss in tropical forests. Various reports exist which show that measured loss-versus-distance, loss-versus-frequency, and loss-versus-antenna height trends are often consistent with the trends predicted by the lateral-wave model. At this point in time, however, it does not appear that the theoretical lateral-wave models represent a practical means for accurately predicting the actual basic-transmission loss.

Comparisons between the theoretical model predictions and measurements are also listed in TABLE 11-3. The predicted values were computed by Hagn[11-28] using the equations of Dence and Tamir (see Reference 11-26). The physical parameters of the forest -- conductivity, dielectric constant, and height -- that were used as model inputs were values measured by Hagn. The computed rms prediction errors of the theoretical model with these inputs range from 24 to 56 dB.

11-23 Sachs, D. L. and Wyatt, P. J., "A Conducting Slab Model Electromagnetic Propagation Within a Jungle Medium," Radio Science, February 1968.

11-24 Tamir, T., "Radio Wave Propagation in Forest Environments," IEEE Transactions on Antennas and Propagation, November 1967.

11-25 Tamir, T., Radio Wave Propagation Along Mixed Paths in Forest Environments," IEEE Transactions on Antenna and Propagation, July 1977.

11-26 Dence, D. and Tamir, T., "Radio Loss of Lateral Waves in Forest Environments," Radio Science, April 1969.

11-27 Ott, R. H and Wait, J. R., Excitation Mechanisms for Forest-Covered and Vegetated Media, Tech. Report ACC-ACO-8-73, Institute of Telecommunications Science (ITS), Boulder, CO, November 1973.

11-28 Hagn, G. H., Shrauger, N. K., and Shepherd, R. A., VHF Propagation Results Using Low Antenna Heights in Tropical Forests, Special Technical Report 46, Stanford Research Institute, Menlo Park, CA, March 1973.

In another comparison between theoretical model predictions and measurements, Ott (see Reference 11-27) reported that his version of the lateral-wave model over-predicted the loss measured in the 50 to 300 MHz range by 18 dB.

The Jansky and Bailey research team also investigated[11-29] a version of the lateral-wave model. They demonstrated that the model would yield quite accurate results if carefully selected "effective" values of the forest's physical parameters were used as model inputs. They obtained their effective values through an iterative process in which comparisons were continuously made between model predictions and the loss values measured at a particular site. The effective values were different for each site investigated. No clear-cut procedure was defined to determine the effective values for a site at which loss measurements had not yet been made. Four years later researchers from Jansky and Bailey and SRI observed that this problem remained.[11-30] To this author's knowledge no further progress had been made on this aspect of the use of the lateral-wave model prior to the preparation of this report.

11.5.3.3 Use of the Jansky-and-Bailey Empirical Model for Other Antenna Heights

Reference 11-5 includes guidance for applying the empirical model to problems in which one or both of the antennas are higher than 7 meters. Studies conducted by this author have shown that the errors are larger than those shown in TABLE 11-3 when this modified procedure is used. The measurements examined were those documented in References 11-5 and 11-29.

11-29 Hicks, J. J., et al., Tropical Propagation Research, Final Report, Vol. II, Atlantic Research Corporation, Alexandria, VA, November 1969.

11-30 Wait, J., Ott, R., and Telfer, T., editors, Workshop on Radio Systems in Forested and/or Vegetated Environments, AD 780-712, Institute of Telecommunications Science (ITS), Boulder, CO, February 1974, pp. I-E-2, I-E-4, and I-C-10.

11.6 THE VARIATION OF SIGNAL STRENGTH WITH POSITION IN A FOREST

11.6.1 Introduction

The preceding subsections provided formulas for predicting the mean loss between two antennas separated by foliage. This subsection provides information about the distribution of loss values about this mean. Such information is important since the actual loss between the two antennas can take on any of the values allowed by the distribution.

The mathematical framework for describing the distributions is based on the work of Norton.[11-31, 11-32] The parameters for a forest environment were reported by Robertson[11-33] and Okumura,[11-34] Josephson,[11-35] and Englund.[11-36]

In a forest environment, transmitted waves may reach the receiver via a number of paths, e.g., direct, ground-reflected, lateral-wave,

---

[11-31] Norton, K. A., et al., "The Probability Distribution of the Amplitude of a Constant Vector Plus a Rayleigh-Distributed Vector," Proc. IRE, October 1955.

[11-32] Rice, P. L., Longley, A. G., Norton, K. A., and Barsis, A. P., Transmission Loss Predictions for Tropospheric Communication Circuits, National Bureau of Standards TN 101, Boulder, CO, Revised, January 1967.

[11-33] Robertson, R. G., et al., Tropical Propagation Research, Final Report, Vol. III, Atlantic Research Corporation, Alexandria, VA, 1969, p. 31.

[11-34] Okumura, Y., et. al., "Field Strength and Its Variability in VHF and UHF Land Mobile Radio Service," Review of the Tokyo Electrical Communication Laboratory, September-October 1968.

[11-35] Josephson, B. and Blomquist, A., "The Influence of Moisture in the Ground, Temperature and Terrain on Ground Wave Propagation in the VHF-Band," IRE Trans. on Ant. and Propagation, April 1958.

[11-36] Englund, C. R., et al., "Some Results of a Study of Ultra-Short-Wave Transmission Phenomena," Proc. IRE, March 1933.

air-tree-interface-reflected, single-tree-scattered, and multiple-tree-scattered. Because each path will generally have a length that is different from that of the other paths, the phase of a signal received over one path will be different from that of a signal received from another path. Signals from several paths will usually be received at any specified point. The combination of signals with differing phases results in phenomena that appear in the space, frequency, and time domains. The phenomena in the space (position) domain will be discussed in this section. Figure 11-9 is an illustration of the actual spatial variation that was observed in a field test. Such variation is typical of that observed in a multipath environment.

The Rayleigh and the Nakagami-Rice distributions are two idealized models that can be used to describe the distribution of losses about the mean. These are described in the next subsection.

11.6.2 The Rayleigh and Nakagami-Rice Distributions

If the signal strength at a point can be modeled with these assumptions:

1. The total field is due to contributions from many paths. The magnitudes of the component vectors are random, but the total power of the sum of the vectors is constant.[a]
2. The contribution of any one vector to the total received power is small.
3. The phase of each vector is a random variable that is uniformly distributed over the range 0-2π

then, the probability that the amplitude of the resultant vector is greater than A, P(A) is given by the Rayleigh distribution:

[a]Rayleigh stipulated that the amplitudes were equal; Norton showed that this condition was not necessary.

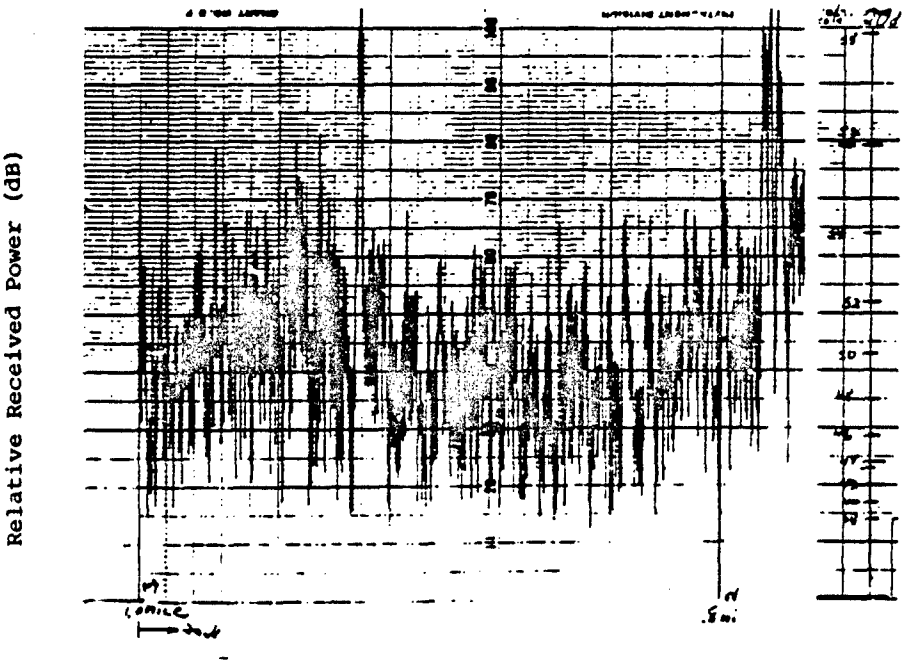

Figure 11-9. An illustration of the spatial variation in received power, due to multipath in a forest environment. The frequency is 250 MHz, polarization is vertical, and the receiver is located in a tropical forest in central Thailand (see Reference 11-5, p. 104). The signal is shown to vary over a range of more than 20 dB as the antenna is moved along a 1000-foot course.

$$P(A) = \exp(-A^2/A_R^2) \qquad (11\text{-}5)$$

where A_R is the RMS value of the resultant vector.

When Equation 11-5 is solved for P(A) = 0.5, the median amplitude, $A_{0.5}$, is found to be equal to $A_R \sqrt{\ln 2}$. Thus, Equation 11-5 is equivalent to:

$$P(A) = \exp \frac{-A^2 \ln 2}{A_{0.5}^2} \qquad (11\text{-}6)$$

Values from Equation 11-5 and 11-6 are shown on the last line of TABLE 11-4.

TABLE 11-4

CHARACTERISTICS OF THE RAYLEIGH AND NAKAGAMI-RICE DISTRIBUTIONS (Reference 11-32)

10 log Γ_F (dB)	$L_{.01}-L_{.5}$ (dB)	$L_{.1}-L_{.5}$ (dB)	$\bar{L}-L_{.5}$ (dB)	$L_{.9}-L_{.5}$ (dB)	$L_{.99}-L_{.5}$ (dB)	α (dB)
∞*	0.00	0.00	0.00	0.00	0.00	0.00
10	3.54	2.12	-0.21	-2.80	-5.98	2.00
0	7.02	4.48	-0.94	-7.53	-17.55	5.09
-10	8.19	5.20	-0.92	-8.18	-18.38	5.56
-∞**	8.22	5.21	-0.92	-8.18	-18.39	5.57

For Γ_F, see Equation 11-7.

*Constant signal.

**Rayleigh signal.

$L_{.xx}$ = Loss not exceeded at xx% of the locations = 10 log $A_{.xx}$.

If the field at any point in the midst of or "near" a forest is due to a multitude of components that satisfy the three criteria listed above, Equation 11-5 or 11-6 can be used to estimate the probability that the field strength

will have a particular amplitude. (The problem with quantifying the word "near" is discussed in Subsection 11.6.3). At another point in the forest that is "far" from the first point, the phases and amplitudes of the components that contribute to the resultant field strength vector will be uncorrelated with the phases and amplitudes of the components of the field at the first point considered. The field strength at this second point can be considered as another random variable with an amplitude probability determined by Equations 11-5 and 11-6. (The term "far" is given a quantitative definition in subsection 11.6.3.) Thus, the voltage at the input terminals to a receiver that is moving in this forest environment will be characterized by a Rayleigh distribution. (Motion of the trees will also cause fluctuations at the terminals of a fixed receiver.)

The Nakagami-Rice distribution describes the field obtained when a constant vector is added to a Rayleigh-distributed vector. It will apply to situations in which one component of the field at a receiver remains relatively constant for small changes in position, but a multitude of scattered components, also contributing to the field, change randomly as the receiver is moved. The probability of the normalized resultant amplitude being larger than A, P(A) is given by:

$$P(A) = \int_{a=A}^{\infty} 2a\,\Gamma_F\, I_o\,[2a\,\Gamma_F]\,\exp\,[-\Gamma_F(a^2 + 1)]\,da \qquad (11\text{-}7)$$

where

A = resultant amplitude A_s

$\Gamma_F = A_s^2/2\sigma^2$

$A_s^2/2$ = the power in the constant vector

σ^2 = the power in the Rayleigh distributed vector

I_o = the modified Bessel function of the first kind, zeroth order.

This distribution was derived independently by M. Nakagami in 1940 and S. O. Rice in 1944. TABLE 11-4 shows the distribution with 10 log Γ_F as a parameter. When this parameter is equal to $-\infty$, there is no constant component, and a Rayleigh distribution results.

When the criteria for this model are met, movement of an antenna from place to place produces a voltage at the receiver input terminals that has a Nakagami-Rice distribution. The movements have to be in an area small enough so that Γ_F remains relatively constant.

Subsection 11.6.3 summarizes measured values of Γ_F.

11.6.3 Measured Values of the Distribution of Field Strengths that Results from Movement of a Terminal

Robertson (Reference 11-33) measured the distribution of received signals that occurred when a receiver was moved about in a dense tropical rain forest in southern Thailand. His study covered the 50 to 150 MHz band. His work is summarized in the next paragraphs. It is followed by a summary of Okumura's (see Reference 11-34), Josephson's (see Reference 11-35), and Englund's (see Reference 11-36) observations in temperate forests.

Robertson's experiments involved path lengths in the 1000' to 8000' range. Transmitter heights varied from 13' to 200', and receiver heights from 6' to 20'. The tree canopy height varied from 65' to 120'. The number of trunks per acre was 590.

Robertson observed that:

1. For receivers within the forest, the field strength can be characterized by a Nakagami-Rice distribution ($\Gamma_F > 0$) for horizontal polarization and by a Rayleigh distribution ($\Gamma_F = 0$) for vertical polarization.

2. Γ_F is larger in clearings than it is in the forest. That is, the steady component of the signal is more significant in relation to the randomly varying component when the receiver is in a clearing.
3. Γ_F becomes smaller as frequency increases. That is, the randomly varying component of the signal increases in significance as the frequency increases.
4. In some cases, raising the antenna height increases Γ_F. In other cases, there is no change.
5. Γ_F becomes smaller as the height and density of the forest increase.

For horizontal polarization, 10 log Γ_F was always less than 11 dB for receivers in the forest. In 22 percent of the cases, the Rayleigh distribution (10 log $\Gamma_F = -\infty$) provided a suitable model. For receivers in clearings, 10 log Γ_F was as high as 18 dB; the Rayleigh distribution applied in 7 percent of the cases.

For vertical polarization with the receiving antenna in the forest, 10 log Γ_F was always less than 4 dB. The Rayleigh distribution applied in 69 percent of the cases. With the receiver in a clearing, 10 log Γ_F was as high as 10 dB, and the Rayleigh distribution was suitable for modeling 11 percent of the cases. (It is possible that horizontal and vertical polarization will be scattered equally well as frequency increases. This will result in an increase in the likelihood of Rayleigh fading for a horizontally polarized system.)

It was previously mentioned that the Rayleigh and Nakagami-Rice distributions applied to receivers in the midst of or "near" a forest. There is not enough data to support an empirical definition of "near." It is to be noted, however, that Robertson did observe a Rayleigh distribution with the receiver 200 feet from the trees. This observation was made for both polarizations. Antenna heights were less than 20 feet.

The separation between the terminal and the trees that is required to preclude multipath effects is a function of the many parameters that influence propagation in a forest environment: antenna heights, path length, terrain features, height and density of the trees, seasonal variations of foliage, polarization, and frequency. Generalization from a small number of observations is not recommended.

In the Rayleigh model description, it was mentioned that two points would have to be separated "far enough" from each other for the field strength at one point to be uncorrelated with the field strength at another point. Robertson observed that 0.5 λ was a sufficient separation for reception points located along the same great circle path to the receiver. 1.0 λ separation was needed if the two reception points were on a line transverse to the great circle path.

In another area of Thailand, Jansky and Bailey crews found 0.37 λ was sufficient for uncorrelated amplitudes. This was based on measurements taken along a single great circle path from the transmitter. This result was found to be independent of frequency in the 25 to 400 MHz band (see Reference 11-5, p. 107).

These measurements confirm a theoretical prediction by Gans.[11-37] He determined that 0.5 λ would be appropriate for the separation between receiving antennas along the same great circle path. He showed that the distance will increase if the receiver is moved away from the scatterers.

Measured values of the distribution of field strengths resulting from the movement of a terminal in temperate forests have been reported by Josephson (see Reference 11-35), Okumura (see Reference 11-34), and Englund (see Reference 11-36).

[11-37] Gans, M. J., "A Power Spectral Theory of Propagation in the Mobile Radio Environment," IEEE Transactions on Vehicular Technology, February 1972.

Josephson published a graph, reproduced here as Figure 11-10, that shows the range of small scale variability of VHF signals in a pine forest. The variability is described as the difference between the levels not exceeded at 10% and at 90% of the locations. From TABLE 11-4 one can see that this difference is 13.5 dB for a Rayleigh distributed signal. This difference is reached at 80 MHz.

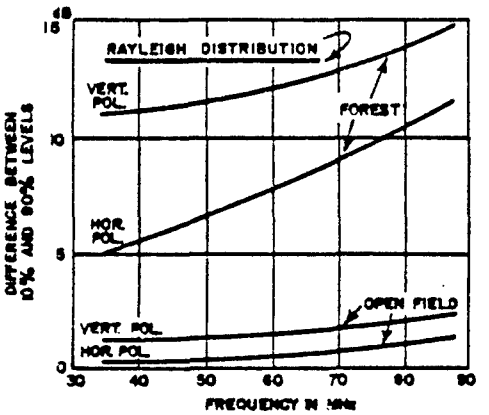

Figure 11-10. The observed variability of the signal received in a nontropical forest (Reference 11-35).

Okumura showed that measurements taken at 450, 900, and 1900 MHz "in or behind" a forest were Rayleigh distributed. The antennas were vertically polarized.

Englund reported a fluctuation of about 10 dB, peak-to-peak, in the 60 to 80 MHz band in woods and at the edge of the woods in New Jersey. This is less severe than the fluctuation of Rayleigh-distributed signals. Vertical polarization was used in this test.

11.7 ESTIMATING THE EFFECTS OF URBAN STRUCTURES ON PATH LOSS

This section pertains to estimating the additional loss caused by single buildings or large clusters of buildings intervening between a transmitting

and receiving antenna. Generally this loss will become greater as frequency increases, the height of the structure relative to the antennas increases, and the distance between the structure and the antennas decreases.

Measurements in Boston showed that building-shadow effects averaged 12 dB at 35 MHz.[11-38]

Measurements in Birmingham, England revealed that the man-made features in the city reduced signal levels by 16 dB at 85.9 MHz, 20 dB at 167.2 MHz, and 35 dB at 441.0 MHz. (H_{tx} = 35 meters, H_{rx} = 1 meter, vertical polarization, path lengths = 1-10 km).[11-39]

Studies in Tokyo at 450 MHz indicate that regions in which 50% of the surface was covered by buildings had losses that were typically 25 dB more than the losses in regions in which only 5% of the surface was built-up (see Reference 11-38). The results at 800 MHz were essentially identical to the lower frequency data.

At 820 MHz, the path loss over urban circuits was 11.9 dB more than the loss for relatively unobstructed suburban paths.[11-40]

At 922, 1317, and 1430 MHz, the average additional attenuations caused by the urban clutter of Tokyo were 27, 28, and 29 dB.[11-41]

11-38 Longley, A. G., Radio Propagation in Urban Areas, OT Report 78-144, Institute for Telecommunications Sciences, Boulder, CO, April 1978.

11-39 Allsebrook, K. and Parsons, J. D., "Mobile Radio Propagation in British Cities at Frequencies in the VHF and UHF Bands," IEEE Trans. on Veh. Tech., November 1978.

11-40 Kelly, K. K. II, "Flat Suburban Area Propagation at 820 MHz," IEEE Trans. on Veh. Tech., November 1978.

11-41 Kozono, S. and Watanabe, K., "Influence of Environmental Buildings on Land Mobile Radio Propagation," IEEE Trans. on Comm. Tech., Vol. 25, No. 10, 1977.

Kinase's clutter model (Reference 11-4) can be used to estimate urban effects in the 3-1000 MHz band. This model applies to cases in which one antenna is elevated above the clutter, as at a base station. It is a graphical procedure, and the necessary figures are reproduced in Subsection 11.4 of this Handbook.

Another commonly cited model for predicting the effects of urban structures was developed by Okumura (see Reference 11-34). There has been no comprehensive comparison of the relative merits of his model and Kinase's. The Kinase model was selected for the Handbook because the use of the parameter η allows users to readily quantify the degree of urban buildup that is present. Okumura's model depends on the hard-to-define terms "urban," "suburban," and "quasi-open".

For predicting urban effects in the 1-2 GHz range, however, Okumura's model is the only one of these two that applies. (The Hata model[11-42] consists of equations developed from Okumura's graphs.)

Kozono (see Reference 11-41) showed how a parameter like Kinase's η could be worked into Okumura's model. Further validation is needed to determine if the resulting procedure is more accurate than Kinase's.

Malaga[11-43] recently summarized 3 - 450 MHz measurements taken in urban (Boston, MA) and suburban (Lexington, MA) areas. Both the transmitting the receiving antenna heights were about 1 m above the ground. An empirical model is shown in his paper, as well as a succinct review of other urban propagation models. He observes that no other models are available for the 3 - 80 MHz portion of his model's range of applicability.

11-42 Hata, M., "Empirical Formula for Propagation Loss in Land Mobile Radio Service," IEEE Trans. on Veh. Tech. August, 1980.

11-43 Malaga, A. "An Empirical Path Loss Model for HF, VHF Propagation in Urban Areas", Radio Science, May 1981.

If a single building obstructs the ray path between a transmitter and receiver, and the relative location of this building is known, then a modified knife-edge diffraction calculation can be used to estimate the increase in loss caused by this building (see References 11-38 and 11-39). Figure 11-5 is a graphical procedure for determining the knife-edge loss. Figure 11-11 shows Allsebrook's empirical correction to be added to the value from Figure 11-5. This correction is due, presumably, to the finite extent of the building, i.e., the fact that it is not an infinitely thin knife-edge.

If the mobile receiver is moved through the urban areas, multipath effects will cause fading. Okumura reports that a Rayleigh distribution will very often accurately characterize the spatial variability (see Reference 11-34, Section 5.1.1). This is based on analysis of data in a dense urban area at 450, 900 and 1900 MHz. When this result is true, the figures on the last line of TABLE 11-4 can be used to estimate the additional loss due to multipath.

Analysts should be aware that pulses in an urban environment will arrive at a reciever over a period of time that is longer than the original duration of the transmitted signal. References 11-44 through 11-48 contain measured values

---

11-44 Young, W. R. and Lacy, L. Y., "Echoes in Transmission at 450 Megacycles From Land-to-car Radio Units", Proceedings of the IRE, March 1950.

11-45 Turin, G. L., et al., "A Statistical Model of Urban Multipath Propagation", IEEE Transactions on Vehicular Technology, February 1972.

11-46 Cox, D. C., "Time-and Frequency-domain Characerizations of Multipath Propagation at 910 MHz in a Suburban Mobile Radio Environment", Radio Science, December 1972.

11-47 Cox, D. C. and Leck, R. P., "Distributions of Multipath Delay Spread and Average Excess Delay for 910-MHz Urban Mobile Radio Paths", IEEE Transactions on Antennas and Propagation, March 1975.

11-48 Nielson, D. L., Microwave Propagation and Noise Measurements for Mobile Digital Radio Application, Pocket Radio Note 4, SRI, Menlo Park, CA, January 1975.

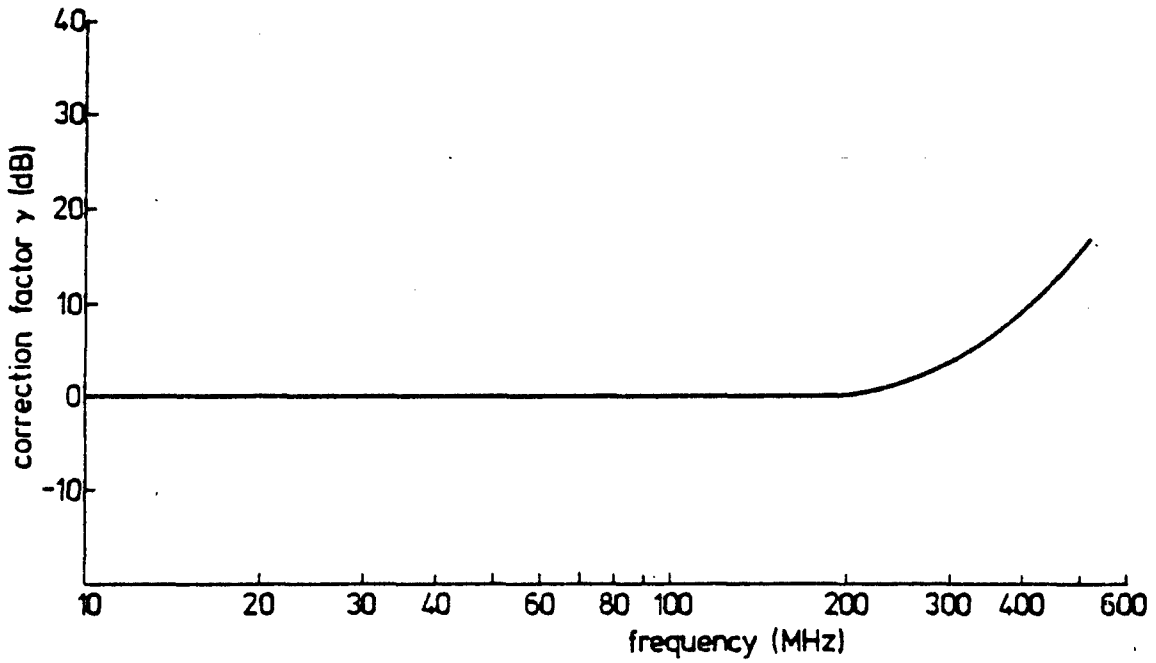

Figure 11-11. Empirical correction to knife-edge diffraction calculations in an urban environment (Reference 11-39). The diffraction procedure has been validated by comparison with data at frequencies above 85 MHz.

of this time spreading. Figure 11-12 is an example of a received-power-versus-time observation in a suburban area. The impact of this phenomenon on digital and wideband-analog system performance is discussed in References 11-49 through 11-52.

11.8 CONCLUDING REMARKS

1. The EXD model is based on a value of α that is a function of frequency and the depth of the forest. It would be interesting to see the development of a more sophisticated equation for α. Factors that should be taken into account are listed below.

a. Have the trees been rained on?
b. How dense is the forest?
c. Are the trees in-leaf?
d. Do the electrical properties of the vegetation vary with season?
e. What is the type of the trees?
f. What is the polarization?
g. What is the height of the antenna relative to the trees?
h. What is the antenna beamwidth?

11-49 Hubbard, R. W., et al., Measuring Characteristics of Microwave Mobile Channels, NTIA Report 78-5, Institute for Telecommunication Sciences, Boulder, CO, June 1978.

11-50 Linfield, R. F., Radio Channel Capacity Limitations, OT Report 77-132, Institute for Telecommunicaton Sciences, Boulder, CO, November 1977.

11-51 Turin, G. L., "Introduction to Spread-Spectrum Antimultipath Techniques and Their Application to Urban Digital Radio," Proceedings of the IEEE, March 1980.

11-50 Jakes, W. C., ed., Microwave Mobile Communications, New York, John Wiley, 1974.

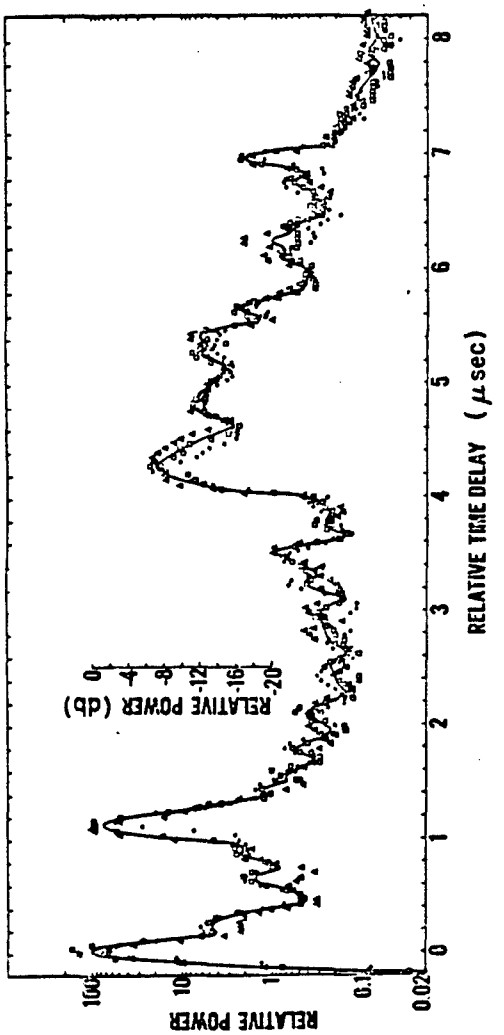

Figure 11-12. An example of echoes observed when a pulse is transmitted in a suburban environment. The transmitter is located about 100 m above the buildings. The receiving antenna, located on top of a van, is 5 km away. The frequency is 910 MHz (from Reference 11-46).

The Hughes and SRI data (see References 11-17, 11-53, 11-54, and 11-55) collected at several locations in Eglin Air Force Base, FL, and Arnold Air Force Station, TN, for the PLRS and JTIDS programs will be valuable for this development effort. Comparing the results of measurements taken in dissimilar tropical forests, such as those listed in TABLE 11-4 will also be useful. More measurements taken in forests after a rainstorm are needed.

2. There is no widely accepted empirical or theoretical procedure for predicting the loss when the antennas are immersed in a temperate forest and are separated by a distance of more than 400 meters. The JTIDS and PLRS measurements would be useful in developing or validating such a procedure. In 1982, the U.S. Army was funding CYBERCOM to study the applicability of electromagnetic scattering theory to the problem of communications in a forest environment. The results of this study may be helpful in solving the long-path problem.

3. A better analysis of the diffraction models and applicable data is needed to resolve the question of when the knife-edge and when the smooth-sphere model should be used. Kinase (see Reference 11-4) presents formulas for diffraction over an extended slab that may also be applicable to this problem.

4. The spreading in time of pulses and the reduction in usable bandwidth due to multipath in a forest environment has not generally been quantified. Only a small amount of contradictory VHF data has been reported

---

11-53 Presnell, R. I., PLRS Ground-to-Ground Propagation Measurements, SRI Project 8171, SRI International, Menlo Park, CA, June 1980.

11-54 Presnell, R. I., JTIDS Ground-to-Ground Propagation Measurements, SRI Project 8171, SRI International, Menlo Park, CA, June 1980.

11-55 Kivett, J. A., and Diedericks, P. J., PLRS Ground-to-Ground Propagation Test Technical Report, RF-80-14-6, Hughes Aircraft Company, Los Angeles, CA, 1980.

for tropical forests.[11-56,11-57] For temperate forests, existing data consists of a few UHF measurements.[11-58]

5. The least-squares procedure used to develop the MED equation for α is not necessarily the optimum one. It would be of value to see the results of alternate approaches.

6. The urban-effects models generally have not been compared with data sets other than the ones used in their development. It is desirable to determine if some prediction biases exist due to the particular data sets initially used.

[11-56] Jakes, W. C., "An Approximate Method to Estimate an Upper Bound on the Effect of Multipath Delay Distortion on Digital Transmission", IEEE Transactions on Communications, January 1979.

[11-57] Hicks, J. J., et al., Tropical Propagation Research, Final Report, Vol. IV, Atlantic Research Corporation, Alexandria, VA, December 1972.

[11-58] Hufford, G. A., Hubbard, R. W., et al., Wideband Propagation Measurements in the Presence of Forests, CECOM-82-CS029-F, Institute for Telecommunication Sciences, Boulder, CO, January, 1982.

CHAPTER 12

MILLIMETER WAVE PROPAGATION

By: R. Meidenbauer

12.1 INTRODUCTION

The millimeter wave band consists of frequencies between 30 and 300 GHz. The most significant difference between the propagation characteristics of millimeter waves and those of lower frequency waves is the large effect of the earth's atmosphere on the transmitted signal. Throughout this band, absorption by the molecular constituents of the atmosphere and attenuation caused by hydrometeors are large contributors to total path loss.

12.2 CAPABILITIES

A summary of the recent work at ECAC in the area of millimeter wave propagation is given below. This chapter will be expanded in a future edition of this handbook to include appropriate manual techniques for millimeter wave propagation analysis and to include a more thorough discussion of available automated models.

An overview of the propagation phenomena in the millimeter wave band is provided in Reference 12-1. Factors contributing to the attenuation of millimeter waves are discussed, including free-space spreading loss, molecular absorption, and attenuation due to rain and other hydrometeors, aerosols, terrain obstacles, and foliage. Other effects on the signal are also treated, including scintillation and fading, angle-of-arrival fluctuations,

---

12-1 Meidenbauer, R., Summary of Millimeter Wave Propagation Phenomena, ECAC-TN-80-023, October 1980.

depolarization, and bandwidth limitations. Simple manual techniques are presented for predicting these effects wherever possible. Appropriate measurements are summarized and extensive references are cited.

Reference 12-2 describes an automated millimeter wave propagation prediction program MMWPROP. This model is currently operational at ECAC and may be used to predict the attenuation due to free space spreading, molecular absorption, and rain absorption and scattering not exceeded P% of the time on a given SHF or EHF (1-300 GHz) link through any one of six model atmospheres. Estimates of molecular phase dispersion may also be obtained. Link predictions are currently limited to radio-line-of-sight paths. A topographic data-handling routine is included so that the ECAC topographic data base may be accessed to check line-of-sight clearance. The MMWPROP model has been shown to provide reasonable agreement with measured data.

12-2 Meidenbauer, R., A Millimeter Wave Propagation Prediction Model - MMWPROP, ECAC-TN-81-046, September 1981.

CHAPTER 13

PROPAGATION AT FREQUENCIES USED

BY ELECTRO-OPTICAL SYSTEMS

By: D. Reed

13.1 INTRODUCTION

Electro-optical (E-O) propagation includes those frequencies in the ultraviolet (UV), visible, and infrared (IR) portions of the spectrum. ECAC has acquired several models to calculate attenuation of radiation through the atmosphere in the spectral regions. These models were utilized on the XM-1 tank laser rangefinder[13-1] and Combat Identification System/Battlefield IFF (CIS/BIFF)[13-2] projects.

13.2 CAPABILITIES

The E-O propagation models which have been acquired to date are: 1) LOWTRAN 5,[13-3] 2) EOSAEL-80,[13-4] 3) LASER,[13-5] and 4) FASCODE1.[13-6] Of these, LOWTRAN 5 and EOSAEL-80 are presently sufficient for ECAC uses and are

---

13-1 Reed, David J., EMC Consideration of the XM-1 Tank Laser Rangefinder, ECAC-PR-80-028, December 1980.

13-2 Osborne, R., Reed, D., Rose, D., and Sautter, P., Preliminary EMC Considerations of the Combat Identification System/Battlefield IFF (CIS/BIFF), ECAC-CR-81-105, September 1981.

13-3 Kneizyr, F. X., et al, Atmospheric Transmittance/Radiance: Computer Code LOWTRAN5, AFGL-TR-80-0067, Air Force Geophysics Laboratory, Hanscom AF, Mass., 21 February 1980.

13-4 Duncan, L. D., EOSAEL 80-Vol. I, ASL-TR-0072, Atmospheric Sciences Laboratory, WSMR, NM, January 1981.

13-5 McClatchey, R. A. and D'Agati, A. P., Atmospheric Transmission of Laser Radiation: Computer Code LASER, AFGL-TR-78-0029, 31 January 1978.

13-6 Smith, H. J. P., et al, FASCODE - Fast Atmospheric Signature Code (Spectral Transmittance and Radiance), AFGL-TR-78-0081, 16 January 1978.

the only ones maintained. References 13-3 through 13-6 provide a good discussion on E-O propagation. However, much of this material has been summarized in APPENDIX A to ECAC-TN-80-025 and in ECAC-TN-81-058. Electro-optical propagation capabilities will continue to be developed as updates to the models are made, and these developments will be documented in future TN's and potentially an ECAC E-O propagation handbook. This chapter will be completed in future editions of this handbook.

CHAPTER 14

COUPLING BETWEEN ANTENNAS ON AN AIRFRAME

By: F. Boldissar

14.1 INTRODUCTION

Section 14.2 of this chapter provides a set of formulas to be used in the calculation of the power coupled between two antennas located on a perfectly conducting airframe. The formulas apply to problems in which the airframe can be represented as either a flat plate, a circular cylinder, a circular cone, or a knife-edge. The cylinder and cone formulations apply to structures in which the radii of curvature are greater than two wavelengths. Further, in all formulations the antennas should be separated by at least one wavelength.

Section 14.3, contributed by W. Stuart and K. O'Haver, provides the current status on a study of computer models designed to solve airframe coupling problems for both small (as in the case of the Section 14.2 formulas) and large wavelength signals. Section 14.4 lists some documents in which comparisons between the Section 14.2 predictions and measurements are presented.

14.2 MANUAL METHODS

This section provides a list of formulas amenable to hand calculation that can be used to estimate coupling losses over perfectly-conducting

airframes. The equations have been extracted from References 14-1 through 14-6. Ambiguities and inconsistencies in several of these documents have been resolved in the preparation of this section.

14.2.1 Loss Over Flat, Perfectly-Conducting Surfaces

Basic transmission loss between antennas located on an aircraft depends upon the geometry of the aircraft and the locations of the antennas. If the antennas are both located on a flat, perfectly-conducting surface, the loss may be computed from the free-space formula,

$$L_{bfs} = 20 \log f + 20 \log d - 37.87 \qquad (14\text{-}1)$$

where L_{bfs} is in dB, f is the frequency in MHz, and d is the distance between the antennas in feet. This equation can also be used when the antennas are within line-of-sight of each other.

14-1 Haseltine, R., Avionics Interference Prediction Model (AVPAK), ECAC-TN-75-020, ECAC, Annapolis, MD, September 1975.

14-2 Hasserjian, G., and Ishimaru, A., "Excitation of a Conducting Cylindrical Surface of Large Radius of Curvature," IRE Trans. on Antennas and Propagation, May 1962.

14-3 Siegel, M.D., Aircraft Coupled Interference Analysis, IEEE EMC Symposium Record, 1969.

14-4 Lyon, J.A.M., et. al., Derivation of Aerospace Antenna Coupling Factor Interference Prediction Techniques, AFAL-TR-66-57, The University of Michigan, Ann Arbor, MI, April 1966.

14-5 Morgan, G., Avionics Interference Prediction Model, FAA-RD-71-10 (ESD-TR-70-286), ECAC, Annapolis, MD, December 1970.

14-6 Jordan, E.C., and Balmain, K.G., Electromagnetic Waves and Radiating Systems, 2nd Edition, Prentice-Hall, Englewood Cliffs NJ, 1968.

14.2.2 Loss Over a Cylindrical Airframe

If the radio ray must travel along the curved surface of the aircraft's fuselage to reach the receiving antenna, the loss is then given by

$$L_b = L_{bfs} + F(y) \text{ dB} \qquad (14\text{-}2)$$

where L_{bfs} is the free-space loss computed over the total distance traversed, and F(y) is the curvature factor shown in Figure 14-1. If the fuselage is modeled as a right circular cylinder with radius of curvature ρ (Figure 14-2), the distance between two antennas located on the surface of the cylinder is given by

$$d_c = \sqrt{[\rho(\phi_1-\phi_2)]^2 + (z_1-z_2)^2} \text{ feet} \qquad (14\text{-}3)$$

where (ρ, ϕ_1, z_1) and (ρ, ϕ_2, z_2) are the cylindrical coordinates of the antennas when the axis of the cylinder is coincident with the z-axis of a cylindrical coordinate system (distances in feet, angles in radians). The dimensionless variable y is given by

$$y = 0.080\,\rho\,(\phi_1-\phi_2)^2\sqrt{\frac{f}{d_c}} \qquad (14\text{-}4)$$

where f is the frequency in megahertz, and the other parameters have previously been defined.

When one of the antennas has been raised above the fuselage, as in Figure 14-3, the total distance used in the free-space equation is the sum of the cylindrical-spiral distance d_c and the straight line distance

$$d_s = \sqrt{\rho_1^2 + \rho_2^2 - 2\rho_1\rho_2\cos(\phi_1 - \phi_2) + (z_1 - z_2)^2} \text{ feet} \qquad (14\text{-}5)$$

where the distances and angles given in Figure 14-3 are in feet and radians, respectively. Expressions for the ϕ and z coordinates of the tangent point (i.e., the point at which the straight line segment of the path joins the cylindrical-spiral segment) are given below.

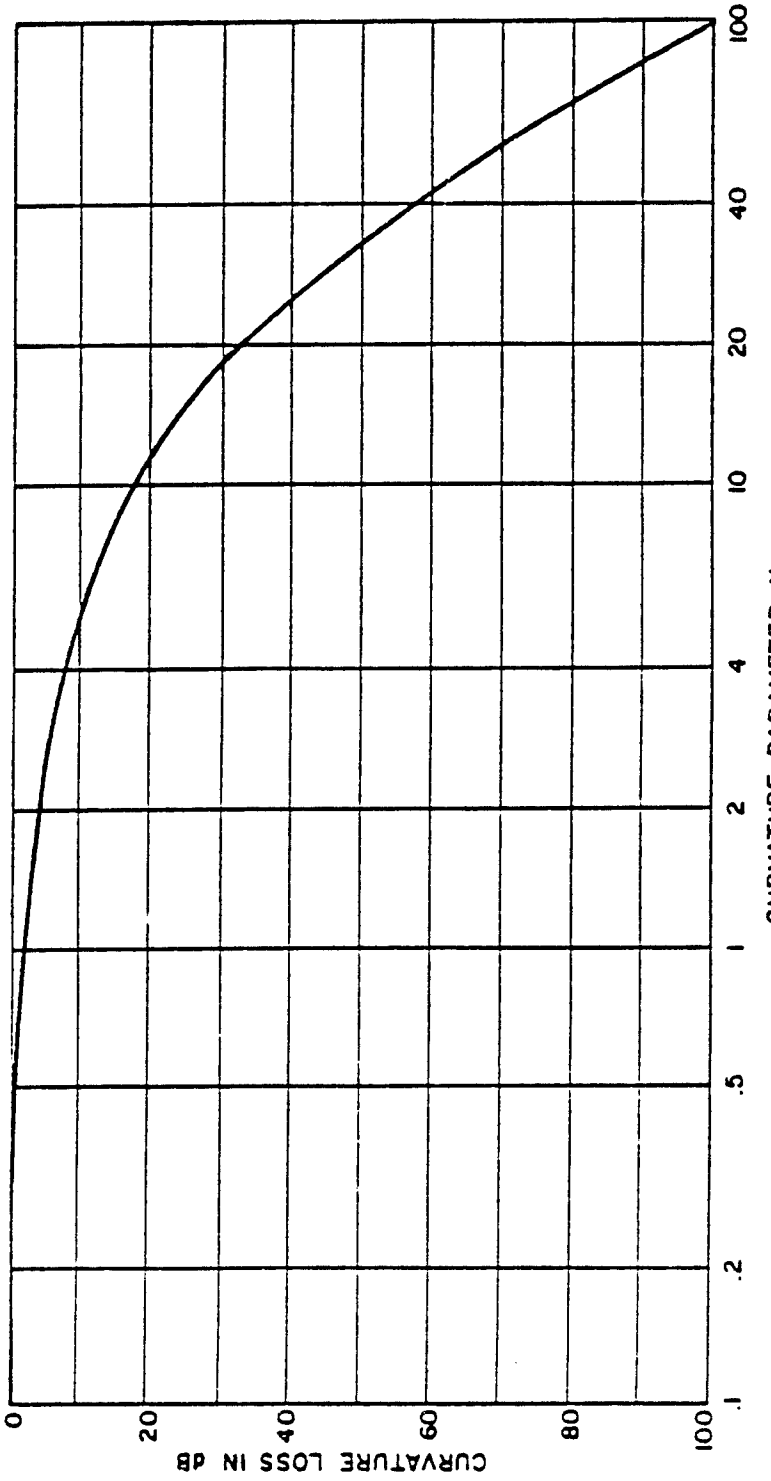

Figure 14-1. Additional loss due to curvature of a cylinder.

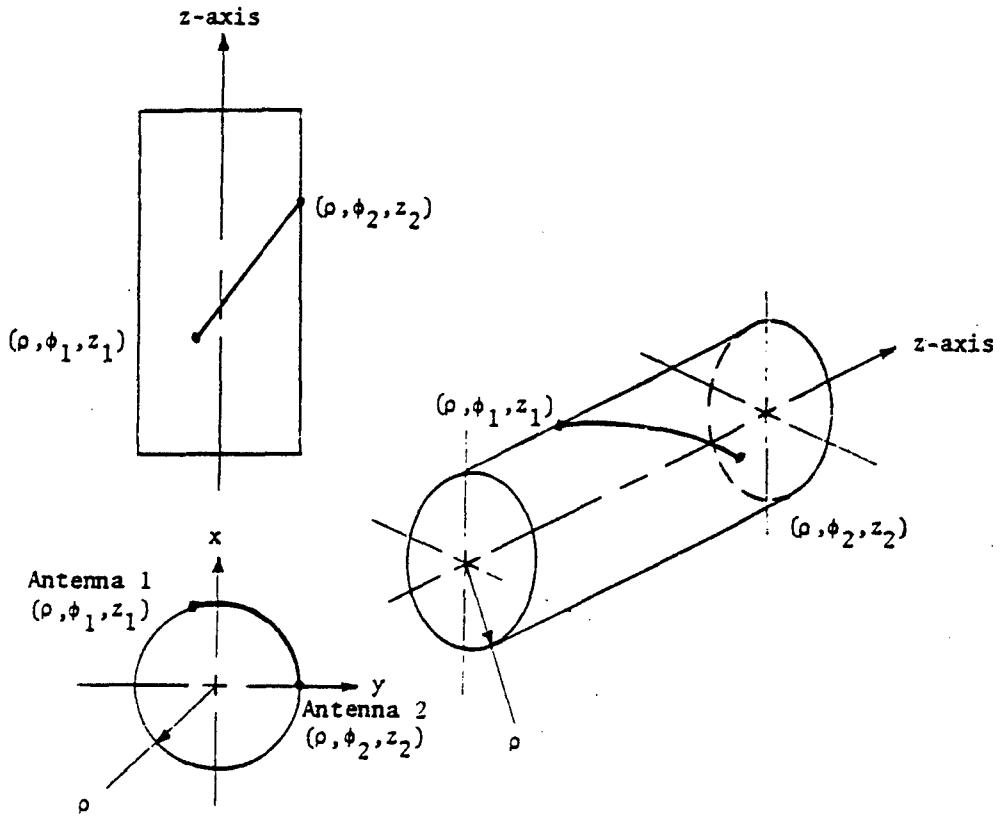

Figure 14-2. Three views of a fuselage modeled as a right circular cylinder with both antennas on the surface.

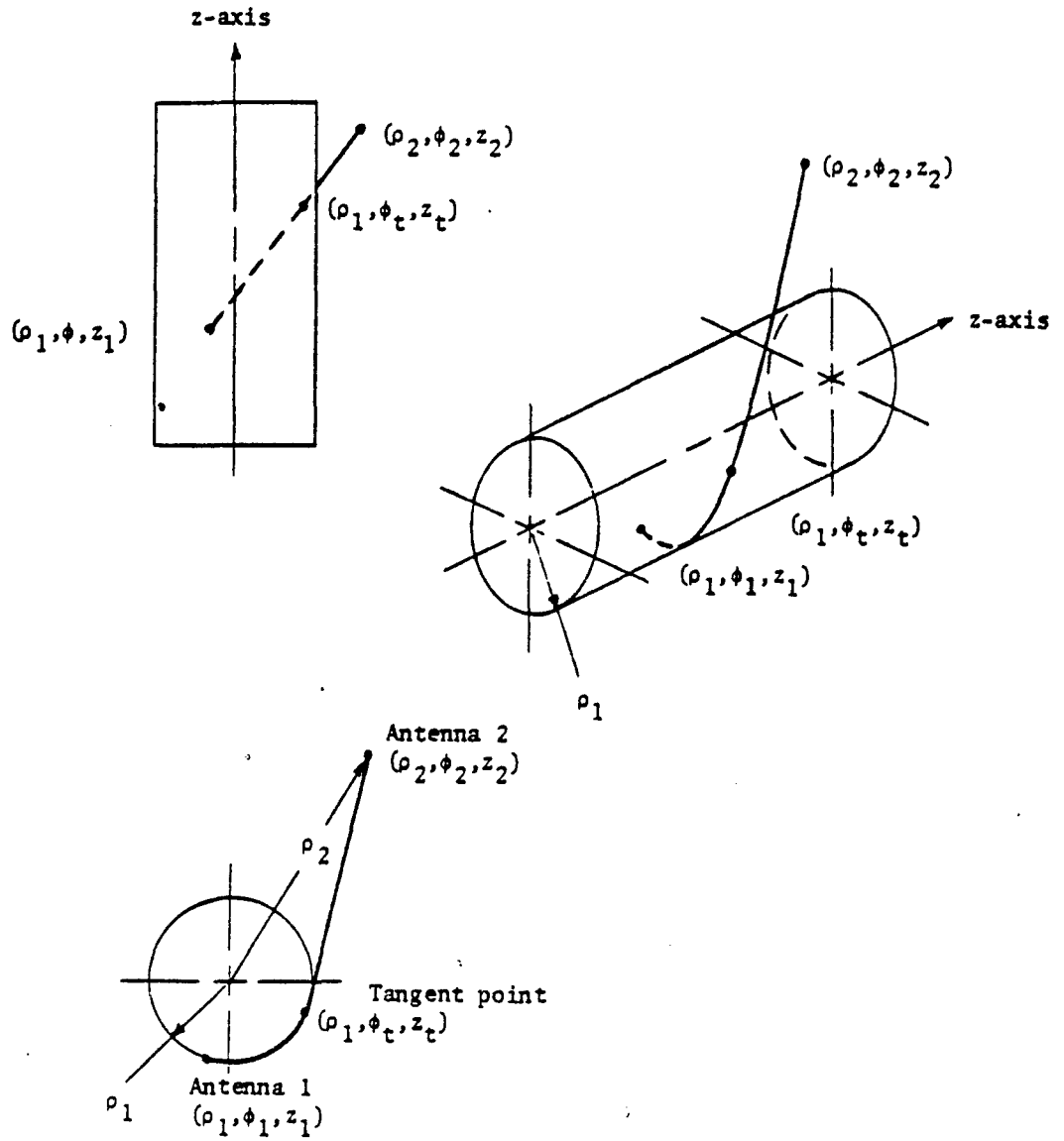

Figure 14-3. Three views of a fuselage modeled as a right circular cylinder with one antenna raised above the surface.

$$\phi_t = \phi_2 \pm \tan^{-1}\left[\frac{\sqrt{\rho_2^2 - \rho_1^2}}{\rho_1}\right] \quad \text{radians} \qquad (14\text{-}6)$$

$$z_t = \frac{\rho_1|\phi_1-\phi_t|z_2 + z_1\sqrt{\rho_2^2 - \rho_1^2}}{\rho_1|\phi_1-\phi_t| + \sqrt{\rho_2^2 - \rho_1^2}} \quad \text{feet} \qquad (14\text{-}7)$$

The appropriate sign in the expression for ϕ_t is that which produces a minimum total distance.

When both antennas are raised above the fuselage, the total path consists of two straight line segments and one cylindrical-spiral segment as shown in Figure 14-4. There are now two tangent points, the coordinates of which are given by

$$\phi_{t1} = \phi_1 \pm \tan^{-1}\left[\frac{\sqrt{\rho_1^2 - \rho_c^2}}{\rho_c}\right] \quad \text{radians} \qquad (14\text{-}8)$$

$$\phi_{t2} = \phi_2 \pm \tan^{-1}\left[\frac{\sqrt{\rho_2^2 - \rho_c^2}}{\rho_c}\right] \quad \text{radians} \qquad (14\text{-}9)$$

$$z_{t1} = \frac{DE-F}{CE-1} \quad \text{feet} \qquad (14\text{-}10)$$

$$z_{t2} = \frac{CF-D}{CE-1} \quad \text{feet} \qquad (14\text{-}11)$$

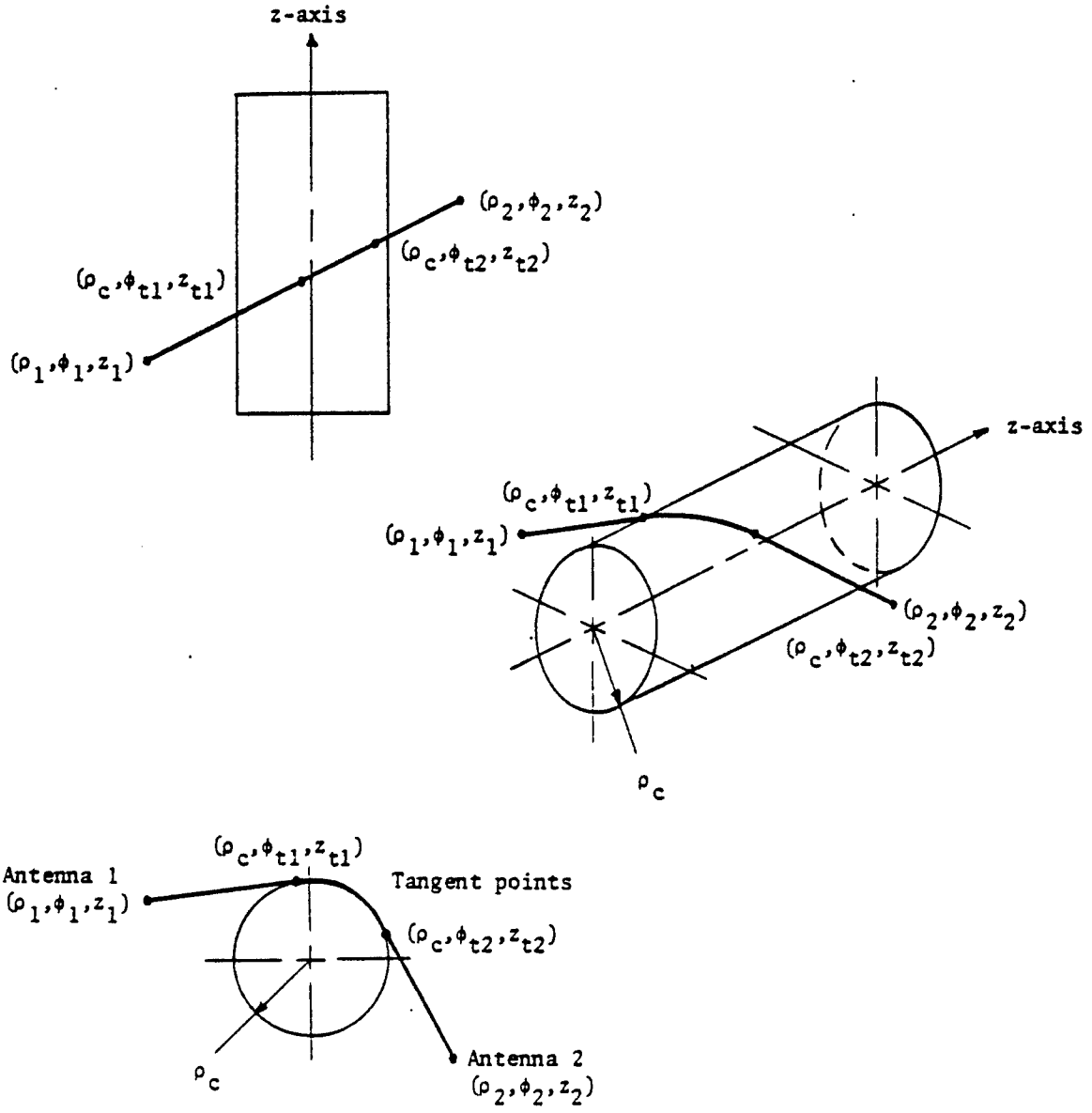

Figure 14-4. Three views of a fuselage modeled as a right circular cylinder with both antennas raised above the surface.

where

$$C = -(A_1 + B)/A_1$$

$$D = -B/A_1$$

$$E = -(A_2 + B)/A_2$$

$$F = -B/A_2$$

$$B = \rho_c|\phi_{t1} - \phi_{t2}|$$

$$A_1 = \sqrt{\rho_1^2 - \rho_c^2}$$

$$A_2 = \sqrt{\rho_2^2 - \rho_c^2}$$

ρ_c = radius of the fuselage (feet)

For these coordinates, the straight line distances and the cylindrical spiral distances are given by Equations 14-5 and 14-3, respectively.

Propagation paths involving more than one cylinder (Figure 14-5) can be handled by computing the curvature factors for each cylinder and summing them with the free-space loss. The total distance used in the free-space formula will include the distance between the curved surfaces. Thus, the total loss is given by

$$L_b = L_{bfs} + \Sigma F(y) \text{ dB} \qquad (14\text{-}12)$$

where

L_{bfs} = free-space loss computed with total path distance

$\Sigma F(y)$ = sum of the curvature factors due to each surface encountered.

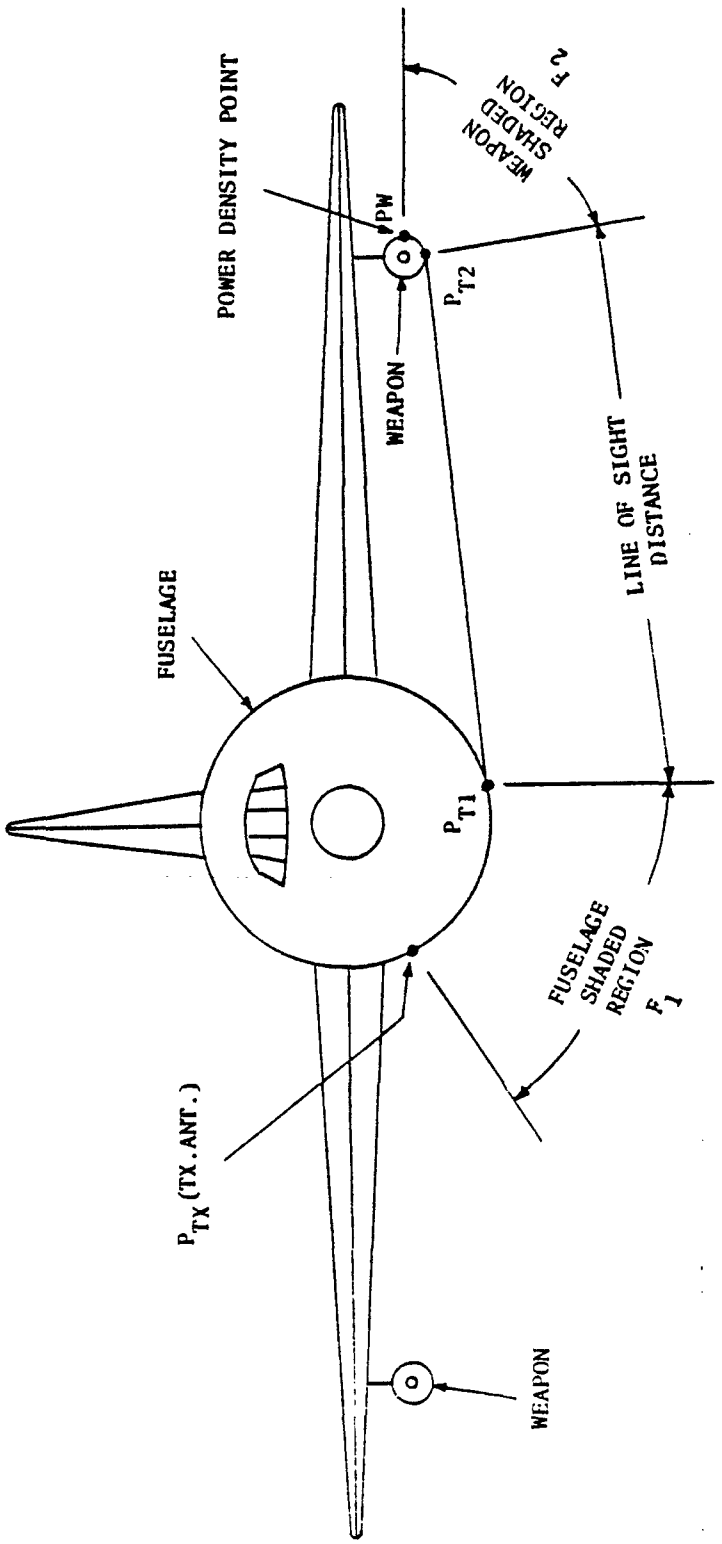

$L_B = L_{bfs} + F_1 + F_2$

L_{bfs} = FREE SPACE LOSS DUE TO (FUSELAGE SHADED DISTANCE + LINE OF SIGHT DISTANCE + WEAPON SHADED DISTANCE)

Figure 14-5. Hypothetical configuration demonstrating shading of the transmission path by both the fuselage and a weapon.

14.2.3 Loss Over a Conical Airframe

Sometimes, a circular cone is more repesentative of an aircraft's fuselage than a cylinder (Figure 14-6). If this is the case, the curved-surface loss may be approximated by using the cylinder formulas except that the radius of the cylinder in the expression for y is replaced with the geometric mean of the maximum and minimum radii of curvature, ρ_1 and ρ_2 (i.e., in Equation 14-4, replace ρ with $\sqrt{\rho_1\rho_2}$). Also the distance d_c becomes the distance between two points on a cone,

$$d_c = \left| \frac{\phi_1 C - \phi_2 D}{2} + \frac{A^2 + B^2}{2A} \ln \left| \frac{A\phi_1 + C}{A\phi_2 + D} \right| \right| \qquad (14\text{-}13)$$

where

$$A = \frac{\rho_2 - \rho_1}{\phi_2 - \phi_1}$$

$$B = \frac{z_2 - z_1}{\phi_2 - \phi_1}$$

$$C = \sqrt{A^2 + B^2 + A^2 \phi_1^2}$$

$$D = \sqrt{A^2 + B^2 + A^2 \phi_1^2}$$

(ρ_1, ϕ_1, z_1) and (ρ_2, ϕ_2, z_2) are the coordinates of the antennas.

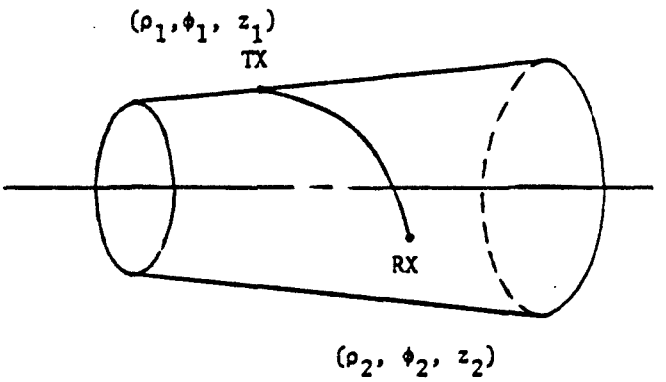

Figure 14-6. Fuselage modeled as a truncated cone with both antennas on the surface.

14.2.4 Knife-Edge Calculations

The knife-edge-diffraction formulations (see Chapter 9 of this handbook) can be used to handle propagation paths with wedge-shaped obstacles such as antennas in the aircraft's bulkhead and wing effects.

14.2.5 Limitations

The above methods are limited in that multipath phenomena are not considered. The cylinder and cone formulations are restricted to bodies with radii of curvature greater than two wavelengths. The distance separation between the antennas must be large enough so that each antenna is in the far field of the other antenna.

14.3 COMPUTER MODELS

Several computer models are currently (FY82) being evaluated to determine their ability to achieve consistently accurate predictions. These include the UNIVAC version of AVPAK[14-1,14-7], the hand-calculator version of AVPAK[14-8], Aircraft Intra-Antenna Propagation with Graphics (AAPG)[14-9], and the General Electromagnetic Model for the Analysis of Complex Systems (GEMACS)[14-10,14-11].

AVPAK and AAPG are computer models for evaluating interference between antennas on a metallic airframe at frequencies above about 50 MHz. For each transmitter receiver pair, AVPAK predicts interference if the on-tune power input to the receiver exceeds its sensitivity threshold. The present version, AVPAK3 (see Reference 14-7), includes an antenna-gain subroutine and data bases containing nominal characteristics of commonly used avionics equipment. Antenna-to-antenna coupling includes free-space loss and losses due to cylindrical curvature, bulkhead diffraction, and wing shading. There is also an option to calculate the power density at any user-specified point on the aircraft.

14-7 Dwyer, Priscilla A., A Model to Predict Mutual Interference on an Airframe, ECAC-PR-76-067, April 1977.

14-8 EMC Analysis Capabilities for Programmable Calculators, ECAC-PD-75-003, 1975.

14-9 Kubina, S.J., Input Formats and Organization for AAPG, Preliminary, EMC Laboratory, TM-7802, Department of Electrical Engineering, Concordia University, Loyola Campus, Montreal Quebec, H4BIR6.

14-10 General Electromagnetic Model for the analysis of Complex Systems, Volume I, User's Manual, RADC-TR-77-137, The BDM Corporation, April 1977.

14-11 General Electromagnetic Model for the Analysis of Complex Systems, Volume II, Engineering Manual, RADC-TR-77-137, The BDM Corporation, April 1977.

AAPG predicts electromagnetic interference (EMI) between a transmitter and receiver if there is frequency coincidence. The EMI margin is determined by

$$EMI = P_R - S_R$$

where P_R is the power received, and S_R is the receiver sensitivity threshold. A positive EMI indicates potential interference. Antenna-to-antenna coupling includes free-space loss, coaxial cable losses, shading due to conical or cylindrical surfaces, and diffraction around wings. There also is a subroutine to calculate antenna gains in the coupling-path direction. AAPG is more user-oriented than AVPAK because it includes a graphics package with an interactive display. These features are extremely useful in an EMC analysis because the antennas can be interactively relocated on the airframe model. Thus, EMI margins for various antenna locations are easily obtained. At present, only AVPAK is ECAC-approved. However, AAPG is being documented for ECAC approval.

GEMACS is available at ECAC to calculate coupling losses on a structure at frequencies between 10 kHz and 40 MHz. GEMACS is a thin-wire code, meaning that the model consists of wire segments connected in a way that approximates the actual structure. GEMACS uses a Method of Moments (MOM) formulation to obtain the current on each wire segment. Linear simultaneous equations arising from the MOM formulation are solved by using the Banded Matrix Interation (BMI) technique. GEMACS is designed for large structures, since the BMI technique requires less computer resources than other solution techniques. However, the BMI technique requires careful modeling and numbering of the wire segments. There is a present ECAC effort to verify the operation of the code.

A detailed discussion of the models recommended will be prepared for insertion in this chapter after completion of the FY-82 Capability Development Task. Coupling over non-metallic and lossy metallic airframes will be investigated in later fiscal years and supplements will be added to this chapter as appropriate.

14.4 VALIDATION

Comparisons between predictions based on the formulas presented in Section 14.2 and measurements are provided in References 14-5, 14-12 and 14-13.

14-12 Friske, Leo, An Extended Avionics Interference Prediction Model, FAA-RD-73-9, ECAC, Annapolis, MD, June 1973.

14-13 Hernandez, A.A., Airframe Antenna Coupling Losses for Obstructed or Unobstructed Paths, ECAC-TN-73-026, revised, 13 May 1974.

APPENDIX A

DERIVATION OF TWO BASIC EQUATIONS FOR L_B

By: M. Weissberger

Section 2 of the Handbook presented a derivation of the basic free-space transmission loss, L_{bfs}. This appendix presents derivations of two equations for the more general quantity, basic transmission loss, L_b. The equations developed are generally only used as building blocks for more complex models that allow state-of-the-art predictions for real problems. They are presented to give engineers some insight as to the basics of the more complex models. The limitations of the equations derived here are cited.

A.1 BASIC TRANSMISSION LOSS (L_b) WHEN THERE IS ATMOSPHERIC ABSORPTION

In this example, assume that in addition to the $1/(4\pi r^2)$ spreading loss there is also absorption by oxygen and water vapor molecules. This additional loss is well modeled by the relationship expressed as: "The decrease in power density, dp_d, of a ray as it flows across a segment of length dr is proportional to the power density flowing into the segment, p_d, the length of the segment, dr, and an absorption coefficient, α." An appropriate equation for this decrease is:

$$dp_d = -\alpha p_d \, dr \qquad \text{(A-1)}$$

$$\frac{dp_d}{p_d} = -\alpha \, dr$$

Integrate both sides:

$$\ln p_d \Big|_{p_d(\text{initial})}^{p_d(\text{final})} = -\alpha \, r \Big|_{r\ (\text{initial})}^{r\ (\text{final})}$$

$$\ln \frac{p_d(\text{final})}{p_d(\text{initial})} = -\alpha \left[r\ (\underline{\text{final}}) - r\ (\underline{\text{initial}}) \right]$$

Let r (final) = r, r (initial) = 0. Then,

$$\ln \frac{p_d(\text{final})}{p_d(\text{initial})} = -\alpha r \qquad \text{(A-2)}$$

Use each side of this equation as an exponent for e:

$$\frac{p_d(\text{final})}{p_d(\text{initial})} = e^{-\alpha r}$$

$$p_d(\text{final}) = p_d(\text{initial})\ e^{-\alpha r} \qquad \text{(A-3)}$$

Thus, there is an exponential decay of the power density, in addition to the $1/(4\pi R^2)$ spreading loss.

Take the $\log_{10}$ of both sides of Equation A-3:

$$p_d(\text{final}) = p_d(\text{initial}) - \alpha r \cdot 10 \log e$$

Note: $\log a^x = x \log a$

or

$$p_d(\text{final}) = p_d(\text{initial}) - \gamma \cdot r \qquad \text{(A-4)}$$

where p_d is the power density in logarithmic units such as dBm/m^2, $\gamma = \alpha \cdot \log e$ is the absorption coefficient in dB/km, and r is the path length in km. (The distance units for γ and r need not be km).

If the power density decreases by this amount, then the power which can be received also decreases by this amount. (From Equation 2-3, received power = power density x effective aperture of the receiving antenna). If the received power decreases by this amount [in addition to the $1/(4\pi R^2)$ spreading loss] then the loss, L_b, (See Equation 2-12) is increased by this amount. Therefore:

$$L_b = L_{bfs} + \gamma \cdot r \qquad \text{(A-5)}$$

where L_{bfs} accounts for the $a/(4\pi R^2)$ spreading, as before.

In general, γ is a function of position. Thus:

$$L_b = L_{bfs} + \int \gamma\,(r)dr \qquad \text{(A-6)}$$

In the earth's atmosphere, oxygen and water vapor each contribute to the absorption at microwave frequencies. Each constituent has its own absorption coefficient. Therefore, L_b is calculated in this fashion:

$$L_b = L_{bfs} + \int \left[\gamma_w(r) + \gamma_o(r)\right] dr \qquad \text{(A-7)}$$

where γ_w is the absorption due to water vapor in dB/km and γ_o is the absorption coefficient due to oxygen in dB/km.

If $\gamma_w(r)$ and $\gamma_o(r)$ are approximately constant,

$$L_b = L_{bfs} + (\gamma_w + \gamma_o) \cdot r \qquad \text{(A-8)}$$

Values for γ_w and γ_o at sea level are shown on the following page (see Figure A-1).

Equation A-8 could be used to estimate the absorption expected on a short line-of-sight link if the antenna were located near sea level. If both antennas were at the same height above sea level, then the equation could be used, but the values of γ should be reduced to account for the less dense atmosphere that exists at this altitude. Approximate formulas[A-1] are: For $0 < h < 12$ km,

$$\gamma_w(h) = \gamma_{wo} \exp(-0.6\ h) \text{ dB/km} \qquad \text{(A-9)}$$

$$\gamma_o(h) = \gamma_{oo} \exp(-b_o h) \text{ dB/km} \qquad \text{(A-10)}$$

with

$$b_o = 0.25\ (-0.5/f_{GHz}) \text{ for } 0.1 \leq f \leq 10 \text{ GHz} \qquad \text{(A-11)}$$

and

$$b_o = 0.25 \quad \text{for } f > 10 \text{ GHz} \qquad \text{(A-12)}$$

[A-1] Rice, P. L., and Herbstreit, J. W., "Tropospheric Propagation", Advances in Electronic and Electron Physics, ed. L. Marton, Academic Press, New York, 1964.

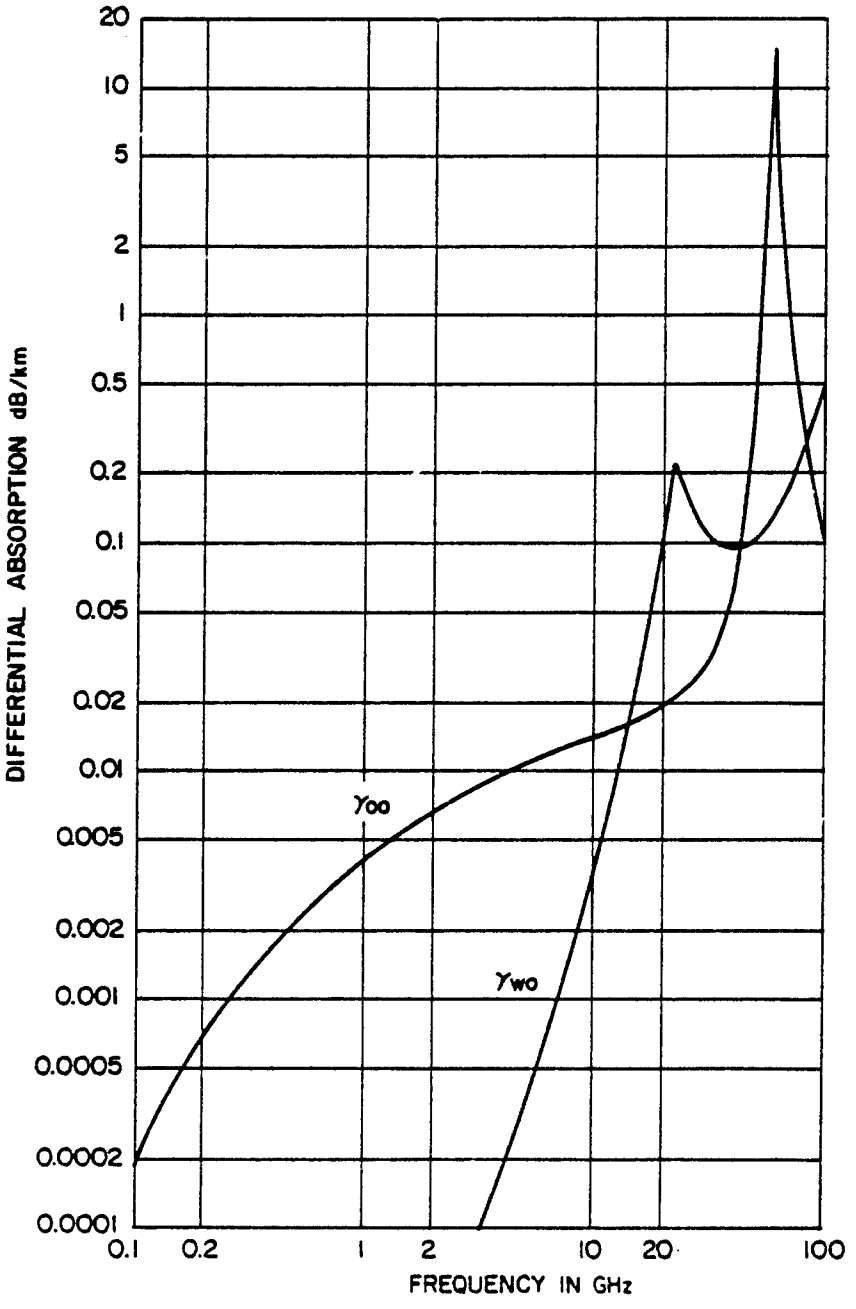

Figure A-1. Estimated values of the sea-level values of γ_w and γ_o. Pressure, 760 mm Hg; temperature, 20° c, water vapor density, 10 gm/m^3. From Reference A-1. Frequency is in GHz.

For $h > 12$ km and $0.1 \leq f \leq 100$ GHz,

$$\gamma_o(h) = \gamma_o(12)\exp(-0.3(h-12)) \text{ dB/km} \qquad \text{(A-13)}$$

The greatest accuracy is achieved using Equation A-7. TIREM executes a form of this integral for terrestrial paths (see Chapter 9 of this handbook). SATPROP does this for earth-space links (Chapter 7), and IF-77 for air-ground links (Chapter 8).

Equation A-6 is also the basis for state-of-the-art calculations of rain-attenuation. Model details are presented in Chapter 7 for earth-space links and in Chapter 10 for terrestrial links. The equation is recommended by some authors for predicting the attenuation due to propagation through foliage. Chapter 11 of this handbook explains the limitations of this procedure.

A.2 BASIC TRANSMISSION LOSS OVER A PLANE EARTH

This sample derivation is included to give engineers an intuitive feel for why increasing antenna height decreases loss -- even for antennas that are within line-of-sight of each other. It also helps explain why loss increases at a rate closer to 40 log D than to 20 log D (as in free-space) when the antennas are near the earth's surface.

The material follows Bullington's writeup.[A-2] Similar information also appears in Jordan and Balmain.[A-3] The equation developed is not suggested as an alternative to the general models presented in Chapters 6, 8 and 9. It

---

[A-2] Bullington, K., "Radio Propagation Fundamentals," Bell System Technical Journal, May 1957, pp. 596-597.

[A-3] Jordan, E. C. and Balmain, K. G., Electromagnetic Waves and Radiating Systems, 2nd Edition, 1968, pp. 653-654.

will produce equivalent results, however, for specific parameter ranges. The mode selection scheme in IPS defines these ranges.[A-4]

Consider the geometry shown in Figure A-2. If the antennas are more than about one wavelength above a normal earth or more than about 10 wave lengths above sea water, and the antennas are well within the line-of-sight of each other, (See References A-3 and A-5), then the total electric field is given by:

$$E_{TOTAL} = E_{DIRECT} + E_{REFLECTED} \qquad \text{(A-14)}$$

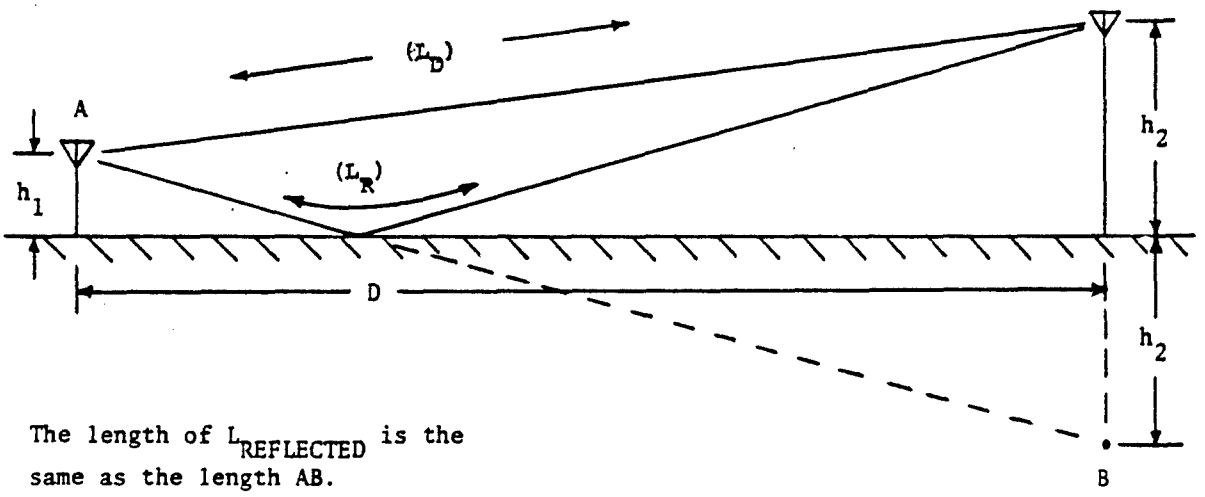

The length of $L_{REFLECTED}$ is the same as the length AB.

Figure A-2. Geometry for the plane-earth loss equation.

A-4 Meidenbauer, R. and Chang, S., A Status Report on the Integrated Propagation System, ECAC-TN-78-025, Electromagnetic Compatibility Analysis Center, Annapolis, MD, November 1978, pp. 9-15.

If the distance between the antennas is much greater than the antenna heights, then the magnitude of the spreading loss of the direct and ground-reflected rays is approximately equal. The difference between the two rays is due to the reflection coefficient (R) and to the difference in phase between the two rays caused by the slightly different path lengths ($\Delta\phi$). Thus:

$$E_{TOTAL} = E_D + E_R = E_D + E_D \cdot R \cdot e^{j\Delta\phi} \qquad \text{(A-15)}$$

Now for grazing incidence over a relatively smooth earth $R \approx -1$.

$$\text{So,} \quad E_{TOTAL} \approx E_D \, (1-e^{j\Delta\phi}) \qquad \text{(A-16)}$$

The phase shift resulting from the difference in path lengths is:

$$\Delta\phi = \frac{2\pi}{\lambda} \, (L_R - L_D) \qquad \text{(A-17)}$$

From the figure it is seen that L_{DIRECT} (L_D) is the hypotenuse of a right triangle with sides D and $(h_2 - h_1)$. So:

$$L_D = \sqrt{D^2 + (h_2 - h_1)^2}$$

$$= \sqrt{D^2 + \left(h_2^2 - 2h_1h_2 + h_1^2\right)} \qquad \text{(A-18)}$$

$$= \sqrt{D^2 \left(1 + \frac{h_2^2 - 2h_1h_2 + h_1^2}{D^2}\right)}$$

Now D >> h_1 or h_2, so the second term is <<1. Since $(1 + X)^{1/2} \approx 1 + 1/2\ X$,

$$L_D \approx D\left(1 + \frac{(h_2^2 - 2h_1 h_2 + h_1^2)}{2D^2}\right) \qquad (A\text{-}19)$$

Now the reflected ray is the hypotenuse of a right triangle with sides D and $(h_1 + h_2)$. Therefore:

$$L_R \approx D\left(1 + \frac{(h_2^2 + 2h_1h_2 + h_1^2)}{2D^2}\right) \qquad (A\text{-}20)$$

Therefore

$$L_R - L_D = D\left(0 + \frac{4h_1h_2}{2D^2}\right) = \left(\frac{2h_1h_2}{D}\right), \qquad (A\text{-}21)$$

and

$$\Delta\phi = \frac{2\pi}{\lambda}(L_R - L_D) = \frac{4\pi\ h_1h_2}{\lambda D} \qquad (A\text{-}22)$$

Insert this into Equation A-16:

$$E_{TOTAL} = E_D\ (1 - e^{j\Delta\phi}) = E_D\left(1 - e^{j\ \frac{4\pi\ h_1h_2}{\lambda D}}\right) \qquad (A\text{-}23)$$

Now,

$$e^X = 1 + X + \frac{X^2}{2!} \ldots \approx 1 + X \text{ for small } x$$

So, for $\Delta\phi < \pi/2$ (see Reference A-2)

$$E_T \approx E_D (1 - 1 - j\Delta\phi) = -j E_D \cdot \frac{4\pi h_1 h_2}{\lambda D} \quad \text{(A-24)}$$

Phase shifts have been considered where they were essential -- in combining the two waves. For further work, they are not needed, so:

$$E_T = E_D \frac{4\pi h_1 h_2}{\lambda D} \quad \text{(A-25)}$$

Since power density, P_D, is proportional to E^2,

$$P_{D,\ TOTAL} = P_{D,\ Direct} \cdot \left(\frac{4\pi h_1 h_2}{\lambda D}\right)^2 \quad \text{(A-26)}$$

The received power is the effective aperture times the power density. So reducing the power density by $\left(\frac{4\pi h_1 h_2}{\lambda D}\right)^2$ will reduce the received power by this amount. From Equation 2-3,

$$\text{Power Received from the Direct ray} = P_t \left(\frac{\lambda}{4\pi L_D}\right)^2 \quad \text{(A-27)}$$

The total received power, P_r, is:

$$P_r = P_t \left(\frac{\lambda}{4\pi L_D}\right)^2 \cdot \left(\frac{4\pi h_1 h_2}{\lambda D}\right)^2 \quad \text{(A-28)}$$

Now, for h_1, $h_2 << D$, $L_D = D$,

so

$$P_r = P_t \left(\frac{h_1 h_2}{D^2}\right)^2 \qquad \text{(A-29)}$$

Basic transmission loss is:

$$L_b = \frac{P_t}{P_r} = \left(\frac{D^2}{h_1 h_2}\right)^2 \qquad \text{(A-30)}$$

(Note that the equation, as written, is only true for lossless isotropic antennas).

In dB, with h_1 and h_2 in feet and D in miles,

$$L_B = 40 \log D - 20 \log h_1 - 20 \log h_2 + 148.91 \qquad \text{(A-31a)}$$

With h_1 and h_2 in meters and D in km,

$$L_B = 40 \log D - 20 \log h_1 - 20 \log h_2 + 120.00 \qquad \text{(A-31b)}$$

One example of a problem for which the equation yields accurate predictions was reported by Hopner and Cushing.[A-5] This was a line-of-sight over-water link at 243 and 455 MHz between Vancouver Island and the mainland city of Vancouver. Measurements on the 84 km path demonstrated that:

A-5 Hopner, E. and Cushing, T. D., "Comparative Propagation Studies on 250 and 450 Megacycles," Record of the AIEE Summer and Pacific General Meeting, Los Angeles, CA, June 21-25, 1954.

a) The measured losses were greater than free-space by amounts predicted by Equation A-31. (The Equation overpredicted the measured loss by 1 dB at 455 MHz; it underpredicted the loss by 1 dB at 243 MHz.)

b) Even though the free-space loss at 243 MHz is 5.5 dB lower than the free-space loss at 455 MHz, the measured losses were within 2 dB of each other. (The predicted difference is 0 dB).

One measured result that is not predicted by Equation A-31 was the existence of substantial time variability of the signals. The 243 MHz signal fluctuated over a 29 dB range and the 455 MHz signal varied 35 dB in intensity. The comparison cited above was between the most probable measured values and the predicted values. Reasons for the time variability of signals on line-of-sight paths are discussed in Chapter 10 of the text.

Egli[A-6] developed an equation which was based on Equation A-31 but included empirical terms to account for deviations measured in the 40-900 MHz band and paths over rough terrain.

Adams[A-7] demonstrated a means for applying the basic two-ray model to problems in which the terrain is not smooth. The method presumes that the analyst has detailed information about the topographic profile between the transmitter and receiver. The procedure was shown to be accurate in the 30-900 MHz range.

[A-6] Egli, J. J., "Radio Propagation Above 40 MC Over Irregular Terrain," Proc. IRE, October 1957.

[A-7] Adams, B. W. P., "An Empirical Routine for Estimating Reflection Loss in Military Radio Paths in the VHF and UHF Bands," IEE Conference Publication 169, IEE, London, England, 1978.

Hufford[A-8] observed that Equation A-31b had to be modified by using Bullington's effective antenna height in order to provide a reasonable estimate of the mean loss measured on circuits between two low (1-9 m) antennas along 5-80 km paths in the Colorado Plains and Northeastern Ohio. The frequencies ranged from 20 to 100 MHz. The effective antenna heights are computational devices for taking into account the surface wave - a component which exists for low antennas. See the heading "Modified Plane Earth" in Chapter 9.2.1 for more information on this subject.

A-8 Hufford, G. A., and Montgomery, J. L., On the Statistics of VHF Field Strength Measurements Using Low Antenna Heights - I, NBS Report 9223, ITSA, Boulder, CO, May 1966.

APPENDIX B

A DETAILED FLOW DIAGRAM OF TIREM

By: R. Meidenbauer

This appendix contains a flow diagram of the Terrain Integrated Rough Earth Model (TIREM). The text describing this model appears in Chapter 9.

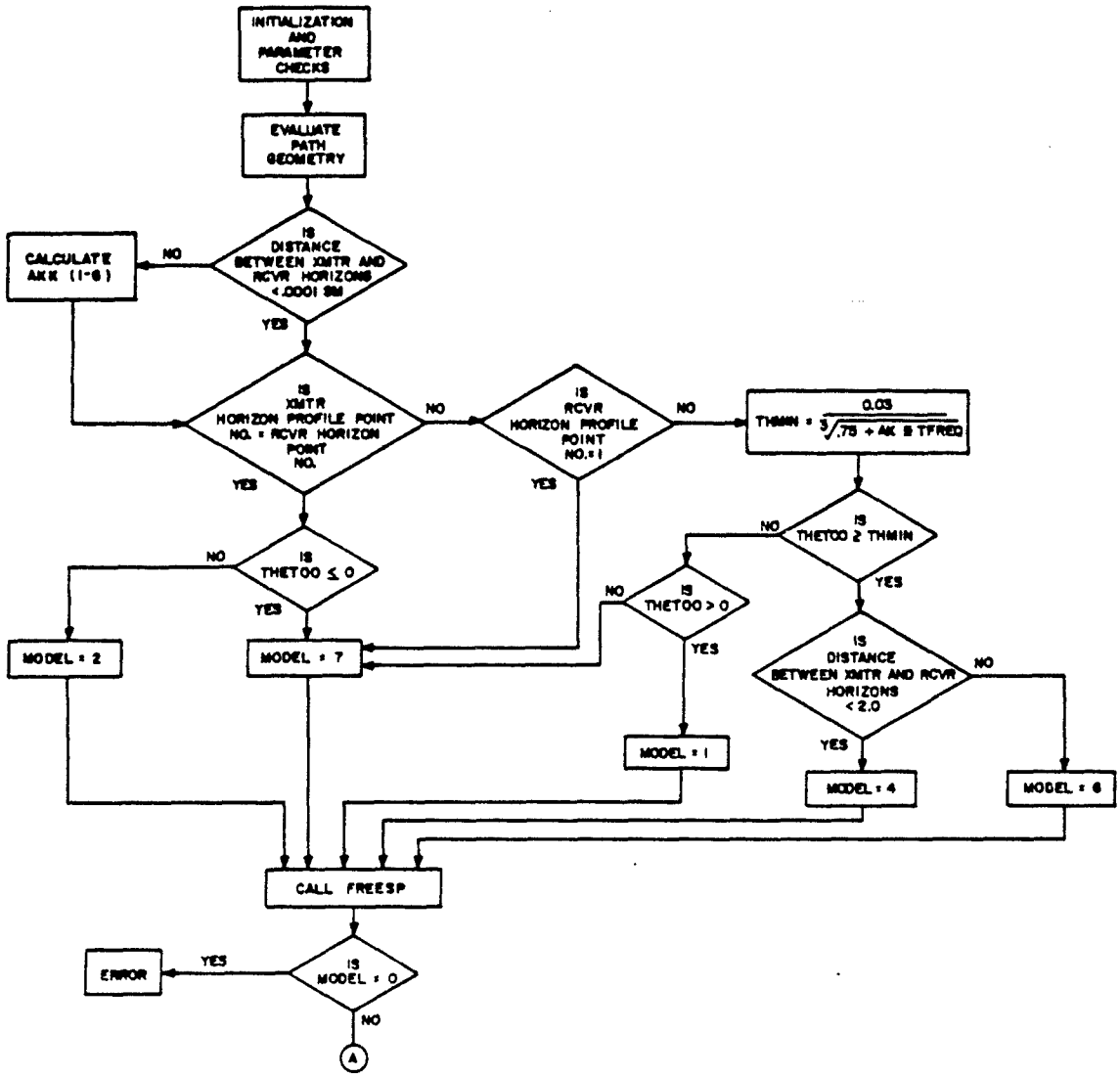
INITIALIZATION AND PARAMETER CHECKS
EVALUATE PATH GEOMETRY
IS DISTANCE BETWEEN XMTR AND RCVR HORIZONS < .0001 SM
NO
CALCULATE AKK (1-6)
YES
IS XMTR HORIZON PROFILE POINT NO. = RCVR HORIZON POINT NO.
NO
IS RCVR HORIZON PROFILE POINT NO.=1
NO
THMIN = 0.03 / ∛(.75 + AK * TFREQ)
YES
YES
IS THETOO ≤ 0
NO
YES
MODEL = 2
MODEL = 7
IS THETOO > 0
NO
YES
MODEL = 1
IS THETOO ≥ THMIN
NO
YES
IS DISTANCE BETWEEN XMTR AND RCVR HORIZONS < 2.0
NO
YES
MODEL = 4
MODEL = 6
CALL FREESP
IS MODEL = 0
YES
ERROR
NO
A

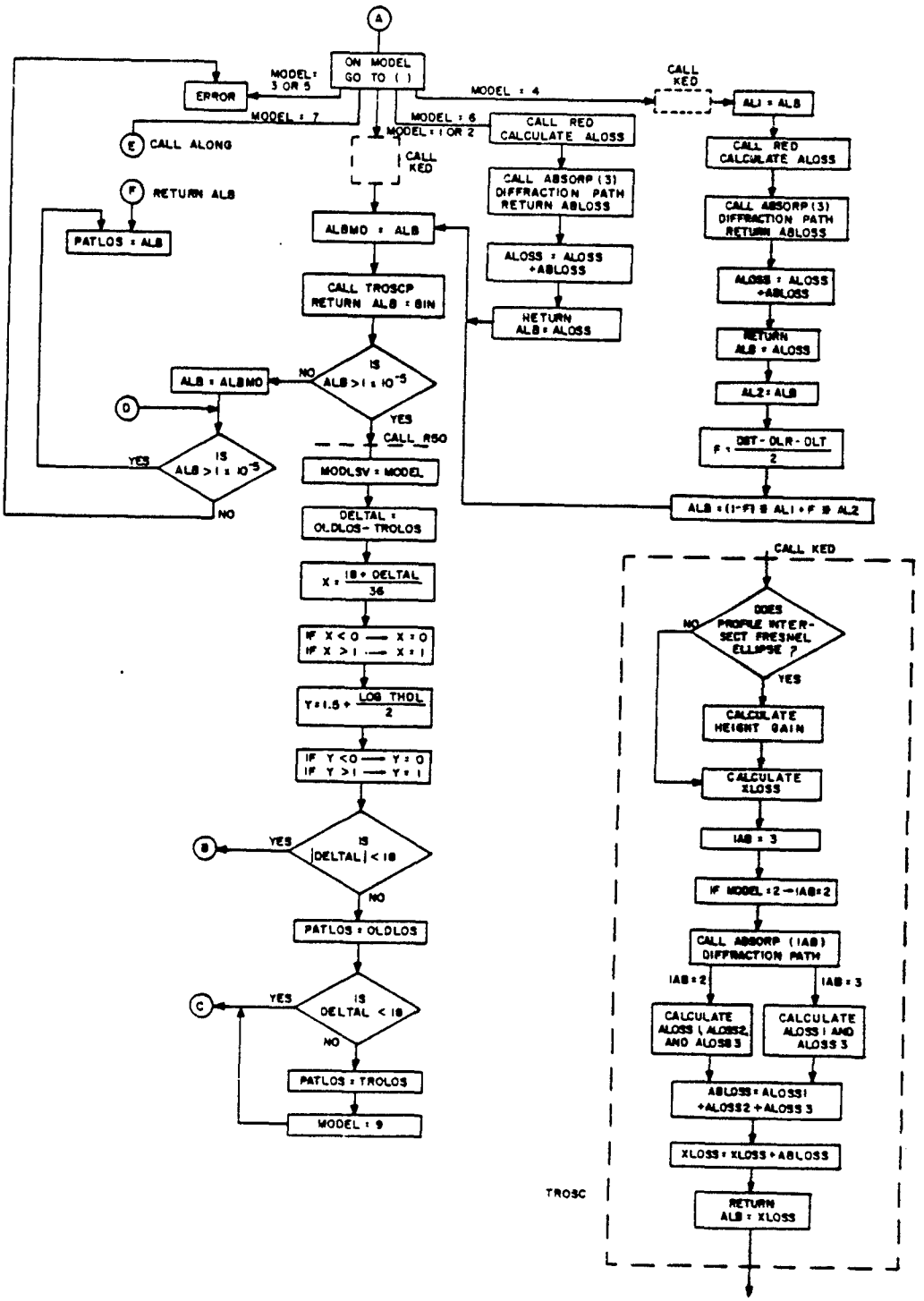
A
ON MODEL GO TO ( )
MODEL = 3 OR 5
ERROR
MODEL = 7
E CALL ALONG
F RETURN ALB
PATLOS = ALB
MODEL = 4
CALL KED
ALI = ALB
CALL RED CALCULATE ALOSS
CALL ABSORP (3) DIFFRACTION PATH RETURN ABLOSS
ALOSS = ALOSS +ABLOSS
RETURN ALB = ALOSS
AL2 = ALB
F = DBT - OLR - OLT / 2
ALB = (1-F) @ ALI + F @ AL2
MODEL = 6
CALL RED CALCULATE ALOSS
CALL ABSORP (3) DIFFRACTION PATH RETURN ABLOSS
ALOSS = ALOSS +ABLOSS
RETURN ALB = ALOSS
MODEL = 1 OR 2
CALL KED
ALBMO = ALB
CALL TROSCP RETURN ALB = SIN
IS ALB > 1 - 10^-5
NO
ALB = ALBMO
D
IS ALB > 1 - 10^-5
YES
NO
YES
CALL RSO
MODLSV = MODEL
DELTAL = OLDLOS - TROLOS
X = 18 + DELTAL / 36
IF X < 0 — X = 0
IF X > 1 — X = 1
Y = 1.5 + LOG THDL / 2
IF Y < 0 — Y = 0
IF Y > 1 — Y = 1
IS |DELTAL| < 18
YES
B
NO
PATLOS = OLDLOS
IS DELTAL < 18
YES
C
NO
PATLOS = TROLOS
MODEL = 9
CALL KED
DOES PROFILE INTER-SECT FRESNEL ELLIPSE ?
NO
YES
CALCULATE HEIGHT GAIN
CALCULATE XLOSS
IAB = 3
IF MODEL = 2 — IAB = 2
CALL ABSORP (IAB) DIFFRACTION PATH
IAB = 2
IAB = 3
CALCULATE ALOSS 1, ALOSS 2, AND ALOSS 3
CALCULATE ALOSS 1 AND ALOSS 3
ABLOSS = ALOSS1 +ALOSS2 + ALOSS 3
XLOSS = XLOSS + ABLOSS
RETURN ALB = XLOSS
TROSC

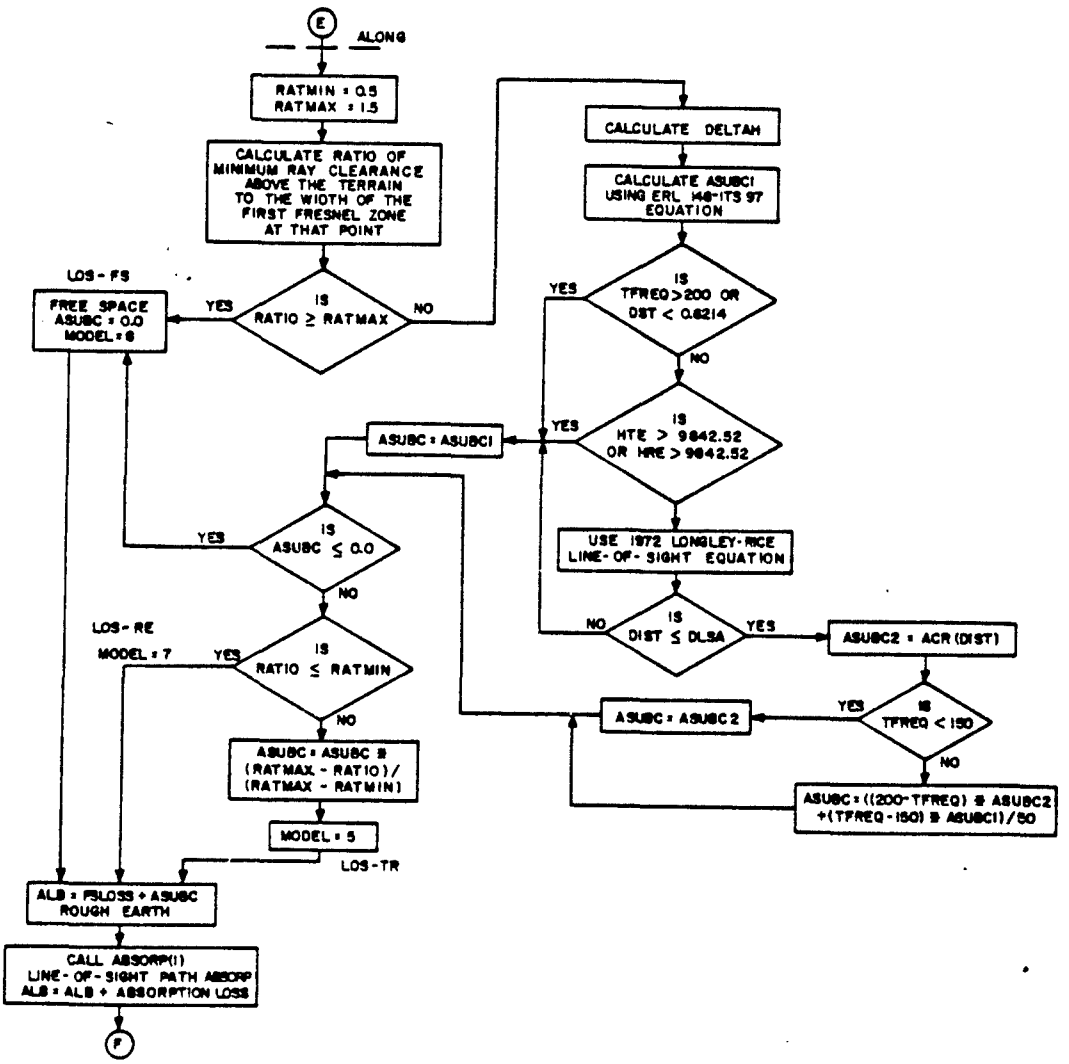
E
ALONG
RATMIN = 0.5
RATMAX = 1.5
CALCULATE RATIO OF MINIMUM RAY CLEARANCE ABOVE THE TERRAIN TO THE WIDTH OF THE FIRST FRESNEL ZONE AT THAT POINT
LOS-FS
FREE SPACE ASUBC = 0.0 MODEL = 6
IS RATIO ≥ RATMAX
YES
NO
CALCULATE DELTAH
CALCULATE ASUBC1 USING ERL 146-ITS 97 EQUATION
IS TFREQ>200 OR DST < 0.6214
YES
NO
IS HTE > 9642.52 OR HRE > 9642.52
YES
ASUBC = ASUBC1
USE 1972 LONGLEY-RICE LINE-OF-SIGHT EQUATION
IS DIST ≤ DLSA
NO
YES
ASUBC2 = ACR(DIST)
IS TFREQ < 150
YES
NO
ASUBC = ASUBC2
ASUBC = ((200-TFREQ) * ASUBC2 +(TFREQ-150) * ASUBC1)/50
IS ASUBC ≤ 0.0
YES
NO
LOS-RE
MODEL = 7
IS RATIO ≤ RATMIN
YES
NO
ASUBC = ASUBC * (RATMAX - RATIO)/ (RATMAX - RATMIN)
MODEL = 5
LOS-TR
ALS = FSLOSS + ASUBC ROUGH EARTH
CALL ABSORP(1) LINE-OF-SIGHT PATH ABSORP ALS = ALS + ABSORPTION LOSS
F

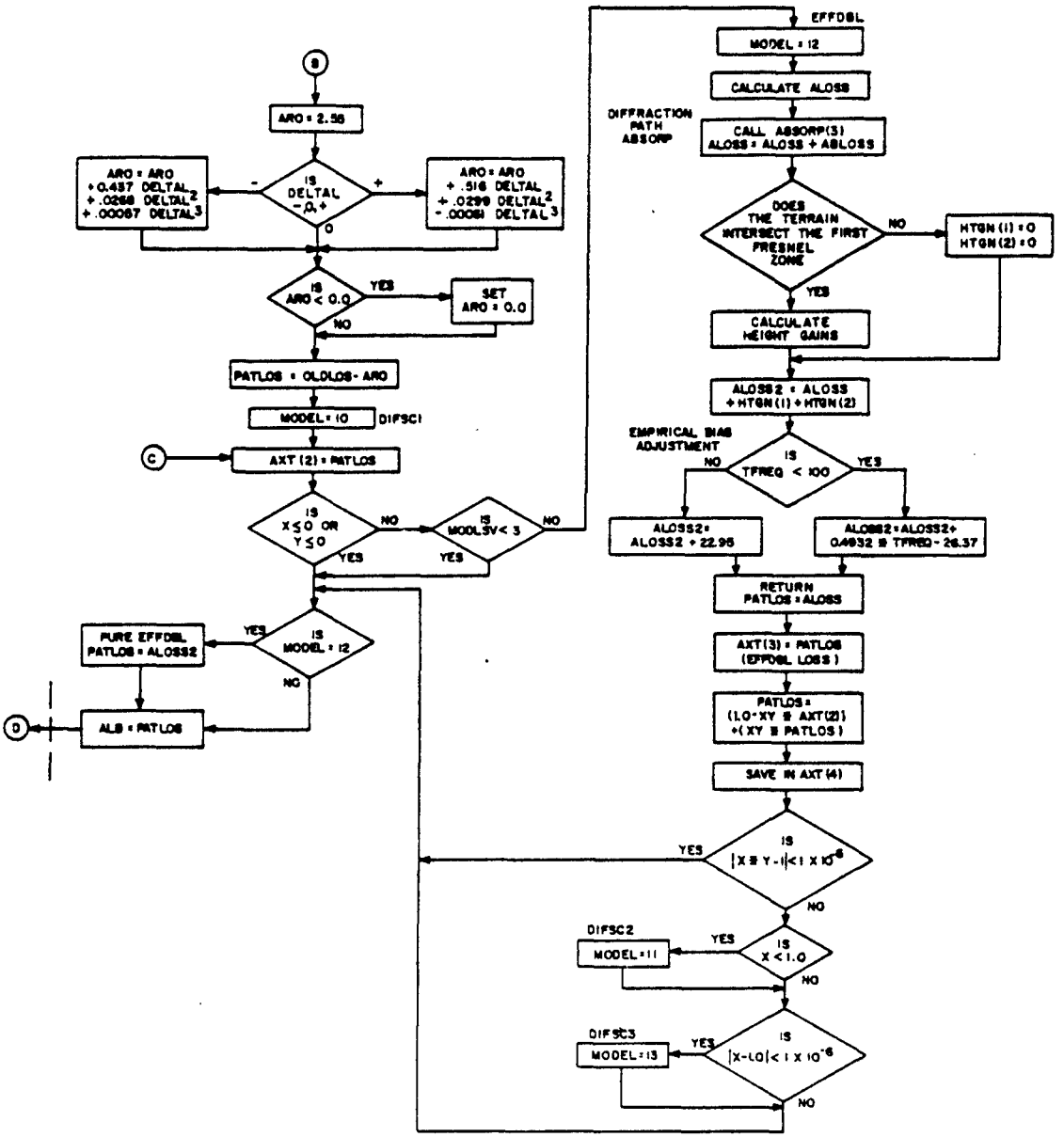
B
ARO = 2.56
IS DELTAL -,0,+
ARO = ARO + 0.487 DELTAL + .0268 DELTAL² + .00067 DELTAL³
ARO = ARO + .516 DELTAL + .0299 DELTAL² - .0008 DELTAL³
IS ARO < 0.0
SET ARO = 0.0
PATLOS = OLDLOS - ARO
MODEL = 10
DIFSC1
C
AXT(2) = PATLOS
IS X≤0 OR Y≤0
IS MODL3V < 3
IS MODEL = 12
PURE EFFDBL PATLOS = ALOSS2
D
ALS = PATLOS
EFFDBL
MODEL = 12
CALCULATE ALOSS
DIFFRACTION PATH ABSORP
CALL ABSORP(3) ALOSS = ALOSS + ABLOSS
DOES THE TERRAIN INTERSECT THE FIRST FRESNEL ZONE
HTGN(1) = 0 HTGN(2) = 0
CALCULATE HEIGHT GAINS
ALOSS2 = ALOSS + HTGN(1) + HTGN(2)
EMPIRICAL BIAS ADJUSTMENT
IS TFREQ < 100
ALOSS2 = ALOSS2 + 22.96
ALOSS2 = ALOSS2 + 0.4932 * TFREQ - 26.37
RETURN PATLOS = ALOSS
AXT(3) = PATLOS (EFFDBL LOSS)
PATLOS = (1.0-XY * AXT(2)) + (XY * PATLOS)
SAVE IN AXT(4)
IS |X * Y-1| < 1 X 10⁻⁶
DIFSC2
MODEL = 11
IS X < 1.0
DIFSC3
MODEL = 13
IS |X-LO| < 1 X 10⁻⁶
YES
NO

APPENDIX C
DETERMINING STATISTICAL TOLERANCE LIMITS FOR A PROPAGATION MODEL - AN EXAMPLE

By: M. Weissberger

INTRODUCTION

The objective of this appendix is to document a procedure for adjusting basic-transmission-loss predictions made using the Integrated Propagation System (IPS) so that observed differences between these predictions and measured data are taken into account. EMC engineers can apply this procedure as a means of increasing the reliability of predictions made using analysis models that include IPS as a subroutine. TENIAS, FDRCAL, and MODEL-B are three models of this type.

The next section discusses the comparison between measured loss values and IPS predictions. The following paragraphs show how a probability distribution of prediction errors may be developed from this comparison. This is followed by an explanation of how to use this distribution to compute the adjustment to the IPS prediction that is needed to produce a given amount of reliability. An example is presented and limitations of the procedure are discussed.

COMPARISONS BETWEEN MEASURED BASIC-TRANSMISSION LOSS VALUES AND IPS PREDICTIONS

Meidenbauer, et al.[C-1] presented the results of a comparison between 5015 measurements and corresponding IPS predictions. These results are

---

[C-1] Meidenbauer, R., Chang, S., and Duncan, M., A Status Report on the Integrated Propagation System, ECAC-TN-78-023, Electromagnetic Compatibility Analysis Center, September 1978, p. 106.

summarized in TABLE C-1. They are similar to the data reported earlier by Lustgarten and Madison.[C-2]

The "prediction error" was determined for each path. This is defined as the predicted loss minus the measured loss, all three quantities in dB. The mean and standard deviation of the prediction errors was computed for each of the 23 groups of paths. These are included in TABLE C-1.

It is to be noted that the measured loss values included in the study were all taken over relatively short time periods -- typically less than 10 minutes.[C-3,C-4] Thus, any particular "error" includes the difference between the long-term median signal level and the signal level which existed when the measurement was made. Thus the distribution of error statistics can be considered to include the distribution of the signal strengths with time. Therefore, no further adjustments need to be made for this factor. It is assumed here that the different measurement programs considered in this study took place over a period of time long enough so that the individual path measurements represent a reasonable sample of different parts of the time-variability distribution.

The two groups of Colorado-Mountains measurements were not used in the remainder of this study. This is because IPS was not designed for use over

---

C-2 Lustgarten, M.N., and Madison, J.A., "An Empirical Propagation Model (EPM-73)", IEEE Transactions on EMC, August 1977.

C-3 Johnson, M.E., et. al., Tabulations of VHF Propagation Data Obtained Over Irregular Terrain at 20, 50, and 100 MHz, ESSA Technical Report IER 38 - ITSA 38, May 1967, p. 10.

C-4 McQuate, P.L., et. al., Tabulations of Propagation Data Over Irregular Terrain in the 230 to 9200 MHz Range, Part I: Gunbarrel Hill Receiver Site, ESSA Technical Report ERL 65-ITS 58, March 1968, p. 21.

TABLE C-1

IPS PREDICTION ERROR

(From Reference C-1)

Freq (MHz)	Location	Number of Paths	Mean Error (dB)	σ of Error (db)
20.1	Colorado Plains	393	-5.1	6.0
49.7	Colorado Plains	393	-0.6	8.3
101.5	Colorado Plains	447	5.9	9.8
101.5	Colorado Plains	444	5.7	10.1
101.5	Colorado Plains	447	8.1	9.3
101.5	Colorado Plains	444	7.3	11.9
101.5	Colorado Mountains	137	-10.4	11.5
101.5	Colorado Mountains	137	-13.4	11.6
101.8	Northeast Ohio	67	13.5	12.2
101.8	Northeast Ohio	70	7.1	10.5
101.8	Northeast Ohio	70	7.5	11.2
910	Colorado Plains	105	3.8	12.8
910	Colorado Plains	104	3.3	12.2
910	Colorado Plains	148	0.5	13.3
1846	Colorado Plains	115	-2.1	15.8
1846	Colorado Plains	129	-3.6	17.0
1846	Colorado Plains	129	-5.4	15.6
4595	Colorado Plains	178	-2.0	21.2
4595	Colorado Plains	206	-6.4	20.7
4595	Colorado Plains	179	-7.2	20.6
9190	Colorado Plains	213	-1.9	25.3
9190	Colorado Plains	227	-5.1	25.7
9190	Colorado Plains	233	-7.1	23.2

Error = Predicted loss (dB) - Measured loss (dB).

such irregular terrain and because the two groups did not represent a large enough sample of data from which to draw meaningful conclusions about IPS prediction accuracy for rough-earth paths.

There were 4741 measurements in the remaining 21 groups that were used in the study.

The Distribution of the Prediction Errors

Each of the 21 groups of prediction errors has its own mean and standard deviation. Typically, these two parameters for one group differ from those of the other groups. The question of how to select a typical value for each parameter now arises.

A straightforward approach would be to analytically determine a single mean and standard deviation that would characterize all 4741 measurements. It is more informative, however, to examine the variation of these parameters from group to group.

There is a strong linear correlation ($\rho^2 = .88$) between the standard deviation of a group and the frequency at which the measurements in the group were made. The correlation between σ and the logarithm of frequency is even greater ($\rho^2 = .89$). It is therefore reasonable to model the standard deviation as a linear function of log f. Greater accuracy in describing the standard deviation can be obtained by using separate linear relationships for each of three frequency bands. Regression yields these formulas:

$$\sigma_1 = 6.784 \log_{10} f - 3.078 \quad (f < 101.8) \tag{1a}$$

$$\sigma_1 = 2.157 \log_{10} f + 6.384 \quad (101.8 \leq f \leq 910.0) \tag{1b}$$

$$\sigma_1 = 11.910 \log_{10} f - 22.624 \quad (f > 910.0) \tag{1c}$$

where σ_1 is the standard deviation of the prediction error in dB and f is the frequency in MHz. The data and the curve fits are shown in Figure C-1.

The variation of the mean prediction error of each group with the measurement frequency was also investigated. The following observations can be made:

1. The linear correlation between the two parameters is low: $\rho^2 = 0.40$.
2. The linear correlation between the mean and the log of frequency is also low: $\rho^2 = 0.43$.
3. The scattergram of the points (Figure C-2) yields no signs that other functions could be used to categorize a relationship between the mean error and frequency.
4. There is no apparent physical reason to expect a dependent relationship.

Because of these reasons, it was decided to model the mean error as being independent of frequency.

It is now assumed that the 21 means are normally distributed with an estimated mean and standard deviation of 0.77 and 6.07 dB. A Chi-square goodness-of-fit test was done to verify that this assumption is satisfactory. The procedure described in Reference C-5 was used. The data was categorized into four groups. χ^2 was 3.19 for the data. This implies that the assumption of a normal distribution is valid at the .05 level of significance. Use of the Chernoff and Lehman approach described in Reference C-6 leads to even greater confidence in the validity of the assumption.

C-5 Alder, H.L., and Roessler, E.B., Introduction to Probability and Statistics, W. H. Freeman and Company, San Francisco, CA, 1972, Section 13.5.

C-6 Blum, J.R. and Rosenblatt, J., Probability and Statistics, W.B. Saunders, Toronto, 1972, Section 12.2.3.

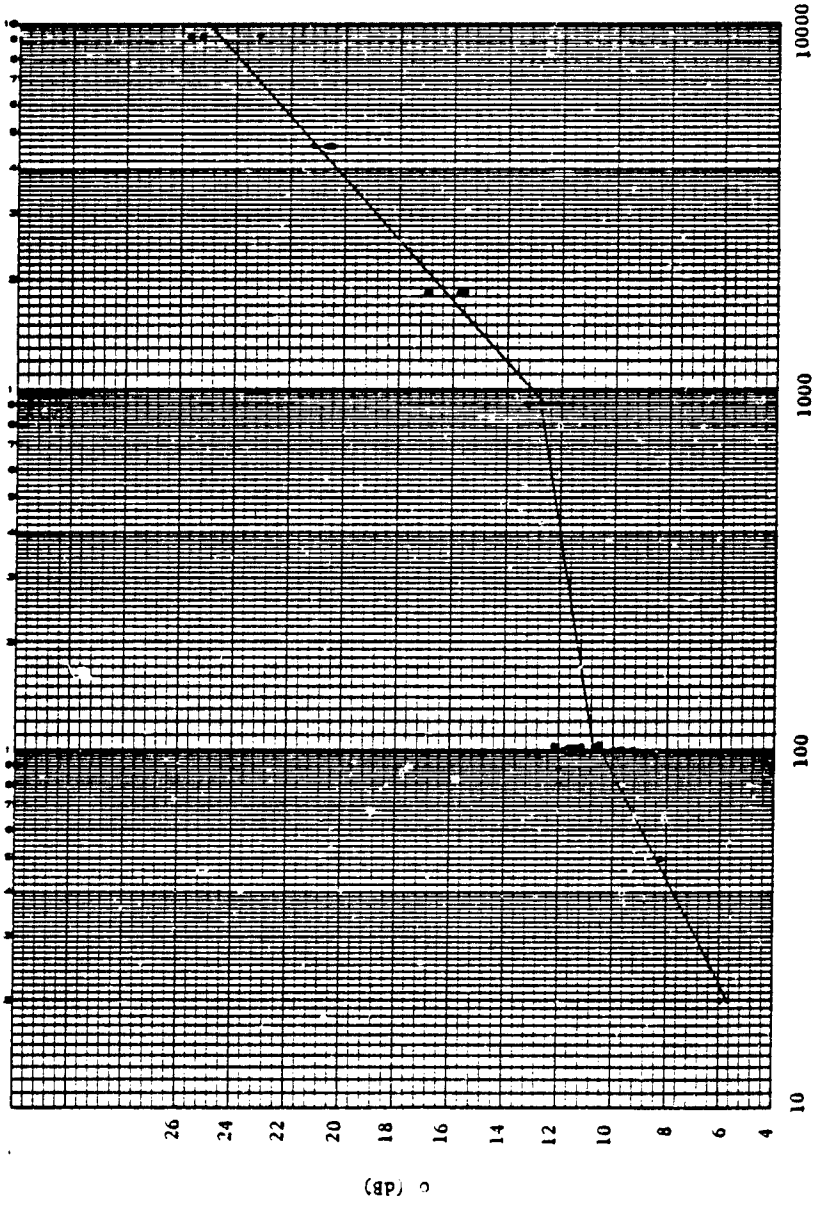

Figure C-1. The standard deviation of the prediction error vs. frequency for the 23 groups of measurements. The two groups from the Colorado Mountains are the 11.5 and 11.6 dB points at 100 MHz. ρ^2, excluding the mountain data is 0.89. The straight lines represent the regression fit given by Equations 1a, 1b, and 1c.

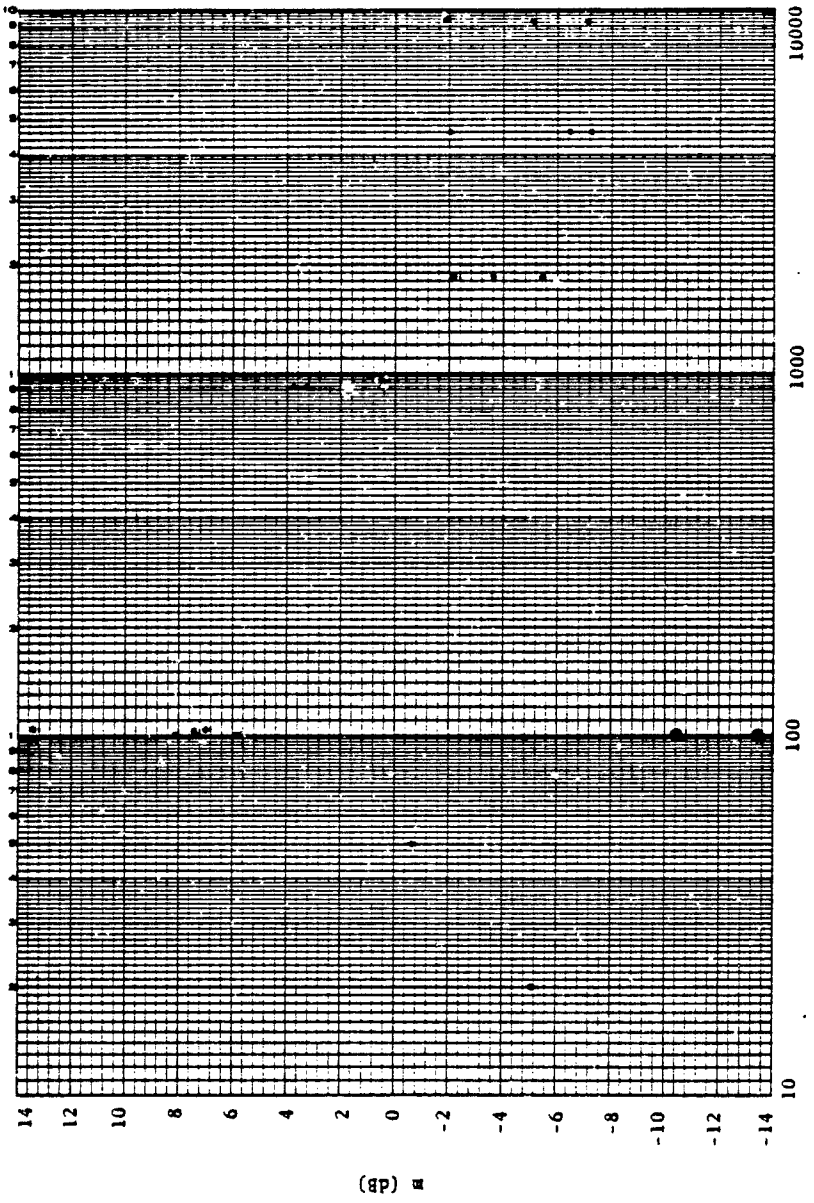

Figure C-2. Mean prediction error vs. frequency for the 23 groups of measurements. The two groups from the Colorado Mountains are circled. The value of ρ^2, excluding the mountain data, is 0.43. In the procedure outlined in this appendix, m and f are assumed to be independent.

Figure C-3 is a graphical comparison between the measured distribution and a normal distribution with the same mean and σ.

The distribution of the prediction errors in each group about the mean error of the group is now assumed normal. Chi-square testing of two arbitrarily selected groups (Ohio, 101.8 MHz, 10'-10' and Colorado Plains, 910 MHz, 24' - 39') indicates that this is a reasonable assumption at the .05 level of significance. (For Ohio, χ^2 = 3.37 for 4 groups of data, and for the Colorado Plains, χ^2 = 21.7 for 16 groups of data.) Figures C-4 and C-5 are graphical comparisons between the measured and normal distributions.

The relationship between the mean of a group and the standard deviation of the group was investigated. These observations can be made:

1. The linear correlation between the two parameters is low: ρ^2 = 0.37.
2. The scattergram of the points (Figure C-6) yields no signs that other functions could be used to categorize a relationship between the mean error and the standard deviation.
3. There is no apparent physical reason to expect a dependent relationship.

Because of these reasons it was decided to model the standard deviation as being independent of the mean error.

The type of information that is needed about the prediction errors is the probability of a given error being greater than X dB. This probability is the probability that the sum of the mean error plus the deviation from this mean is greater than X dB. Since the distribution of the mean errors and the distribution of errors about the mean have been found to be normal and the two distributions have been found to be approximately independent, then the desired probability can be calculated from the probability that a single normal distribution exceeds X dB. This single distribution has a mean of 0.77 dB and a standard deviation of:

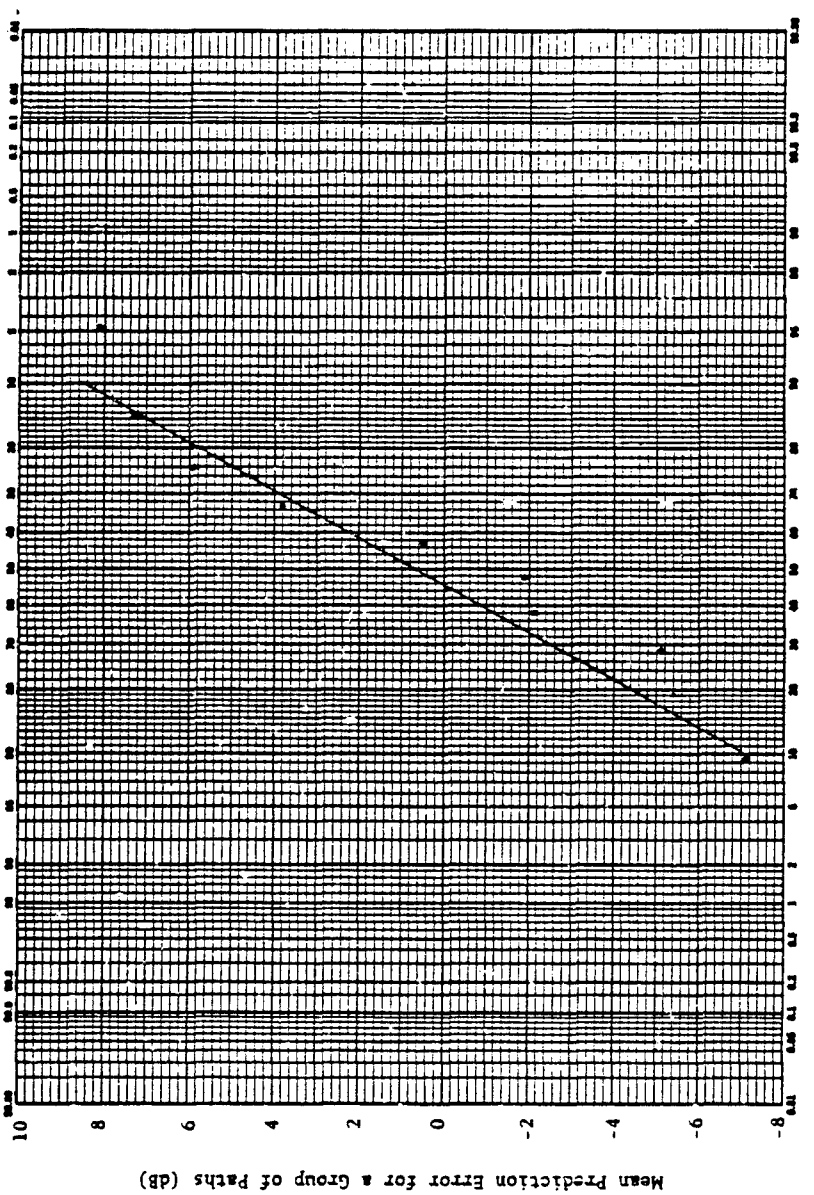

Figure C-3. Distribution of the mean prediction error for the 21 groups of data. The solid line is the theoretical normal distribution having the same mean and σ. In addition to this graph, Chi-square testing supports the assumption that the distribution is normal.

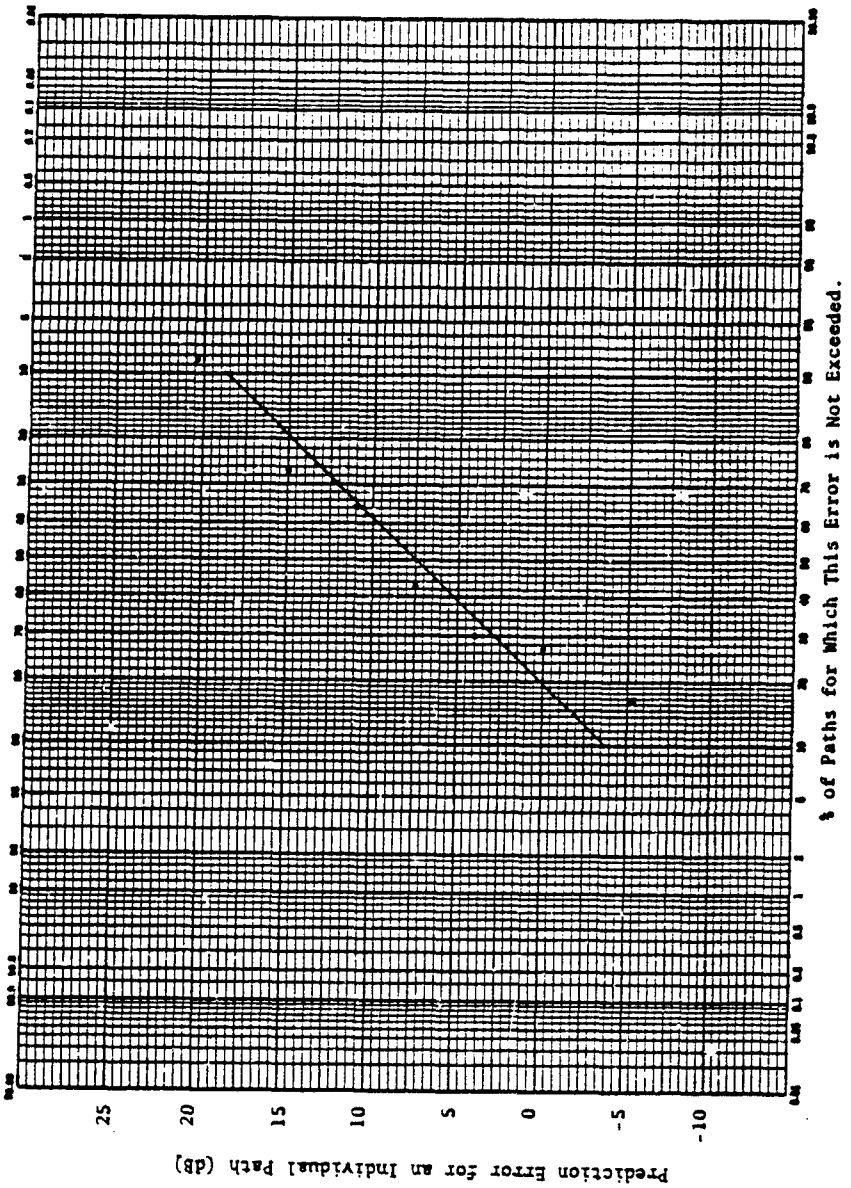

Figure C-4. Distribution of prediction errors for 70 paths in N.E. Ohio at 101.8 MHz. The solid line is the theoretical normal distribution having the same mean and σ. In addition to this graph, Chi-square testing supports the assumption that the distribution is normal.

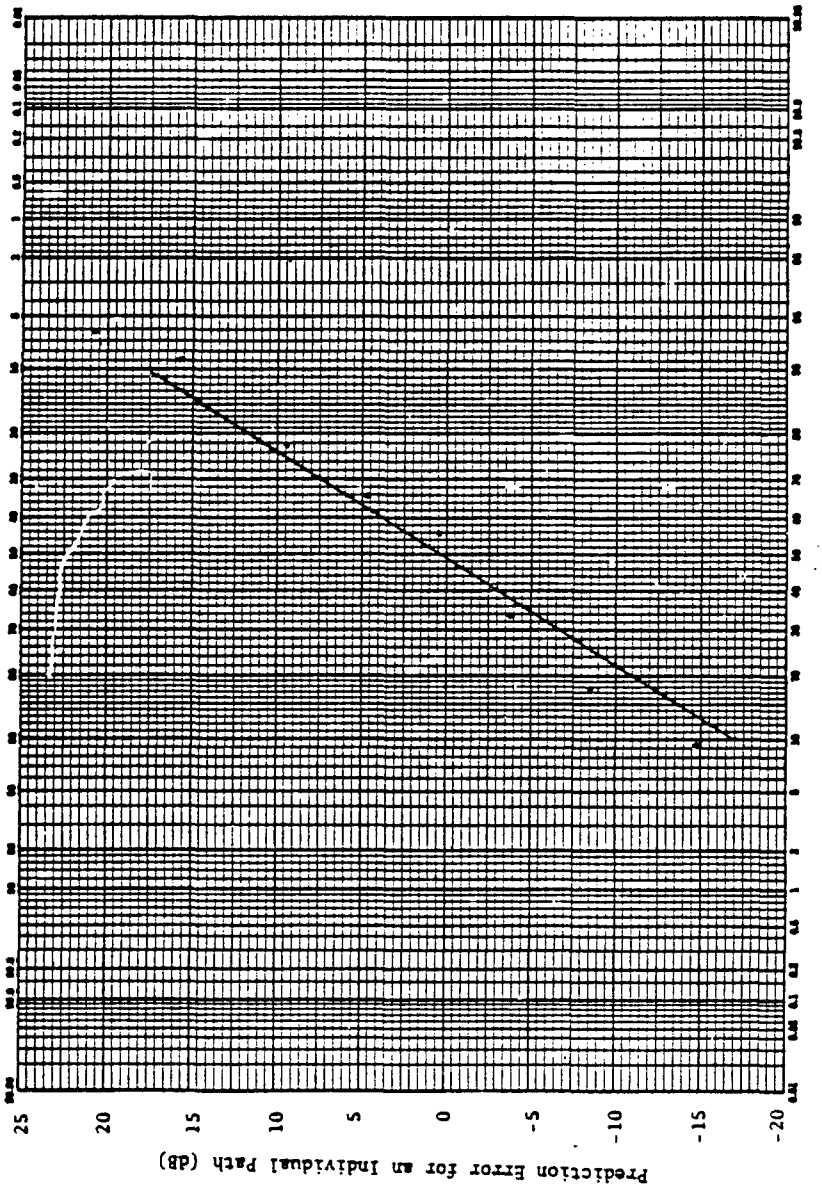

Figure C-5. Distribution of prediction errors for 148 paths in the Colorado Plains at 910 MHz. The solid line is the theoretical normal distribution having the same mean and σ. In addition to this graph, Chi-square testing supports the assumption that the distribution is normal.

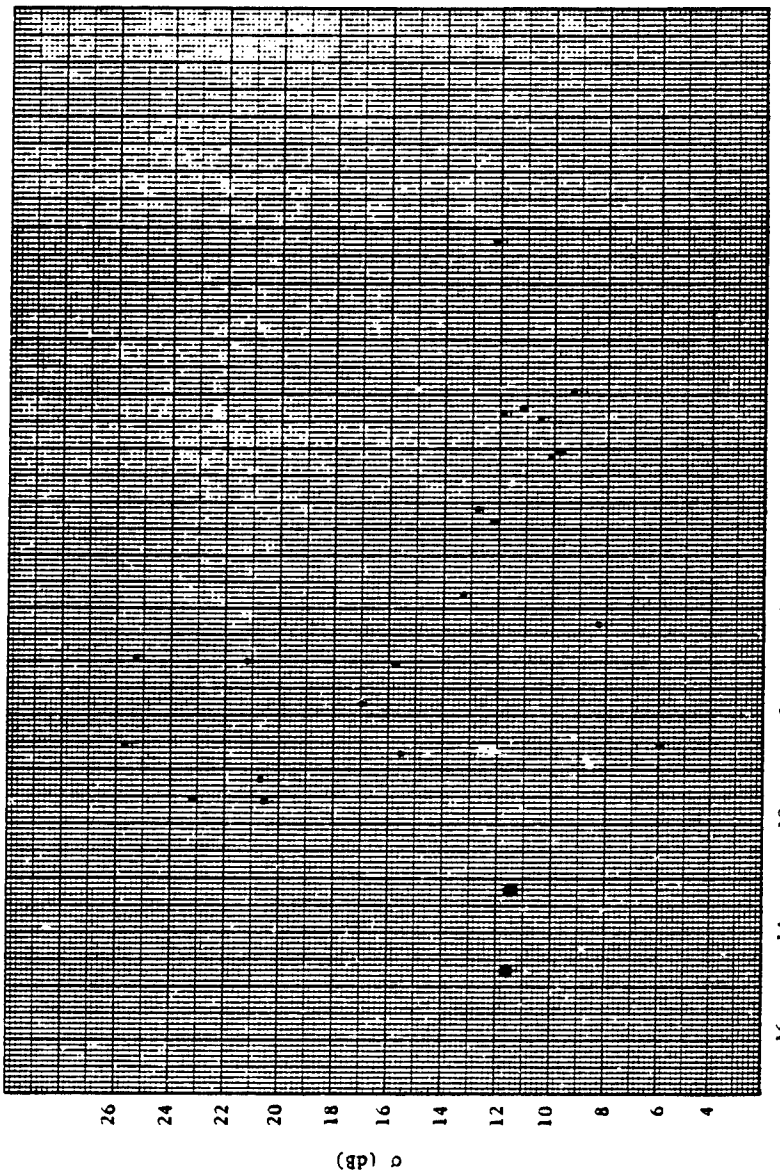

Figure C-6. Standard deviation of a group of prediction errors vs. the mean prediction error of the group. Data for the two Colorado Mountains groups are circled. ρ^2, excluding the mountain data, is 0.37. In the procedure outlined in this memorandum, σ and m are assumed to be independent.

$$\sigma = \sqrt{(6.07)^2 + \sigma_1^2} \qquad (2)$$

where σ_1 is given by Equation 1. (See, for example, Reference C-6, Section 4.6.)

Combining Equations 1 and 2 results in these formulas:

$$\sigma = \sqrt{46.32 - 41.76 \log f + 46.02 \log^2 f} \qquad (3a)$$
$$(f < 101.8)$$

$$\sigma = \sqrt{77.60 + 27.54 \log f + 4.65 \log^2 f} \qquad (3b)$$
$$(101.8 \leq f \leq 910.0)$$

$$\sigma = \sqrt{548.69 - 538.90 \log f + 141.85 \log^2 f} \qquad (3c)$$
$$(f > 910.0)$$

Statistical Tolerance Limits

If the set of prediction errors available was infinite in size, then there would be precise knowledge of the mean and standard deviation of the set of errors. Furthermore, if these data were normally distributed, then the probability of an error being greater than X dB could be determined, with 100% confidence, from a table of the cumulative normal distribution.

The actual data is limited, however, to 4741 measurements. At some frequencies there were as few as 357 measurements. And the model of the error distribution is based on a set of 21 means and sigmas. Thus there is uncertainty in the knowledge of the actual mean and standard deviation of the set of all possible prediction errors.

Since the actual distribution is approximately normal, the noncentral-t distribution can be used to quantify the uncertainty in the knowledge of the spread of prediction errors.[C-7] One can then determine, for a specified degree of confidence, the magnitude of the prediction error that will not be exceeded for a specified fraction of the cases investigated. This magnitude can be calculated as minus the mean error plus $k\sigma$, where the mean error is 0.77 dB, σ is given by Equation 3, and k is from TABLE C-2.

TABLE C-2

VALUES OF K

		Confidence Level 90%	95%
Fraction of the cases for which the error will not be exceeded	0.900	1.470	1.527
	0.950	1.861	1.927
	0.990	2.601	2.684
	0.999	3.435	3.539

The values of k were obtained from Reference C-7. The sample size was assumed to be 100, this being a reasonable compromise between the three possible choices (4741, 357, and 21). It can be shown that this choice is conservative for frequencies greater than or equal to 101.8 MHz.

EXAMPLE

At 200 MHz, increase the loss predicted by IPS by:

$$-0.77 + 1.527\sqrt{77.60 + (27.54 \log 200) + (4.65 \log^2 200)}$$

$$= -0.77 + 19.65 = 18.88 \text{ dB}$$

[C-7] Owen, D.B., Handbook of Statistical Tables, Addison - Wesley Publishing Co., Reading, MA, 1962, Section 5.3.

Now, if groups of 100 instantaneous (i.e. less than about 10 minutes) measurements are examined, the predicted loss will exceed the measured loss in at least 90 cases in each group for 95% of the groups.

If the IPS prediction is reduced by - 0.77 - 19.65 = -20.42 dB, then the measured loss will exceed the predicted loss in at least 90 cases in each group for 95% of the groups.

LIMITATIONS

The error statistics in Reference C-1 are based on measurements in the 20-9190 MHz band. Path lengths ranged from 0.3 to 73.8 statute miles. Antenna heights varied from 10 to 40 feet. All paths were overland in the United States. As actual path parameters diverge from this range of conditions, the confidence that may be placed in the accuracy of the error distribution diminishes.

The measurements discussed in this study were taken over relatively smooth terrain (ΔH = 90 meters). This was because the IPS is intended for application to this type of problem. When the model is used over more irregular terrain, it should be expected that the distribution of prediction errors will broaden and adjustments larger than those recommended in this appendix will be needed. This source of inaccuracy will become more severe as frequency increases.

Loss values predicted by this procedure should be limited to a minimum value of 6 dB less than the free-space loss.

This appendix addresses tolerance levels associated with one parameter - the basic transmission loss between two stations. In actual interference analyses there will be other parameters that are statistical in nature, e.g., antenna gains, noise levels, duty cycles, and (assuming that the IPS prediction is used for the interfering-signal level prediction) the desired signal strength. Techniques that can be used to account for the random nature of several variables are discussed in, for example, APPENDIX D and Reference C-8.

C-8 Lustgarten, M.N., A Generalized Procedure for Prediction or Evaluation of Frequency/Distance Separation Requirements, ECAC-TN-75-026, Electromagnetic Compatibility Analysis Center, December 1975.

ESTIMATING OUTAGE TIME IN TERRESTRIAL MICROWAVE SYSTEMS CAUSED BY MOBILE OR STATIONARY IN-BAND INTERFERENCE SOURCES [a]

Mark A. Weissberger, Robert L. Hinkle*, William T. Shelton
The IIT Research Institute Staff
At The Department of Defense
Electromagnetic Compatibility Analysis Center
Annapolis, Maryland 21402

Summary

Terrestrial line-of-sight microwave communications systems typically have a large enough median carrier-to-noise ratio to prevent loss of intelligence during periods of fading. The surplus carrier power can serve to mask interfering signals when fading is not occurring. This situation should be taken into account when estimating the degree of interference that in-band transmitters would cause. This paper presents a procedure for predicting interference in such cases. The measure of interference used is the increase in outage time (time during which the signal-to-interference-plus-noise ratio falls below the minimum acceptable value for the circuit) that the interfering source will produce during normal operation. An example is presented which results in an estimate of the outage caused by an airborne transmitter to a one hop circuit at 7.5 GHz. Multiple hop interference calculations are also described.

Introduction

Microwave line-of-sight radio links are designed with a median carrier power large enough to prevent loss of communications during all but the most severe periods of fading. The extra desired signal power will serve to mask interference when deep fading is not occurring. A realistic analysis of the impact of in-band interference should take this situation into account.

This paper presents an analysis technique that includes the effects of fade protection designed into terrestrial line-of-sight microwave systems. The result of the analysis is an estimate of the increase in outage time that the interfering source will produce during normal operation.. (Outage time is the time during which the desired signal-to-interference-plus-noise ratio falls below the minimum acceptable level for the circuit.)

The analysis procedure allows the engineer to include descriptions of the durations of the expected levels of desired signal power, interfering signal power, and background noise in the microwave receiver. Variations in the desired signal level would be due to fading and equipment failure. Variations in the interfering signal level would be due to movement of the interfering transmitter, changes in the orientation of its antenna, fading, and periods of no transmission. Variations in background noise would be due to fading and interference in the preceding hops of a multiple-hop system.

Outage time is computed from the probability of outage, P(O). This is the fraction of time that the system can be expected to experience an outage. The relation between outage time and P(O) is:

$$T_O = P(O) \times T_T \quad (1)$$

where

T_O = Outage time (seconds).

T_T = Total time period considered (seconds).

Typical T_T values would be 3600 seconds (one hour) and 2.592×10^6 seconds (one month).

An assumption used in the analysis is that the desired signal is always being transmitted. Therefore the probability of outage can be converted to a percent time available by using this formula:

$$\% \text{ time available} = (1 - P(O)) \times 10^{+2} \quad (2)$$

This factor is often called circuit reliability.

This analysis employs probability techniques. Parameters that are deterministic in nature (such as duty cycle and expected movement of the interfering source) can be accurately modeled and included in the analysis. Appropriate procedures are illustrated by an example.

Probability of Outage for a Single Hop Circuit

Condition for an Outage

The minimum acceptable signal-to-interference-plus-noise ratio at the receiver output can be related to a minimum carrier-to-interference-plus-noise ratio at the receiver input. For a given interference-plus-noise level at the receiver input, a minimum acceptable carrier level will exist. An outage occurs when:

$$c < c_{RIN} \quad (3)$$

where

c = Actual carrier power at receiver input (mW).

c_{RIN} = Carrier power required in the presence of interference and noise (mW).

The relation between the carrier power required in the presence of background noise only and the carrier power required in the presence of background noise and noiselike interference is:

* Mr. Hinkle is now with the U.S. Department of Commerce, Office of Telecommunications, Annapolis, Maryland.

[a] Originally published in the 1975 IEEE Electromagnetic Compatibility Symposium Record. This Appendix is provided as an example of an approach for integrating time variability data into a band sharing study.

$$c_{RIN} = c_{RN} \times \left(\frac{n_o + i}{n_o}\right) \quad (4)$$

where

c_{RN} = Carrier power required at the receiver input in the presence of noise only (mW).

n_o = Background internal noise level referenced to receiver input (mW).

i = Interfering power at the receiver input within the limits of the receiver IF bandwidth (mW).

The actual carrier power at the receiver input, c, is:

$$c = c_{RN} \times \left(\frac{f_M}{l_{AD}}\right) \quad (5)$$

where

f_M = Fade margin (ratio).

l_{AD} = Propagation loss, in addition to basic medium propagation loss, experienced by the desired signal (ratio). This is the depth of the fade.

Combining (3), (4) and (5) leads to the following test for outage in a single microwave hop:

$$\left(\frac{f_M}{l_{AD}}\right) \times \left(\frac{n_o}{n_o + i}\right) < 1 \quad (6a)$$

In logarithmic units this is:

$$F_M - L_{AD} + N_o$$

$$-10 \log (10^{N_o/10} + 10^{I/10}) < 0 \quad (6b)$$

where

F_M = f_M, expressed in dB.

L_{AD} = l_{AD}, expressed in dB.

N_o = n_o, expressed in dBm.

I = i, expressed in dBm.

When inequality (6a) or (6b) is satisfied, an outage occurs.

Using Monte Carlo Techniques to Determine P(O)

The probability of outage, P(O), can be determined from (6b) by formal analytic means when the probability density functions for both L_{AD} and I are available in closed form. Typically the density function for I is not available*. In any event, solving for P(O) by such means is cumbersome for the single hop problem and very cumbersome for the multiple hop problem. The use of Monte Carlo techniques involves many repetitive calculations and therefore requires the use of a computer. However the calculations are not complicated and are easily programmed. A closed form of the density function of I is not required. A further advantage is that the complexity of multiple hop problems is not significantly greater than the complexity of single hop problems. For these reasons the Monte Carlo procedure will be described and used in this paper.

The Monte Carlo procedure consists of repeatedly entering sample values of L_{AD} and I into (6b). After each sample pair has been entered, the result of the outage test is noted. After a sufficient number of samples has been tried, P(O) is calculated. Its value will be the number of trials in which an outage is predicted divided by the total number of trials.

Procedures for selecting L_{AD} and I sample values appear in the next two sections. These parameters are assumed to be independent and samples are selected independently.

Selecting Sample L_{AD} Values

Figure 1 is a set of plots of the cumulative distribution function of fade depths expected in a 7.5 GHz non-diversity system. The function used for deep fading (depths greater than 15 dB) is given by Equation (12) from Reference 2. The function is derived from the results of studies done by W. Barnett. It is sensitive to frequency, terrain type, climate zone and path length. The function used for fade depths less than 15 dB is derived from Figure 5 of Reference 3.

Figure 2 is a set of plots of the cumulative distribution of fade depths for a 7.5 GHz system with dual space diversity. For fades greater than 15 dB, it is assumed that a correlation coefficient of 0.5 relates the strengths of the two desired signals. (See Reference 2, Equation (18).) It is assumed that the degree of correlation increases for the less severe fades.

Choosing sample L_{AD} values is done graphically by repeating this procedure:

1. Choose a random number, from a uniform distribution, on the interval [0,1]. The number should have eight or more digits.
2. Use this as a Y-axis value on Figure 1 or 2.
3. Determine the corresponding L_{AD} (X-axis) value.

The process can be done analytically by using the inverse of the functions on Figure 1 and 2. The following equations are these inverse functions and will yield sample L_{AD} values as a function of a random number:

* A noteworthy exception is the case where both the desired signal and the interfering signal undergo Rayleigh fading. The solution to this problem appears in a paper by Bond.[1] Such a problem arises when the interfering transmitter is at a fixed location fairly distant from the microwave receiver. Bond concludes that the fading of the interfering signal does not significantly improve the chances of receiving the desired signal.

$$L_{AD} = \begin{cases} -A - B \log Q & 0 \le Q \le a \\ -C - D \log Q & a < Q \le .5 \\ 0 & .5 < Q \le 1 \end{cases} \quad (7)$$

where Q is a random number from a uniform distribution on the interval [0,1]. All other parameters are in TABLE 1.

Selecting Sample I Values

The received interference power at the microwave receiver can be computed from this relation:

$$I = P_T + G_T + G_R - L_{BM} - L_{AI} - OFR - \Delta BW \quad (8)$$

where

- I = Interference power at the receiver input within the limits of the receiver IF bandwidth (dBm).
- P_T = Power of interfering transmitter (dBm).
- G_T = Gain of interfering transmitting antenna (dBi).
- G_R = Gain of receiving antenna (dBi).
- L_{BM} = Basic median propagation loss for the interfering signal (dB).
- L_{AI} = Additional propagation loss, experienced by the interfering signal, due to fading (dB).
- OFR = Off-frequency-rejection caused by receiver selectivity to signals not co-channel with the receiver (dB).
- $\Delta BW = \begin{cases} 10 \log (BW_E/BW_{IF}), & \text{when } BW_E/BW_{IF} \ge 1 \\ 0, & \text{when } BW_E/BW_{IF} < 1 \end{cases}$
- BW_E = 3 dB emission bandwidth of the interfering source (Hz).
- BW_{IF} = Receiver 3 dB IF bandwidth (Hz).

When the interfering source is stationary and operates continuously, variations in I will be due to fading of the interfering signal. This is based on the assumption that the antenna of the interfering source is not being steered. In this case sample values of I can be generated by choosing sample values of L_{AI} and entering them into (8). The sample values of I are then entered into (6b). The sample values of L_{AI} are selected by using the inverse of the distribution function of fade depths appropriate for the path between the interfering transmitter and the victim receiver. (The solution to the problem where the interfering signal and the desired signal both undergo Rayleigh fading appears in Reference 1.)

When the interfering transmitter is mobile, I will vary because of changes in L_{BM}, G_T, G_R and L_{AI}. L_{BM} varies as the path length from the interfering transmitter to the victim receiver changes. G_T and G_R vary as the angle of the ray between this transmitter and receiver changes. L_{AI} changes due to fading of the interfering signal. Figures 3 and 4 illustrate the variation of I that would be produced as an airborne 125 watt transmitter was moved about at an elevation of 10,000 feet. The transmitter antenna gain is 5 dBi for all angles in the lower hemisphere. The microwave receiver antenna gain is 39 dBi in the main beam (circular with a 2° diameter) and -5 dBi for all other angles. The frequency is 7.5 GHz for both transmitter and receiver. ΔBW and OFR are 0. It is assumed that fading of the interfering signal (L_{AI}) is not significant.

Figure 4 is based on an output from the Airborne Flight Analysis Model (AFAM). This model allows the user to input full descriptions of the transmitter and receiver antenna patterns. L_{BI} values computed in the AFAM model can be based on smooth earth considerations or can take into account the shielding effects of the actual terrain. Figure 4 is based on a smooth earth assumption.

Consider a potential flight path along the section line A-A shown in Figure 3. Figure 5 illustrates the I values that would impact the microwave receiver as the airborne transmitter moved along this path. The total path length considered is 144 nmi. If the aircraft moves along this path with constant speed, then random numbers uniformly distributed on the interval [0,144] will provide proper sample values of the aircraft's position. The corresponding I values on Figure 5 are therefore appropriate sample values to enter into (6b) for outage tests. In actual calculations, the function illustrated in Figure 5 is approximated by a series of linear functions.

Example

The interference scenario plotted in Figure 5 was used in a test problem. The victim receiver was an AN/GSC operated in a system with a 20 dB fade margin, no diversity. The background noise level, N_o, was assumed to be -87 dBm (thermal noise in a 25 MHz bandwidth increased by a 13 dB noise figure). The fading samples used were for a 30 mile path in a temperate climate zone. Outage probabilities were calculated for both the interference and no-interference situations. A sample size of 20,000 was used. The results showed a probability of outage with no interference of 1.9×10^{-3} (reliability = 99.81%), and a probability of outage of 6.28×10^{-2} (reliability = 93.72%) with the interference. Another test problem solved was the case where the flight path was 144 miles long and went over the receiver but diverted away from the main beam region. In this case the probability of outage was 2.3×10^{-4} (reliability = 99.77%).

Probability of Outage for a Multiple Hop Circuit

The cumulative effects of interference and noise should be considered when doing outage calculations for

systems that consist of several hops in tandem. Fading in one section will produce an increase in noise which is passed on to other sections.[a] The interfering power introduced into one section is also transmitted to other sections.

Consider a system with N hops as illustrated in Figure 6. The total noise and noise-like interference into the jth receiver will be:

$$n_{TOT}(j) = n_o + i(j) + n_{PH}(j) + i_{PH}(j) \quad (10)$$

where

$i(j)$ = the interfering power entering the jth receiver directly from the interfering source (mW).

$n_{PH}(j)$ = noise accumulated in preceding hops and transmitted to the jth receiver by the jth microwave transmitter (mW).

$i_{PH}(j)$ = interfering power accumulated in preceding hops and transmitted to the jth receiver by the jth microwave transmitter (mW).

It is assumed that the interfering power from different hops (and different carriers) will add incoherently even though it may have all originated from the same source. The accumulated noise and interference are given by these equations:

$$n_{PH}(j) = \sum_{k=1}^{j-1} n_o \frac{l_{AD}(k)}{l_{AD}(j)} \quad (11)$$

and

$$i_{PH}(j) = \sum_{k=1}^{j-1} i(k) \frac{l_{AD}(k)}{l_{AD}(j)} \quad (12)$$

The factor $l_{AD}(k)$ accounts for the AGC of the kth receiver amplifying the interference and noise entering this receiver. The amount of gain is equal to the depth of the fade in the kth hop, $l_{AD}(k)$. The factor $l_{AD}(j)$ accounts for the attenuation of this retransmitted interference and noise by fading in the jth hop.

The carrier power at the input to the jth receiver will be:

$$c(j) = \frac{c_{KN} \times f_M(j)}{l_{AD}(j)} \quad (13)$$

where $f_M(j)$ is the fade margin (ratio) designed into the jth hop.

The test for outage at the jth receiver will be (by analogy to (6a)):

$$\left(\frac{f_M(j)}{l_{AD}(j)}\right) \times \left(\frac{n_o(j)}{n_{TOT}(j)}\right) < 1 \quad (14)$$

where

$$n_o(j) = n_o \times j \quad (15)$$

When the condition in (14) is satisfied, an outage occurs. Equation (15) reflects the fact that the quiescent (no fading) noise level into the jth receiver contains an accumulation of noise from the preceding hops. $f_M(j)$ is the protection ratio relative to this quantity.

Acknowledgement

The above work was performed under Contract No. F-19628-75-C-0002 and F-19628-73-C-0031 with the Electronics Systems Division, Air Force Systems Command. The Airborne Flight Analysis Model was programmed by Mr. T. Cochrane. The Monte Carlo procedure used for the example was programmed by Mr. K. Lawnes.

References

1. Bond, F. E. and Meyer, H. F., "The Effect of Fading on Communication Circuits Subject to Interference," *Proc. of IRE, Vol. 45*, May 1957.

2. *Engineering Considerations for Microwave Communications Systems*, Lenkurt Electric Co., Inc., San Carlos, CA, June 1970.

3. Pearson, K. W., "Method for the Prediction of the Fading Performance of a Multisection Microwave Link," *Proc. IEE, Vol. 112*, No. 7, July 1965[a].

4. Panter, P. F., *Communications System Design: Line-of-Sight and Tropocatter Systems*, McGraw-Hill, New York, 1972.

[a] See Chapter 10 of this Handbook for an updated guide to models for predicting fade distributions for microwave links.

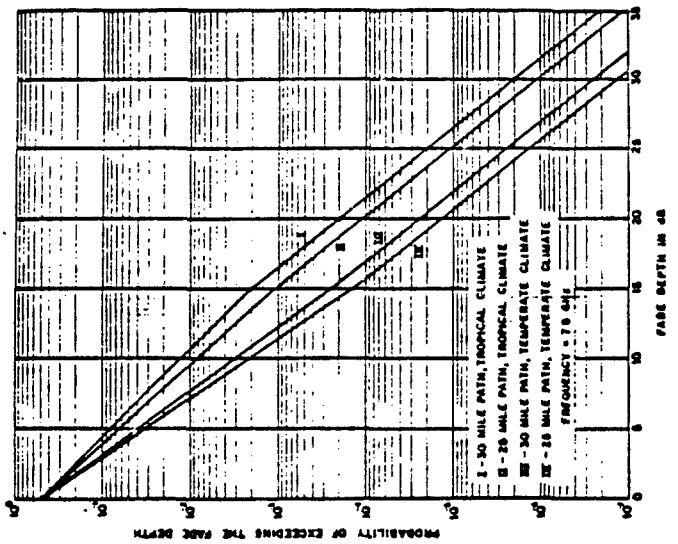

Figure 2. Cumulative fading distribution (dual space diversity).

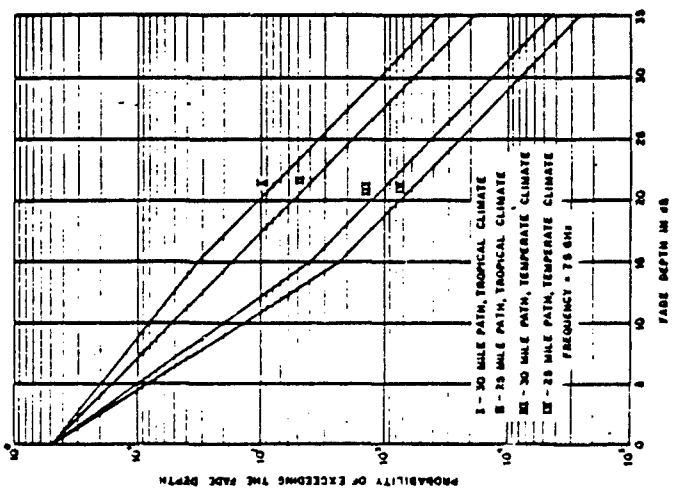

Figure 1. Cumulative fading distribution (non diversity).

4 A III b 5

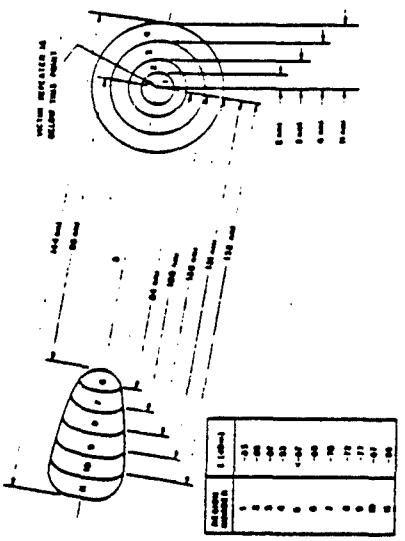

Figure 4. Detailed view of interference regions.

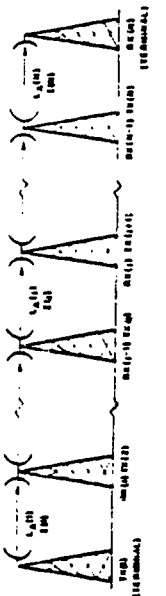

Figure 6. The multiple-hop system.

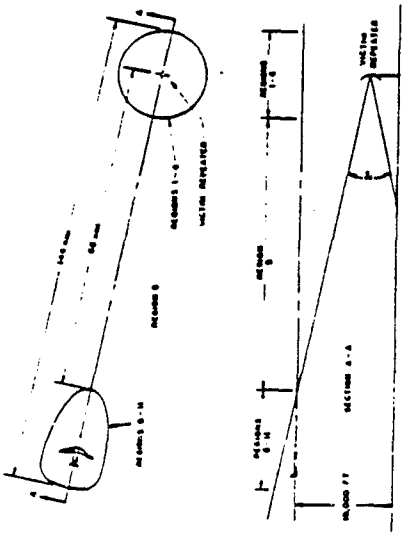

Figure 3. Interference regions produced by airborne source.

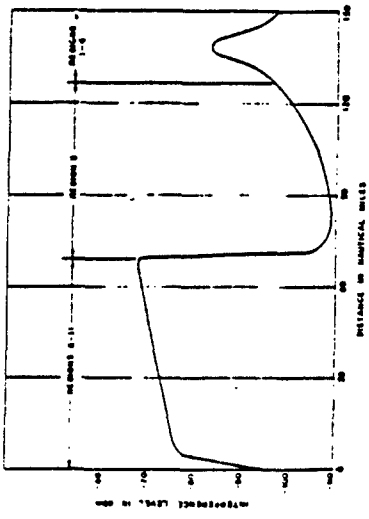

Figure 5. Interference levels produced as aircraft flies over path A-A.

TABLE 1

CONSTANTS FOR EQUATION 7

	Diversity				Non-Diversity			
	Temperate		Tropical		Temperate		Tropical	
	25 Miles	30 Miles	25 Miles	30 Miles	25 Miles	30 Miles	25 Miles	30 Miles
A	4.16	2.98	-.34	-1.54	11.4	8.98	2.32	-.050
B	5.0	5.0	5.0	5.0	10.0	10.0	10.0	10.0
C	1.28	1.37	1.72	1.89	1.93	2.15	3.16	3.78
D	4.25	4.55	5.70	6.27	6.43	7.15	10.5	12.6
α	$1.47_{4} \times 10^{-4}$	$2.53_{4} \times 10^{-4}$	$1.17_{3} \times 10^{-3}$	$2.03_{3} \times 10^{-3}$	$2.32_{3} \times 10^{-3}$	$4.00_{3} \times 10^{-3}$	$1.85_{2} \times 10^{-2}$	$3.20_{2} \times 10^{-2}$

DISTRIBUTION LIST FOR
RADIO WAVE PROPAGATION: A HANDBOOK OF
PRACTICAL TECHNIQUES FOR COMPUTING BASIC
TRANSMISSION LOSS AND FIELD STRENGTH
ECAC-HDBK-82-049

ADDRESS	NO. COPIES
ARMY	
HQDA DAMO-C4Z-S (PAUL PHILLIPS) WASHINGTON DC 20310	2
DIRECTOR USA SWL ATTN: DELSW-PP(MR CRAIG) VINT HILL FARMS STA WARRENTON VA 22186	1
US ARMY C-E SERVICES OFFICE ATTN: CC-OPS-CE-S WASHINGTON DC 20310	3
COMMANDER USA ERADCOM ATTN:CM/CCM (MR SCZEPANSKI) 2800 POWDER MILL RD ADELPHI MD 20783	1
PROJECT MANAGER SGT YORK GUN SYSTEM ATTN: DRCPM-ADG-E(C CHRISTIANSON) DOVER NJ 07801	1
CDR, USAAVRADCOM ATTN: DRCPM-ASE-PA(MR.F.ROHNE) 4300 GOODFELLOW BLVD ST LOUIS MO 63120	1
CDR, USAAVRADCOM ATTN: DRCPM-ASE-PA (LETA BROWER) 4300 GOODFELLOW BLVD ST LOUIS MO 63120	1
CDR, USACECOM ATTN: DRSEL-COM-RF-2 (P. SASS) FORT MONMOUTH NJ 07703	1
CDR, USAERADCOM(PM SOTAS) ATTN: DRSEL-CT-R (M. SHULHANDER) FORT MONMOUTH NJ 07703	1

DISTRIBUTION (Continued)
ECAC-HDBK-82-049

ADDRESS	NO. COPIES
CDR, USACECOM ATTN: DRSEL-COM-RY-3 FORT MONMOUTH NJ 07703	2
CDR, USACECOM ATTN: DRDCO-COM-RY-5 (W. KESSLEMAN) FORT MONMOUTH NJ 07703	2
CDR, USAMICOM ATTN: DRSMI-RE(D SMITH) REDSTONE ARSENAL AL 35898	1
CDR, USAMICOM ATTN: DRSMI-RTE (C PONDS) REDSTONE ARSENAL AL 35898	1
CDR, USAMICOM ATTN: DRCPM-HAE REDSTONE ARSENAL AL 35898	1
CDR, USAMICOM ATTN: DRCPM-ROL-E (L SMITH) REDSTONE ARSENAL AL 35898	1
CDR, USAMICOM ATTN: DRCMP-HFE (R SMITH) REDSTONE ARSENAL AL 35898	1
CDR, 7TH SIGNAL BRIGADE ATTN AEUSC-OA (CPT J NYERE) APO NY 09028	1
CDR, USATECOM ATTN: DRSTE-EL (MAJ ANGEL) ABERDEEN PROVING GPOUND MD 21005	2
CDR, USACC AGENCY-WHITE SANDS ATTN: CC-NC-TWS-F WSMR NM 88002	1
CDP, USACC ATTN: CC-OPS-W (H. WILSON) FORT HUACHUCA AZ 85613	1
CDR, USA CEE1A ATTN: CCC-EMEO-ECD FORT HUACHUCA AZ 85613	3

DISTRIBUTION (Continued)
ECAC-HDBK-82-049

ADDRESS	NO. COPIES
USA CONCEPTS ANALYSIS AGENCY ATTN: LTC STILWELL 8120 WOODMONT AVE BETHESDA MD 20014	1
CDR, USAEPG ATTN: STEEP-MT-M (LTC TURPIN) FORT HUACHUCA AZ 85613	2
CDR USACECOM ATTN: DRCPM-TDS-PL (H BAHR, J LIOY) FORT MONMOUTH NJ 07703	2
CDR, USACEEIA ATTN: CCC-EMEO-ECD(MR K BREWINGTON) FORT HUACHUCA AZ 85613	1
CDR, USACEEIA ATTN: CCC-EMEO (MR H MERKEL) FORT HUACHUCA AZ 85613	1
OFFICE OF THE AREA FREQUENCY COORDINATOR ATTN: DOD AFC ARIZONA FORT HUACHUCA AZ 85613	1
ARMY FREQUENCY COORDINATOR EASTERN US ATTN: CC-OPS-CE-UE (CHRIS WALL) FORT MEADE MD 20755	1
ARMY FREQUENCY COORDINATOR CENTRAL US ATTN: CC-OPS-CE-UC (J WEIBLE) FORT SAM HOUSTON TX 78234	1
ARMY FREQUENCY COORDINATOR ATTN: CC-OPS-CE-UW (J BARR) PRESIDIO OF SAN FRANCISCO SAN FRANCISCO CA 94129	1
ARMY FREQUENCY COORDINATOR ATTN: MDW-OMD-AFC (HARRY COLE) FORT MCNAIR WASHINGTON DC 20319	1

DISTRIBUTION (Continued)
ECAC-HDBK-82-049

ADDRESS	NO. COPIES
DOD AREA FREQUENCY COORDINATOR ATTN: MR. G. HUNGATE WSMR NM 88002	1
CDR, USACC AGENCY ATTN: CCNR-SLI-AF FORT SLISS TX 79916	1
CDR USARMY ENVIRONMENTAL HYGIENE AGENCY ATTN:HSE-RL(J TAYLOR) ABERDEEN PROVING GROUND MD 21005	1
COMMANDER-IN-CHIEF US EUROPEAN COMMAND ATTN: ECC3S-SPF(LTC HODGSON) APO NY 09128	1
COMMANDER USARMY SIGNAL CTR&FT GORDON ATTN: ATZH-CD-CS FORT GORDON GA 30905	2
USCORADCOM PROJECT MANAGER SINCGARS ATTN: DRCPM-GARS (C FISHMAN) FORT MONMOUTH NJ 07703	1
PROJECT MANAGER PATRIOT MISSILE SYSTEM, USADARCOM ATTN: DRCPM-MD-8 REDSTONE ARSENAL AL 35898	1
DIRECTOR SIGNAL WARFARE LAB ATTN: DELSW-PS (DR F WILLIAMS) VINT HILL FARMS STATION WARRENTON VA 22186	1
DIRECTOR, SIGNAL WARFARE LAB ATTN: DELSW-EE (C. STEPHENSON) VINT HILL FARMS STATION WARRENTON VA 22186	1

DISTRIBUTION (Continued)
ECAC-HDBK-82-049

ADDRESS	NO. COPIES
COMMANDER USARMY SIGNAL CENTER & FORT GORDON ATTN: ATZH-CDM (W BROOKSHIRE) FORT GORDON GA 30905	1
COMMANDER USARMY COMBINED ARMS CD ACTIVITY ATTN: ATCA-C3I(MAJ SCUREMAN) FORT LEAVENWORTH KS 66027	1
PRESIDENT US ARMY C-E TEST BOARD ATTN: ATZH-BD (J LYLE) FORT GORDON GA 30905	1
COMMANDER USARMY TRAINING & DOCTRINE COMMAND ATTN: ATTNG-NTC(COL R EDWARDS) FORT MONROE VA 23651	1
AIR FORCE	
HQ ASD/ENACE WRIGHT-PATTERSON AFB OH 45433	1
1839TH EIG/EIE KEESLER AFB MS 39534	1
EIC/EIEUS OKLAHOMA CITY AFS OK 73145	1
NAVY	
CHIEF OF NAVAL OPERATIONS (OP-941F) NAVY DEPARTMENT WASHINGTON DC 20350	1
DIRECTOR NAVAL ELECTROMAGNETIC SPECTRUM CENTER 4401 MASSACHUSETTS AVE NW WASHINGTON DC 20390	1
COMMANDER (ELEX-832T) NAVAL ELECTRONIC SYSTEMS COMMAND WASHINGTON DC 20363	1

DISTRIBUTION (Continued)
ECAC-HDBK-82-049

ADDRESS	NO. COPIES
DIRECTOR DEFENSE COMMUNICATIONS AGENCY ATTN: B303 WASHINGTON DC 20305	1
DOD & OTHERS	
DIRECTOR NATIONAL SECURITY AGENCY ATTN: W36/MR. V. MCCONNELL FT. GEORGE G. MEADE MD 20755	2
FEDERAL AVIATION ADMINISTRATION FOB 10A/RM 512 ATTN: ARD-450 800 INDEPENDENCE AVE SW WASHINGTON DC 20591	1
NATIONAL AERONAUTICS & SPACE ADMINISTRATION GODDARD SPACE FLIGHT CENTER ATTN: CODE 801/JIM SCOTT GREENBELT MD 20771	1
COMMANDER IN CHIEF US EUROPEAN COMMAND ATTN: C3S-SP APO NY 09128	1
COMMANDER IN CHIEF PACIFIC ATTN: C3STM BOX 29/32A CP HM SMITH HI 96861	1
DCA EUR (CODE E-400) APO NY 09131	1
ALASKAN AREA FREQUENCY COORDINATOR C/O AAC/DCXC ELMENDORF AFB AL 99506	1
COMMANDER IN CHIEF US SOUTHERN COMMAND ATTN: SC-G APO MIAMI 34003	1

ADDRESS	NO. COPIES
COMMANDER, CECOM ATTN:DRSEL-SEI(L DIEDRECHSEN) FORT MONMOUTH NJ 07703	3
CDR USATECOM ATTN:DRSTE-CT-CE(J RUSSELL) 5001 EISENHOWER AVE ALEXANDRIA VA 22333	1
USAAMSAA ATTN: E BARTHEL ABERDEEN PROVING GROUND MD 21005	1
USCINCEUR RAFLO BONN BOX 65 (MAJ H FAIRCLOTH) US EMBASSY APO NY 09080	1
COMMANDER USA NATIONAL TRAINING CTR ATTN: AFZJ-SMO (D GETZ) FORT IRWIN CA 92311	1
CDR, 5TH SIGNAL COMMAND ATTN: CCC-PO-TS APO NY 09056	1
CDR, USATECOM ATTN: DRSTE-CT-C ABERDEEN PROVING GROUND MD 21005	1
COMMANDER IN CHIEF US READINESS COMMAND ATTN: RCJ6-T (MR. RED MC CARRON) MACDILL AFB FL 33608	1
DIRECTOR US ARMY COMBAT SURVEILLANCE AND TARGET ACQ LAB ATTN: DELCS-R (LONGINOTTI) FORT MONMOUTH NJ 07703	1

ADDRESS	NO. COPIES
COMMANDER IN CHIEF ATLANTIC NORFOLK VA 23511	1
COMMANDER IN CHIEF U.S. READINESS COMMAND ATTN: RCJ6-O MACDILL AFB FL 33608	1
COMMANDER IN CHIEF STRATEGIC AIR COMMAND OFFUTT AFB NE 68113	1
COMMANDER IN CHIEF CONTINENTAL AIR DEFENSE COMMAND ENT AFB COLORADO SPRINGS CO 80912	1
MAJ C BAK ASSISTANT US MEMBER ARFA US DELEGATION/NATO MIL COMMITTEE APO NY 09667	1
NATIONAL TELECOMMUNICATIONS & INFORMATION ADMIN ATTN: MR ROBERT MAYHER 179 ADMIRAL COCHRANE DRIVE ANNAPOLIS MD 21401	1
DCEC ATTN: (R 410) 1860 WIEHLE AVENUE RESTON VA 22090	1
JOINT FREQUENCY MANAGEMENT AND SPECTRUM ENGINEERING OFFICE ATLANTIC NAVAL BASE BLDG N26 NORFOLK VA 23511	1

DISTRIBUTION (Continued)
ECAC-HDBK-82-049

ADDRESS	NO. COPIES
DIRECTOR DEFENSE COMMUNICATIONS AGENCY OPERATIONS CENTER ATTN: N24C WASHINGTON DC 20305	3
RAPID DEPLOYMENT AGENCY ATTN: RDJ6-T MACDILL AFB FL 33608	1
MAJ F J NEWMAN OJCS/C3S, JTD DIVISION RM 1C826, PENTAGON WASHINGTON DC 20301	1
TEMPORARY ADDRESSES	
COMMANDER NAVAL OCEAN SYSTEMS CENTER SAN DIEGO CA 92152	1
SUPERINTENDENT NAVAL POSTGRADUATE SCHOOL MONTEREY CA 93940	1
THE US ENVIRONMENTAL PROTECTION AGENCY ATTN: MR N HANKIN, ANR 461 CRYSTAL MALL II 401 M STREET SW WASHINGTON DC 20460	1
MR RICHARD TELL,BRANCH CHIEF, NRSB USEPA PO BOX 18416 LAS VEGAS NV 89114	1
CPT GUY JONES 5TH SIGNAL COMMAND FMO FREQ MGT BRANCH WORMS, FRG APO NY 09128	1
PROFESSOR W L STUTZMAN VPI AND STATE UNIVERSITY BLACKSBURG VA 20461	1

ADDRESS	NO. COPIES
PROFESSOR ROBERT E MCINTOSH UNIVERSITY OF MASSACHUSETTS AMHERST MA 01003	1
DR D V ROGERS COMSAT LABS BOX 115 CLARKSBURG MD 20734	1
DR TA-SHING CHU BELL LABORATORIES CRAWFORDS CORNER ROAD HOLMDEL NJ 07733	1
DR ERNEST K SMITH JET PROPULSION LABORATORY CALIFORNIA INSTITUTE OF TECHNOLOGY 4800 OAK GROVE DR PASADENA CA 91103	1
USAF FMO ATTN: NELSON POLLACK WASHINGTON DC 20330	1
MR S . PENNINGTON, CODE 5707.3 NAVAL RESEARCH LABORATORY WASHINGTON DC 20375	1
MR DOUGLAS J DUPEROW CONSUMERS POWER COMPANY 212 WEST MICHIGAN AVE JACKSON MI 49201	1
CDR, USAERADCOM ATTN: DRDCO-COM-RF-2(P SASS) FORT MONMOUTH NJ 07703	1
CMDR HQ CECOM ATTN: DRSEL-COM-RY-2 MR PAUL A MAJOR FT MONMOUTH NJ 07703	1

DISTRIBUTION (Continued)
ECAC-HDBK-82-049

ADDRESS	NO. COPIES
MR DAVID PRICHARD US ARMY SYSTEMS ANALYSIS ACTIVITY ABERDEEN PROVING GROUND MD 21005	1
FEDERAL AVIATION ADMINISTRATION FOB 10A/RM 512 ATTN: ARD-450, C CRAM 800 INDEPENDENCE AVE SW WASHINGTON DC 20591	1
MR WILLIAM FRAZIER US DEPARTMENT OF COMMERCE NTIA ADMIRAL COCHRANE DR ANNAPOLIS MD 21401	1
DR LOUIS IPPOLITO, MANAGER PROPAGATION AND GROUND TERMINAL PROGRAMS WASHINGTON DC 20546	1
INSTITUE FOR TELECOMMUNICATION SCIENCES DR HAROLD T DOUGHERTY BOULDER CO 80303	1
MR GEORGE HAGN SRI INTERNATIONAL 1611 NORTH KENT ST ARLINGTON VA 22209	1
COMMANDER-IN-CHIEF US EUROPEAN COMMAND ATTN: MAJ, MARTY SASS APO NY 09128	1
MR W DANIEL OFFICE OF THE CHIEF ENGINEER RESEARCH DIV., FCC 1909 M STREET NW WASHINGTON DC 20554	1
DR GEORGE HUFFORD INSTITUTE FOR TELECOMMUNICATION SCIENCES BOULDER CO 80303	1

DISTRIBUTION (Continued)
ECAC-HDBK-82-049

ADDRESS	NO. COPIES
DEFENSE TECHNICAL INFORMATION CENTER CAMERON STATION ALEXANDRIA VA 22314	12
485 EIG/EIEUS GRIFFISS AFB NY 13441	1
6545TH TEST GROUP HILL AFB UTAH 84056	2
1843 EIG/EIEM WHEELER AFB HI 96854	1
AFEWC/SAT ATTN: J OLIVER SAN ANTONIO TX 78243	1
JEWC/TAM ATTN: CAPT BAKER SAN ANTONIO TX 78243	1
JEWC/OPT ATTN: A BLACK SAN ANTONIO TX 78243	1
FTD/TQC ATTN: J WISE WRIGHT PATTERSON AFB OH 45433	1
JEWC/TA ATTN: BOB MILLET SAN ANTONIO TX 78243	2

ECAC INTERNAL DISTRIBUTION

CA/R TITUS	6
DO/J SCOTT/T BODE/S CAMERON	1
XM/J JANOSKI	1

DISTRIBUTION (Continued)
ECAC-HDBK-82-049

ADDRESS	NO. COPIES
DI/W GREENE	1
DIB/E FOWLER	1
DIC/C LADY	1
DID/R BREDESON	1
DIO/F TUSHOPH	1
DR/K KONTSON	1
DRC/T REILLY	1
DRD/A FITCH	3
DRM/D MACKIN	1
DRM/M WEISSBERGER	5
DRS/C JONES	1
DRS/M GRUENDL	1
DS/R CRISAFULLI	1
DSA/G ROMANOWSKI	1
DSB/J BENISCHEK	1
DSF/D DOYEN	1
DST/J FAROE	1
DC/R CRAWFORD	1
DCB/W KLESSE	1
DCC/C GETTIER	1
DCF/R SLYE	1
DCI/P SAUTTER	1

DISTRIBUTION (Continued)
ECAC-HDBK-82-049

ADDRESS	NO. COPIES
DF/R WILLATS	1
DFA/L SKEWS	1
DFB/H KNOWLTON	1
DFS/J SMITHMYER	1
DN/J JONES	1
DNA/R TAYLOR	1
DNM/G IMHOF	1
CF/L KIMMONS	1
CF/P KERR	1
CF/R CANFIELD	1
CF/P MAGER	1
CF/LT MORAITES	1
CF/S SAFFERMAN	1
CF/CAPT LUKE	1
CF/R LARSON	1
DNN/D BARAN	1
DQ/E JACKSON	2
DQT/R WHITEMAN	1
DIL	15
CCN/J ATKINSON	1
CD/J A ZOELLNER	1
DIO/T WILSON	1